



Université  
de Lille  
1 SCIENCES  
ET TECHNOLOGIES

## **THESE**

Présentée à

**L'Université des Sciences et Technologies de Lille**

Pour obtenir le titre de

**DOCTEUR EN CHIMIE**

Spécialité: Sciences de la Matière, du Rayonnement et de l'Environnement

par

**Javier IBÁÑEZ ABAD**

**Développement de nouveaux catalyseurs hétérogènes sélectifs  
pour l'amination directe des alcools**

Soutenue le 15 Novembre 2017 devant la commission d'examen suivante :

### **Rapporteurs**

M. Dmitry Yu. MURZIN, Professeur, Åbo Akademi University (Finland)

M. Marco DATURI, Professeur, Université Caen Basse-Normandie (France)

### **Examineurs**

M. Franck DUMEIGNIL, Professeur, Université Lille 1 Sciences et Technologies (France)

Mme. Anne PONCHEL, Professeur, Université d'Artois (France)

M. Maarten K. SABBE, Maître de conférences, Université de Gent (Belgique)

### **Directeurs**

M. Sébastien PAUL, Professeur, Ecole Centrale de Lille (France)

M. Marc PERA TITUS, Chargé de Recherche CNRS, E2P2L Shanghai (Chine)





Université  
de Lille  
1 SCIENCES  
ET TECHNOLOGIES

## THESE

**L'Université des Sciences et Technologies de Lille**

For obtaining a title of

**DOCTOR IN CHEMISTRY**

Mention: Sciences de la Matière, du Rayonnement et de l'Environnement

by

**Javier IBÁÑEZ ABAD**

**Development of Novel Heterogeneous Selective Catalysts for the Direct  
Amination of Alcohols**

Defended on 15 November 2017 in front of the following examination committee:

### **Reviewers**

M. Dmitry Yu. MURZIN, Professor, Åbo Akademi University (Finland)

M. Marco DATURI, Professor, Université Caen Basse-Normandie (France)

### **Examiners**

M. Franck DUMEIGNIL, Professor, Université Lille 1 Sciences et Technologies (France)

Mme. Anne PONCHEL, Professor, Université d'Artois (France)

M. Maarten K. SABBE, Assistant professor, Université de Gent (Belgique)

### **Directors**

M. Sébastien PAUL, Professeur, Ecole Centrale de Lille (France)

M. Marc PERA TITUS, Chargé de Recherche CNRS, E2P2L Shanghai (Chine)



Dedicado a la memoria de Trinidad,  
María del Carmen  
y Daniel.

## ACKNOWLEDGMENTS

---

First, I would like to thank the Agence National de la Recherche and the CNRS for the financial support through the ANR SHAPes program during my doctoral studies. I would like to extend my gratitude to Dr. Marc Pera Titus, Dr. Sébastien Paul, Dr. Floryan Decampo, Dr. Armin Liebens and Dr. Franck Dumeignil for offering me this opportunity and allowing me to pursue research in the UCCS and E2P2 laboratories in Lille and Shanghai, as well as in the REALCAT platform in Lille.

Besides providing me this opportunity, the role of Dr. Sébastien Paul and Dr. Marc Pera Titus as my doctoral advisors goes way beyond that. Their experience, knowledge and guidance has been key to the development of my doctoral work. Dr. Marcia Araque Marin, as my doctoral mentor, has always been available for the day-to-day discussions, helping me to solve numerous scientific and technical questions. She has always provided me with the most valuable advice and guidance during these years. For all that and more, I would like to express my most sincere gratitude to my supervisors. Their scientific and personal support, their trust and the freedom they gave me have helped me in all time during my research and writing of this thesis.

I am especially honored by the acceptance Dr. Dmitry Yu Murzin and Dr. Marco Daturi to review my doctoral work. Likewise, I would like to thank Dr. Franck Dumeignil, Dr. Anne Ponchel and Dr. Maarten Koenraad Sabbe for agreeing to take part in the dissertation committee.

I wish to express my gratitude to Dr. Zhen Yan for his help during my stay in Shanghai. His scientific advice, his great experimental experience and the numerous scientific discussions have been key throughout the completion of my thesis. I would like to extend my gratitude to the colleagues who I was lucky to work with and with whom I share unforgettable memories from Shanghai. In particular, I would like to thank Javier Diaz Maroto, Dr. Bright Kusema, Dr. Jonathan Lai, Dr. Fang Lin, Dr. Raphael Wischert, Dr. Renate Schwiedernoch, Dr. Jerry-Peng Li, Dr. Mengjia Wu, Dr. Fengzheng Su, Dr. Fan Jiang and Dr. Wenjuan Zhou.

I am indebted to numerous people that helped me during my stay in Lille. Firstly, I would like to thank Johann Jezequel, Gérard Cambien and Pascale Dewalle for their valuable technical assistance. I would also like to thank David Porier, Barbara Declerck-Boulanger and Zohra Gueroui for their help with all the paperwork and reservations during my thesis. An especial mention should be done to Svetlana Heyte and Joëlle Thuriot for their valuable help while I worked on the REALCAT platform. Not only their technical help and analytical work but their positive attitude have been invaluable during these years. I would also like to thank Dr. Benjamin Katryniok, Dr. Andrei Khodakov, Dr. Vitaly Ordonsky and Dr. Robert Wojcieszak for their help and fruitful scientific discussions.

I would like to extend my gratitude to the many fellow graduate and postdoctoral students with whom I had the pleasure to share space and time in Lille. Especial thanks to Marco and Unai for helping me the first days and introducing me to the city. I would also

like to thank Anouchka, Mehdi, Ana, Nuno, Haiqin, Xuemei, Xiaofeng, Tong, Dmitry, Bang, Alexandre, Thomas, Samadhan, Ajay G., David and many others for the day-to-day discussions, coffees and all the good moments in Lille. An especial mention to my friend and colleague Ajay Tomer, for the scientific discussions and the many great moments in Lille and Shanghai.

I am especially grateful to my great friends in Lille, who have supported me during these years. I wish to thank Natalia, Estitxu and Rocio for being there since day 1 and throughout these years. Thanks to Caroline, Marion, Maxime, Alix and Tommy for the great moments we've shared in 421 and after. Thank you for your openness and your positive spirit. You have all been my family in Lille.

I would like to express my most personal acknowledgment to Julia. Thanks to you for your invaluable support, unconditional love and your contagious smile.

Last, but not least, I would like to thank my parents, Juan de Dios and Maria del Carmen, my aunts Petra and Paquita and my brothers Juan, Daniel and Miguel for more than I could ever express here.

### **Funding and Organization**

This work was supported by the French National Agency of Research (ANR) through the SHAPes program (contract 13-CDII-0004-06).

The REALCAT platform is benefiting from a state subsidy administrated by the French National Research Agency (ANR) within the frame of the 'Future Investments' program (PIA), with the contractual reference 'ANR-11-EQPX-0037'. The European Union, through the ERDF funding administered by the Hauts-de-France Region, has co-financed the platform. Centrale Lille, the CNRS, and Lille 1 University as well as the Centrale Initiatives Foundation, are thanked for their financial contributions to the acquisition and implementation of the equipment of the REALCAT platform.

## RESUMÉ

---

Les amines sont des composés utilisés dans de nombreux secteurs de l'industrie chimique et dont, au vu d'études récentes, la demande devrait augmenter dans les années à venir. À cet égard, le développement de technologies efficaces et écologiquement responsables pour leur production est nécessaire pour notre société. La transformation des alcools en amines via le mécanisme «d'emprunt d'hydrogène» (*borrowing hydrogen*) apparaît comme une voie performante et durable.

Ce travail se concentre sur le développement de nouvelles formulations de catalyseurs hétérogènes permettant de synthétiser de manière sélective des amines primaires à partir d'alcools et d'ammoniac. Deux formulations bimétalliques supportées sur alumine ont été développées à partir d'une stratégie séquentielle de criblage intensif et d'optimisation des catalyseurs. Ces formulations montrent d'excellentes activité et sélectivité vers l'amine primaire ciblée: la *n*-octylamine.

Finalement, un modèle cinétique a été développé sur la base des données expérimentales collectées. Il permet de bien rendre compte de l'ensemble complexe de réactions en cascade du mécanisme.

## ABSTRACT

---

Amines are important building blocks for many fields of the chemical industry and, according to recent studies, their demand is foreseen to increase over the following years. In this regard, the development of efficient and ecologically responsible technologies for their production is necessary for our society. The transformation of alcohols into amines via the so-called *borrowing hydrogen* mechanism stands out as an efficient and ecological route.

This work centers its efforts on the development of novel heterogeneous formulations for the selective synthesis of amines from alcohols and ammonia via a sequential screening and optimization of monometallic and bimetallic supported catalysts. Two bimetallic formulations supported on alumina have been developed showing excellent activity and selectivity towards the targeted primary amine: the *n*-octylamine.

Finally, a kinetic model has been developed on the basis of the experimental data collected. It correctly predicts the reaction rates of the complex ensemble of cascade reactions of the mechanism.



# Table of Contents

---

## **Chapter 1 General Introduction and Bibliographic Study .....1**

1.1	Amines: Generalities and Market .....	3
1.1.1	Industrial Context: A Brief Introduction.....	3
1.2	Synthesis of (Alkyl) Amines .....	5
1.2.1	Halide Amination Process.....	5
1.2.2	Olefin Amination Process (Hydroamination) .....	6
1.2.3	Nitrile Hydrogenation Process .....	7
1.2.4	Carbonyl Reductive Amination Process .....	8
1.2.5	Direct Alcohol Amination Process .....	9
1.3	Kinetic Modelling for the Amination of Alcohols .....	19
1.4	Conclusion .....	26
1.5	Nomenclature.....	27
1.6	References.....	28

## **Chapter 2 Materials and Methods .....39**

2.1	Materials .....	41
2.2	Synthesis of Heterogeneous Catalysts .....	42
2.2.1	Synthesis of bimetallic supported catalysts .....	42
2.3	Characterization Methods.....	43
2.3.1	Elemental Analysis (ICP-oES) .....	43
2.3.2	Specific Surface Area Measurement (BET-BJH) .....	44
2.3.3	X-Ray Powder Diffraction (XRD).....	44
2.3.4	Scanning Transmission Electron Microscopy –EELS/EDS .....	44
2.3.5	Temperature Programmed Reduction (H <sub>2</sub> –TPR).....	44
2.3.6	Temperature Programmed Pulse Oxidation (O <sub>2</sub> Pulse–TPO).....	45
2.4	Catalytic Tests .....	46
2.4.1	Three Parallel Fixed Bed Reactor – MPRS-3TC.....	46
2.4.2	High Pressure Fixed Bed Reactor – TERCH.....	48

2.4.3	High-Throughput Experiments – Flowrence® Unit .....	49
2.5	Kinetic Modeling .....	52
2.5.1	Fixed Bed Flow Model .....	52
2.5.2	Mathematical description of the reactor hydrodynamics .....	54
2.5.3	Least Squares - Kinetic Fitting .....	55
2.5.4	Quality of the Fittings – Statistical Analysis .....	56
2.6	Nomenclature.....	59
2.7	References .....	60

### **Chapter 3 Cobalt-based Bimetallic Catalysts for the Direct Amination of *n*-octanol .....61**

3.1	Background.....	63
3.2	Effect of the nature of the dopant .....	64
3.3	Effect of the Impregnation Sequence for Ru- and Ag-doped 5%Co/Al <sub>2</sub> O <sub>3</sub> .66	
3.3.1	Catalytic Activity .....	66
3.3.2	Cobalt Reducibility .....	67
3.4	Optimization of the Dopant Loading.....	71
3.4.1	Catalytic activity .....	71
3.4.2	X-Ray Diffraction .....	77
3.4.3	STEM/EDS-SDD .....	77
3.5	Effect of the H <sub>2</sub> pressure at variable NH <sub>3</sub> -to-alcohol ratios .....	78
3.6	Optimization of Process Conditions .....	79
3.6.1	Conclusions.....	82
3.7	References .....	84

### **Chapter 4 Kinetic modeling of *n*-octanol amination .....87**

4.1	Background.....	89
4.2	Reaction Network .....	89
4.3	Experimental trends .....	89
4.4	Development of kinetic models .....	92
4.4.1	Rationalization of the experimental trends .....	92

4.4.2	Hypotheses and approximations .....	95
4.4.3	Formulation of kinetic expressions .....	97
4.5	Kinetic Fitting .....	101
4.5.1	Discrimination of the different deactivation mechanisms .....	101
4.5.2	Kinetic Model Optimization .....	105
4.5.3	Validation of experimental trends for model M.V_B .....	109
4.5.4	Mapping of Process Conditions .....	112
4.6	Conclusions .....	114
4.7	Nomenclature.....	116
4.8	References.....	117

## **Chapter 5 General conclusions and perspectives .....119**

5.1	General Conclusions.....	121
5.2	Perspectives .....	122

## **Annexes .....125**

Annex I.	Summary of the screening of mono-metallic catalysts.....	127
I.1.	Introduction.....	127
I.2.	Materials and Methods.....	127
I.3.	Results.....	127
Annex II.	Kinetic experiments and table of results.....	134
Annex III.	Validation of the proposed hydrodynamic model.....	142
Annex IV.	Development of the kinetic expressions .....	146
Annex V.	Matlab code for the kinetic optimization of model M.V_B .....	150
	References of the annexes .....	159



---

# **Chapter 1**

## **General Introduction and Bibliographic Study**

---



## 1.1 Amines: Generalities and Market

Amines are organic compounds derived from ammonia where one or more of the hydrogen atoms has been replaced by an alkyl or aryl group. Depending on the number of organic substituents amines can be classified as primary, secondary and tertiary [1,2].

### 1.1.1 Industrial Context: A Brief Introduction

During the first decade of the 20<sup>th</sup> century the German chemists Fritz Haber and Carl Bosch developed a process that can efficiently transform atmospheric nitrogen into ammonia by reaction with hydrogen. In 1913, the Haber-Bosch process was implemented by the chemical company BASF and, ever since then, ammonia has been readily available at large scale, exceeding an annual production of a 100 million metric tons, thus consuming over 1% of the world energy resources [3,4]. At present, virtually all the manufactured amines are issued directly or indirectly from ammonia, representing a total amine production of about 6 to 7 million metric tons per year [5,6].

Amines are commodity chemicals with a wide variety of applications, serving as building blocks in the manufacture of agrochemicals, surfactants, polymers, water treatment chemicals, pharmaceuticals, solvents and dyes (Figure 1-1). In particular, alkylamines and their derivatives have been extensively used in a broad range of applications, including fabric softening or other antistatic uses [7–10], shampoos and hair conditioners [11,12], cleaners and detergents including hard surface cleaners [13], corrosion inhibitors [14], and agricultural surfactants [15,16]. For example, fatty amine ethoxylates are nonionic surfactants used as wetting and dispersing agents, stabilizers, sanitizers and defoaming agents in various industries like textile, paper, drilling and chemical paints [17]. Cationic derivatives issued from fatty amines have a marked degree of substantivity (adhesion) for solid surfaces (*e.g.*, wool, leather, cotton, plastics, dye pigments, metals) allowing the formation of firm cationic films with tunable properties for a broad range of applications [10]. It is forecasted that the global demand of amines will increase in the following years, especially driven by the Chinese and other Asian markets. Overall, the demand for amines is foreseen to increase at an annual growth rate of 4 to 8% during the next decade [6,18–20].

Even though the amine industry has reached a position of maturity, it still faces numerous challenges, especially regarding the synthesis of primary alkylamines. The existing processes often lack of selectivity, producing an equilibrium mixture of amines [21], and/or encompass hazardous reagents and byproducts [22,23]. Both industry and academia have tried to tackle this issue, as testified by the increasing number of patents and scientific papers in this topic during the last decade. In Figure 1-2 (a) we can observe how the main body of granted patents in the period 2007-2016 has mainly focused on hydrogenation of nitriles and direct amination of alcohols, while the scientific community - Figure 1-2 (b) - has concentrated its interest mostly on the direct amination of alcohols as a route towards the synthesis of primary amines, with more than 300 scientific publications published in peer-reviewed journals related to the topic along this period.

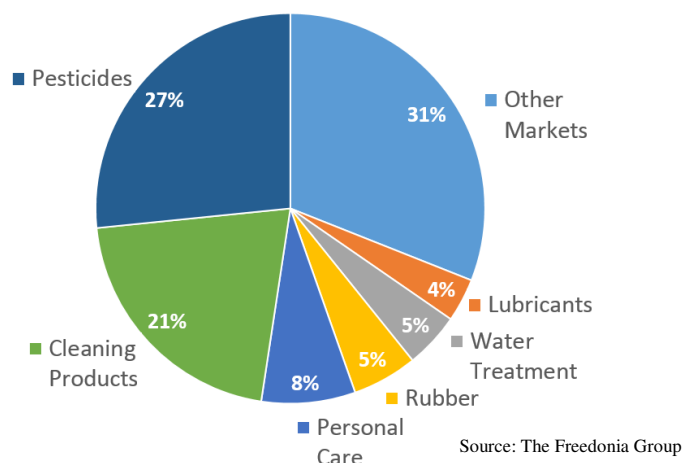


**Figure 1-1** Global market for amines, 2015 (6.1 million tons in total) (Data replotted from The Freedonia Group Study) [24].

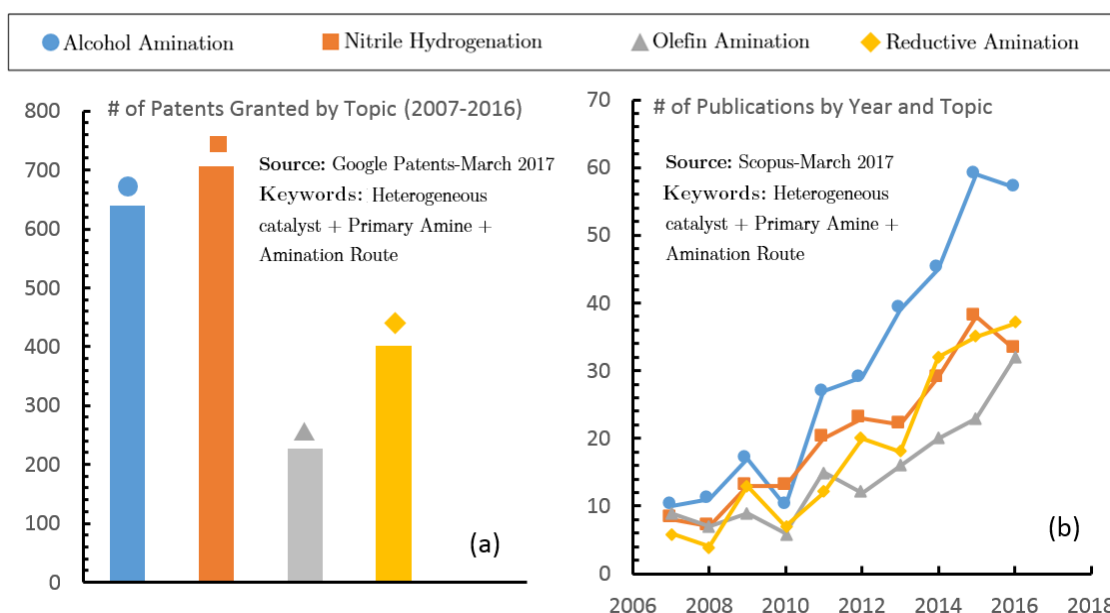


**Figure 1-2** (a) Number of patents granted from 2007 to 2016 regarding different amination routes. (b) Number of publications by year and amination route (2007-2016).

Below we summarize the different processes for amine manufacture, with a special focus on the synthesis of primary alkylamines *via* heterogeneously catalyzed processes, which are of greater relevance for large-scale production. In the forthcoming chapters, the reader will find a compilation of the most recent advances on heterogeneous catalysts for the direct amination of alcohols as an efficient and sustainable route towards the synthesis of primary amines.

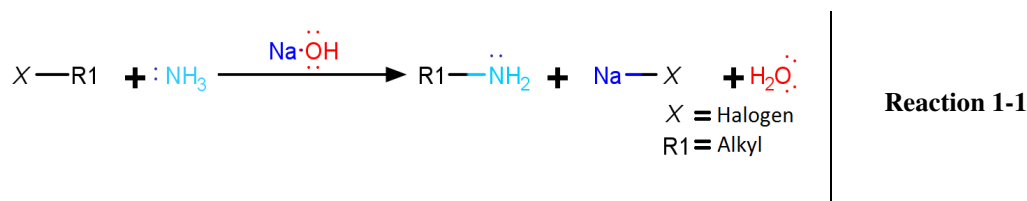
## 1.2 Synthesis of (Alkyl) Amines

Various reactions and processes are well known for the synthesis of amines, most of them for more than a century. As early as 1849, the French chemist Charles-Adolphe Wurtz already reported the synthesis of methyl and ethylamine by the hydrolysis of the corresponding alkyl isocyanate [5,25]. In 1901, the alkylation of aniline with sodium alkoxides was described by John Ulrich Nef [26]. Further on, Sabatier and Mailhe [27] reported in 1909 the synthesis of amines by contacting alcohols and ammonia at high temperatures (250-350 °C) in the presence of an acid thoria catalyst. This reaction is interesting due to the availability of inexpensive alcohols derived from processes such as hydroformylation/reduction of olefins, hydration of olefins, fermentation of sugars, or directly produced from syngas. Moreover, the reaction is atom efficient, does not involve hazardous compounds and generates water as sole byproduct [28,29]. Since these earlier discoveries, many processes have been implemented for the synthesis of alkylamines *via* the vapor-phase amination of alcohols with ammonia [30–32]. All these processes rely on the direct amination of alcohols operating at high temperatures and pressures.

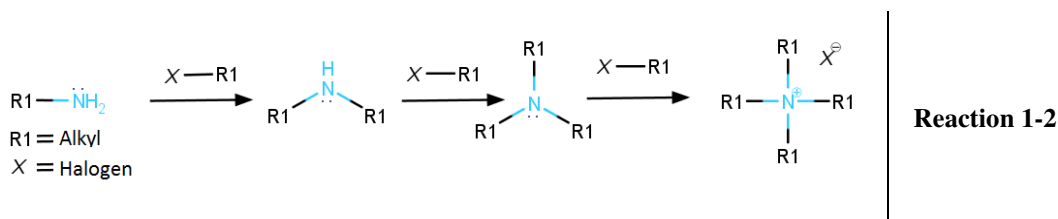
At present, the industrial production of amines is achieved through several different processes involving different feedstocks, catalysts and reaction conditions. In sections 1.2.1 to 1.2.5, we discuss the most relevant processes for the manufacture of amines, as well as their main advantages and drawbacks.

### 1.2.1 Halide Amination Process

The reaction between ammonia and halocarbon compounds is one of the oldest known technologies for manufacturing amines [33,34]. The reaction occurs through a two-step mechanism: first the nitrogen atom from ammonia attacks the electrophilic carbon atom of the alkyl halide, creating a new carbon-nitrogen bond and displacing the halogen. The positively charged nitrogen (ammonium) will be deprotonated by either the excess ammonia, or by an externally added base, thus producing the primary amine and the corresponding salt (see Reaction 1-1).



The produced primary amine, being a stronger nucleophile than ammonia, will readily react with the alkyl halide following Reaction 1-2, producing a mixture of primary, secondary, tertiary amines and quaternary ammonium salt, making it difficult to control the reaction selectivity.



The reaction occurs under mild conditions in the absence of catalyst for alkyl and activated aryl halides with strong electron withdrawing groups. For the amination of non-activated aryl halides, the reactions can be assisted by an homogeneous palladium catalyst following the Buchwald-Hartwig reaction [35].

Although this route represents a standard synthesis method at laboratory scale, the amination of haloalkanes is not the preferred process for the industrial production of amines. The difficulty to control the reaction selectivity, the higher price of the starting materials and the disposal of stoichiometrically generated salts limit the economic feasibility of the process at a large production scale [10,36].

Despite the above stated shortcomings, this route is still relevant for the manufacture of allylamines, where other routes typically result in the hydrogenation of the double bond or promote undesired side reactions (*e.g.*, polymerization, cyclization) [37,38]. In 2012, Kalpataru *et al.* [39] demonstrated the direct catalytic amination of allylic alcohols using a Pt/DPEphos homogeneous catalyst attaining yields above 70% towards several amines, proving the viability of a more eco-efficient selective synthesis of primary allylamines.

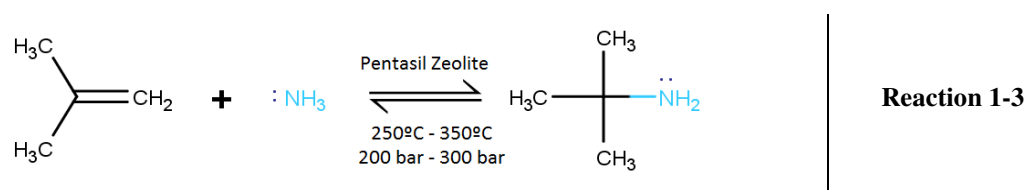
### 1.2.2 Olefin Amination Process (Hydroamination)

Hydroamination refers to the addition of a new C-N bond across an unsaturated C-C bond. This route is inherently atom efficient and green, affording the transformation of inexpensive and readily available alkenes and alkynes into amines [40].

The inclusion of the amine group is slightly exothermic and has negative entropy, being thermodynamically favored at low temperatures and high pressures. Nonetheless, the reaction presents a high energy barrier for activation, especially in the case of alkenes, making it necessary the use of catalysts affording energetically-favored reaction pathways [41]. The catalyst choice will determine the reaction route and the reaction products, favoring Markovnikov or anti-Markonikov addition [42]. In practice, hydroamination reactions are typically conducted at high temperature (200-350 °C) to overcome the energy barrier, but it is limited thermodynamically by equilibrium to low conversions (typically 2%-10%). The use of pressures as high as 300 bar are necessary to shift the equilibrium and limit the formation of side products such as nitriles [19].

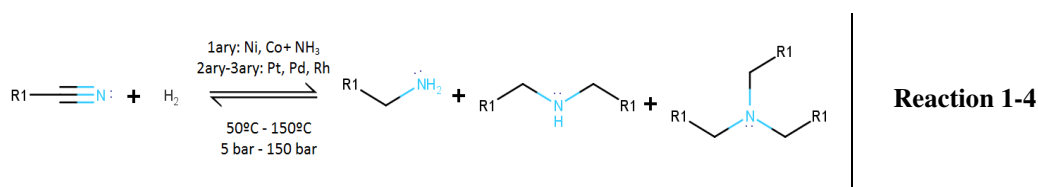
Over the past 15 years, the interest in hydroamination reactions has experienced a dramatic increase, as evidenced by the volume of published work in this field, especially in the development of homogeneous catalysts. Despite these efforts, the development of heterogeneous catalysts, of greater interest for industrial manufacture, is still limited [41]. Some examples of heterogeneous catalysts for hydroamination reactions can be found in the open literature relying on the use of immobilized homogeneous catalysts. The study reported by Jimenez *et al.* [43] on the immobilization of organometallic Pd complexes constitutes an illustrative example.

Despite the progress in the field, the thermodynamic and kinetic limitations make often hydroamination reactions non-economically feasible for a large-scale manufacture of amines. To the best of our knowledge, the only commercial amine produced by this route is *tert*-butylamine (see Reaction 1-3), being produced by BASF [44].



### 1.2.3 Nitrile Hydrogenation Process

The transformation of nitriles into alkylamines can be achieved by reduction over a hydrogenation catalyst, typically based on Ni, Pt, Pd or Rh (see Reaction 1-4). The reaction occurs *via* the formation of an imine or enamine intermediate that can further react to form secondary and tertiary amines [40,45].

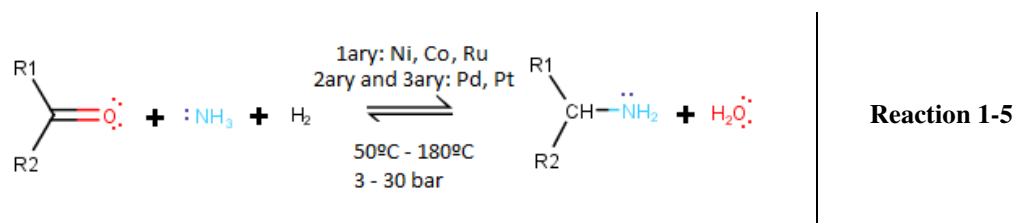


The selectivity of the reaction can be controlled by the catalyst choice and the process conditions. On the one hand, primary amines can be obtained using Ni or Co-based catalysts together with the presence of ammonia [46]. On the other hand, Pt, Pd and Rh catalysts are preferred for the synthesis of secondary and tertiary amines [19,45]. Extensive research has also been addressed to the use of additives for tuning the acidity of the catalysts. For instance, Verhaak *et al.* [47] modified a Ni catalyst supported over alumina with sodium and potassium, achieving excellent selectivity to primary amines. Likewise, Air Products and Chemicals patented a lithium hydroxide treated Raney Co catalyst exhibiting over 95% selectivity to primary amines [48].

A commercial example of the above stated process encompasses the industrial production of hexamethylenediamine (HMDA) from adiponitrile, which is used for the production of Nylon 6,6 *via* condensation with adipic acid. Typically, adiponitrile is obtained from the hydrocyanation of butadiene (derived from oil feedstocks) over a Ni catalyst, exploiting the technology originally developed by Drinkard (DuPont, 1970) [49].

## 1.2.4 Carbonyl Reductive Amination Process

The amination of carbonyl compounds occurs over hydrogenation catalysts (*e.g.*, based on Ni, Co, Ru, copper chromite, Pt or Pd) *via* the formation of an imine or enamine intermediate depending on whether ammonia or an amine is used, which undergoes metal-catalyzed hydrogenation to form an amine. The reaction is conducted at moderate temperature and moderate-to-high pressure, according to Reaction 1-5 [19,40].



The reaction selectivity depends strongly on the carbonyl substrate and can be controlled to a certain extent by selecting the reaction conditions and the catalytic formulation. An ammonia excess, high hydrogen pressure and Ru, Co or Ni-based catalysts are often used for the synthesis of primary amines, whereas lower ammonia-to-substrate ratios and noble metal catalysts are preferred for the synthesis of secondary and tertiary amines [40].

The selective synthesis of primary amines *via* reductive amination with ammonia was first reported by Beller *et al.* in 2002 [50]. The reaction is assisted by a homogeneous Rh catalyst at 135 °C, 65 bar of hydrogen pressure and 8:1 ammonia-to-substrate molar ratio. Good-to-excellent yields towards several benzylamines were obtained (up to 86% for aniline), but the synthesis of primary aliphatic amines proved to be more challenging. More recently, other groups have reported the homogeneously-catalyzed selective synthesis of primary amines by substituting hydrogen with other reducing agents such as sodium borohydride [51], ammonium formate [52], or silanes [53]. For instance, Miriyala *et al.* [51] achieved good-to-excellent yields (>80-90%) for a diversity of primary amines starting from ketones using titanium(IV) isopropoxide as catalyst and sodium borohydride as reducing agent.

Regarding the use of heterogeneous catalysts, an excellent study was reported by Müller *et al.* [54] on the reductive amination of butyraldehyde with ammonia over noble metal catalysts (Ru, Rh, Pd and Pt). The authors suggested a competitive mechanism between hydrogenolysis and hydrogenation reactions controlling the product selectivity (Figure 1-3). Metals such as Ru or Rh appear to promote the synthesis of primary amines, whereas Pd or Pt favor the formation of secondary amines.

The reductive amination of aldehydes and ketones is used at industrial scale in preference to alcohol amination whenever the carbonyl compound is cheaper than the corresponding alcohol (*e.g.*, acetone and lower aldehydes manufactured by hydroformylation) [40]. However, the difficulty to control the product distribution and the extension of side reactions of the reactive carbonyl group (*e.g.*, hydrogenation to alcohol, aldol condensation) constitute the main challenges. Moreover, the need of exogenous hydrogen makes the reaction less attractive from an atom economy standpoint.

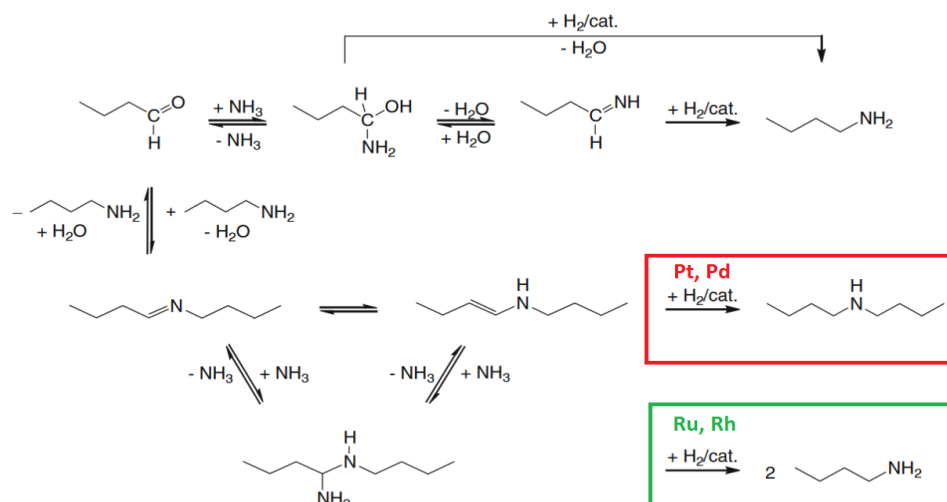
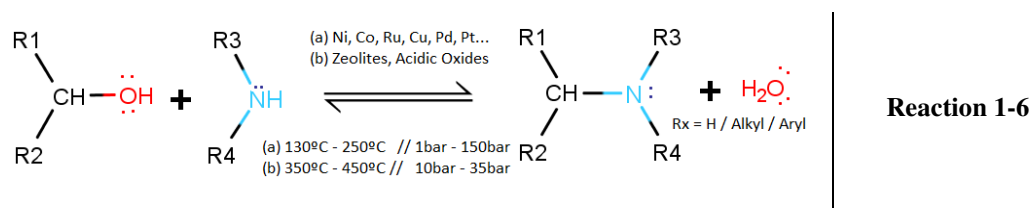


**Figure 1-3** Proposed reaction pathway for the reductive amination of butyraldehyde (Adapted from ref. [54]).

## 1.2.5 Direct Alcohol Amination Process

Alcohols react with ammonia or amines in the presence of a catalyst according to Reaction 1-6, producing the corresponding amine compound and water as the only by-product [28]



Two main classes of catalyst are used for the direct amination of alcohols, namely metal catalysts and acid metal oxides. While the activity of metal-based catalysts resides in their ability to dehydrogenate the alcohol to a more reactive carbonyl compound, metal oxides typically proceed by acid-catalyzed dehydration *via* nucleophilic substitution pathways [40]. Higher temperatures (350-450 °C) and pressures (10-35 bar) are usually required for the dehydration route [55–57], while the metal catalyzed amination typically is conducted at temperatures in the range 130-250 °C [10,20]. As in the case of alkyl halide amination and reductive amination of carbonyl compounds (see sections 1.2.1 and 1.2.4), the main challenge is to avoid overalkylation of the substrate with the produced amines.

The product distribution (either kinetically or thermodynamically controlled) depends on the nature of the substrate, the catalyst type and the process conditions. On the one hand, alcohol dehydration and self-condensation are the main competing reactions over acid metal oxides, yielding alkenes and ethers. On the other hand, dehydrogenation of the amine to the corresponding nitrile is promoted over metal catalysts, as it is a thermodynamically-driven reaction. The formation of nitrile can be avoided by decreasing the temperature, increasing the total pressure and/or increasing the hydrogen partial pressure in the system.

An example of acid-catalyzed dehydration of alcohols at industrial level can be found in the synthesis of methylamines from methanol *via* the so called Leonard process [21,58]. Typically, methanol and ammonia are contacted at temperatures about 400-420 °C over an amorphous silica-alumina catalyst, producing an equilibrium mixture of monomethyl, dimethyl and trimethylamine. The different amines are further separated by sequential distillation and recycled according to market requirements. The equilibrium mixture of amines is unlikely to match the market demand, which is usually higher for dimethylamine. In this view, many efforts have been made aiming at developing more selective catalysts yielding a non-equilibrated amine mixture, both by tuning the acido-basicity of the catalyst [31,59] and by developing shape-selective materials [30,56,57,60,61]. In the case of longer (fatty) alkylamines, the economic feasibility of the process is compromised due to the excessive loss of alcohol attributed to competing reactions, yielding alkenes and/or ethers [62,63].

As an alternative to nucleophilic substitution, the H<sub>2</sub> borrowing or H<sub>2</sub> auto-transfer mechanism can be used for preparing amines from alcohols [64–69]. This mechanism relies on three steps (Figure 1-4):

- (i) The alcohol is dehydrogenated, forming a more reactive carbonyl compound;
- (ii) The carbonyl compound undergoes nucleophilic addition with the ammonia or amine molecule, yielding an imine or enamine intermediate with concomitant C-o cleavage by either dehydration or hydrogenolysis;
- (iii) The intermediate imine or enamine is reduced to the corresponding amine, returning the borrowed hydrogen.

In this mechanism, H<sub>2</sub> is temporally borrowed by the action of a catalyst. Unlike reductive amination, no external H<sub>2</sub> supply is in principle required. Furthermore, parasite reactions such as aldol condensation over the carbonyl groups can be avoided. Furthermore, the metal-activated reaction occurs at milder temperatures (130-250 °C) compared to the acid-catalyzed route, avoiding the undesired side reactions and affording excellent selectivity to amines.

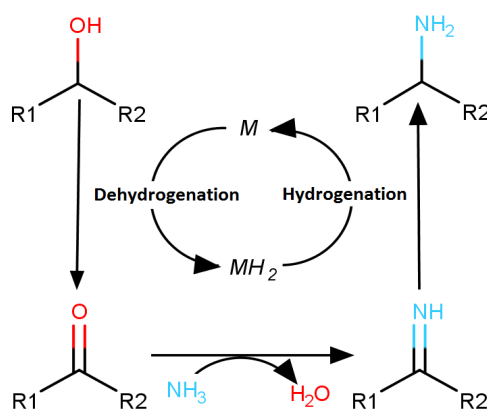


**Figure 1-4** Borrowing Hydrogen Mechanism.

Light alkylamines (C<sub>2</sub>-C<sub>5</sub>) and fatty amines are preferentially manufactured *via* metal-catalyzed amination, since the acid-catalyzed route often leads to the formation of alkenes and ethers [20,21]. As in the dehydration route, equilibrium mixtures of amines are typically obtained and the development of novel catalytic formulations is necessary to overcome this issue, especially regarding the synthesis of primary alkylamines.

To summarize, the H<sub>2</sub> auto-transfer strategy stands out as an efficient and green route towards the synthesis of amines. Nevertheless, various challenges still need to be addressed, especially regarding the synthesis of primary amines. Selective formation of primary amines from alcohols is challenging, since ammonia is less nucleophilic and thus less reactive than primary and secondary amines in the sequential formation of secondary and tertiary amines, respectively [70]. Moreover, once generated, primary amines can react with aldehydes/ketones, producing secondary amines that can also react to give tertiary amines, leading to the formation of a mixture of products [71].

In sections 1.2.5.1 and 1.2.5.2 we introduce the most recent developments in the design of homogeneous and heterogeneous catalysts for the direct amination of alcohols, with special emphasis on the selective synthesis of primary alkylamines.

### 1.2.5.1 Homogeneously catalyzed amination of alcohols

The first examples of homogeneously-catalyzed amination of alcohols date back to the early 1980s. In 1981 the *n*-alkylation of several primary and secondary amines over Re, Ir and Ru metal-phosphine complexes was demonstrated by Grigg *et al.* [72]. In parallel, Watanabe *et al.* [73] reported the activity of a Ru-based phosphine complex for the *n*-alkylation of aniline with several saturated and unsaturated alcohols (*e.g.*, methanol, ethanol, allyl alcohol). Different Ru-phosphine complexes were described in the following years, typically involving high temperatures (180 °C) and limited to primary alcohols [74,75].

More recently, most of the reported studies have concentrated on the development of Ru(II) [76–80] and Ir(III) [81–84] homogeneous complexes. These catalysts afford the synthesis of secondary and tertiary amines from alcohols under mild conditions, often with the help of a basic co-catalyst to promote alcohol dehydrogenation (see Figure 1-5).

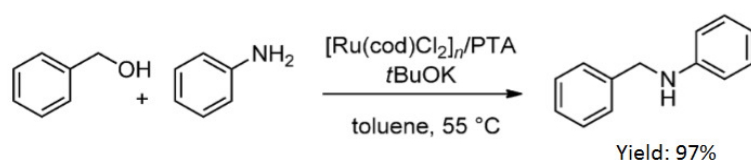


**Figure 1-5** N-Alkylation of aniline with benzyl alcohol over Ru-based homogeneous catalyst, assisted by potassium *tert*-butoxide (Adapted from ref. [76]).

In particular, Fujita *et al.* reported the alkylation of aqueous ammonia over a Cp\*Ir-amine complex [85], but only the synthesis of secondary and tertiary amines was observed. In this regard, the first selective synthesis of primary amines from alcohols and ammonia was described by Milstein *et al.* [71] using a Ru(II) pincer-type phosphine complex (Figure

1-6), but the system was ineffective for the amination of secondary alcohols. Later on, Vogt *et al.* [69] successfully reacted cyclohexanol and ammonia over  $[\text{Ru}_3(\text{CO})_{12}]$  and a phosphine ligand, affording selectivities up to 75% to the primary amine, even at 90% conversion. Similarly, Beller [70,86] and Deutsch [87] reported the selective synthesis of primary amines from primary and secondary alcohols over different Ru PNP pincer complexes using cheaper ligands than those reported by Milstein.

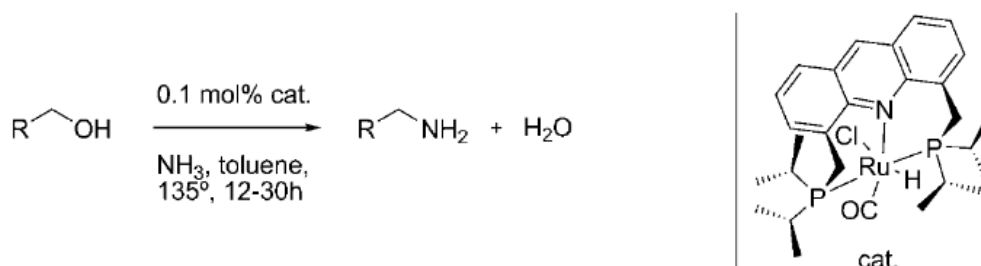


**Figure 1-6** Selective synthesis of primary amines by Gunanathan and Milstein over Ru/PNP pincer complex (Adapted from ref. [71]).

In the last years, most of the efforts have concentrated on the discovery of more available and lower-cost substitutes to traditional precious metal complexes [88]. In this regard, Barta *et al.* [89] demonstrated the applicability of Knölker Fe complex for the monoalkylation of anilines and benzylamines with several alcohols and diols (*e.g.*, *n*-pentanol, ethylene glycol). Co [90] and Mn [91] pincer-type phosphine complexes were reported as a competitive alternatives to Ru(II) and Ir(III) organometallic catalysts for the synthesis of secondary amines. Nevertheless, progress is still required towards the selective synthesis of primary amines.

### 1.2.5.2 Heterogeneously catalyzed amination of alcohols

Early reports on the use of metallic hydrogenation catalysts for the amination of short-chain alcohols with amines and ammonia operating *via* the borrowing H<sub>2</sub> mechanism consisted of metal catalysts, typically Ni, Co or Cu supported over silica and alumina [92–101]. Typically, alcohols and ammonia are contacted at 150–250 °C under pressure, affording high alcohol conversion and amines yield (above 95%). The reaction produces an equilibrium mixture of primary, secondary and tertiary amines. In these examples, the reaction was carried out under a H<sub>2</sub> atmosphere to maintain the catalyst activity [102–104]. Unsupported Co-Fe catalysts prepared by co-precipitation [105–107], and Cu/Ni/Ca/Ba colloidal mixed-oxide catalysts prepared from stearate precursors were selective in the synthesis of primary diamines from diols [108]. In the former case, the catalyst was stabilized by Fe, which appeared to kinetically preserve the otherwise thermodynamically unstable  $\beta$ -Co active phase. A yield up to 32% to 1,3-diaminopropane was achieved under supercritical ammonia conditions. Similarly, the introduction of noble metals on Ni and Co based catalysts was reported to facilitate the reduction of the active phase and increase the catalytic activity. For instance, 15–20 wt% Ni or Co supported over alumina, silica or titania were modified with 0.5–3 wt% Pd, Pt, Rh, Ru or Cu, favoring the catalytic activity [109].

The catalytic activity in alcohol amination over supported metal catalysts is often conditioned by the alcohol dehydrogenation reaction, this being the rate-limiting step of the overall process. This fact explains the low reactivity and high temperatures (150-210 °C) and pressures (18-200 bar) commonly required for achieving high activity. Some studies have shown that Co-based catalysts exhibit higher activity relative to Ni counterparts [110], the activity being related to the amount of reduced Co available [111]. Other bimetallic catalysts (15-20% Ni or Co + 0.5-3% Pd on alumina, silica or titania) [109] exhibit higher activity and can be usually activated at lower temperatures (200 °C vs. 400 °C). Co-exchanged Y-zeolite catalysts were also developed favoring the formation of primary and secondary amines relative to tertiary ones [112].

Despite the great progress in the topic, none of the aforementioned heterogeneous catalysts was successful in the selective synthesis of primary amines. Sewell and coworkers did a comparative study between Co and Ni catalysts, supported on silica, regarding the direct amination of ethanol [110]. Higher reactivity and selectivity of Co towards the less substituted amines was evidenced despite strong metal-support interactions. Similarly, Co [103] and Ni [104] catalysts supported over  $\gamma$ -Al<sub>2</sub>O<sub>3</sub> were studied by Cho *et al.* Both catalysts proved excellent selectivity towards the primary amine for ethanol amination with ammonia with yields of 80% and 76%, respectively.

Since these earlier studies, a great deal of work was dedicated to the quest of more active and selective heterogeneous catalysts for the direct amination of alcohols. Excellent reports and reviews can be found in the literature exemplifying the amination of alcohols over a variety of supported and unsupported metal catalysts. In these studies, the acido-basic and/or redox properties of the support were correlated to the activity and selectivity for alcohol amination. In this regard, we review below the reported literature concerning the effect of the support properties of the catalysts on the activity and selectivity for alcohol amination.

#### (i) Catalytic supports with acid-base properties

This family of catalysts relies on the Brønsted and Lewis acid-basic properties of the metal oxide support. For instance, Corma and coworkers [113] reported the use of Pd/MgO basic catalyst for the synthesis of N-phenylbenzylamine in the reaction of benzyl alcohol with aniline at 180 °C at short reaction times (<2 h). The initial reaction rate was enhanced by decreasing the Pd nanoparticle size, revealing the structure sensitivity of the hydrogen transfer process. The importance of the basic nature of the support was evidenced when comparing the catalytic activity to that achieved over a Pd/C, which afforded lower activity and selectivity to the desired product.

Ishida *et al.* [114] studied the influence of the support on the catalytic activity and selectivity of supported Au nanoparticles for the reaction between benzyl alcohol and aniline. Despite a higher activity of Au/CeO<sub>2</sub> for the alcohol dehydrogenation step, surface hydroxyl moieties present on ZrO<sub>2</sub> played an important role on the overall hydrogen transfer efficiency of Au/ZrO<sub>2</sub> (Figure 1-7). The authors proposed a plausible mechanism where the alcohol deprotonation was promoted by surface basic sites, while acid -OH groups

and hydrides on Au nanoparticles protonated the intermediate hemiaminal, stating the relevance of the amphoteric nature of the support for the tandem reaction.

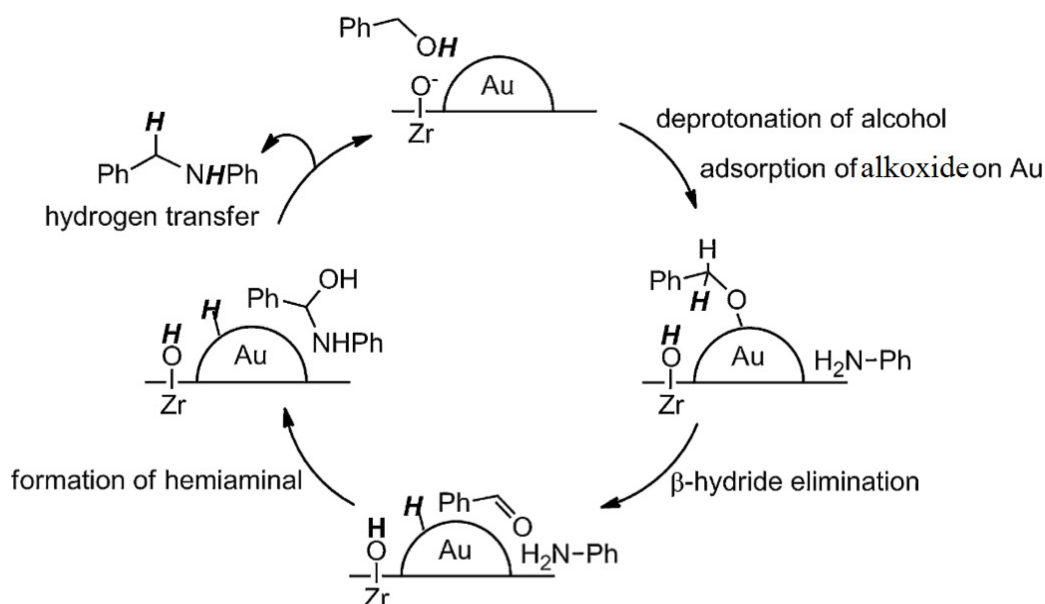


**Figure 1-7** Proposed reaction pathway by Ishida *et al.* for the *n*-alkylation of aniline with benzyl alcohol over Au/ZrO<sub>2</sub> (Adapted from ref. [114]).

Shimizu and coworkers [115,116] stated the importance of the amphoteric nature of the support. In the first study, regarding the *n*-alkylation of aniline with *n*-octanol and benzyl alcohol, a positive correlation between the acidity of the oxide support and the reaction rate for supports with basic to amphoteric nature (CaO ~ Al<sub>2</sub>O<sub>3</sub>) was found. In contrast, acid supports exerted a negative impact on the catalytic activity (Figure 1-8-(a)). Moreover, the basic and acid sites of the best performing catalyst (Ni/ $\theta$ -Al<sub>2</sub>O<sub>3</sub>) were selectively poisoned, impacting negatively the catalytic activity (Figure 1-8-(b-c)). Comparable results were obtained for the reaction between 2-octanol and ammonia [116].

In summary, basic and amphoteric supports are beneficial for alcohol amination, proving the active role of both moderately acid and basic sites of the support. However, differences may arise regarding the reacting substrate and the metal-support combination.

## (ii) Catalytic supports with redox properties

This family of supports covers metal oxides with redox properties. These supports can effectively store and release oxygen, potentially affecting the oxidation state of the supported metal. This flexibility on their oxidation state can effectively promote the hydrogen transfer efficiency.

For instance, a Pd/Fe<sub>2</sub>O<sub>3</sub> catalyst was developed by Zhang and coworkers [117] by co-precipitation of Pd and Fe precursors followed by calcination. A reaction mechanism was proposed operating *via* a redox cycle based on active Pd(IV) and Pd(II) species (Figure 1-9) as inferred from experimental results and DFT calculations. More recently, a Pd/CeO<sub>2</sub> catalyst has been reported by Yan *et al.* [118]. The reversible hydride transfer between Pd

and the support was key to the overall activity. Interestingly, the reversible hydrogen storage capacity of the catalyst could be tuned by thermal treatment and correlated with the catalytic activity.

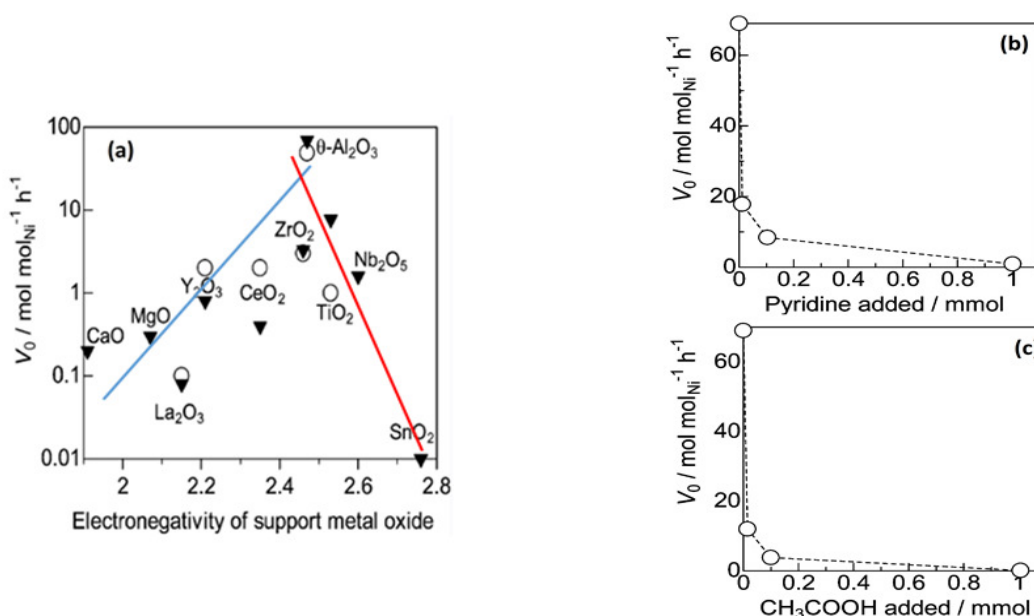


**Figure 1-8** (a) Rate of N-alkylation of aniline with (○) *n*-octanol or (▼) benzyl alcohol (144°C, Ni/support) as a function of the electronegativity of the support metal oxide ( $\infty$  acidity). (Lines for tendency added to original plot) (b) and (c) Rate of N-alkylation of aniline with (○) *n*-octanol as a function of the concentration of pyridine and acetic acid (Adapted from ref. [115]).

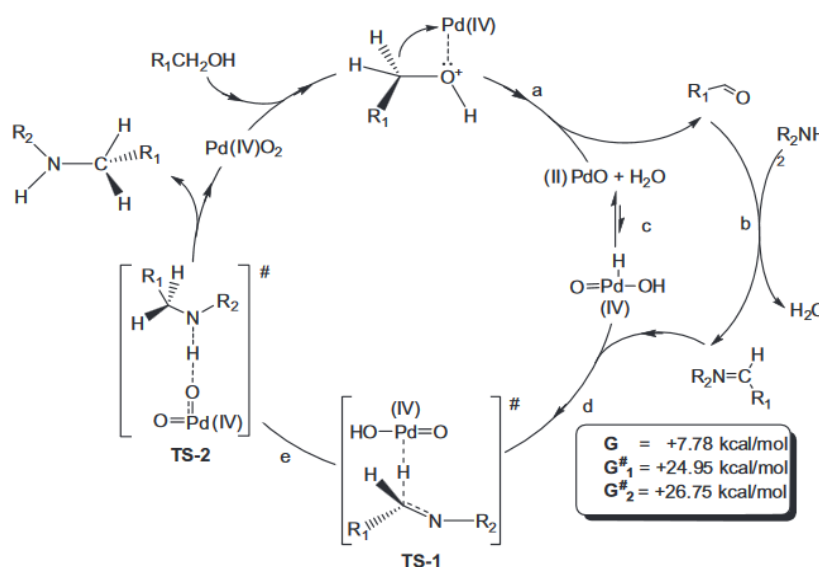


**Figure 1-9** Proposed mechanism for the Pd/Fe<sub>2</sub>O<sub>3</sub> catalyzed N-alkylation of amines with alcohols by Zhang *et al.* (Adapted from ref. [117]).

Multimetallic Ni-Cu-Fe<sub>2</sub>O<sub>3</sub> formulations were also reported as active in the N-alkylation of ammonia and amines with alcohols, exhibiting outstanding moisture and air stability [119]. Likewise, 95 wt% Co – 5 wt% Fe formulations were developed by Fischer

*et al.* [105]. As pointed out above, Fe effectively hindered the phase transformation of Co, stabilizing the thermodynamically disfavored  $\beta$ -Co phase. The absence of strong acid and basic sites was argued as crucial to improve the catalytic selectivity, avoiding side reactions.

Finally, ceria was demonstrated to behave as a promoter of noble-metal catalysts for amination. For instance, Au/CeO<sub>2</sub> (2.5 wt.%Au) afforded the coupling of two multistep catalytic cycles for the one-pot synthesis of propargylamines from N-benzylamine and benzyl alcohol [120]. Recently, M. Ousmane *et al.* [121] also reported a Pd-substituted octahedral molecular sieve (Pd/K-oMS-2) for the amination of benzyl alcohol with aniline. The catalyst presented a prominent catalytic performance that was ascribed to the *in situ* generation of an active Pd/Mn<sub>3</sub>O<sub>4</sub> phase during the reaction with a large density of surface oxygen moieties and Pd(IV)/Pd(II) active sites. The same team reported a Pd/CeO<sub>2</sub> catalyst with a prominent reversible H<sub>2</sub> storage capacity which revealed a high activity and selectivity in the direct amination of benzyl alcohol with aniline and ammonia via hydrogen borrowing mechanism [118].

### 1.2.5.3 Amination of fatty alcohols

Most of the studies reported above focus on the amination of cyclic, aromatic and substituted or branched alcohols over metal-supported catalysts. However, only few studies were reported on the direct amination of aliphatic alcohols. In this section, the reader will find a brief compilation of studies targeting fatty amines.

The most studied heterogeneous catalysts for the direct synthesis of amines from long-chain (fatty) alcohols *via* the borrowing H<sub>2</sub> mechanism rely on the Ni-Cu couple comprising Raney Ni [122,123], as well as Ni [101,109,115,116,124,125], Cu [126–131], NiCu [132–134], NiCuFeO<sub>x</sub> [119], NiCuZn [135], CuAl [136], CuAg [137] and CuCr [138] supported over alkaline or amphoteric oxides (*e.g.*,  $\gamma$ - and  $\theta$ -Al<sub>2</sub>O<sub>3</sub>). The reactions are most often carried out at laboratory scale in liquid phase in the presence of a solvent (*e.g.*, *t*-amyl alcohol, *o*-xylene). In particular, Cu-Ni formulations have been extensively studied, offering tunable selectivities to the desired amines by varying the Cu/Ni ratio or by adding a third element. In 2002, Li. *et al.* [135] studied the amination of fatty alcohols catalyzed by Cu-Ni supported over CaCO<sub>3</sub>. The promotional effect of Zn or Mg (as a third element) could be related to the Ni reducibility in the catalyst. In general, lower reducibility of Ni<sup>2+</sup> led to higher selectivity. Kimura *et al.* [132] reported the one-step amination of dodecyl alcohol and dimethyl amine to N,N-dimethyl dodecylamine using Cu/Ni/Ca/Ba colloidal catalysts with a selectivity of 98% and an alcohol conversion of 99% at 210 °C for 4 h.

Alternative metal formulations have been explored for the liquid-phase synthesis of alkylamines, but with poor success. For instance, Co either unsupported or supported over silica, was reported as a highly selective catalyst for the direct amination of short-chain alcohols (see section 1.2.5.2) [103,110], ethoxylated alcohols [139] and diols [105,107], but with few examples of developments for fatty alcohols [131]. Finally, as a rule, noble metals such as Ru, Pd and Pt usually suffer from lower productivity for amination and lower selectivity to monoalkylation, favoring C-C and C-o cleavage pathways [116,130,140,141].

One of the first systematic reports on metal-supported catalysts was published by Kliger *et al.* [142] in 1961 describing the amination of butyl alcohol over an Fe catalyst. The optimal reaction conditions were 230 °C, 20 bar, a WHSV of 1200 h<sup>-1</sup> and 43.5% v/v NH<sub>3</sub> in the feed, obtaining a 76% yield to amines. A positive correlation was evidenced between the ammonia content, the yield to amines and the catalyst productivity. Later on, studies on the influence of the alcohol structure [143] and its molecular weight [144] on the amination reaction were reported by the same group. The amination of C<sub>8</sub>-alcohols was inhibited when shifting the hydroxyl group from the first and second carbon atoms towards the chain center, while it kept unaffected by the length of the carbon chain (in the range C<sub>5</sub>-C<sub>18</sub>). On the contrary, an increase of the molecular weight promoted the formation of secondary and tertiary amines.

In an interesting work, Shimizu *et al.* [116] recently studied the effectiveness of several transition metal catalysts supported over  $\gamma$ -Al<sub>2</sub>O<sub>3</sub> for the amination of 2-octanol. Overall, Pt, Ni and Ir afforded the highest conversions. While noble metals (Pt, Ir) afforded a mixture of primary and secondary amines and the ketone, Ni transformed selectively the 1- and 2-octanol into the corresponding primary amines. Likewise, Murzin *et al.* [141] investigated the direct amination of *n*-dodecanol over Ru, Pd, Pt Ir and Os supported over carbon. Similar activities (in terms of TOF) were achieved for Ru, Pd and Pt, which afforded the highest conversions. Pd maintained an excellent selectivity towards dodecylamine over the studied range of conversion (>95% selectivity up to 77% conversion), while Ru and Pt promoted the formation of the secondary amine and dodecane.

Despite the great progress in the topic, important challenges still need to be overcome, especially regarding the selective synthesis of primary amines. In this regard, the reaction between *n*-octanol and ammonia will be chosen along this study as a model reaction for assessing the efficiency of novel heterogeneous catalysts. The most relevant literature on the amination of *n*-octanol and other aliphatic alcohols with ammonia is summarized in Table 1-1. Mizuno and coworkers [140] reported the direct amination of *n*-octanol using 0.2 equivalents of NH<sub>3</sub> (aq. NH<sub>3</sub> 28%) under Ar atmosphere using Ru(OH)<sub>x</sub>/TiO<sub>2</sub> as a catalyst. The tertiary amine was obtained as main product with 88% yield relative to the initial ammonia. In 2011, Li *et al.* [134] reported a Ni-Cu (1.25:1)/diatomite catalyst for *n*-octanol amination with 3 equivalents of NH<sub>3</sub> at 230 °C for 5 h in NH<sub>3</sub>/H<sub>2</sub> (40/60 v/v%). A 97% yield towards the tertiary amine was obtained at almost full conversion. Likewise, Shi and coworkers [119] reported a Ni-Cu-FeO<sub>x</sub> catalyst for *n*-octanol amination with 1.2 mmol NH<sub>3</sub> at 200 °C for 24 h, achieving 61% yield to the secondary amine. In 2013, Shimizu and coworkers [116] reported for the first time the synthesis of primary amines from secondary alcohols and NH<sub>3</sub> at high yields using Ni/Al<sub>2</sub>O<sub>3</sub> as a catalyst under relatively mild conditions and without additional H<sub>2</sub> supply (Table 1-1). A yield >80% to 2-octylamine was achieved at 160 °C for 4 h under 4 bar NH<sub>3</sub> using 1 mol% of 10 wt.%Ni/ $\gamma$ -Al<sub>2</sub>O<sub>3</sub> or  $\theta$ -Al<sub>2</sub>O<sub>3</sub>. For *n*-octanol amination, the authors only reported an example, underlying 70% *n*-octylamine yield at 90% conversion using 5 mol% of 10 wt.%Ni/ $\theta$ -Al<sub>2</sub>O<sub>3</sub> at 160 °C for 13 h. The authors argued about a major role of surface metallic Ni nanoparticles in strong synergy with acid and basic groups of the support.

**Table 1-1** Relevant examples on heterogeneously catalyzed ammonia alkylation with fatty alcohols (C<sub>8</sub> and related)

Catalyst	Alcohol	Gas (Press.)	Temp.	H <sub>2</sub> : NH <sub>3</sub> : R-OH	Conv.(%)	Yield Amines (%)			Ref.				
		Liquid (Solv.)				1ary	2ary	3ary					
Fused Fe	<i>n</i> -octanol	G – 50bar	240°C	23 : 16 : 1	95%	71% <sup>(a,c)</sup>	15% <sup>(a,c)</sup>	3% <sup>(a,c)</sup>	[143]				
	2-octanol					83% <sup>(a,c)</sup>	4.5% <sup>(a,c)</sup>	4.5% <sup>(a,c)</sup>					
Ni.Cu.FeO <sub>x</sub>	<i>n</i> -octanol	L – xylene	200°C	0 : 1.2 : 1	-	-	61%	-	[119]				
Ni-Cu/ Diatomite	<i>n</i> -octanol	L – no solvent	230°C	40% : 60% H <sub>2</sub> :NH <sub>3</sub>	100%	<3%	<3%	97%	[134]				
Ru(OH) <sub>x</sub> /TiO <sub>2</sub>	<i>n</i> -octanol	L – mesitylene	141°C	0 : 0.2 : 1	-	-	-	88% <sup>(b)</sup>	[140]				
	<i>n</i> -octanol									90%	70%	7%	-
	2-octanol									93%	88%	5%	-
10% Ni/ θ -Al <sub>2</sub> O <sub>3</sub>	2-octanol	L – o-xylene	160°C	4 bar NH <sub>3</sub> , no H <sub>2</sub>	93%	88%	5%	-	[116]				
	4-octanol									94%	85%	3%	-
Ni or Co / SiO <sub>2</sub> , ZrO <sub>2</sub>	2ary C <sub>16</sub> – C <sub>24</sub>	L – no solvent	270°C	20bar H <sub>2</sub>	93%	81%	7%	-	[131]				
1-10% Co or Ni + dopant/ ZSM-5	C <sub>2</sub> – C <sub>4</sub> (Butanol)	G – 20-25bar	190°C –	5.3 : 5.4 : 1	60% - 90%	40% -	20% -	<5% <sup>(c)</sup>	[101]				
			210°C			60% <sup>(c)</sup>	30% <sup>(c)</sup>						
17% Ni/γ-Al <sub>2</sub> O <sub>3</sub>	2-Propanol	G – 1 bar	170°C	6 : 8 : 1	93%	77 %	11%	-	[104]				
23% Co/γ-Al <sub>2</sub> O <sub>3</sub>			190°C	12 : 6 : 1	90%	80%	-	-	[103]				
Ru/C	<i>n</i> -Dodecanol	L – Decane	200°C	4 bar NH <sub>3</sub> , 2 bar H <sub>2</sub>	99%	69%	18%	-	[141]				
Pd/C					77%	74%	-	-					

(a) Obtained by potentiometric titration; (b) Yield based on the nitrogen source; (c) Calculated from data in the original document

### 1.3 Kinetic Modelling for the Amination of Alcohols

Despite the vast efforts dedicated to the discovery of novel catalytic formulations for direct alcohol amination reactions, only few representative kinetic models can be found in the open literature. The complexity of the reaction network (Figure 1-10) and the need of large sets of experimental data have apparently limited the research on this topic. In the forthcoming sections we will introduce the existing kinetic models comprising, (i) direct alcohol amination, as well as (ii) relevant kinetic models reported in the literature on alcohol dehydrogenation with neither ammonia nor amines, and (iii) reductive amination of carbonyl compounds. These models are useful not only for rationalizing the different reaction pathways present during alcohol amination, but also for further reactor engineering and design to help optimizing the yield to the desired amine (in our case primary amines).

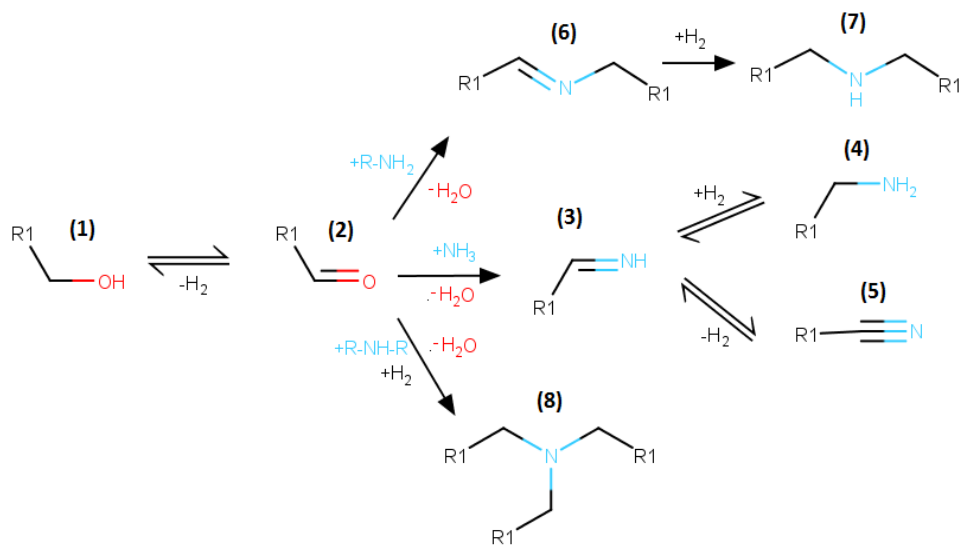


Figure 1-10 Reaction network scheme for the amination of alcohols.

#### (i) Kinetic Models for Alcohol Amination

The first kinetic models accounting for direct alcohol amination were developed by Kliger [145,146] and Baiker [147] encompassing the gas-phase reaction of *n*-octanol with ammonia, monomethylamine and dimethylamine under hydrogen pressure over molten iron and copper catalysts. The reaction rate of the overall process was described using the following equation (Eq. 1-1). A detailed nomenclature is given in section 1.5.

$$r = \frac{kK_{ROH}P_{ROH}}{\left[1 + K_{ROH}P_{ROH} + K_{H_2O}P_{H_2O} + K_{NS}P_{NS}\right]^2} \quad \text{Eq. 1-1}$$

This model relies on two main assumptions: (i) the rate-determining step involves the abstraction of a  $\alpha$ -hydrogen from the alcohol and its transfer to an adjacent vacant site of the catalyst, and (ii) equilibrated single-site Langmuir adsorption of the reactants and products. The inhibition of the reaction was considered to be significant at a 95% confidence interval for *n*-octanol, water and dimethylamine. A high concentration of the

intermediate aldehyde was found to compete for the adsorption sites, but its concentration was irrelevant at the studied reaction conditions. Similarly, under the tested conditions (1-40 kPa), competitive adsorption by hydrogen was regarded as negligible.

In a subsequent study, Bassili and Baiker [148] adapted this kinetic equation to describe the amination of 1-methoxypropan-2-ol with ammonia over a Ni/SiO<sub>2</sub> catalyst (Eq. 1-2). In this case, the dissociative adsorption of hydrogen and the amine product were considered as the only adsorbates inhibiting the reaction.

$$r = \frac{k K_{ROH} P_{ROH}}{\left[ 1 + \sqrt{K_{H_2} P_{H_2}} + K_{RNH_2} P_{RNH_2} \right]^2} \quad \Bigg| \quad \text{Eq. 1-2}$$

The role of hydrogen, otherwise not necessary from a stoichiometric point of view, was attributed to the inhibition of catalytic deactivation by ammonia, forming the corresponding metal nitride. Overall, the model could satisfactorily describe the kinetics of the reaction except for low ammonia-to-alcohol molar ratios, where the considered hydrogen effect failed to explain the experimental results.

More recent work has been dedicated to the development of kinetic models for the *n*-alkylation of aniline. Zotova *et al.* [149] developed a model describing the reaction between aniline and benzyl alcohol over a Au/TiO<sub>2</sub> catalyst. As in the previously described models, the model was built on the basis of a Langmuir-Hinshelwood (LH) type kinetic equation, considering in this case the formation of the carbonyl compound as the rate-limiting step. The formed aldehyde could desorb from the catalyst and undergo competitive non-catalytic condensation with aniline in the liquid phase (Figure 1-11). An Increase of the temperature boosted the rate of the surface reaction, improving the selectivity towards the primary amine. A similar mechanism was described by Demidova and coworkers [150] accounting for the reaction between aniline and myrtenol. The catalytic and non-catalytic reaction between the aldehyde and the amine were considered in parallel. Furthermore, the hydrogen transfer steps were determined to exclusively occur on the catalyst surface. Interestingly, a deactivation term was considered, modeling the decrease in active sites by means of coke deposition during the time on stream. The intermediate imine was proposed as coke source.

The exogenous hydrogen pressure is known to promote the catalytic activity in the amination of aliphatic alcohols operated under the H<sub>2</sub> borrowing mechanism [103,104,147]. This effect has been the subject of study by several groups. Baiker *et al.* [102] studied the influence of hydrogen pressure on the amination of *n*-dodecanol with dimethylamine over a supported Cu catalyst. It was concluded that ammonia, formed *via* disproportionation of dimethylamine, could transform the metallic Cu into inactive Cu nitride species. The presence of hydrogen in the feed could effectively recover the activity of the catalyst by reducing the formed Cu nitride. Detailed temperature-programmed desorption and differential scanning calorimetry studies conducted by Baiker [151,152] and Cho *et al.* [103,104] pointed out that the same deactivation mechanism could be extrapolated to Co and Ni based catalysts. In the latter studies, equivalent flows of hydrogen and nitrogen were

alternated in the feed. Whenever hydrogen was removed from the feed, the conversion rapidly decreased, recovering immediately its original value after the hydrogen feed was restored (Figure 1-12).

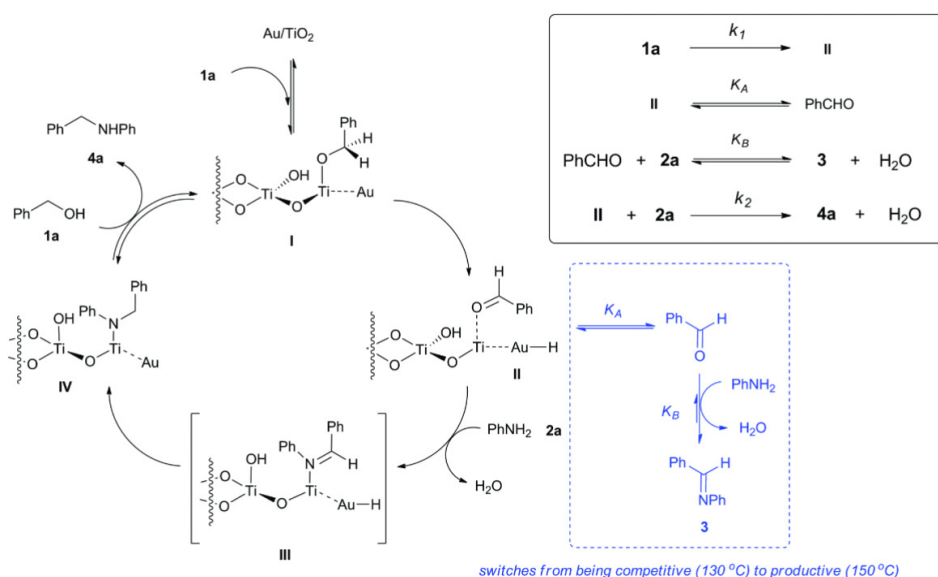


**Figure 1-11** Proposed catalytic cycle for the reaction between benzyl alcohols and aniline over Au/TiO<sub>2</sub> (Adapted from ref.[149]).

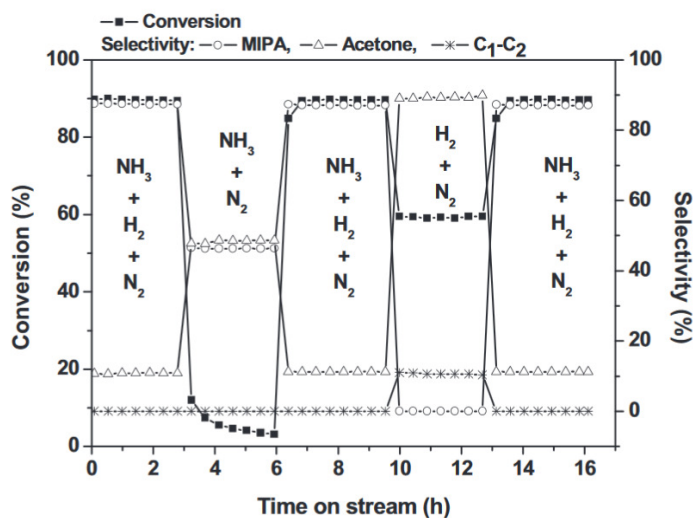


**Figure 1-12** Evolution of 2-propanol amination over a Co/Al<sub>2</sub>O<sub>3</sub> catalyst both in the presence and absence of exogenous hydrogen (Adapted from ref. [103]).

An alternative mechanism was recently proposed by Murzin *et al.* [141] relying on a complete kinetic study on the amination of 1-dodecanol with ammonia over a Ru/C catalyst. The positive order of reaction with respect to hydrogen was attributed to a partial surface regeneration of the catalyst from coke deposition. In this view, a term accounting for reversible deactivation was included in the kinetic model affording a successful description of the experimental results. As in previous studies, the activation-deactivation cycle was found to be very fast, reaching equilibrium along the reaction (Eq. 1-3). The

effect of hydrogen on the reaction selectivity was evidenced and explained by the proposed kinetic model.

$$r = \frac{kC_{ROH}}{1 + K_1C_{ROH}} \frac{P_{H_2}}{k'' + P_{H_2}} \frac{1}{1 + \sqrt{K_3K_4P_{H_2}} + K_3P_{H_2}} \quad \text{Eq. 1-3}$$

Overall, most of the proposed kinetic models agree to designate the initial hydride abstraction from the alcohol as rate-determining step. The relative rates of the consecutive condensation reactions with ammonia or amines and hydrogenation of the intermediate imine/enamine will dictate afterwards the product selectivity.

### (ii) Kinetic Models for Alcohol Dehydrogenation into Carbonyl Compounds

Various kinetic studies regarding alcohol dehydrogenation into aldehydes and ketones can be found in the open literature [153–163]. The dehydrogenation of 2-butanol into methyl ethyl ketone (MEK) over a solid brass catalyst was studied by Thodos *et al.* [153,154] in the late 50s. In these studies, a change in the rate-controlling step was evidenced by tuning the reaction conditions. The reaction was carried out in a differential reactor in the temperature range 290-370 °C and pressures range 1-15 atm. Various reaction mechanisms were proposed considering the adsorption/desorption and the surface reaction as rate-limiting step. The shape of the initial rate vs. total pressure curves at different temperatures was used to discriminate between different reaction mechanisms. The experimental results, presented in Figure 1-13-(b), provided evidence of a change in the reaction mechanism above 600 °F (316 °C). At lower temperatures, the results were properly fitted by a mechanism involving a dual-site surface reaction-limiting step (Eq. 1-4). An alcohol molecule, adsorbed on a single site, was involved with an adjacent site to produce the ketone and molecular hydrogen. The alcohol, the aldehyde and molecular hydrogen were considered to compete for adsorption on the active sites.

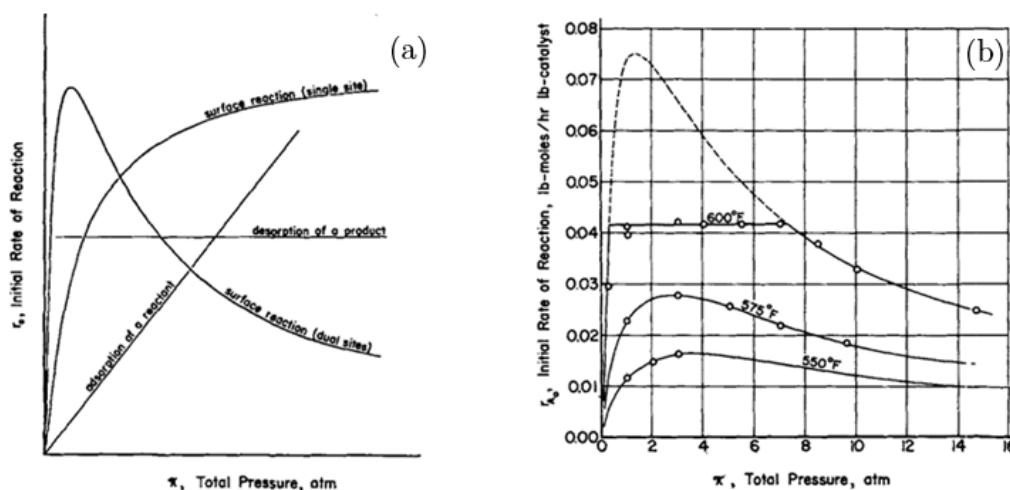


**Figure 1-13** (a) Variation of initial rates with the total pressure for different rate-controlling steps. (b) Initial rate of reaction vs. pressure for the dehydrogenation of 2-butanol (Adapted from ref. [154]).

$$r = \frac{k \left[ P_{ROH} - \frac{P_{R=O} P_{H_2}}{K_{eq}} \right]}{\left[ 1 + K_{ROH} P_{ROH} + K_{R=O} P_{R=O} + K_{H_2} P_{H_2} \right]^2} \quad \text{Eq. 1-4}$$

As can be observed in Figure 1-13-(b) the reaction followed a different mechanism when the temperature was increased above 600 °F (316 °C). In this case, the authors proposed a kinetic model comprising hydrogen desorption as the rate-determining step. Later on, Ford and Perlmutter [162] studied the dehydrogenation of 2-butanol over brass catalyst, corroborating the temperature-dependency of the reaction mechanism. The authors proposed a mechanism controlled by a single-site surface reaction at lower temperatures (Eq. 1-5), while the adsorption of the alcohol became rate controlling at temperatures between 350 °C and 400 °C. When the temperature was increased above 425 °C, the single-site surface reaction became again the rate-controlling step.

$$r = \frac{k P_{ROH}}{\left[ 1 + K_{ROH} P_{ROH} + K_{H_2} P_{H_2} \right]} \quad \text{Eq. 1-5}$$

The dehydrogenation of ethanol was studied by Franckaerts and Froment [155] over CuO with 5% CoO and 1% Cr<sub>2</sub>O<sub>3</sub> supported over an asbestos catalyst. The study covered reaction temperatures in the range 225-285 °C and pressures between 1 and 10 atm. The shape of the alcohol pressure vs. initial reaction rate curves suggested a mechanism controlled by the surface reaction on dual sites (Figure 1-14), in agreement with the model proposed by Thodos and Thaller [154] presented in Eq. 1-4. Similar results were further reported by Peloso *et al.* [158].

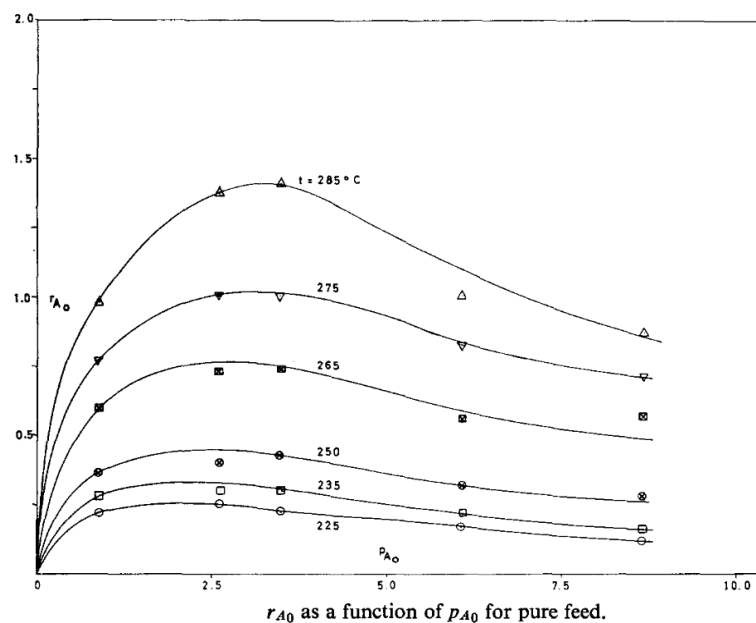


**Figure 1-14** Initial rate of reaction vs. pressure of alcohol for the dehydrogenation of ethanol (Adapted from ref. [155]).

In 2001, Keuler and co-workers [163] studied the dehydrogenation of 2-butanol over Cu catalysts supported over MgO and SiO<sub>2</sub>. The data were properly described by Eq. 1-4, suggesting a mechanism limited by a dual-site surface reaction. Interestingly, a negative value for the hydrogen adsorption equilibrium constant (impossible according to thermodynamics) was obtained, evidencing a promoting role of hydrogen on the reaction rate. This effect, counterintuitive for a dehydrogenation reaction, was attributed to a decoking role of hydrogen. In line with this study, Sheintuch and Dessau [164] reported examples comprising the dehydrogenation of alcohols and alkanes, where the presence of hydrogen promoted the reaction rate.

More recently, Crivello *et al.* [160] studied the dehydrogenation of *n*-octanol over a Cu-Mg catalyst in the temperature range 225-280 °C. The data were properly represented by a mechanism driven by a dual-site surface reaction. Opposing to previous models, hydrogen was considered to dissociate on the catalyst, giving the rate expression in Eq. 1-6. The activation energy of the rate-determining step was determined at 4.76 kcal/mol.

$$r = \frac{kP_{ROH}}{\left[1 + K_{ROH}P_{ROH} + K_{R=O}P_{R=O} + \sqrt{K_{H_2}P_{H_2}}\right]^2} \quad \text{Eq. 1-6}$$

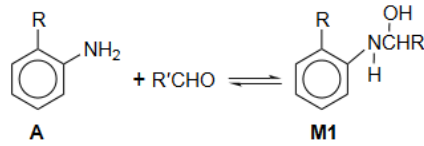
To summarize, various kinetic models can be found in the literature describing alcohol dehydrogenation. Overall, there is consensus about a mechanism controlled by the surface reaction below 300 °C. The equilibrium constants for aldehyde adsorption are generally high, resulting in a relevant inhibition of the reaction. The discrepancy between single- and dual-site mechanisms may be related either to differences in process conditions, or to the nature of the catalysts.

### (iii) Amination of Carbonyl Compounds

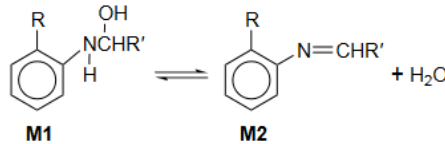
Only a very few number of kinetic models are available in the literature accounting for reductive amination of carbonyl compounds, mostly covering the alkylation of anilines. The condensation reaction between amines and aldehydes or ketones occurs fast in the homogeneous phase without the need of a catalyst, producing the corresponding imine/enamine and water. The imine/enamine is then hydrogenated in the presence of a catalyst to form the corresponding amine [165]. The combination of homogeneous and heterogeneous reactions, together with the high reactivity of carbonyl compounds, makes it difficult to elucidate the surface catalytic mechanism.

Lehtonen *et al.* [165] studied the liquid-phase amination of anilines over a Pt/C catalyst at 15 bar H<sub>2</sub> pressure in the temperature range 30-75 °C. The authors proposed a mechanism combining liquid-phase (non-catalytic) and surface reactions, as summarized in Figure 1-15. The first homogeneous step (1) and the latter surface reaction (3) were considered as rate determining. The surface reaction was described using Eq. 1-7, considering dissociative hydrogen adsorption. Nonetheless, several competing kinetic models could fit the data, comprising either competitive or non-competitive adsorption of the aromatic molecules. Similarly, it was impossible to statistically discern if hydrogen adsorbed molecularly or dissociated on the Pt surface.

1. homogeneous reaction in the liquid phase



2. homogeneous reaction in the liquid phase



3. heterogeneous surface reaction

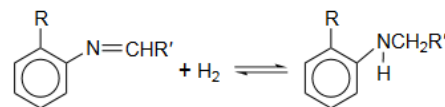


**Figure 1-15** Proposed reaction scheme for the reductive alkylation of anilines by Lehtonen *et al.* (Adapted from ref. [165]).

$$r = \frac{kC_{R=N-R}C_{H_2}}{\left[1 + K_{R=N-R}C_{R=N-R} + \sqrt{K_{H_2}C_{H_2}} + \sum K_i C_i\right]^3} \quad \text{Eq. 1-7}$$

Similar kinetic models were further developed by Roy *et al.* [166,167]. In an interesting experiment, these authors sorted out the homogeneous and surface reactions by carrying out the reaction (i) in the absence of catalyst and H<sub>2</sub>, (ii) with H<sub>2</sub> but no catalyst, and (iii) with catalyst but no H<sub>2</sub> (Figure 1-16). Similar results were obtained by Gomez *et al.* [168] for the formation of dibenzylimine from benzaldehyde and benzylamine.

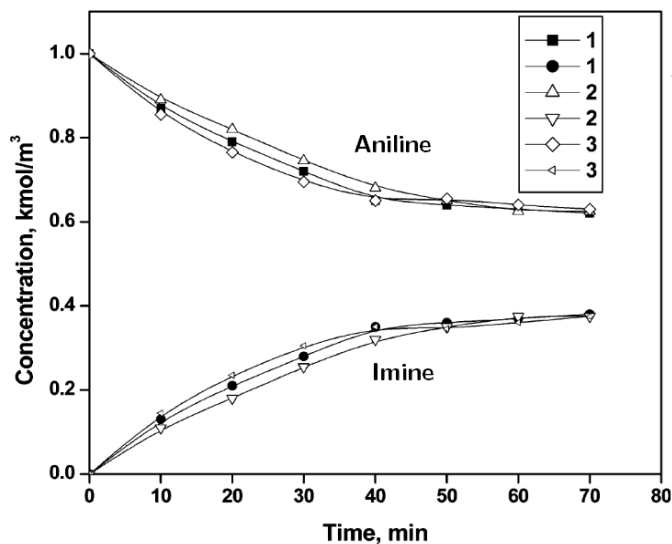


**Figure 1-16** Concentration vs time profiles for the homogeneous reaction between aniline and acetone: effect of H<sub>2</sub> and Pd/Al<sub>2</sub>O<sub>3</sub>. (1,1) in the absence of catalyst and H<sub>2</sub>, (2,2) with H<sub>2</sub> but no catalyst and (3,3) with catalyst but no H<sub>2</sub> (Adapted from ref. [166]).

In 2004 Gomez *et al.* [169] studied the reaction between benzaldehyde and NH<sub>3</sub>

over Pd/C and Ru/C catalysts. The reaction kinetics over the different catalysts was explained using a general mass action law model, considering a nearly empty catalytic surface. No simplifications regarding the rate-determining step were considered, solving a set of 5 differential equations that described the formation rate of the primary and secondary amines. Interestingly, the selectivity difference between the Pd/C and Ru/C catalysts could be rationalized from the fitted parameters. While both catalysts led to a similar rate of formation of dibenzylimine (DBI), Ru/C seemed to promote DBI transimination to BI and BA. In contrast, Pd/C was more effective in DBI hydrogenation towards the secondary amine (DBA). A similar mechanism was proposed by Lercher *et al.* [52] for the reductive amination of butyraldehyde (Figure 1-3)

#### (iv) Summary

As discussed above, very few examples of representative kinetic models for the metal-catalyzed amination of alcohols have been reported. Nonetheless, interesting information can be obtained from relevant studies regarding the dehydrogenation of alcohols and the amination of carbonyl compounds. In this context, new kinetic studies could help to integrate the information gathered in the presented studies and help to better rationalize the reaction mechanism for alcohol amination driven by the borrowing hydrogen mechanism. This information is also required to assist reactor design for target amination reactions.

## 1.4 Conclusion

As previously stated, amines are important building blocks for many fields of the chemical industry and their demand is foreseen to increase over the following years. In this regard, the development of efficient and ecologically responsible technologies for its production is a societal need. In this frame, the transformation of alcohols into amines via the so-called *borrowing hydrogen* mechanism stands out as an efficient and eco-efficient route. This route has already attracted the attention of both academia and industry and noticeable progress has been made in the last years.

The breakthrough developments in homogeneous catalysis (*e.g.*, Milstein [71], Beller [70,86], Deutsch [87]) represent an important milestone, allowing the selective synthesis of primary amines from alcohols and ammonia. Nevertheless, as a rule, such homogeneous catalysts rely on expensive organometallic complexes and ligands, which are also difficult to be recovered and reused, having a limited scale-up feasibility. As a way out, the development of inexpensive and reusable heterogeneous catalysts is an urgent need for the industrial production of amines. It is relevant to mention the latest contributions by Cho [103,104], Shimizu [116] and Murzin [141], achieving promising selectivities for primary amines over metal-supported catalysts. Nevertheless, there is still room for improvement through the development of better performing formulations.

In this context, this work will center its efforts on the development of novel heterogeneous formulations for the selective synthesis of primary amines from alcohols and ammonia. The reaction between *n*-octanol and ammonia will be chosen as a model

reaction and the efficiency of the catalysts will be evaluated in terms of activity and selectivity towards the synthesis of *n*-octylamine.

The problem will be approached *via* a sequential catalytic screening and formulation optimization. An initial library of catalysts will be tested relying both on the open and patent literature to move to novel multimetallic formulations in a second step (Chapter 3). Ultimately, a kinetic model will be developed for the best performing catalyst (Chapter 4), allowing a better understanding of the role of the different process variables on the catalytic properties.

## 1.5 Nomenclature

k	=	Kinetic constant
K <sub>eq</sub>	=	Chemical equilibrium constant
K <sub>i</sub>	=	Adsorption equilibrium constant
r	=	Reaction rate

### Subscripts:

H	=	Hydride
H <sub>2</sub>	=	Molecular Hydrogen
H <sub>2</sub> O	=	Water
NS	=	Nitrogen source (ammonia or amine)
R=N-R	=	Secondary Imine
R=O	=	Aldehyde or Ketone
ROH	=	Alcohol

## 1.6 References

- [1] A. Stevenson, J. Pearsall, eds., Oxford dictionary of English, 3. ed, Oxford Univ. Press, Oxford, 2010.
- [2] J.E. McMurry, Organic Chemistry, 9th edition, CENGAGE Learning Custom Publishing, Boston, MA, USA, 2015.
- [3] Mineral Commodities Summaries, 2015.  
<https://minerals.usgs.gov/minerals/pubs/mcs/2016/mcs2016.pdf>
- [4] J.I. van der Vlugt, Advances in selective activation and application of ammonia in homogeneous catalysis, Chem. Soc. Rev. 39 (2010) 2302–2322. doi:10.1039/B925794M.
- [5] S.A. Lawrence, Amines: Synthesis, Properties and Applications, Cambridge University Press, 2004.
- [6] World Amines Market, (n.d.). <http://www.prnewswire.com/news-releases/world-amines-market-274542701.html> (accessed March 15, 2017).
- [7] C.L. Roggenkamp, Acidic emollient liquid detergent composition, US3943234 A, 1976. <http://www.google.ch/patents/US3943234> (accessed April 24, 2017).
- [8] W.H. Scepaniski, Solid cast fabric softening compositions for application in a washing machine, US6110886 A, 2000. <http://www.google.fr/patents/US6110886> (accessed April 24, 2017).
- [9] E.C. Sherburne, Antistatic materials, US3468869 A, 1969. <http://www.google.com/patents/US3468869> (accessed April 24, 2017).
- [10] K. Eller, E. Henkes, R. Roszbacher, H. Höke, Amines, Aliphatic, in: Ullmanns Encycl. Ind. Chem., Wiley-VCH Verlag GmbH & Co. KGaA, 2000. doi:10.1002/14356007.a02\_001.
- [11] T. Gerstein, Low pH hair conditioner compositions containing amine oxides, US4714610 A, 1987. <http://www.google.com/patents/US4714610> (accessed April 24, 2017).
- [12] J.E. Borland, T. Crutcher, J.D. Sauer, K.R. Smith, Amine oxide surfactant compositions, US5167864 A, 1992. <http://www.google.com/patents/US5167864> (accessed April 24, 2017).
- [13] O.D. Stringer, S.H. Abbas, R. Subramanyam, Cleaning compositions containing amine oxide and formic acid, US5858955 A, 1999. <http://www.google.ch/patents/US5858955> (accessed April 24, 2017).
- [14] D.A. Williams, J.R. Looney, D.S. Sullivan, B.I. Bourland, J.A. Haslegrave, P.J. Clewlow, N. Carruthers, T.M. O'Brien, Amine derivatives as corrosion inhibitors, US5322630 A, 1994. <http://www.google.com/patents/US5322630> (accessed April 24, 2017).
- [15] W.T. Hulshof, Herbicides and fungicides containing activity promoting additives, US5226943 A, 1993. <http://www.google.com/patents/US5226943> (accessed April 24, 2017).
- [16] J.C. Forbes, M.M. Henriët, S. Hewitt, R.W. Mitchell, Glyphosate formulations comprising alkoxyated amine surfactants, US5668085 A, 1997. <http://www.google.com/patents/US5668085> (accessed April 24, 2017).
- [17] Application of Surfactants - Fatty Amine Ethoxylates, (n.d.). <http://www.rimpro-india.com/articles1/application-of-surfactants-fatty-amine-ethoxylates.html> (accessed April 24, 2017).
- [18] Amines Market by Amine Type & Application - 2020 | MarketsandMarkets, (n.d.). <http://www.marketsandmarkets.com> (accessed March 15, 2017).

- [19] P. Roose, M.G. Turcotte, Amines, Lower Aliphatic, in: Kirk-othmer Encycl. Chem. Technol., John Wiley & Sons, Inc., 2000. doi:10.1002/0471238961.1215230520211803.a01.pub3.
- [20] K. Visek, Amines, Fatty, in: Kirk-othmer Encycl. Chem. Technol., John Wiley & Sons, Inc., 2000. doi:10.1002/0471238961.0601202022091905.a01.pub2.
- [21] K.S. Hayes, Industrial processes for manufacturing amines, Appl. Catal. Gen. 221 (2001) 187–195. doi:10.1016/S0926-860X(01)00813-4.
- [22] V.A. Nekrasova, N.I. Shulkin, Catalytic alkylation of ammonia with halogen derivatives of alkanes and cyclanes Part 2. Effect of the nature of the halogen and of its position in the molecule on amination of alkyl halides, Bull. Acad. Sci. USSR Div. Chem. Sci. 1 (1952) 599–600. doi:10.1007/BF01164924.
- [23] C.W. Cheung, X. Hu, Amine synthesis via iron-catalysed reductive coupling of nitroarenes with alkyl halides, Nat. Commun. 7 (2016). doi:10.1038/ncomms12494.
- [24] B.B. Bureau, Asia-Pacific region to propel global demand for amines in cleaning products, Bus. Stand. India. (2016). <http://www.business-standard.com> (accessed March 16, 2017).
- [25] Académie des sciences (France), Comptes rendus hebdomadaires des séances de l'Académie des sciences, Gauthier-Villars, Paris, 1849. <http://gallica.bnf.fr/ark:/12148/bpt6k29859> (accessed March 17, 2017).
- [26] J.U. Nef, Dissociationsvorgänge bei den einatomigen Alkoholen, Aethern und Salzen, Justus Liebigs Ann. Chem. 318 (1901) 137–230. doi:10.1002/jlac.19013180202.
- [27] P. Sabatier, Catalysis in organic chemistry, D. Van Nostrand Company, 1922.
- [28] S. Bähn, S. Imm, L. Neubert, M. Zhang, H. Neumann, M. Beller, The Catalytic Amination of Alcohols, ChemCatChem. 3 (2011) 1853–1864. doi:10.1002/cctc.201100255.
- [29] T.W.G. Solomons, C.B. Fryhle, S.A. Snyder, Organic chemistry, 11th edition, Wiley, Hoboken, NJ, 2013.
- [30] Y. Ashina, M. Fukatsu, Process for producing methylamines, US4485261 A, 1984. <http://www.google.com/patents/US4485261> (accessed March 22, 2017).
- [31] Y. Ashina, T. Fujita, M. Fukatsu, J. Yagi, Process for producing dimethylamine in preference to mono- or trimethylamine by vapor-phase catalytic reaction of methanol and ammonia, US4578516 A, 1986. <http://www.google.com/patents/US4578516> (accessed March 22, 2017).
- [32] L.J. D, Process for the manufacture of methylamines, US3387032 A, 1968. <http://www.google.com/patents/US3387032> (accessed April 24, 2017).
- [33] B.C. Challis, A.R. Butler, Substitution at an amino nitrogen, in: S. Patai (Ed.), Amino Group 1968, John Wiley & Sons, Ltd., 1968: pp. 277–347. doi:10.1002/9780470771082.ch6.
- [34] F. Effenberger, The Chemistry of Open-chain Organic Nitrogen Compounds. Von P. A. S. Smith. Verlag W. A. Benjamin, Inc., New York-Amsterdam. Angew. Chem. 79 (1967) 283–284. doi:10.1002/ange.19670790630.
- [35] J.F. Hartwig, Organotransition metal chemistry: from bonding to catalysis, University Science Books, Sausalito, Calif, 2010.
- [36] R.N. Salvatore, C.H. Yoon, K.W. Jung, Synthesis of secondary amines, Tetrahedron. 57 (2001) 7785–7811.
- [37] C. Willard, Process for production of unsaturated amines, US2216548 A, 1940. <http://www.google.ch/patents/US2216548> (accessed March 18, 2017).
- [38] W.E. Carroll, R.J. Daughenbaugh, D.D. Dixon, M.E. Ford, M. Deeba, Allylamine from allyl alcohol, J. Mol. Catal. 44 (1988) 213–215.

- [39] K. Das, R. Shibuya, Y. Nakahara, N. Germain, T. Ohshima, K. Mashima, Platinum-Catalyzed Direct Amination of Allylic Alcohols with Aqueous Ammonia: Selective Synthesis of Primary Allylamines, *Angew. Chem. Int. Ed.* 51 (2012) 150–154. doi:10.1002/anie.201106737.
- [40] G. Ertl, ed., *Handbook of heterogeneous catalysis: 8 volumes, 2., completely rev. and enl. ed.*, WILEY-VCH, Weinheim, 2008.
- [41] T.E. Müller, K.C. Hultsch, M. Yus, F. Foubelo, M. Tada, Hydroamination: Direct Addition of Amines to Alkenes and Alkynes, *Chem. Rev.* 108 (2008) 3795–3892. doi:10.1021/cr0306788.
- [42] M. Beller, J. Seayad, A. Tillack, H. Jiao, Catalytic Markovnikov and anti-Markovnikov Functionalization of Alkenes and Alkynes: Recent Developments and Trends, *Angew. Chem. Int. Ed.* 43 (2004) 3368–3398. doi:10.1002/anie.200300616.
- [43] O. Jimenez, T.E. Müller, C. Sievers, A. Spirkel, J.A. Lercher, Markovnikov and anti-Markovnikov hydroamination with palladium catalysts immobilized in thin films of silica supported ionic liquids, *Chem. Commun.* (2006) 2974–2976. doi:10.1039/B605567B.
- [44] Preparation of tert-butylamine from isobutene, n.d. <http://www.google.com/patents/US4929758> (accessed March 20, 2017).
- [45] Y. Huang, W.M.H. Sachtler, On the mechanism of catalytic hydrogenation of nitriles to amines over supported metal catalysts, *Appl. Catal. Gen.* 182 (1999) 365–378. doi:10.1016/S0926-860X(99)00035-6.
- [46] Hydrogenation of nitriles in ammonia and water, n.d. <http://www.google.com/patents/US4248799> (accessed March 20, 2017).
- [47] M. Verhaak, A.J. Van Dillen, J.W. Geus, The selective hydrogenation of acetonitrile on supported nickel catalysts, *Catal. Lett.* 26 (1994) 37–53.
- [48] Hydrogenation of nitriles to produce amines, n.d. <http://www.google.com/patents/US5869653> (accessed March 20, 2017).
- [49] Hydrocyanation of olefins, 1967. <https://patents.google.com/patent/US3496217A/en> (accessed March 21, 2017).
- [50] T. Gross, A.M. Seayad, M. Ahmad, M. Beller, Synthesis of Primary Amines: First Homogeneously Catalyzed Reductive Amination with Ammonia, *Org. Lett.* 4 (2002) 2055–2058. doi:10.1021/ol0200605.
- [51] B. Miriyala, S. Bhattacharyya, J.S. Williamson, Chemoselective reductive alkylation of ammonia with carbonyl compounds: synthesis of primary and symmetrical secondary amines, *Tetrahedron.* 60 (2004) 1463–1471. doi:10.1016/j.tet.2003.12.024.
- [52] S. Ogo, K. Uehara, T. Abura, S. Fukuzumi, pH-Dependent Chemoselective Synthesis of  $\alpha$ -Amino Acids. Reductive Amination of  $\alpha$ -Keto Acids with Ammonia Catalyzed by Acid-Stable Iridium Hydride Complexes in Water, *J. Am. Chem. Soc.* 126 (2004) 3020–3021. doi:10.1021/ja031633r.
- [53] D. Menche, F. Arikan, J. Li, S. Rudolph, Directed Reductive Amination of  $\beta$ -Hydroxy-ketones: Convergent Assembly of the Ritonavir/Lopinavir Core, *Org. Lett.* 9 (2007) 267–270. doi:10.1021/ol062715y.
- [54] J. Bódis, L. Lefferts, T.E. Müller, R. Pestman, J.A. Lercher, Activity and Selectivity Control in Reductive Amination of Butyraldehyde over Noble Metal Catalysts, *Catal. Lett.* 104 (2005) 23–28. doi:10.1007/s10562-005-7431-4.
- [55] T. Mallat, A. Baiker, W. Kleist, K. Köhler, Amination Reactions, in: *Handb. Heterog. Catal.*, Wiley-VCH Verlag GmbH & Co. KGaA, 2008. doi:10.1002/9783527610044.hetcat0182.
- [56] R.S. Egly, E.F. Smith, Effect of operating variables on methylamine production, *Chem. Eng. Prog.* 44 (1948) 387–397.

- [57] A.C. Stevenson, *Ammonolysis*, *Ind. Eng. Chem.* 41 (1949) 1846–1851.
- [58] Process for the manufacture of methylamines, n.d.  
<http://www.google.com/patents/US3387032> (accessed March 22, 2017).
- [59] C. Gründling, G.C. Eder-Mirth, J.A. Lercher, Selectivity enhancement in methylamine synthesis via postsynthesis modification of brønsted acidic mordenite, *J. Catal.* 160 (1996) 299–308.
- [60] B. Tijsebaert, B. Yilmaz, U. Müller, H. Gies, W. Zhang, X. Bao, F.-S. Xiao, T. Tatsumi, D. De Vos, Shape-selective synthesis of methylamines over the RRO zeolite Al-RUB-41, *J. Catal.* 278 (2011) 246–252. doi:10.1016/j.jcat.2010.12.010.
- [61] F.C. Wilhelm, G.E. Parris, B.A. Aufdembrink, T.R. Gaffney, Preparation of methylamines using shape selective chabazites, US5399769 A, 1995.  
<http://www.google.com/patents/US5399769> (accessed March 22, 2017).
- [62] J.A. Kent, *Riegel's Handbook of Industrial Chemistry.*, Springer Netherlands, Dordrecht, 1993. <http://public.eblib.com/choice/publicfullrecord.aspx?p=3568168> (accessed April 2, 2017).
- [63] V.A. Veeffkind, J.A. Lercher, On the elementary steps of acid zeolite catalyzed amination of light alcohols, *Appl. Catal. Gen.* 181 (1999) 245–255.
- [64] T.D. Nixon, M.K. Whittlesey, J.M.J. Williams, Transition metal catalysed reactions of alcohols using borrowing hydrogen methodology, *Dalton Trans.* (2009) 753–762. doi:10.1039/B813383B.
- [65] M.H.S.A. Hamid, P.A. Slatford, J.M.J. Williams, Borrowing Hydrogen in the Activation of Alcohols, *Adv. Synth. Catal.* 349 (2007) 1555–1575. doi:10.1002/adsc.200600638.
- [66] G.E. Dobereiner, R.H. Crabtree, Dehydrogenation as a Substrate-Activating Strategy in Homogeneous Transition-Metal Catalysis, *Chem. Rev.* 110 (2010) 681–703. doi:10.1021/cr900202j.
- [67] G. Guillena, D.J. Ramón, M. Yus, Hydrogen Autotransfer in the *N*-Alkylation of Amines and Related Compounds using Alcohols and Amines as Electrophiles, *Chem. Rev.* 110 (2010) 1611–1641. doi:10.1021/cr9002159.
- [68] A.J.A. Watson, J.M.J. Williams, The Give and Take of Alcohol Activation, *Science.* 329 (2010) 635–636. doi:10.1126/science.1191843.
- [69] D. Pingen, C. Müller, D. Vogt, Direct Amination of Secondary Alcohols Using Ammonia, *Angew. Chem. Int. Ed.* 49 (2010) 8130–8133. doi:10.1002/anie.201002583.
- [70] S. Imm, S. Bähn, L. Neubert, H. Neumann, M. Beller, An Efficient and General Synthesis of Primary Amines by Ruthenium-Catalyzed Amination of Secondary Alcohols with Ammonia, *Angew. Chem. Int. Ed.* 49 (2010) 8126–8129. doi:10.1002/anie.201002576.
- [71] C. Gunanathan, D. Milstein, Selective Synthesis of Primary Amines Directly from Alcohols and Ammonia, *Angew. Chem.* 120 (2008) 8789–8792. doi:10.1002/ange.200803229.
- [72] R. Grigg, T.R.B. Mitchell, S. Sutthivaiyakit, N. Tongpenyai, Transition metal-catalysed *N*-alkylation of amines by alcohols, *J. Chem. Soc. Chem. Commun.* (1981) 611–612. doi:10.1039/C39810000611.
- [73] Y. Watanabe, Y. Tsuji, Y. Ohsugi, The ruthenium catalyzed *N*-alkylation and *N*-heterocyclization of aniline using alcohols and aldehydes, *Tetrahedron Lett.* 22 (1981) 2667–2670. doi:10.1016/S0040-4039(01)92965-X.

- [74] S. Ganguly, F.L. Joslin, D.M. Roundhill, Conversion of long-chain terminal alcohols and secondary amines into tertiary amines using dichlorotris(triphenylphosphine)ruthenium(II) as catalyst, *Inorg. Chem.* 28 (1989) 4562–4564. doi:10.1021/ic00325a004.
- [75] Y. Tsuji, S. Kotachi, K.T. Huh, Y. Watanabe, Ruthenium-catalyzed dehydrogenative N-heterocyclization. Indoles from 2-aminophenethyl alcohols and 2-nitrophenethyl alcohols, *J. Org. Chem.* 55 (1990) 580–584. doi:10.1021/jo00289a036.
- [76] V.R. Jumde, L. Gonsalvi, A. Guerriero, M. Peruzzini, M. Taddei, A Ruthenium-Based Catalytic System for a Mild Borrowing-Hydrogen Process, *Eur. J. Org. Chem.* 2015 (2015) 1829–1833. doi:10.1002/ejoc.201403636.
- [77] X. Cui, Y. Deng, F. Shi, Reductive N-Alkylation of Nitro Compounds to N-Alkyl and N,N-Dialkyl Amines with Glycerol as the Hydrogen Source, *ACS Catal.* 3 (2013) 808–811. doi:10.1021/cs400049b.
- [78] K.O. Marichev, J.M. Takacs, Ruthenium-Catalyzed Amination of Secondary Alcohols Using Borrowing Hydrogen Methodology, *ACS Catal.* 6 (2016) 2205–2210. doi:10.1021/acscatal.6b00175.
- [79] M.H.S.A. Hamid, C.L. Allen, G.W. Lamb, A.C. Maxwell, H.C. Maytum, A.J.A. Watson, J.M.J. Williams, Ruthenium-catalyzed N-alkylation of amines and sulfonamides using borrowing hydrogen methodology, *J. Am. Chem. Soc.* 131 (2009) 1766–1774. doi:10.1021/ja807323a.
- [80] A.B. Enyong, B. Moasser, Ruthenium-catalyzed N-alkylation of amines with alcohols under mild conditions using the borrowing hydrogen methodology, *J. Org. Chem.* 79 (2014) 7553–7563. doi:10.1021/jo501273t.
- [81] K.-I. Fujita, T. Fujii, R. Yamaguchi, CpIr complex-catalyzed N-heterocyclization of primary amines with diols: a new catalytic system for environmentally benign synthesis of cyclic amines, *Org. Lett.* 6 (2004) 3525–3528. doi:10.1021/ol048619j.
- [82] K. Yuan, F. Jiang, Z. Sahli, M. Achard, T. Roisnel, C. Bruneau, Iridium-catalyzed oxidant-free dehydrogenative C-H bond functionalization: selective preparation of N-arylpiperidines through tandem hydrogen transfers, *Angew. Chem. Int. Ed Engl.* 51 (2012) 8876–8880. doi:10.1002/anie.201204582.
- [83] S. Ruch, T. Irrgang, R. Kempe, New iridium catalysts for the selective alkylation of amines by alcohols under mild conditions and for the synthesis of quinolines by acceptor-less dehydrogenative condensation, *Chem. Weinh. Bergstr. Ger.* 20 (2014) 13279–13285. doi:10.1002/chem.201402952.
- [84] A. Wetzel, S. Wöckel, M. Schelwies, M.K. Brinks, F. Rominger, P. Hofmann, M. Limbach, Selective alkylation of amines with alcohols by Cp\*-iridium(III) half-sandwich complexes, *Org. Lett.* 15 (2013) 266–269. doi:10.1021/ol303075h.
- [85] R. Kawahara, K. Fujita, R. Yamaguchi, Multialkylation of Aqueous Ammonia with Alcohols Catalyzed by Water-Soluble Cp\*Ir–Ammine Complexes, *J. Am. Chem. Soc.* 132 (2010) 15108–15111. doi:10.1021/ja107274w.
- [86] S. Imm, S. Bähn, M. Zhang, L. Neubert, H. Neumann, F. Klasovsky, J. Pfeffer, T. Haas, M. Beller, Improved Ruthenium-Catalyzed Amination of Alcohols with Ammonia: Synthesis of Diamines and Amino Esters, *Angew. Chem. Int. Ed.* 50 (2011) 7599–7603. doi:10.1002/anie.201103199.
- [87] W. Baumann, A. Spannenberg, J. Pfeffer, T. Haas, A. Köckritz, A. Martin, J. Deutsch, Utilization of Common Ligands for the Ruthenium-Catalyzed Amination of Alcohols, *Chem. – Eur. J.* 19 (2013) 17702–17706. doi:10.1002/chem.201302774.
- [88] R.M. Bullock, ed., *Catalysis without precious metals*, Wiley-VCH, Weinheim, 2010.
- [89] T. Yan, B.L. Feringa, K. Barta, Iron catalysed direct alkylation of amines with alcohols, *Nat. Commun.* 5 (2014) 5602. doi:10.1038/ncomms6602.

- [90] G. Zhang, Z. Yin, S. Zheng, Cobalt-Catalyzed N-Alkylation of Amines with Alcohols, *Org. Lett.* 18 (2016) 300–303. doi:10.1021/acs.orglett.5b03461.
- [91] S. Elangovan, J. Neumann, J.-B. Sortais, K. Junge, C. Darcel, M. Beller, Efficient and selective N-alkylation of amines with alcohols catalysed by manganese pincer complexes, *Nat. Commun.* 7 (2016). doi:10.1038/ncomms12641.
- [92] Cyclohexanedimethanamine by direct amination of cyclohexanedimethanol, 2009. <https://patents.google.com/patent/EP2262762A4/en> (accessed April 27, 2017).
- [93] A.K. Rausch, E. van Steen, F. Roessner, New aspects for heterogeneous cobalt-catalyzed hydroamination of ethanol, *J. Catal.* 253 (2008) 111–118. doi:10.1016/j.jcat.2007.10.013.
- [94] A. Fischer, T. Mallat, A. Baiker, Nickel-catalyzed amination of 1,3-propanediols differently substituted at C2-position: influence of reactant structure on diamine production, *J. Mol. Catal. Chem.* 149 (1999) 197–204. doi:10.1016/S1381-1169(99)00174-0.
- [95] O.J. Frank, M.J. Francis, Manufacture of aliphatic amines, US2365721 A, 1944. <http://www.google.com/patents/US2365721> (accessed April 6, 2017).
- [96] D. Phineas, R.P. William, C.R. Reid, T.A.W. Charles, Production of amines, US2609394 A, 1952. <http://www.google.ch/patents/US2609394> (accessed April 6, 2017).
- [97] T.A.W. Charles, R.P. William, Production of amines, US2636902 A, 1953. <http://www.google.com/patents/US2636902> (accessed April 6, 2017).
- [98] D. a Gardner, R.T. Clark, Catalytic process for preparing ethyl amines, US4255357 (A), 1981. [http://worldwide.espacenet.com/publicationDetails/biblio?FT=D&date=19810310&DB=EPODOC&locale=en\\_EP&CC=US&NR=4255357A&KC=A&ND=4](http://worldwide.espacenet.com/publicationDetails/biblio?FT=D&date=19810310&DB=EPODOC&locale=en_EP&CC=US&NR=4255357A&KC=A&ND=4) (accessed December 22, 2015).
- [99] J.V.M. de Pinillos, R.L. Fowlkes, Synthesis of lower alkyl amines, US4314084 A, 1982. <http://www.google.ch/patents/US4314084> (accessed April 6, 2017).
- [100] F. Santoro, R. Psaro, N. Ravasio, F. Zaccheria, Reductive Amination of Ketones or Amination of Alcohols over Heterogeneous Cu Catalysts: Matching the Catalyst Support with the N-Alkylating Agent, *ChemCatChem.* 4 (2012) 1249–1254. doi:10.1002/cctc.201200213.
- [101] G.A. Vedage, L.A. Emig, H.-X. Li, J.N. Armor, Metal exchanged zeolite catalysts for alcohol amination, Google Patents, 1999. <https://www.google.com/patents/US5917092> (accessed December 17, 2015).
- [102] A. Baiker, Catalytic amination of aliphatic alcohols. Role of hydrogen as inhibitor for catalyst deactivation, *Ind. Eng. Chem. Prod. Res. Dev.* 20 (1981) 615–618. doi:10.1021/i300004a006.
- [103] J.H. Cho, J.H. Park, T.-S. Chang, G. Seo, C.-H. Shin, Reductive amination of 2-propanol to monoisopropylamine over Co/ $\gamma$ -Al<sub>2</sub>O<sub>3</sub> catalysts, *Appl. Catal. Gen.* 417–418 (2012) 313–319. doi:10.1016/j.apcata.2012.01.011.
- [104] J.H. Cho, J.-H. Park, T.-S. Chang, J.-E. Kim, C.-H. Shin, Reductive Amination of 2-Propanol to Monoisopropylamine Over Ni/ $\gamma$ -Al<sub>2</sub>O<sub>3</sub> Catalysts, *Catal. Lett.* 143 (2013) 1319–1327. doi:10.1007/s10562-013-1086-3.
- [105] A. Fischer, M. Maciejewski, T. Bürgi, T. Mallat, A. Baiker, Cobalt-Catalyzed Amination of 1,3-Propanediol: Effects of Catalyst Promotion and Use of Supercritical Ammonia as Solvent and Reactant, *J. Catal.* 183 (1999) 373–383. doi:10.1006/jcat.1999.2408.

- [106] G. Jenzer, T. Mallat, A. Baiker, Cobalt-catalyzed amination of 1,3-cyclohexanediol and 2,4-pentanediol in supercritical ammonia, *Catal. Lett.* 61 (1999) 111–114. doi:10.1023/A:1019045527193.
- [107] A. Fischer, T. Mallat, A. Baiker, Synthesis of 1,4-Diaminocyclohexane in Supercritical Ammonia, *J. Catal.* 182 (1999) 289–291. doi:10.1006/jcat.1999.2410.
- [108] M. Imabeppu, K. Kiyoga, S. Okamura, H. Shoho, H. Kimura, One-step amination of  $\alpha,\omega$ -alkylenediols over Cu/Ni-based catalysts, *Catal. Commun.* 10 (2009) 753–757. doi:10.1016/j.catcom.2008.10.046.
- [109] G.A. Vedage, K.S. Hayes, M. Leeaphon, J.N. Armor, Multi-metallic actalysts for amination of alcohols to form alkylamines, Google Patents, 1999. <https://www.google.com/patents/US5932769> (accessed December 17, 2015).
- [110] G. Sewell, C. O'Connor, E. van Steen, Reductive amination of ethanol with silica-supported cobalt and nickel catalysts, *Appl. Catal. Gen.* 125 (1995) 99–112. doi:10.1016/0926-860X(95)00010-0.
- [111] G.S. Sewell, C.T. O'Connor, E. van Steen, Effect of Activation Procedure and Support on the Reductive Amination of Ethanol Using Supported Cobalt Catalysts, *J. Catal.* 167 (1997) 513–521. doi:10.1006/jcat.1997.1596.
- [112] M. Deeba, Shape selective catalysts for C2 to C4 alkanol amination, US4918234 A, 1990. <http://www.google.com/patents/US4918234> (accessed April 27, 2017).
- [113] A. Corma, T. Ródenas, M.J. Sabater, A Bifunctional Pd/MgO Solid Catalyst for the One-Pot Selective N-Monoalkylation of Amines with Alcohols, *Chem. – Eur. J.* 16 (2010) 254–260. doi:10.1002/chem.200901501.
- [114] T. Ishida, R. Takamura, T. Takei, T. Akita, M. Haruta, Support effects of metal oxides on gold-catalyzed one-pot N-alkylation of amine with alcohol, *Appl. Catal. Gen.* 413–414 (2012) 261–266. doi:10.1016/j.apcata.2011.11.017.
- [115] K. Shimizu, N. Imaiida, K. Kon, S.M.A. Hakim Siddiki, A. Satsuma, Heterogeneous Ni Catalysts for N-Alkylation of Amines with Alcohols, *ACS Catal.* 3 (2013) 998–1005. doi:10.1021/cs4001267.
- [116] K. Shimizu, K. Kon, W. Onodera, H. Yamazaki, J.N. Kondo, Heterogeneous Ni Catalyst for Direct Synthesis of Primary Amines from Alcohols and Ammonia, *ACS Catal.* 3 (2013) 112–117. doi:10.1021/cs3007473.
- [117] Y. Zhang, X. Qi, X. Cui, F. Shi, Y. Deng, Palladium catalyzed N-alkylation of amines with alcohols, *Tetrahedron Lett.* 52 (2011) 1334–1338. doi:10.1016/j.tetlet.2011.01.059.
- [118] Z. Yan, A. Tomer, G. Perrussel, M. Ousmane, B. Katryniok, F. Dumeignil, A. Ponchel, A. Liebens, M. Pera-Titus, A Pd/CeO<sub>2</sub> “H<sub>2</sub> Pump” for the Direct Amination of Alcohols, *ChemCatChem.* 8 (2016) 3347–3352. doi:10.1002/cctc.201600855.
- [119] X. Cui, X. Dai, Y. Deng, F. Shi, Development of a General Non-Noble Metal Catalyst for the Benign Amination of Alcohols with Amines and Ammonia, *Chem. – Eur. J.* 19 (2013) 3665–3675. doi:10.1002/chem.201203417.
- [120] A. Corma, J. Navas, M.J. Sabater, Coupling of Two Multistep Catalytic Cycles for the One-Pot Synthesis of Propargylamines from Alcohols and Primary Amines on a Nanoparticulated Gold Catalyst, *Chem. – Eur. J.* 18 (2012) 14150–14156. doi:10.1002/chem.201201837.
- [121] M. Ousmane, G. Perrussel, Z. Yan, J.-M. Clacens, F. De Campo, M. Pera-Titus, Highly selective direct amination of primary alcohols over a Pd/K-oMS-2 catalyst, *J. Catal.* 309 (2014) 439–452. doi:10.1016/j.jcat.2013.10.003.
- [122] R.G. Rice, E.J. Kohn, Raney Nickel Catalyzed N-Alkylation of Aniline and Benzidine with Alcohols, *J. Am. Chem. Soc.* 77 (1955) 4052–4054. doi:10.1021/ja01620a026.

- [123] A. Mehta, A. Thaker, V. Londhe, S.R. Nandan, Reinvestigating Raney nickel mediated selective alkylation of amines with alcohols via hydrogen autotransfer methodology, *Appl. Catal. Gen.* 478 (2014) 241–251. doi:10.1016/j.apcata.2014.04.009.
- [124] K. Shimizu, S. Kanno, K. Kon, S.M.A. Hakim Siddiki, H. Tanaka, Y. Sakata, N-alkylation of ammonia and amines with alcohols catalyzed by Ni-loaded CaSiO<sub>3</sub>, *Catal. Today*. (n.d.). doi:10.1016/j.cattod.2013.09.002.
- [125] K. Shimizu, Heterogeneous catalysis for the direct synthesis of chemicals by borrowing hydrogen methodology, *Catal. Sci. Technol.* 5 (2015) 1412–1427. doi:10.1039/C4CY01170H.
- [126] R.C. Lemon, R.C. Myerly, Production of amines, US3022349 A, 1962. <http://www.google.fr/patents/US3022349> (accessed April 27, 2017).
- [127] M. Dixit, M. Mishra, P.A. Joshi, D.O. Shah, Clean borrowing hydrogen methodology using hydrotalcite supported copper catalyst, *Catal. Commun.* 33 (2013) 80–83. doi:10.1016/j.catcom.2012.12.027.
- [128] F. Santoro, R. Psaro, N. Ravasio, F. Zaccheria, N -Alkylation of amines through hydrogen borrowing over a heterogeneous Cu catalyst, *RSC Adv.* 4 (2014) 2596–2600. doi:10.1039/C3RA44364G.
- [129] J. He, K. Yamaguchi, N. Mizuno, Selective Synthesis of Secondary Amines via N-Alkylation of Primary Amines and Ammonia with Alcohols by Supported Copper Hydroxide Catalysts, *Chem. Lett.* 39 (2010) 1182–1183.
- [130] A. Baiker, W. Richarz, Catalytic amination of long chain aliphatic alcohols, *Ind. Eng. Chem. Prod. Res. Dev.* 16 (1977) 261–266.
- [131] M. Conrads, A.T. Hermann, E. Scherf, A. Wagner, Production of primary guerbet amines, US5808158 A, 1998. <http://www.google.fr/patents/US5808158> (accessed April 12, 2017).
- [132] H. Kimura, H. Taniguchi, Targeting quantitative synthesis for the one-step amination of fatty alcohols and dimethylamine, *Appl. Catal. Gen.* 287 (2005) 191–196. doi:10.1016/j.apcata.2005.03.041.
- [133] J. Sun, X. Jin, F. Zhang, W. Hu, J. Liu, R. Li, Ni–Cu/ $\gamma$ -Al<sub>2</sub>O<sub>3</sub> catalyzed N-alkylation of amines with alcohols, *Catal. Commun.* 24 (2012) 30–33. doi:10.1016/j.catcom.2012.03.010.
- [134] Y. Li, Q. Li, L. Zhi, M. Zhang, Catalytic Amination of Octanol for Synthesis of Trioctylamine and Catalyst Characterization, *Catal. Lett.* 141 (2011) 1635–1642. doi:10.1007/s10562-011-0686-z.
- [135] L. Qiuxiao, Z. Gaoyong, P. Shaoyi, Study of the amination of fatty alcohols catalyzed by Cu- Ni catalysts, *J. Surfactants Deterg.* 5 (2002) 229–233.
- [136] P.R. Likhar, R. Arundhathi, M.L. Kantam, P.S. Prathima, Amination of Alcohols Catalyzed by Copper-Aluminium Hydrotalcite: A Green Synthesis of Amines, *Eur. J. Org. Chem.* 2009 (2009) 5383–5389. doi:10.1002/ejoc.200900628.
- [137] K. Shimizu, K. Shimura, M. Nishimura, A. Satsuma, Silver cluster-promoted heterogeneous copper catalyst for N-alkylation of amines with alcohols, *RSC Adv.* 1 (2011) 1310–1317. doi:10.1039/C1RA00560J.

- [138] Process for the Continuous Preparation of Saturated and Unsaturated Secondary Fatty Amines., GB1180972 (A), 1970.  
<https://worldwide.espacenet.com/publicationDetails/biblio?FT=D&date=19700211&DB=&locale=&CC=GB&NR=1180972A&KC=A&ND=1> (accessed April 27, 2017).
- [139] P. Kubanek, B.W. Hoffer, E. Schwab, J.-P. Melder, H. Evers, T. Gerlach, Method for producing an amine, US20090286977 A1, 2009.  
<http://www.google.fr/patents/US20090286977> (accessed April 27, 2017).
- [140] K. Yamaguchi, J. He, T. Oishi, N. Mizuno, The “Borrowing Hydrogen Strategy” by Supported Ruthenium Hydroxide Catalysts: Synthetic Scope of Symmetrically and Unsymmetrically Substituted Amines, *Chem. – Eur. J.* 16 (2010) 7199–7207. doi:10.1002/chem.201000149.
- [141] D. Ruiz, A. Aho, T. Saloranta, K. Eränen, J. Wärnå, R. Leino, D.Y. Murzin, Direct amination of dodecanol with NH<sub>3</sub> over heterogeneous catalysts. Catalyst screening and kinetic modelling, *Chem. Eng. J.* 307 (2017) 739–749. doi:10.1016/j.cej.2016.08.083.
- [142] Y.B. Kagan, A.N. Bashkirov, G.A. Kliger, Amination of butyl alcohol over iron catalysts in presence of hydrogen under pressure, *Russ. Chem. Bull.* 10 (1961) 432–436.
- [143] Y. Kagan, A. Bashkirov, G. Kliger, C. Chzhaodi, N. Mak, The reaction of octyl alcohols with ammonia under a pressure of hydrogen over a fused iron catalyst, *Pet. Chem. USSR.* 1 (1962) 300–310. doi:10.1016/0031-6458(62)90038-2.
- [144] Y. Kagan, A. Bashkirov, G. Kliger, C. Chzhaodi, N. Mak, Effect of the molecular weight of an alcohol on its amination, *Pet. Chem. USSR.* 1 (1962) 451–461. doi:10.1016/0031-6458(62)90084-9.
- [145] G.A. Kliger, L.F. Lazutina, R.A. Fridman, Y. KRYUKOV, A.N. Bashkirov, Y.S. Snagovskii, R. SMIRNOVA, SEVERAL ASPECTS OF KINETICS AND MECHANISM OF AMINATION OF OCTANOL ON A MOLTEN IRON CATALYST, *Kinet. Catal.* 16 (1975) 567–570.
- [146] A. Baiker, J. Kijenski, Catalytic Synthesis of Higher Aliphatic Amines from the Corresponding Alcohols, *Catal. Rev.* 27 (1985) 653–697. doi:10.1080/01614948508064235.
- [147] A. Baiker, W. Caprez, W.L. Holstein, Catalytic amination of aliphatic alcohols in the gas and liquid phases: kinetics and reaction pathway, *Ind. Eng. Chem. Prod. Res. Dev.* 22 (1983) 217–225. doi:10.1021/i300010a010.
- [148] V. A. Bassili, A. Baiker, Catalytic amination of 1-methoxypropan-2-ol over silica supported nickel : Modelling of reaction kinetics, *Appl. Catal.* 70 (1991) 325–338. doi:10.1016/S0166-9834(00)84174-3.
- [149] N. Zotova, F.J. Roberts, G.H. Kelsall, A.S. Jessiman, K. Hellgardt, K.K. (Mimi) Hii, Catalysis in flow: Au-catalysed alkylation of amines by alcohols, *Green Chem.* 14 (2012) 226–232. doi:10.1039/C1GC16118K.
- [150] Y.S. Demidova, I.L. Simakova, M. Estrada, S. Beloshapkin, E.V. Suslov, D.V. Korchagina, K.P. Volcho, N.F. Salakhutdinov, A.V. Simakov, D.Y. Murzin, One-pot myrtenol amination over Au nanoparticles supported on different metal oxides, *Appl. Catal. Gen.* 464–465 (2013) 348–356. doi:10.1016/j.apcata.2013.06.013.
- [151] A. Baiker, M. Maciejewski, Formation and thermal stability of copper and nickel nitrides, *J. Chem. Soc. Faraday Trans. 1 Phys. Chem. Condens. Phases.* 80 (1984) 2331–2341. doi:10.1039/F19848002331.

- [152] A. Baiker, D. Monti, Interaction of Ammonia with Metallic Copper, Nickel and Cobalt Catalysts Studied by Temperature Programmed Desorption, *Berichte Bunsenges. Für Phys. Chem.* 87 (1983) 602–605. doi:10.1002/bbpc.19830870714.
- [153] J.J. Perona, G. Thodos, Reaction kinetic studies: Catalytic dehydrogenation of sec-butyl alcohol to methyl ethyl ketone, *AIChE J.* 3 (1957) 230–235. doi:10.1002/aic.690030218.
- [154] L.H. Thaller, G. Thodos, The dual nature of a catalytic reaction: The dehydrogenation of sec-butyl alcohol to methyl ethyl ketone at elevated pressures, *AIChE J.* 6 (1960) 369–373. doi:10.1002/aic.690060306.
- [155] J. Franckaerts, G.F. Froment, Kinetic study of the dehydrogenation of ethanol, *Chem. Eng. Sci.* 19 (1964) 807–818.
- [156] S. Kolboe, Kinetics of dehydrogenation of isopropyl alcohol over a zinc oxide catalyst, *J. Catal.* 13 (1969) 208–214. doi:10.1016/0021-9517(69)90393-5.
- [157] N. Doca, E. Segal, Kinetics of dehydrogenation of low aliphatic alcohols on copper catalysts containing small amounts of Cr, Mn, Fe and Ni, *React. Kinet. Catal. Lett.* 28 (1985) 123–129.
- [158] A. Peloso, M. Moresi, C. Mustachi, B. Soracco, Kinetics of the dehydrogenation of ethanol to acetaldehyde on unsupported catalysts, *Can. J. Chem. Eng.* 57 (1979) 159–164. doi:10.1002/cjce.5450570206.
- [159] M. Boronat, A. Corma, F. Illas, J. Radilla, T. Ródenas, M.J. Sabater, Mechanism of selective alcohol oxidation to aldehydes on gold catalysts: Influence of surface roughness on reactivity, *J. Catal.* 278 (2011) 50–58. doi:10.1016/j.jcat.2010.11.013.
- [160] M.E. Crivello, C.F. Pérez, S.N. Mendieta, S.G. Casuscelli, G.A. Eimer, V.R. Elías, E.R. Herrero, n-octyl alcohol dehydrogenation over copper catalysts, *Catal. Today.* 133–135 (2008) 787–792. doi:10.1016/j.cattod.2007.11.037.
- [161] L.H. Thaller, G. Thodos, The dual nature of a catalytic reaction: The dehydrogenation of sec-butyl alcohol to methyl ethyl ketone at elevated pressures, *AIChE J.* 6 (1960) 369–373. doi:10.1002/aic.690060306.
- [162] F.E. Ford, D.D. Perlmutter, The kinetics of the brass-catalysed dehydrogenation of sec-butyl alcohol, *Chem. Eng. Sci.* 19 (1964) 371–378.
- [163] J.N. Keuler, L. Lorenzen, S. Miachon, The dehydrogenation of 2-butanol over copper-based catalysts: optimising catalyst composition and determining kinetic parameters, *Appl. Catal. Gen.* 218 (2001) 171–180. doi:10.1016/S0926-860X(01)00639-1.
- [164] M. Sheintuch, R.M. Dessau, Observations, modeling and optimization of yield, selectivity and activity during dehydrogenation of isobutane and propane in a Pd membrane reactor, *Chem. Eng. Sci.* 51 (1996) 535–547.
- [165] J. Lehtonen, T. Salmi, A. Vuori, E. Tirronen, On the Principles of Modelling of Homogeneous- Heterogeneous Reactions in the Production of Fine Chemicals. A Case Study: Reductive Alkylation of Aromatic Amines, *Org. Process Res. Dev.* 2 (1998) 78–85.
- [166] D. Roy, R. Jaganathan, R.V. Chaudhari, Kinetic Modeling of Reductive Alkylation of Aniline with Acetone Using Pd/Al<sub>2</sub>O<sub>3</sub> Catalyst in a Batch Slurry Reactor, *Ind. Eng. Chem. Res.* 44 (2005) 5388–5396. doi:10.1021/ie049093+.
- [167] N.G. Patil, D. Roy, A.S. Chaudhari, R.V. Chaudhari, Kinetics of Reductive Alkylation of *p*-Phenylenediamine with Methyl Ethyl Ketone Using 3% Pt/Al<sub>2</sub>O<sub>3</sub> Catalyst in a Slurry Reactor, *Ind. Eng. Chem. Res.* 46 (2007) 3243–3254. doi:10.1021/ie0608556.

- [168] S. Gomez, J.A. Peters, T. Maschmeyer, The reductive amination of aldehydes and ketones and the hydrogenation of nitriles: mechanistic aspects and selectivity control, *Adv. Synth. Catal.* 344 (2002) 1037–1058.
- [169] S. Gomez, J.A. Peters, J.C. van der Waal, P.J. van den Brink, T. Maschmeyer, The rationalization of catalyst behaviour in the reductive amination of benzaldehyde with ammonia using a simple computer model, *Appl. Catal. Gen.* 261 (2004) 119–125. doi:10.1016/j.apcata.2003.10.037.

---

## **Chapter 2**

### **Materials and Methods**

---



## 2.1 Materials

The metal oxides, metal precursors and chemical reagents used in the course of this thesis are listed, respectively, in Table 2-1., Table 2-2. and Table 2-3. All the reagents were used as received, without further purification.

**Table 2-1** List of metal oxides used as supports for the synthesis of heterogeneous catalysts

Metal Oxide	CAS number	Commercial Name	Specific Surface	Provider
$\gamma$ -Al <sub>2</sub> O <sub>3</sub>	1344-28-1	Puralox SCCa-5	~150 m <sup>2</sup> /g	Sasol
TiO <sub>2</sub>	13463-67-7	P25	~50 m <sup>2</sup> /g	Evonik
SiO <sub>2</sub>	112945-52-5	Aerosil 200	~200 m <sup>2</sup> /g	Evonik
Fe <sub>2</sub> O <sub>3</sub>	1309-37-1	-	~150 m <sup>2</sup> /g	Sigma-Aldrich
CeO <sub>2</sub>	1306-38-3	HSA 5	~250 m <sup>2</sup> /g	Solvay

**Table 2-2** List of metal precursors used for the synthesis of heterogeneous catalysts

Metal	Precursor	CAS number	Supplier
Co	Co(NO <sub>3</sub> ) <sub>2</sub> 6H <sub>2</sub> O	10026-22-9	SCR-China, Sigma-Aldrich
Ag	AgNO <sub>3</sub>	7761-88-8	SCR-China, Sigma-Aldrich
Ru	Ru(III) nitrosyl nitrate	34513-98-9	J&K Scientific Sigma-Aldrich
Pt	Pt(NH <sub>3</sub> ) <sub>4</sub> (NO <sub>3</sub> ) <sub>2</sub>	20634-12-2	J&K Scientific
Pd	Pd(NO <sub>3</sub> ) <sub>2</sub> 2H <sub>2</sub> O	32916-07-7	J&K Scientific
Au	HAuCl <sub>4</sub> 3H <sub>2</sub> O	16961-25-4	J&K Scientific
Ni	Ni(NO <sub>3</sub> ) <sub>2</sub> 6H <sub>2</sub> O	13478-00-7	SCR-China, Sigma-Aldrich

**Table 2-3** List of chemical compounds used as reagent or analytical standard

Chemical	CAS Number	Purity	Supplier
<i>n</i> -octanol	111-87-5	≥ 99%	
<i>n</i> -octylamine	111-86-4	99%	
Heptyl Cyanide	124-12-9	97%	
Di- <i>n</i> -octylamine	1120-48-5	98%	J&K
Tri- <i>n</i> -octylamine	1116-76-3	98%	Scientific Sigma-
Octanal	124-13-0	99%	Aldrich
<i>tert</i> -Amyl Alcohol	75-85-4	99%	
Biphenyl	92-52-4	≥ 99%	
1,3-Propanediol	504-63-2	98%	
NH <sub>3</sub>	7664-41-7	≥ 99.9%	
N <sub>2</sub>	7727-37-9	≥ 99.99%	Air Liquide
H <sub>2</sub>	1333-74-0	≥ 99.99%	

## 2.2 Synthesis of Heterogeneous Catalysts

The monometallic and bimetallic catalysts were synthesized by incipient wetness impregnation (IWI) over various supports. This method relies on the use of an impregnation solution with a volume equal to that of the pore volume of the support. The low solution volume favors the dispersion of the active phase driven by capillarity, which is much faster than diffusion. The protocol used for preparing the catalysts is as follows. A weighted amount of metal precursor was dissolved in just enough water to fill the pore volume of the support (*e.g.*,  $0.55 \text{ mL} \cdot \text{g}^{-1}$  for  $\gamma\text{-Al}_2\text{O}_3$ ). The solution was sonicated for 10 min at room temperature to completely dissolve the metal precursor. The resulting solution was then added dropwise to the metal oxide while mixing with a glass bar. The as-obtained mixture was kept at room temperature for 2 h, then dried at  $120 \text{ }^\circ\text{C}$  for 12 h and finally calcined at  $400 \text{ }^\circ\text{C}$  for 4 h using a heating rate of  $2 \text{ }^\circ\text{C} \cdot \text{min}^{-1}$  under static air. A general scheme of the protocol is presented in Figure 2-1.

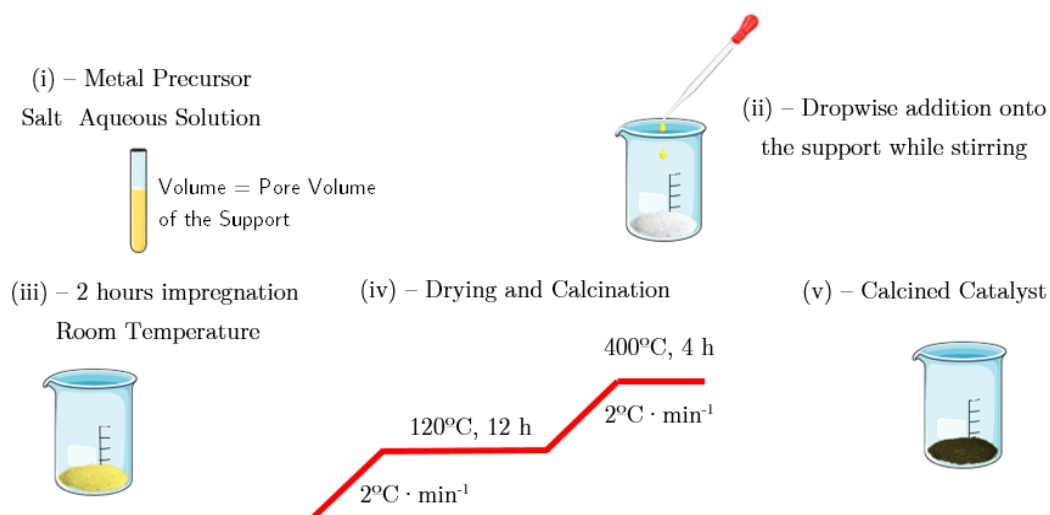


**Figure 2-1** General protocol for the synthesis of supported metallic catalysts by the incipient wetness impregnation method.

The catalysts synthesized by this method will be termed hereinafter as  $M\%/S$ , where  $M$  is the active metal,  $M\%$  is the weight loading of the metal and  $S$  is the support. For instance,  $5\%\text{Co}/\gamma\text{-Al}_2\text{O}_3$  stands for 5% loading by weight of Co supported over  $\gamma\text{-Al}_2\text{O}_3$ .

### 2.2.1 Synthesis of bimetallic supported catalysts

A series of bimetallic formulations based on Co and a noble metal (NM) were prepared. The general scheme of the protocol was similar to that depicted in Figure 2-1 only differing from the impregnation sequence of both metals. In this view, two main sequences were considered, namely sequential impregnation and co-impregnation.

#### (i) Catalysts synthesized by sequential impregnation

This procedure consists of the consecutive impregnation of the two metal precursors. One of the metal precursors was first impregnated over the support followed by drying and

calcination as specified in Figure 2-1. The as-obtained catalyst was further impregnated with the second metal following the same protocol. Two possible sequences were considered, namely Co then NM and NM then Co, and the impregnation order was specified in the nomenclature of the catalyst.

The catalysts synthesized by this procedure will be termed hereinafter by indicating both metals (Co, NM) separated by a hyphen. Likewise, the Co weight loading (M%), the noble metal weight loading (X%) and the support (S) will be specified using the general expression: M% Co-X% NM/S. For instance, 5%Co-0.24%Pt/ $\gamma$ -Al<sub>2</sub>O<sub>3</sub> stands for 5% by weight of Co supported over  $\gamma$ -Al<sub>2</sub>O<sub>3</sub> further doped with 0.24 wt.%Pt. Besides, 0.24%Pt-5%Co/ $\gamma$ -Al<sub>2</sub>O<sub>3</sub> represents a catalyst with the same formulation, but where the noble metal precursor was first impregnated followed by impregnation of the Co precursor.

### (ii) Catalysts synthesized by co-impregnation

This procedure consists of the simultaneous impregnation of Co and the noble metal dopant according to the protocol depicted in Figure 2-1. First, an aqueous solution with the appropriate amount of Co and noble metal precursors was prepared and added dropwise onto the support under mild stirring. The suspension was left at room temperature for 2 h, then dried at 120 °C for 12 h and finally calcined at 400 °C for 4 h.

The catalysts synthesized by this procedure will be termed hereinafter by indicating the dopant weight percent (X%) and nature (NM) in parentheses after Co. Likewise, the Co weight loading (M%) and the support (S) will be specified as M%Co(X%NM)/S. For instance, 5%Co(0.24%Pt)/ $\gamma$ -Al<sub>2</sub>O<sub>3</sub> stands for 5wt%Co supported over  $\gamma$ -Al<sub>2</sub>O<sub>3</sub> doped with a 0.24wt%Pt, where Co and Pt were co-impregnated.

## 2.3 Characterization Methods

### 2.3.1 Elemental Analysis (ICP-OES)

The quantitative analysis of the composition of the different catalysts was carried out by inductive coupled plasma-optic emission spectroscopy using a 720-ES ICP-OES (Agilent) instrument available at the REALCAT platform (UCCS, Lille) equipped with axially viewing, simultaneous CCD detection and ICP Expert™ software (version 2.0.4). The instrument was calibrated using certified standard solutions. Before the analyses, the dried and ground sample (~10 mg) was dissolved in 1.5 mL of concentrated *aqua regia* and 250  $\mu$ L of a 48% hydrofluoric acid (HF) solution. The solution was heated at 50 °C and sonicated for 24 h. After digestion, a solution containing a mixture of the complexing and buffering agents (UNS-1 solution developed by Inorganic Ventures) were used to deactivate HF in excess by increasing the pH to a value between 7.5 and 8.0 and maintain the solubility of the sample by complexation. The solutions were stirred and the volume was adjusted to 50 mL using ultrapure water before analysis.

### 2.3.2 Specific Surface Area Measurement (BET-BJH)

The specific surface area ( $S_{\text{BET}}$ ), the total pore volume ( $V_{\text{p}}$ ) and the mean pore size ( $\overline{d_{\text{p}}}$ ) of the catalysts were characterized by  $\text{N}_2$  adsorption/desorption at  $-196\text{ }^\circ\text{C}$  using a Tristar II Plus apparatus from Micromeritics available at the REALCAT platform (UCCS, Lille). Prior to analysis, the samples were degassed at  $100\text{ }^\circ\text{C}$  overnight. The specific surface area was calculated using the Brunauer-Emmer-Teller (BET) equation in the  $P/P^\circ$  range 0.05-0.25 [1]. The pore size distribution was measured from the desorption isotherm using the Barrett-Joyner-Halenda (BJH) method [2].

### 2.3.3 X-Ray Powder Diffraction (XRD)

The crystalline structure of the samples was analyzed by X-Ray powder diffraction (XRD) using a Bruker D8 Discover diffractometer in Bragg-Brentano geometry equipped with monochromatic  $\text{Cu K}\alpha$  radiation ( $\lambda=0.1538\text{ nm}$ ) and available at the REALCAT platform (UCCS, Lille). Typically, the XRD patterns were recorded at room temperature in the range  $10^\circ < 2\theta < 70^\circ$  with a step-size of  $0.014^\circ$ . The experimental patterns were compared with the ICDD database to identify the crystalline structure of the samples. The average crystallite size of  $\text{Co}_3\text{O}_4$  was estimated from the line broadening at  $2\theta = 36.9^\circ$  corresponding to the (311) crystal plane using the Scherrer equation (see Eq. 2-1)

$$\tau = \frac{K\lambda}{\beta \cos \theta} \quad \Bigg| \quad \text{Eq. 2-1}$$

where  $\tau$  is the mean size of the ordered crystalline domains,  $K$  is a dimensionless shape factor (typically  $\sim 0.9$ ),  $\lambda$  is the X-ray wavelength,  $\beta$  is the peak broadening at half the maximum intensity [ $\Delta(2\theta)$ , in radians] and  $\theta$  is the Bragg angle. The average size of  $\text{Co}^\circ$  crystallite (spherical) was corrected by the factor 0.75 accounting for the density difference between  $\text{Co}^\circ$  and  $\text{Co}_3\text{O}_4$  [3].

The Co dispersion was estimated assuming spherical monocrystalline particles according to Eq. 2-2, where  $\tau$  was expressed in nm [4,5]

$$D\% = 96 / \tau \quad \Bigg| \quad \text{Eq. 2-2}$$

### 2.3.4 Scanning Transmission Electron Microscopy –EELS/EDS

The morphology and elemental composition of the bimetallic Co catalysts were characterized by STEM-EELS/EDS analysis using a 200 kV FEI Tecnai F20 microscope available at ICMPE (CNRS, Paris) [6]. The microscope was equipped with a FEG electron gun, a STEM unit and EDAX Optima T60 SDD EDS spectrometer. The images were analyzed using EDAX Team microanalysis software.

### 2.3.5 Temperature Programmed Reduction ( $\text{H}_2$ -TPR)

The reducibility of the metallic species present in the catalysts was characterized by  $\text{H}_2$ -TPR using a Micromeritics AutoChem 2920 instrument equipped with a thermal

conductivity detector (TCD) and available at E2P2L (Solvay, Shanghai). Typically, ~100 mg of calcined catalyst were placed in a U-shaped quartz reactor and reduced under a 5% v/v H<sub>2</sub>-Ar mixture (40 cm<sup>3</sup>(STP)/min). The sample was gradually heated from room temperature up to 900 °C using a rate of 10 °C·min<sup>-1</sup>. The effluent leaving the reactor was passed through a coil submerged in an isopropyl alcohol slurry cold trap, where any water formed was condensed (Figure 2-2), and further analyzed using a TCD detector. The H<sub>2</sub> profiles were recorded using Autochem II software and the H<sub>2</sub> consumption was measured after band integration.

### 2.3.6 Temperature Programmed Pulse Oxidation (O<sub>2</sub> Pulse–TPO)

The extent of reduction (EOR) of the metallic species present in the catalysts was characterized by O<sub>2</sub> pulse-TPO using a Micromeritics AutoChem 2920 instrument equipped with a thermal conductivity detector (TCD) and available at E2P2L (Solvay, Shanghai). In a typical test, ~100 mg of calcined catalyst were placed in a U-shaped quartz reactor and reduced under a 5% v/v H<sub>2</sub>-Ar flow mixture (40 cm<sup>3</sup>(STP)/min) by heating from room temperature up to 500 °C at a rate of 5 °C·min<sup>-1</sup>, and held at this temperature for 1 h. After reduction, the sample was cooled down to 400 °C under Ar and held at this temperature for 1 h to ensure complete H<sub>2</sub> desorption. Subsequently, O<sub>2</sub> pulses were fed into the reactor until no further O<sub>2</sub> consumption was observed.

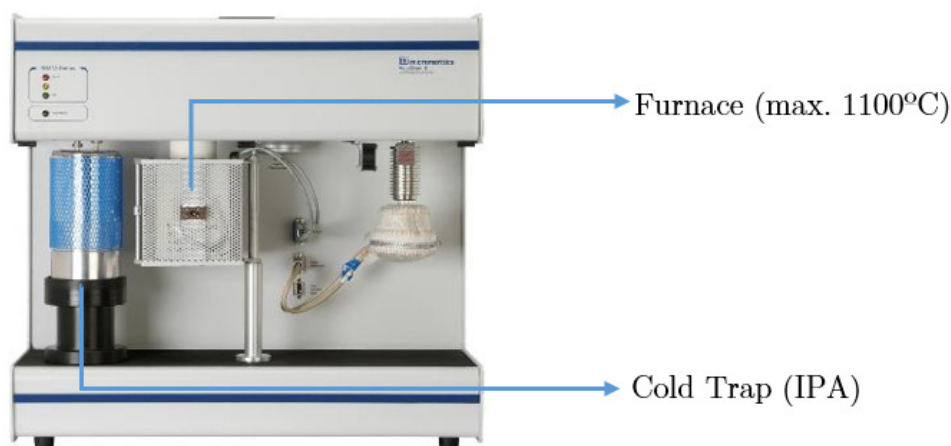
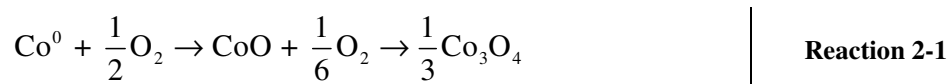


**Figure 2-2** AutoChem 2920 instrument from Micromeritics available at E2P2L.

The O<sub>2</sub> consumption was used to calculate the extent of Co reduction (EOR) using Eq. 2-3 by assuming complete oxidation of CoO and Co<sup>0</sup> species in the sample to Co<sub>3</sub>O<sub>4</sub> [7]. The reactions involved in the oxidation process are specified in Reaction 2-1

$$EOR = \frac{2 \left( N_{O_2} - \frac{N_{Co}}{6} \right)}{N_{Co}} \quad \Bigg| \quad \text{Eq. 2-3}$$

where N<sub>O<sub>2</sub></sub> and N<sub>Co</sub> refer the number of moles of O<sub>2</sub> consumed and the number of moles of Co in the sample, respectively.



## 2.4 Catalytic Tests

### 2.4.1 Three Parallel Fixed Bed Reactor – MPRS-3TC

The catalytic tests were conducted in the MPRS-3TC reactor (Yashentech, China), available at E2P2L (Solvay, Shanghai). The reactor consists of a 3 parallel fixed-bed reactors allowing the simultaneous study of three reactions at the same feed and temperature conditions. The main features of the reactor are summarized in Figure 2-3 together with a process flowsheet diagram of the system. The inlet gas flow rates were adjusted using thermal mass flow controllers ( $\pm 1\%$  accuracy, Seven Star Electronics), while the liquid flow rate was adjusted with a liquid metering pump ( $\pm 3\%$  accuracy, Beijing Satellite Manufacturing).

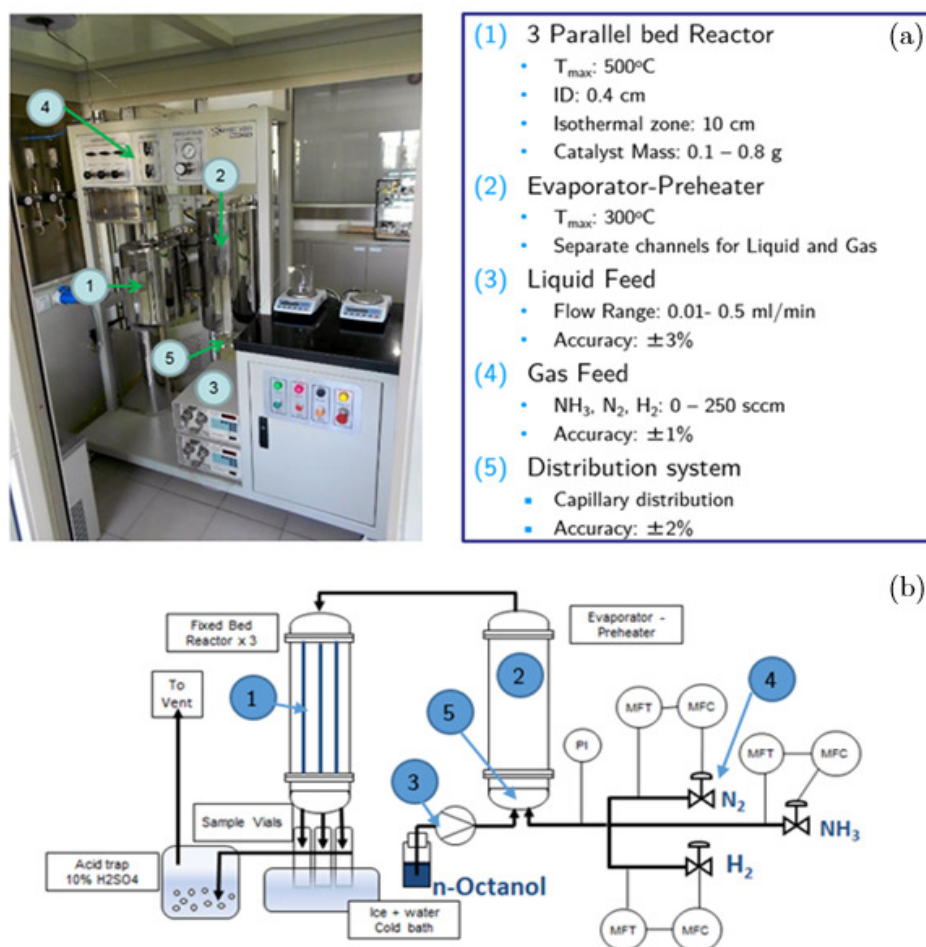


**Figure 2-3** (a) Image and details of the MPRS-3TC 3 parallel fixed bed reactor; and (b) process flowsheet diagram of the MPRS-3TC unit available at E2P2L.

The stainless steel reactors (i.d. 4 mm) were loaded from the bottom to the top as detailed in Figure 2-4. A first layer of 200  $\mu m$  SiC ensured the positioning of the catalyst within the isothermal zone in the reactor. The desired amount of catalyst was loaded as a second layer followed by 200  $\mu m$  SiC that facilitated the feed mixing and brought it up to the reaction temperature. The different layers were separated using glass wool.

Before the reaction, the catalysts were activated under a 20%v/v H<sub>2</sub>-N<sub>2</sub> flow mixture. The reactors were heated up to 500 °C at a rate of 5 °C·min<sup>-1</sup> and held at this temperature for 1 h. The reactors were then cooled down to the desired temperature under a H<sub>2</sub>-N<sub>2</sub> flow mixture. Subsequently, the temperature was stabilized under a N<sub>2</sub> flow, the reaction conditions were set and the system was stabilized for 1 h. The reactor outlet was cooled down to room temperature and liquid samples were recovered every hour. The gas outlet was passed through an acid trap to remove the unreacted NH<sub>3</sub>. Whenever the reaction conditions were changed, the reactor was stabilized for at least 1 h between two consecutive catalytic tests.

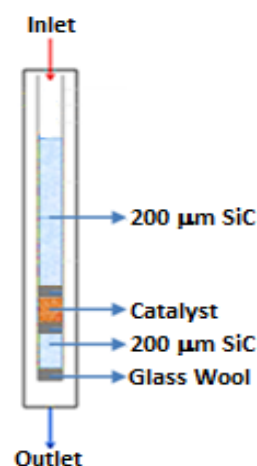


**Figure 2-4** Reactor filling scheme on the MPRS-3TC unit (ID=4 mm, stainless steel).

The reaction conditions RC-1 listed in Table 2-4 were used for screening the performance of monometallic catalysts (Annex I), bimetallic catalysts and the optimization of the impregnation sequence (Chapter 3). Furthermore, the reaction conditions RC-2 listed in Table 2-7 were used for the optimization of the noble metal loading on Ru- and Ag-promoted Co catalysts (Chapter 3).

**Table 2-4** Reaction conditions **RC-1** used for the catalytic screening of monometallic (Annex I) and bimetallic formulations based on Co (Chapter 3)

<b>Catalyst weight</b>	510 mg	[WHSV = 2.9 h <sup>-1</sup> ]
<b>NH<sub>3</sub> flow rate</b>	38.3 cm <sup>3</sup> (STP)/min	[9 equiv]
<b>H<sub>2</sub> flow rate</b>	10.7 cm <sup>3</sup> (STP)/min	[2.5 equiv]
<b>N<sub>2</sub> flow rate</b>	3.8 cm <sup>3</sup> (STP)/min	[0.9 equiv]
<b><i>n</i>-octanol flow rate</b>	1.8 mL·h <sup>-1</sup>	[1 equiv]
<b>Pressure</b>	1 bar	

**Table 2-5** Reaction conditions **RC-2** used for the loading optimization of Ru- and Ag-doped Co bimetallic catalysts (Chapter 3)

<b>Catalyst weight</b>	510 mg	[WHSV = 1.9 h <sup>-1</sup> ]
<b>NH<sub>3</sub> flow rate</b>	25.7 cm <sup>3</sup> (STP)/min	[9 equiv]
<b>H<sub>2</sub> flow rate</b>	9.6 cm <sup>3</sup> (STP)/min	[3.4 equiv]
<b>N<sub>2</sub> flow rate</b>	-	-
<b><i>n</i>-octanol flow rate</b>	1.2 mL·h <sup>-1</sup>	[1 equiv]
<b>Pressure</b>	1 bar	

The recovered liquid samples were analyzed offline using a GC (Agilent GC-7890A) equipped with a 30 m x 0.32 mm x 0.25 μm HP-5 column and a FID detector. The column was programmed with a 3 °C·min<sup>-1</sup> initial ramp from 80 °C to 100 °C followed by a 50 °C·min<sup>-1</sup> ramp to 300 °C and this temperature was held for 3 min. The conversion and yields (based on *n*-octanol) were calculated by interpolation using biphenyl as internal standard.

## 2.4.2 High Pressure Fixed Bed Reactor – TERCH

The catalytic tests for optimizing the process conditions were conducted in a high-pressure continuous fixed-bed reactor (Terch Scientific, Beijing) available at E2P2L (Solvay, China). The reactor was equipped with 3 standardized gas feeding streams, 2 liquid feeding streams, an automatic sampling system for exhaust gas (not used for this project) and a manual sampling system for liquid products. The main features of the system are shown in Figure 2-5. H<sub>2</sub>, N<sub>2</sub> and NH<sub>3</sub> were fed into the reactor using mass flow controllers ( $\pm 1\%$  accuracy) (Seven Star Electronics for H<sub>2</sub> and N<sub>2</sub> and Brooks for NH<sub>3</sub>). The liquid *n*-octanol was weighed using an electronic balance (Hengping/Lianmao, China) and the corresponding flowrate was controlled using a liquid metering pump ( $\pm 1\%$  accuracy, NS Japan). Liquid NH<sub>3</sub> could also be fed with a double-piston metering pump ( $\pm 1\%$  accuracy, Xingda, China). The gas-liquid mixture was prepared in a preheater evaporator and then fed into the reactor.

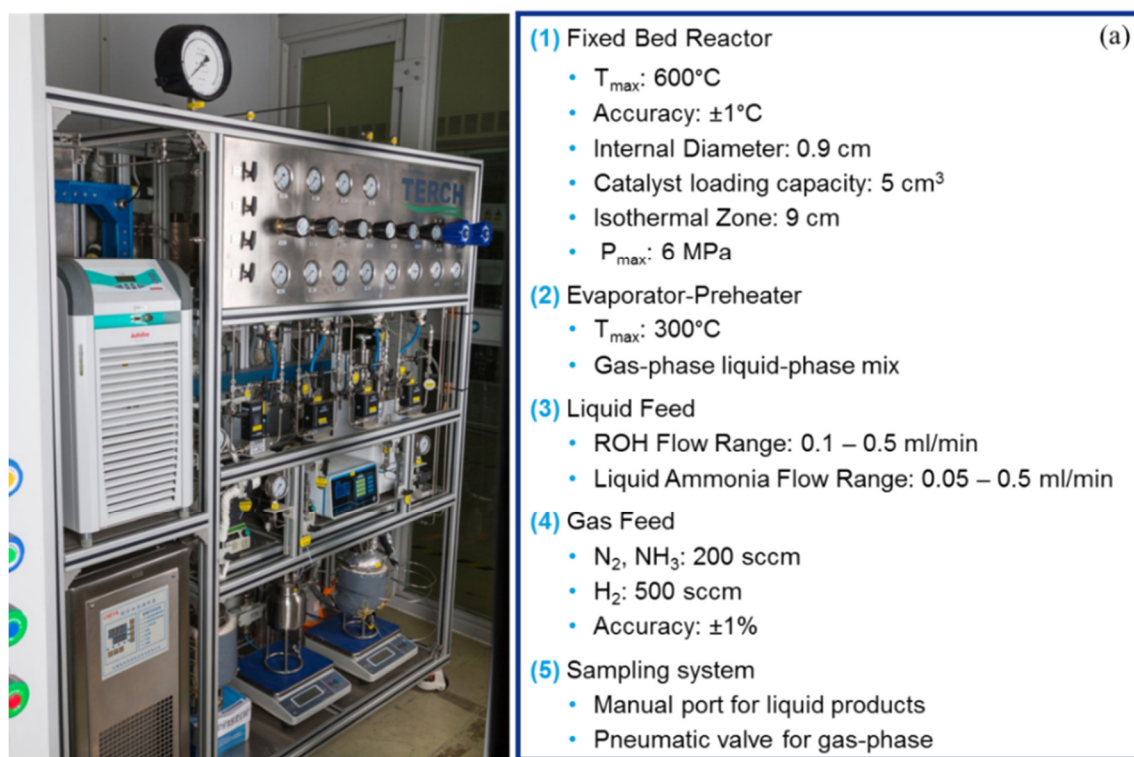
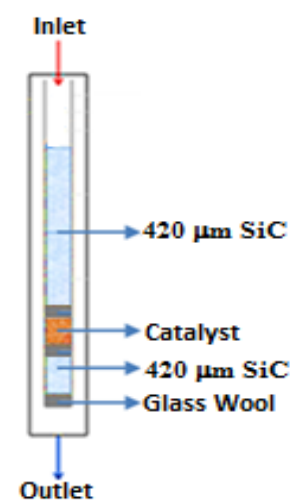


Figure 2-5 Image and details of fixed-bed reactor TERCH

The stainless-steel reactor (i.d. 9 mm, 5 cm<sup>3</sup> catalyst filling capacity) was located at the center of the reactor with an isothermal filling height of 90 mm (Figure 2-6). A bottom layer of 420  $\mu\text{m}$  SiC ensured the positioning of the catalyst within the isothermal zone of the reactor. The desired amount of catalyst was loaded as a middle layer followed by a top layer of 420  $\mu\text{m}$  SiC that facilitated a good feed mixture and brought it up to the reaction temperature. The different layers were separated by glass wool. The reaction mixture was fed from the top inlet radially and out from the bottom outlet axially.

Prior to the amination reaction, the catalyst was activated under a 20%v/v H<sub>2</sub>-N<sub>2</sub> flow mixture. The reactor was heated at 5 °C·min<sup>-1</sup> up to 500 °C and held at 500 °C for 1 h. The reactor was then cooled down to the desired temperature under a H<sub>2</sub>-N<sub>2</sub> flow mixture and further stabilized under a N<sub>2</sub> flow. The reaction mixture was passed through the catalyst bed in downflow mode. The catalysts typically attained steady-state performance after 1 h on stream. Unless otherwise stated, the reaction conditions RC-3 listed in Table 2-6 were used for optimizing the noble metal loading for Ru- and Ag-promoted Co catalysts and assessing the influence of the operational variables on the catalytic performance.

After the reaction, the product mixture entered the gas-liquid separation tank by cooling in a condenser. The condenser and gathering tank were equipped with cooling/heating jackets. The gas-phase mixture containing unreacted NH<sub>3</sub> was sent to a scrubber *via* a venting line. The liquid-phase product samples were collected at the manual sampling port for further analysis. The recovered liquid samples were analyzed in an offline GC (Thermo Scientific, Trace 1300) equipped with a 30 m x 0.32 mm x 0.25 μm Thermo Scientific TG-5MS column and a FID detector. The column was temperature-programmed with a 3 °C·min initial heating rate from 80 °C up to 100 °C, followed by a 50 °C·min<sup>-1</sup> rate up to 300 °C, and held at this temperature for 3 min. The conversion and yields (based on *n*-octanol) were measured by interpolation using biphenyl as internal standard.



**Figure 2-6** Reactor filling scheme on the TERCH reactor (ID=9 mm, stainless steel).

**Table 2-6** Reaction conditions **RC-3** used for the loading optimization of Ag and Ru doped cobalt bimetallic catalysts (Chapter 3).

<b>Catalyst weigh</b>	0.5-4.0 g	
<b>NH<sub>3</sub> flow rate</b>	25-200 cm <sup>3</sup> (STP)/min	[3-21 equiv]
<b>H<sub>2</sub> flow rate</b>	10-100 cm <sup>3</sup> (STP)/min	[3-15 equiv]
<b>N<sub>2</sub> flow rate</b>	-	-
<b><i>n</i>-octanol flow rate</b>	3.9-5.0 mL·h <sup>-1</sup>	[1 equiv]
<b>Pressure</b>	1-15 bar	
<b>Temperature</b>	160-220 °C	

### 2.4.3 High-Throughput Experiments – Flowrence® Unit

The high-throughput (HT) experiments for kinetic modelling were conducted in a Flowrence unit (Avantium, Netherlands) available at the REALCAT platform (UCCS, Lille). The Flowrence unit consists of 16 parallel fixed-bed reactors each one equipped with a liquid and a gas inlet. The 16 reactors are divided within 4 blocks with independent temperature control (Figure 2-7).

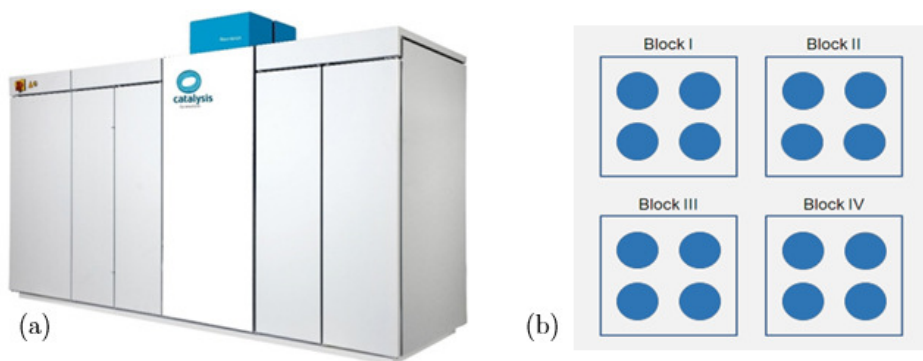


**Figure 2-7** (a) Flowrence unit by Avantium; (b) Reactor Block scheme of the Flowrence unit.

The inlet gas and liquid flowrates were adjusted using thermal mass flow controllers ( $\pm 1\%$  accuracy, Brooks) and a compact HPLC pump ( $\pm 1\%$  accuracy, Jasco PU-2080), respectively. The liquid flowrate variation between the reactors was lower than 3%. The liquid samples were recovered at the outlet of the reactors using a dedicated sampling robot. A simplified process flowsheet diagram of the unit is depicted in Figure 2-8. Fused silica capillaries were used to equalize the pressure drop differences between the reactors ensuring homogeneous flow (Figure 2-10). The stainless steel reactors (i.d. 2.4 mm) were loaded as indicated in Figure 2-9. A first a layer of 100  $\mu\text{m}$  SiC was used to ensure the positioning of the catalyst within the isothermal zone of the reactor. The desired amount of catalyst (10, 20 or 30 mg) was diluted with  $\gamma\text{-Al}_2\text{O}_3$  up to 100 mg and loaded as a second layer followed by 200  $\mu\text{m}$  SiC that facilitated a good mixture of the feed and brought it up to the reaction temperature. On top of the reactor, a glass sock avoided liquid dripping by favoring the liquid-gas contact and in turn its vaporization.

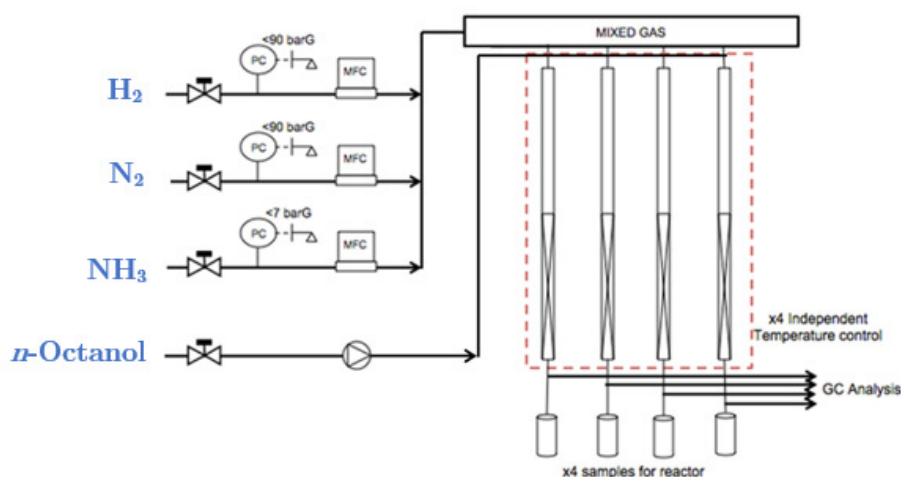


**Figure 2-8** Simplified plug flow diagram of the Flowrence unit.

Before the reaction, the catalysts were activated under a 20% v/v  $\text{H}_2\text{-N}_2$  flow mixture. The reactors were heated using a  $5 \text{ }^\circ\text{C}\cdot\text{min}^{-1}$  rate up to  $500 \text{ }^\circ\text{C}$  and held at this temperature for 1 h. The reactors were then cooled down to the desired temperature under a  $\text{H}_2\text{-N}_2$  flow mixture. After the reduction, the reaction conditions were set. The reaction sampling started after 1 h on stream for stabilization and the sample was collected during 1.5 h. Two

experimental conditions were tested in the course of each run, allowing 1.5 h between them for stabilization.

The recovered liquid samples were analyzed offline using a GC (Agilent GC-2010 Plus) equipped with a 30 m x 0.25 mm x 0.25 μm Zebron ZB-5MS column and a FID detector. The column was programmed with a 3 °C·min<sup>-1</sup> initial heating rate from 80 °C to 100 °C followed by a 50 °C·min<sup>-1</sup> rate to 300 °C and this temperature was held for 3 min. The conversion and yields (based on *n*-octanol) were calculated by interpolation of the calibration curves using 1,3-propanediol as internal standard.

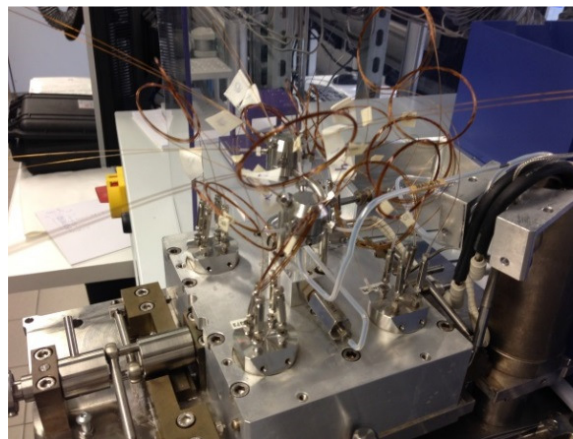


**Figure 2-10** Detail of the capillary distribution system of the Flowrence unit.

A full factorial design of experiments was implemented, affording the study of the influence of the different reaction variables, as well as their interactions. The temperature, the catalyst weight and the H<sub>2</sub> partial pressure were studied over three levels, while the *n*-octanol and NH<sub>3</sub> partial pressures were varied within two levels and a central point allowing a survey of non-linear effects. The range and levels of the studied variables are summarized in Table 2-7. The evaluated feed mixtures are represented within the experimental space in Figure 2-11. The experimental conditions are specified in Table 2-8. Overall, 126 experimental points were obtained and used for the evaluation of different kinetic models. The full list of tests is presented in Annex II.

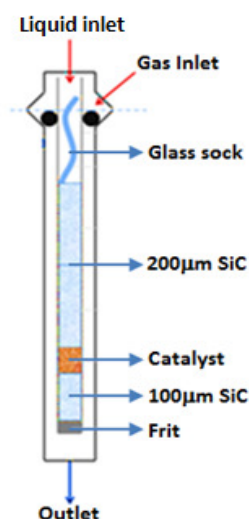


**Figure 2-9** Reactor filling scheme on the Flowrence unit (ID =2.4 mm, stainless steel).

**Table 2-7** Full factorial design of experiments for kinetic modeling (covered in Chapter 4)

Variable	Range	Levels
$P_{H_2}$	0.1-0.5 bar	3
$P_{R-OH}$	0.1-0.2 bar	2 + Central Point
$P_{NH_3}$	0.3-0.6 bar	2 + Central Point
Temperature	160-180 °C	3
Catalyst weight	10-30 mg	3

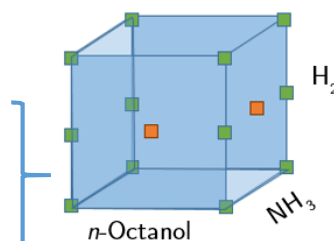


**Figure 2-11** Feed mixtures tested within the full factorial design.

**Table 2-8** Reaction conditions **RC-5** used for kinetic modeling (covered in Chapter 4)

<b>Catalyst weigh</b>	10-20-30 mg	-
<b>NH<sub>3</sub> flowrate</b>	2.8-4.2-5.6 cm <sup>3</sup> (STP)/min	[3-4.5-6 equiv]
<b>H<sub>2</sub> flowrate</b>	0.9-2.8-4.6 cm <sup>3</sup> (STP)/min	[1-3.0-5 equiv]
<b>N<sub>2</sub> flowrate</b>	Fill up to 14.8 cm <sup>3</sup> (STP)/min	-
<b><i>n</i>-octanol flowrate</b>	0.36-0.54-0.72 mL·h <sup>-1</sup>	[1-1.5-2 equiv]
<b>Pressure</b>	2 bar	-
<b>Temperature</b>	160-180°C	-

## 2.5 Kinetic Modeling

A detailed kinetic modeling was carried out to rationalize the influence of the different operation parameters for *n*-octanol amination with NH<sub>3</sub>. As the reaction rates may vary with the position in the reactor, it is necessary to integrate the kinetic expressions over the reactor length/radius and consider an appropriate hydrodynamic model. Overall, the kinetic study comprised the following steps:

1. **Development of kinetic expressions:** different kinetic models were formulated taking into account previous knowledge of the reaction mechanism and the observed experimental trends as a function of the operation variables. The reader will find more detailed information in Chapter 4.
2. **Reactor modeling:** the kinetic expressions were incorporated in the reactor mass balances and integrated over the reactor length/radius. The validity of the proposed flow model is discussed in section 2.5.1 and the corresponding mass balance expressions are presented in section 2.5.2.
3. **Parameter optimization:** the model variables were adjusted using an iterative algorithm that minimizes the sum of square differences between the experimental and predicted data (partial pressures of *n*-octanol and N-products) at the reactor outlet. Further details can be found in section 2.5.3.
4. **Validation of the models:** kinetic models including positive adsorption enthalpies and negative activation energies or rate constants lacking of physical consistency were rejected. Kinetic models providing incoherent values for different parameters due to low sensitivity and correlation effects were also rejected.
5. **Statistical analysis:** the kinetic models were judged by their capacity of convergence, goodness of fit, random error distribution and accuracy of the fitted parameters. More details on the statistical methods used are presented in section 2.5.4.

### 2.5.1 Fixed Bed Flow Model

The kinetic models were implemented by assuming isothermal plug-flow reactor (PFR) hydrodynamics with neither heat nor radial/axial diffusion. This model assumes a flat velocity profile within the reactor, implying an equivalent residence time for all the fluid elements. In the following lines we will assess the validity of this model for describing

the hydrodynamics of our reactor using well-established heuristic criteria and related literature.

(iii) Axial dispersion

Flow-through packed-bed reactors may present some degree of backmixing due to, for instance, molecular diffusion. To minimize this effect, the reactor length must be long enough so that the dispersion front becomes negligible. Mears [8,9] proposed a criterion (Eq. 2-4) for determining the minimum reactor length for mitigating dispersion effects. The application of this criterion (see calculation details in Annex III) validates the assumption of negligible axial dispersion for our reactor.

$$\frac{L}{d_p} > \frac{20}{Pe_a} \ln \frac{C_0}{C_f} \quad \Bigg| \quad \text{Eq. 2-4}$$

Likewise, the effect of temperature differences over the longitudinal axis can be neglected for reactors presenting a length-to-particle diameter ratio above 30 [8]. In our case, since the ratio of bed length (>25 mm) to particle (~0.15 mm) in our reactor (Flowrence unit) was 166, the temperature can be considered constant along the reactor length.

(iv) Radial dispersion

Radial dispersion effects are generally caused by thermal gradients normal to the reactor flow and may drastically alter the reaction rate across the radius. This effect can be minimized when working with small reactor diameters and under bed dilution. In our case, the effect of radial thermal profiles can be neglected considering the small reaction enthalpy ( $\Delta H^\circ = -13 \text{ kJ}\cdot\text{mol}^{-1}$ ) and small reactor diameter (i.d. 2.4 mm). Radial dispersion caused by eddy or molecular diffusion is generally small, since the corresponding Péclet numbers are about one order of magnitude higher than the axial Péclet numbers [10,11] and can accordingly be safely neglected.

(v) Wall effects

Velocity profiles may exist within packed-bed reactors due to local differences in bed porosity. As a rule, the catalyst is less closely packed near to the walls, creating a zone of maximum speed at about one particle diameter from the wall. This effect can be minimized by using larger reactor diameter-to-particle ratios. A minimum ratio between 8 and 15 is commonly proposed to ensure negligible wall effects [12,13]. Since in our reactor the ratio of the reactor diameter (2.4 mm) to particle (~0.15 mm) was 16, wall effects can be regarded as negligible.

(vi) Mass and Heat Transfer Limitations on the Catalyst

The kinetics in catalytic reactors can be affected by heat and mass diffusion between the fluid and the particle (external transfer) and within the catalyst pores (internal transfer). In our case, heat transfer can be omitted due to the low reaction enthalpy for *n*-octanol amination with  $\text{NH}_3$  ( $\Delta H^\circ = -13 \text{ kJ}\cdot\text{mol}^{-1}$ ), the small reactor diameter (i.d. 2.4 mm), and the use of bed dilution (1/10-3/10). The absence of inter- and intraparticle mass/heat transfer

limitations are assessed below on the guidance of well-established heuristic criteria and literature examples.

### External Mass Transfer

External mass transfer can become rate limiting when the reactants are consumed on the catalyst surface at a faster rate than their corresponding diffusion rate from the bulk solution. This effect can be minimized by increasing the reactant flow speed or by decreasing the intrinsic reaction rate (*e.g.*, by decreasing the temperature or the catalyst loading). The criterion proposed by Mears [8] is widely used for assessing the influence of external mass/heat transfer limitations (Eq. 2-5).

$$\frac{-r_{\text{ROH}(obs)} \rho_b R_p n}{k_g C_{\text{ROH}}} < 0.15 \quad \Bigg| \quad \text{Eq. 2-5}$$

In our case, this criterion is satisfied, since Eq. 2-5 is fulfilled (0.07, see calculation details in Annex III). Accordingly, we can safely assume the absence of mass transfer limitations on the measured reaction rates.

### Internal Mass Transfer

Internal mass/heat transfer can become rate-controlling when diffusion within the catalyst pores becomes slower than the intrinsic reaction rate. This effect is especially relevant for fast reactions occurring in micro- and mesoporous catalysts. Internal mass/heat transfer limitations can be discouraged by decreasing the particle size. The Weisz-Prater criterion [14] is generally accepted for assessing the influence of pore diffusion on the experimental reaction rates. For first-order reactions, the criterion is expressed using Eq. 2-6. With a value of 0.09 (see calculation details in Annex III), this criterion is fulfilled for our reactor, confirming negligible contribution of intraparticle mass transfer to the experimental reaction rates.

$$\frac{-r_{\text{ROH}(obs)} \rho_c R_p^2}{D_{\text{ROH}} C_{\text{ROH}}} < 0.6 \quad \Bigg| \quad \text{Eq. 2-6}$$

## **2.5.2 Mathematical description of the reactor hydrodynamics**

As discussed in the previous section, the isothermal PFR model appears to be a good choice for representing the hydrodynamics of our fixed-bed reactor. The PFR model consists of an open tube with material entering and leaving the system boundaries. In this model, mass balances are conducted over a differential volume (plug) of the tube with the assumptions that: (i) all the volume elements have the same residence time on the reactor, (ii) radial mixing is instantaneous, and (iii) no axial mixing exists between adjacent plugs (Figure 2-12). Assuming steady-state operation, the mass balance for a given compound *i* can be represented by an ordinary differential equation (Eq. 2-7).

$$\frac{dF_i}{dM_c} = -r_i \quad \begin{array}{l} \text{Initial conditions:} \\ M_c = 0 \rightarrow F_i = F_{i,0} \end{array} \quad \Bigg| \quad \text{Eq. 2-7}$$

The different kinetic models developed in this study, all based on Langmuir-Hinshelwood type kinetics (see Chapter 4 and Annex IV for details) were incorporated into the material balances and solved numerically using the Matlab functions *ode45* or *ode15s* [15]. The *ode45* function is a one-step solver based on an explicit Runge-Kutta (4,5) formula, while the *ode15s* is a multistep solver based on numerical differentiation formulas, more suitable for stiff systems. Both solvers use adaptive step-size discretization to minimize the integration error (relative error <0.1%) and ensure stability. The solver operates inside a “for” loop, evaluating the 42 experimental conditions.

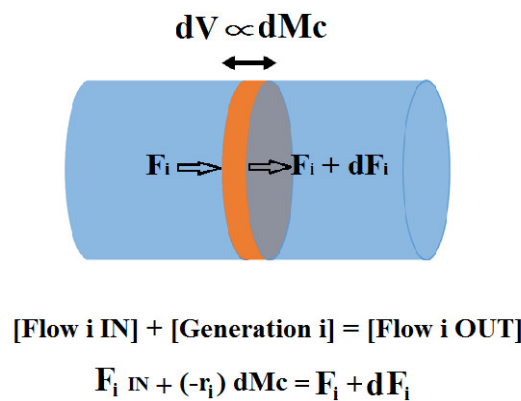


**Figure 2-12** Differential volume ( $dV$ ) or its equivalent in mass of catalyst ( $dM_c$ ) for a PFR, with  $F$  and  $r$  being the flow and rate of consumption per unit mass of catalyst for reactant  $i$ .

### 2.5.3 Least Squares - Kinetic Fitting

The different kinetic models for  $n$ -octanol amination with  $\text{NH}_3$  were fitted using the non-linear curve-fitting function *lsqcurvefit* available in Matlab software [16]. The kinetic and thermodynamic parameters of the models were fitted using the Levenberg-Marquardt or L-M algorithm based on least-square minimization of the square distance between the experimental and predicted partial pressures of  $n$ -octanol and  $N$ -products at the reactor outlet (Eq. 2-8)

$$\min \sum [f(Z, P) - y_{\text{exp.}}]^2 \quad \Bigg| \quad \text{Eq. 2-8}$$

where  $Z$  is a vector including the model parameters,  $P$  is a vector including the reaction variables (feed composition, flow, temperature, pressure and mass of catalyst),  $f(Z, P)$  is a vector including the model output and  $y_{\text{exp}}$  is a vector including the experimental data ( $n$ -octanol conversions, yields to different products).

The L-M algorithm operates through an iterative procedure. To start the optimization, the user provides an initial estimate for  $Z$  named  $Z_0$ . In each iteration the parameter vector  $Z_n$  is replaced by a new estimate ( $Z_n + \delta_K$ ), which is calculated by a linear approximation of  $f(Z, P)$  in the neighborhood of  $Z$ . The algorithm adaptively varies the parameter updates

between the gradient descent and the Gauss-Newton methods using a damping factor  $\gamma$ . Initially, a large  $\gamma$  is set so that first updates are small steps in the steepest-descent direction. As the solution is improved,  $\gamma$  is decreased and the solution accelerates towards the local minimum. In the case an iteration results in a worse approximation,  $\gamma$  is again increased, proceeding through the steepest-descent method. A comprehensive flow-chart is presented in Figure 2-13. More information on the L-M algorithm can be found in dedicated literature [17,18].

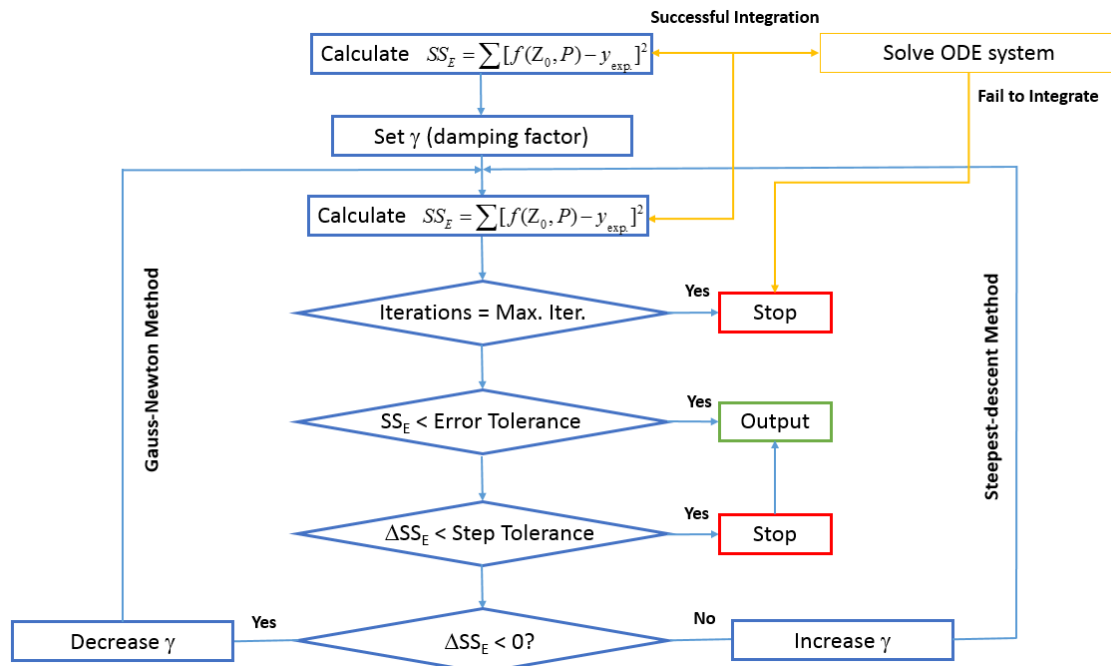


**Figure 2-13** Iterative optimization Levenberg-Marquardt algorithm simplified flow chart ( $SS_E$ =sum of squared error,  $Z$ = vector of parameters,  $P$ =reaction variables and  $y_{exp}$ =experimental values).

## 2.5.4 Quality of the Fittings – Statistical Analysis

The discrimination between the different kinetic models was carried out by statistical analysis of the fittings. The goodness of fit, the correlation matrix and the confidence intervals of the fitted parameters were computed to assess the quality of the fittings. Finally, the residuals were analyzed and checked for establishing their patterns. At equal quality of the fitting, the simpler model would be chosen as the preferred one. The statistical expressions used in this section and summarized below can be found in dedicated literature [19–23].

The goodness of fit was measured in terms of the residual sum of squares ( $SS_E$ ) and the coefficient of determination ( $R^2$ ). Both descriptors were calculated using Eq. 2-9 and Eq. 2-10, respectively. It is important to notice that a superior  $R^2$  value does not imply *per se* a better model unless  $SS_E$  is minimized.

$$SS_E = \sum (y_i - \hat{y}_i)^2 \quad \Bigg| \quad \text{Eq. 2-9}$$

$$R^2 = 1 - \frac{SS_E}{SS_T} = 1 - \frac{\sum (y_i - \hat{y}_i)^2}{\sum (y_i - \bar{y}_i)^2} \quad \text{Eq. 2-10}$$

The 95% confidence interval for the optimized parameters was calculated according to Eq. 2-11, where  $t_{1-\alpha}$  refers to the Student-t (1.96 for 95% confidence interval), and  $\text{cov}_{jj}$  are the diagonal elements of the variance-covariance matrix (Eq. 2-12).

$$CI_j = \pm t_{1-0.05/2} \sqrt{\text{cov}_{jj}} = 1.96 \sqrt{\text{cov}_{jj}} \quad \text{Eq. 2-11}$$

$$\text{cov} = (J^T \times J)^{-1} MS_E = \frac{SS_E}{n_y - n_p} (J^T \times J)^{-1} \quad \text{Eq. 2-12}$$

where J is the Jacobian matrix and  $MS_E$  is the mean square error that is calculated by dividing  $SS_E$  by the number of degrees of freedom  $n_y - n_p$ , where  $n_y$  and  $n_p$  refer to the number of experiments and parameters, respectively.

The Jacobian matrix is a  $(n_y \times n_p)$  matrix representing the first-order partial derivatives of the least-squares function. This matrix is numerically computed at each iteration step of the Levenberg-Marquardt algorithm by evaluating the function change in the vicinity of each parameter as expressed by Eq. 2-13. The approximation of the Jacobian matrix at the optimized solution is retrieved and used to estimate the different parameters.

$$J_{ij} = \frac{\partial f(y_i)}{\partial P_j} \quad \text{Eq. 2-13}$$

where  $f(y_i)$  is the function value at the point  $y_i$ .

The correlation matrix (corr) was calculated as expressed in Eq. 2-14, where % indicates element-wise matrix division. The resulting square matrix is a standardized version with unit variances of the covariance matrix, ranging in values from -1 to +1, both included. Values  $> |0.95|$  indicate high correlation between the fitted parameters.

$$\text{corr} = \text{cov} \% \sqrt{(\text{cov}_{jj} \times \text{cov}_{jj}^T)} \quad \text{Eq. 2-14}$$

Multicollinearity between the fitted parameters was assessed by means of the variance inflation factor (VIF), which was calculated according to Eq. 2-15. A VIF  $> 10$  for a given parameter is generally considered as a sign of multicollinearity for that parameter.

$$VIF = \text{diag}(\text{corr}^{-1}) \quad \text{Eq. 2-15}$$

Finally, the residuals from the regression model were standardized using the sample variance according to Eq. 2-16

$$d_i = \frac{(y_i - \hat{y}_i)}{\sqrt{MS_E}} \quad \text{Eq. 2-16}$$

The standardized residuals were plotted against the experimental values and checked for outliers and patterns. Ideally, 95% of the residuals should fall between  $\pm 1.96\sqrt{MS_E}$ , have an almost zero mean and be randomly distributed. Typical patterns found in residual analysis are summarized in Figure 2-14.

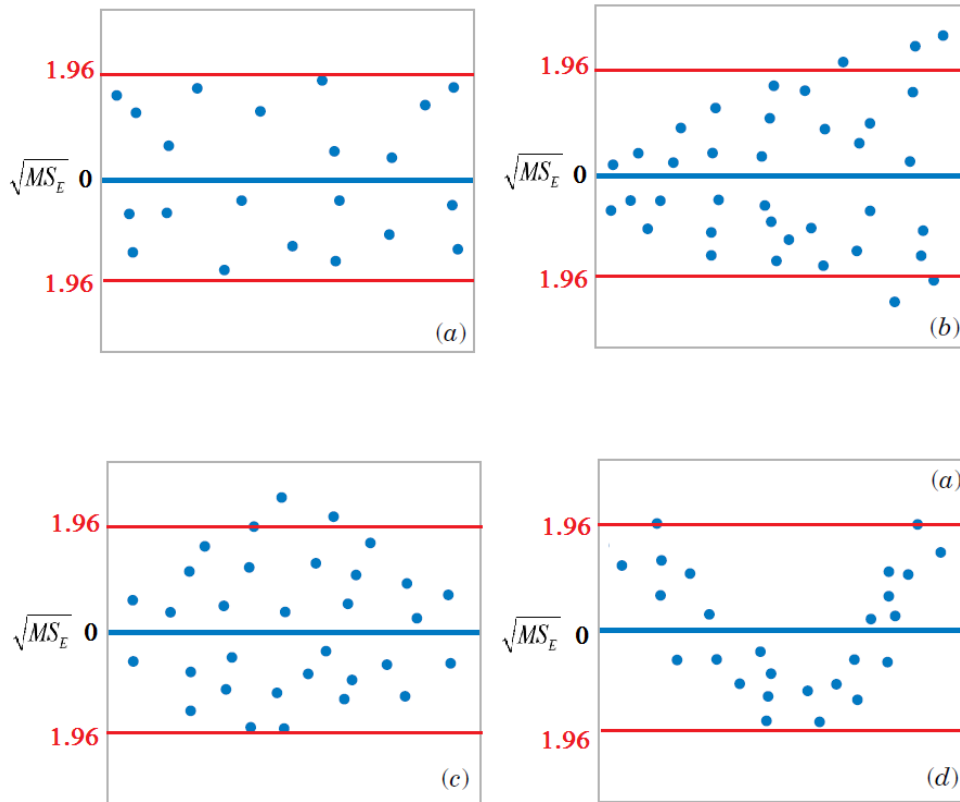


**Figure 2-14** Typical patterns from standardized residual plots, (a) satisfactory, (b) funnel, (c) double bow, and (d) non-linear (Adapted from [19]).

## 2.6 Nomenclature

$y_i$	Experimental data
$\bar{y}_i$	Mean of experimental data
$\hat{y}_i$	Predicted data
C	Concentration ( $\text{mmol}\cdot\text{mL}^{-1}$ )
CI	Confidence interval
corr	Correlation matrix
cov	Variance-covariance matrix
d	Diameter
di	Standardized residuals
F	Mass/Molar Flow
J	Jacobian matrix
K	Dimensionless shape factor ( $\sim 0.9$ )
$k_g$	Mass transport coefficient ( $\text{cm}\cdot\text{s}^{-1}$ )
L	Reactor Length
$\text{MS}_E$	Mean squared error of residuals
N	Number of moles
n	Reaction order
$n_p$	Number of parameters
$n_y$	Number of experimental points
P	Vector of reaction variables
Pe	Péclet number
R	Radius (cm)
r	Reaction rate ( $\text{mmol}\cdot\text{g}\cdot\text{cat}^{-1}\cdot\text{s}^{-1}$ )
R <sup>2</sup>	Coefficient of determination
$\text{SS}_E$	Squared sum of residuals
$\text{SS}_T$	Total sum of squares
Z	Vector of model parameters

### Subscripts:

0	Initial
A	Axial
b	Catalytic Bed
c	Catalyst
exp.	Experimental
f	Final
obs	Observed
p	Particle
r	Radial

### Greek Letters

$\theta$	Diffraction angle
$\delta_K$	Parameter update factor in L-M algorithm
$\beta$	Peak Broadening at half maximum intensity ( $\Delta(2\theta)$ , in radians)
$\gamma$	L-M damping factor
$\lambda$	X-ray wavelength
$\rho$	Density ( $\text{g}\cdot\text{L}^{-1}$ )
$\tau$	Mean crystallite size

## 2.7 References

- [1] S. Brunauer, P.H. Emmett, E. Teller, Adsorption of Gases in Multimolecular Layers, *J. Am. Chem. Soc.* 60 (1938) 309–319. doi:10.1021/ja01269a023.
- [2] E.P. Barrett, L.G. Joyner, P.P. Halenda, others, The determination of pore volume and area distributions in porous substances. I. Computations from nitrogen isotherms, *J Am Chem Soc.* 73 (1951) 373–380.
- [3] H.M. Koo, T. Tran-Phu, G.-R. Yi, C.-H. Shin, C.-H. Chung, J.-W. Bae, Effect of the ordered meso–macroporous structure of Co/SiO<sub>2</sub> on the enhanced activity of hydrogenation of CO to hydrocarbons, *Catal Sci Technol.* 6 (2016) 4221–4231. doi:10.1039/C5CY01685A.
- [4] R.D. Jones, C.H. Bartholomew, Improved flow technique for measurement of hydrogen chemisorption on metal catalysts, *Appl. Catal.* 39 (1988) 77–88. doi:10.1016/S0166-9834(00)80940-9.
- [5] A. Martínez, C. López, F. Márquez, I. Díaz, Fischer–Tropsch synthesis of hydrocarbons over mesoporous Co/SBA-15 catalysts: the influence of metal loading, cobalt precursor, and promoters, *J. Catal.* 220 (2003) 486–499. doi:10.1016/S0021-9517(03)00289-6.
- [6] East Paris Institute of Chemistry and Materials Science - TEM FEI Tecnai F20, (n.d.). <http://www.icmpe.cnrs.fr/spip.php?article740&lang=en> (accessed April 21, 2017).
- [7] G.S. Sewell, E. van Steen, C.T. O'Connor, Use of TPR/TPO for characterization of supported cobalt catalysts, *Catal. Lett.* 37 (1996) 255–260.
- [8] D.E. Mears, Tests for transport limitations in experimental catalytic reactors, *Ind. Eng. Chem. Process Des. Dev.* 10 (1971) 541–547.
- [9] H.F. Rase, Fixed-bed reactor design and diagnostics: gas-phase reactions, Butterworths, Boston, 1990.
- [10] M.E. Davis, R.J. Davis, Fundamentals of chemical reaction engineering, International ed, McGraw-Hill, Boston, 2003.
- [11] R.H. Wilhelm, Progress towards the a priori design of chemical reactors, *Pure Appl. Chem.* 5 (1962). doi:10.1351/pac196205030403.
- [12] M.O. Tarhan, Catalytic reactor design, McGraw-Hill, 1983.
- [13] J. Ancheyta, Modeling and Simulation of Catalytic Reactors for Petroleum Refining, John Wiley & Sons, 2011.
- [14] P.B. Weisz, C.D. Prater, Interpretation of Measurements in Experimental Catalysis, *Adv. Catal.* 6 (1954) 143–196. doi:10.1016/S0360-0564(08)60390-9.
- [15] Choose an ODE Solver - MATLAB & Simulink - MathWorks España, (n.d.). <https://es.mathworks.com/help/matlab/math/choose-an-ode-solver.html> (accessed May 17, 2017).
- [16] Solve nonlinear curve-fitting (data-fitting) problems in least-squares sense - MATLAB lsqcurvefit - MathWorks España, (n.d.). <https://es.mathworks.com/help/optim/ug/lsqcurvefit.html> (accessed April 21, 2017).
- [16] K. Levenberg, A method for the solution of certain non-linear problems in least-squares, *Q. Appl. Math.* 2 (1944) 164–168.
- [18] D. Marquardt, An Algorithm for Least-Squares Estimation of Nonlinear Parameters, *J. Soc. Ind. Appl. Math.* 11 (1963) 431–441. doi:10.1137/0111030.
- [19] D.C. Montgomery, G.C. Runger, Applied statistics and probability for engineers, 3rd ed, Wiley, New York, 2003.
- [20] W.C. Navidi, Statistics for engineers and scientists, 3rd ed, McGraw-Hill, New York, 2011.
- [21] S. Chatterjee, J.S. Simonoff, Handbook of regression analysis, Wiley, Hoboken, New Jersey, 2013.
- [22] D.M. Himmelblau, Process analysis by statistical methods, Wiley, New York, 1970.
- [23] D.A. Belsley, Regression diagnostics: identifying influential data and sources of collinearity, Wiley-Interscience, Hoboken, N.J, 2004.

---

## **Chapter 3**

### **Cobalt-based Bimetallic Catalysts for the Direct Amination of *n*-octanol**

---



### 3.1 Background

As already discussed in Chapter 1, the direct amination of alcohols *via* the H<sub>2</sub> borrowing mechanism emerges as an atom-efficient, step-efficient and ecologically responsible route for the industrial synthesis of amines. Numerous examples of heterogeneous metal-supported catalysts for amination reactions have been reported both in the open and patent literature. However, as of today, the available catalytic formulations suffer from important limitations, especially when regarding the synthesis of primary amines. In this view, the development of efficient and selective catalysts for the mono-alkylation of NH<sub>3</sub> with alcohols could help to diminish the environmental footprint of current industrial processes.

With the purpose of identifying performing catalysts for amination reactions, a library of catalysts was prepared comprising Pd, Pt, Au, Ni, Co and Cu supported over SiO<sub>2</sub>, TiO<sub>2</sub>, Al<sub>2</sub>O<sub>3</sub>, CeO<sub>2</sub> and Fe<sub>2</sub>O<sub>3</sub>. The catalysts were further screened for the gas-phase amination reaction between *n*-octanol and NH<sub>3</sub> (Annex I). From this preliminary study, Co/ $\gamma$ -Al<sub>2</sub>O<sub>3</sub> emerged as the most selective formulation towards aliphatic primary amines. Nonetheless, this catalyst suffers from low activity (molar basis) compared to supported Ni or Pt, most likely due to a strong metal-support interaction [1–3]. Numerous examples of noble-metal dopants used to enhance the Co reducibility can be found in the literature, mostly related to Fischer-Tropsch synthesis [4–12]. Moreover, examples on Pd [13] and Ru-promoted Co catalysts have been reported in the patent literature for direct alcohol amination [14,15]. Since noble metal oxides can be reduced at lower temperatures than cobalt oxide [16], these can dissociatively chemisorb H<sub>2</sub>. The as-generated hydrides can eventually migrate to nearby Co oxide particles, removing oxygen atoms and thus reducing cobalt oxide to its active metallic phase. The nature of the noble metal [10], the impregnation protocol [12], and the metal/Co atomic ratio [11] can greatly impact the catalytic performance.

In this context, a series of noble-metal promoters (*e.g.*, Au, Pd, Pt, Ru and Ag) were used for enhancing the catalytic activity of Co/ $\gamma$ -Al<sub>2</sub>O<sub>3</sub> for conducting the gas-phase amination reaction of *n*-octanol and NH<sub>3</sub> to *n*-octylamine (OA). To survey the promoting effect of the different noble metals and preparation protocols in detail, the different bimetallic catalysts were prepared over the same batch of a model Co catalyst, *i.e.* 5%Co/ $\gamma$ -Al<sub>2</sub>O<sub>3</sub> (see Chapter 2 for details).

Along this chapter, the effect of the nature of the noble metal will be first assessed using the OA yield as descriptor of the catalytic performance. Second, the effect of the type of promoter, impregnation sequence and loading will be evaluated to attain optimal catalytic formulations. Third, the influence of the NH<sub>3</sub> and H<sub>2</sub> partial pressures on the catalytic activity and selectivity will be studied as an attempt to decouple pure Co reduction enhancement effects from a co-catalytic role of the noble metal. Finally, the process conditions will be optimized for the best performing catalyst targeting the highest OA yield. The catalytic results will be analyzed in parallel with relevant characterization techniques (*i.e.* TPR, XRD, STEM-HAADF), allowing a deep understanding of the catalytic behavior.

## 3.2 Effect of the nature of the dopant

A series of 5%Co/ $\gamma$ -Al<sub>2</sub>O<sub>3</sub> catalysts doped with different noble metals (NM) were manually prepared by sequential incipient wetness impregnation (IWI). The promoters were impregnated in a second step over the same catalyst batch (1.5%a/a). This allowed to better study the net influence of the noble metal by minimizing side effects such as changes in Co dispersion. Table 3-1 lists the catalysts prepared, as well as the corresponding weight loading of noble metals.

**Table 3-1** List of catalysts synthesized to study the influence of the nature of the noble metal dopant (1.5% a/a) on the catalytic performance of 5%Co/ $\gamma$ -Al<sub>2</sub>O<sub>3</sub>

Catalyst <sup>(a)</sup>	NM promoter	Promoter a/a
5%Co/ $\gamma$ -Al <sub>2</sub> O <sub>3</sub> -Benchmark	-	-
5%Co-0.25%Pt/ $\gamma$ -Al <sub>2</sub> O <sub>3</sub>	Pt	1.5%
5%Co-0.14%Pd/ $\gamma$ -Al <sub>2</sub> O <sub>3</sub>	Pd	1.5%
5%Co-0.14%Ag/ $\gamma$ -Al <sub>2</sub> O <sub>3</sub>	Ag	1.5%
5%Co-0.25%Au/ $\gamma$ -Al <sub>2</sub> O <sub>3</sub>	Au	1.5%
5%Co-0.13%Ru/ $\gamma$ -Al <sub>2</sub> O <sub>3</sub>	Ru	1.5%

(a) Theoretical weight %; calculated from the mass of precursor used in the preparation

The synthesized catalysts were tested in the gas-phase amination of *n*-octanol with NH<sub>3</sub>. The reaction was carried under the operation conditions RC-1 (Table 2-4). The main products formed were *n*-octylamine (OA), octanenitrile (ON) and di-*n*-octylamine (DOA). Side products such as di-*n*-octylimine (DOI) were detected in trace amounts. The results are compiled in Figure 3-1-(a). Among the different noble metals, Pt and Pd exhibited the highest activity increase, the *n*-octanol conversion being enhanced from 25% for the parent 5%Co/ $\gamma$ -Al<sub>2</sub>O<sub>3</sub> to 44% and 32% for Pt and Pd-promoted catalysts, respectively. Ag and Ru only afforded a slight increase in activity with a *n*-octanol conversion of 28% and 29%, respectively. Opposing these trends, Au dropped the *n*-octanol conversion down to 15%. In terms of TOF, the intrinsic activity of the catalysts decreased with the extent of reduction as shown in Figure 3-1-(b). The Au-promoted catalyst was out of the trend, suggesting a poisoning effect of Au.

Turning now our attention into the selectivity, Pt and Pd exerted a negative impact towards OA, transforming 11% of *n*-octanol into DOA. The remaining noble metals kept the OA selectivity with only traces of DOA (yield <0.5%). Overall, the highest OA yields were achieved with Pt (20%), Ag (18%) and Ru (17%). Since Ag and Ru maintained a good OA selectivity towards, both noble metals were kept in the remainder of our study.

To rationalize the mechanism behind the loss of selectivity over the Pt- and Pd-promoted 5%Co/ $\gamma$ -Al<sub>2</sub>O<sub>3</sub> catalysts, an equimolar mixture of OA, ON and water was fed to the reactor under the same conditions as in the screening tests. The reaction was carried over Pt- and Ru-promoted catalysts as contrasting examples of selectivity. As evidenced from Figure 3-2, the Pt-promoted sample exhibited a much higher capacity for DOA formation. These results suggest the activation of undesired side reactions, such as amine

disproportionation (Reaction 3-1) or nitrile-amine reductive condensation (Reaction 3-2) in the presence of Pt according to the pathway described by Gomez *et al.* [17].

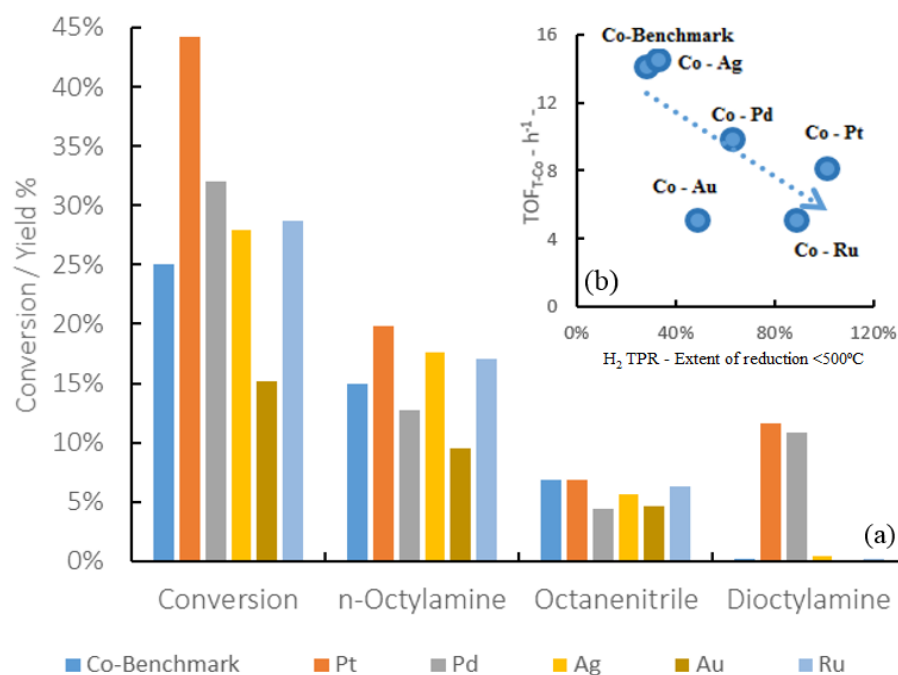


**Figure 3-1** (a) Conversion and yields in the amination of *n*-octanol with NH<sub>3</sub> over 5%Co/ $\gamma$ -Al<sub>2</sub>O<sub>3</sub> doped with noble metals (1.5% a/a Pt, Pd, Ag, Au and Ru). (b) Turnover frequency based on moles of amine formed per hour and per mole of reduced Co vs extent of reduction (calculated from H<sub>2</sub>-TPR <500°C, see below). Catalysts prepared by sequential impregnation, 1<sup>st</sup> Co, 2<sup>nd</sup> NM. Reaction conditions: 180 °C; NH<sub>3</sub> : H<sub>2</sub> : N<sub>2</sub> : ROH (mol%)= 9 : 2.5 : 0.9 : 1; WHSV<sub>ROH</sub> = 2.9 h<sup>-1</sup>; P=1 bar. Carbon balance in the range 95-99% for all the catalytic tests.

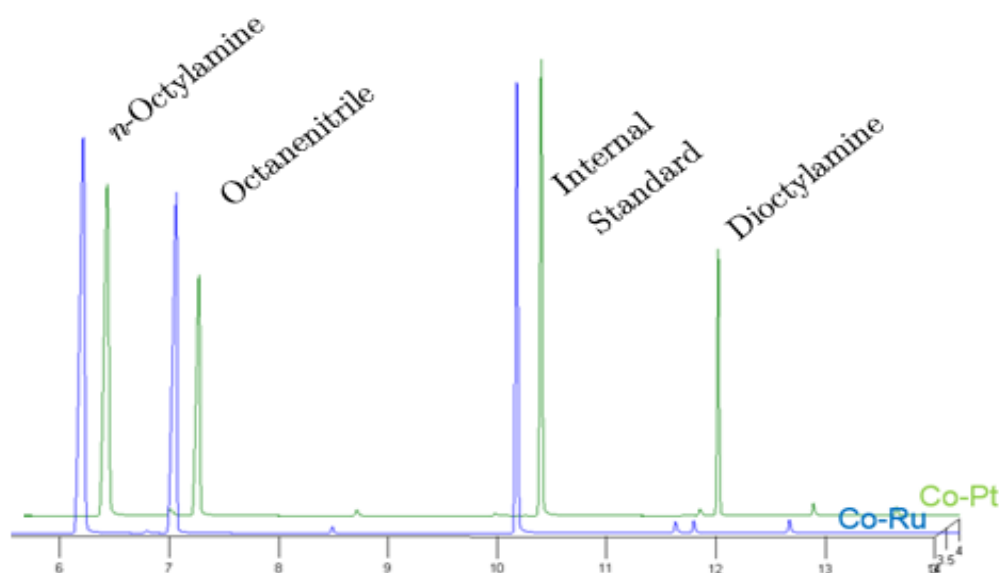
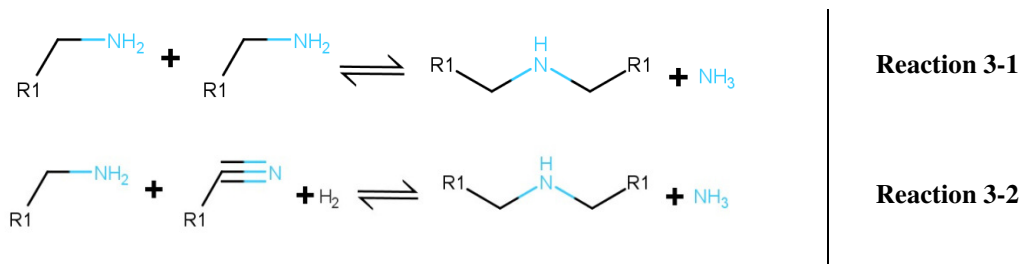


**Figure 3-2** GC chromatograms for the reaction of OA with ON in the presence of water. Reaction conditions: 180 °C; P=1 bar; NH<sub>3</sub> : H<sub>2</sub> : N<sub>2</sub> : ROH (mol%) = 9 : 2.5 : 0.9 : 1; WHSV<sub>ROH</sub> = 2.9 h<sup>-1</sup>.



### 3.3 Effect of the Impregnation Sequence for Ru- and Ag-doped 5%Co/Al<sub>2</sub>O<sub>3</sub>

In a subsequent step, the effect of the impregnation sequence (i.e. sequential impregnation of either Co or the noble metal, and coimpregnation) was studied for Ru- and Ag-doped 5%Co/ $\gamma$ -Al<sub>2</sub>O<sub>3</sub> catalysts (1.5%*a/a*). Overall, six catalysts were prepared according to the protocols described in Chapter 2 (Table 3-2). For clarity, the different catalysts will be termed hereinafter as Co(X) for coimpregnated catalysts and Co-X and X-Co for the sequentially impregnated samples, where X stems for either Ru or Ag.

**Table 3-2** List of catalysts synthesized to study the influence of the impregnation sequence on the promoting effect of Ru and Ag (1.5%*a/a*) over 5%Co/ $\gamma$ -Al<sub>2</sub>O<sub>3</sub>

Catalyst	Promoter	Promoter <i>a/a</i>	Impregnation <sup>(a)</sup>
5%Co/ $\gamma$ -Al <sub>2</sub> O <sub>3</sub> -Benchmark	-	-	-
5%Co-0.13%Ru/ $\gamma$ -Al <sub>2</sub> O <sub>3</sub>		1.5%	S – 1 <sup>st</sup> Co, 2 <sup>nd</sup> Ru
0.13%Ru-5%Co/ $\gamma$ -Al <sub>2</sub> O <sub>3</sub>	Ru	1.5%	S – 1 <sup>st</sup> Ru, 2 <sup>nd</sup> Co
5%Co(0.13%Ru)/ $\gamma$ -Al <sub>2</sub> O <sub>3</sub>		1.5%	Coimpregnation
5%Co-0.14%Ag/ $\gamma$ -Al <sub>2</sub> O <sub>3</sub>		1.5%	S – 1 <sup>st</sup> Co, 2 <sup>nd</sup> Ag
0.14%Ag-5%Co/ $\gamma$ -Al <sub>2</sub> O <sub>3</sub>	Ag	1.5%	S – 1 <sup>st</sup> Ag, 2 <sup>nd</sup> Co
5%Co(0.14%Ag)/ $\gamma$ -Al <sub>2</sub> O <sub>3</sub>		1.5%	Coimpregnation

(a) S stands for sequential impregnation.

#### 3.3.1 Catalytic Activity

The performance of the different catalysts in the amination reaction of *n*-octanol with NH<sub>3</sub> was evaluated under the operation conditions RC-1 (Table 2-4). The results, plotted in Figure 3-3, point out an increase of the *n*-octanol conversion for all the noble-metal promoted samples with respect to the parent 5%Co/ $\gamma$ -Al<sub>2</sub>O<sub>3</sub>. In the case of Ru-promoted 5%Co/ $\gamma$ -Al<sub>2</sub>O<sub>3</sub>, the coimpregnated catalyst [Co(Ru)] afforded the highest OA yield (23%) followed by the catalyst prepared by sequential impregnation of Ru and Co (Ru-Co) with a yield of 20%. Regarding the Ag-promoted 5%Co/ $\gamma$ -Al<sub>2</sub>O<sub>3</sub>, the catalyst prepared by sequential Ag and Co impregnation (Ag-Co) exhibited the most prominent activity enhancement, transforming 25% of *n*-octanol into OA. In contrast, the Co(Ag) and Co-Ag catalysts afforded a yield of 19% and 18%, respectively. No negative effect on the selectivity was evidenced for the different catalysts, the main reaction products being OA and ON.

To summarize, the most promising formulations for *n*-octanol amination with NH<sub>3</sub> were Ag-Co and Co(Ru), affording in each case a 65% and 50% increase of the OA yield. These catalysts have been used in the remainder of this study as the most promising formulations.

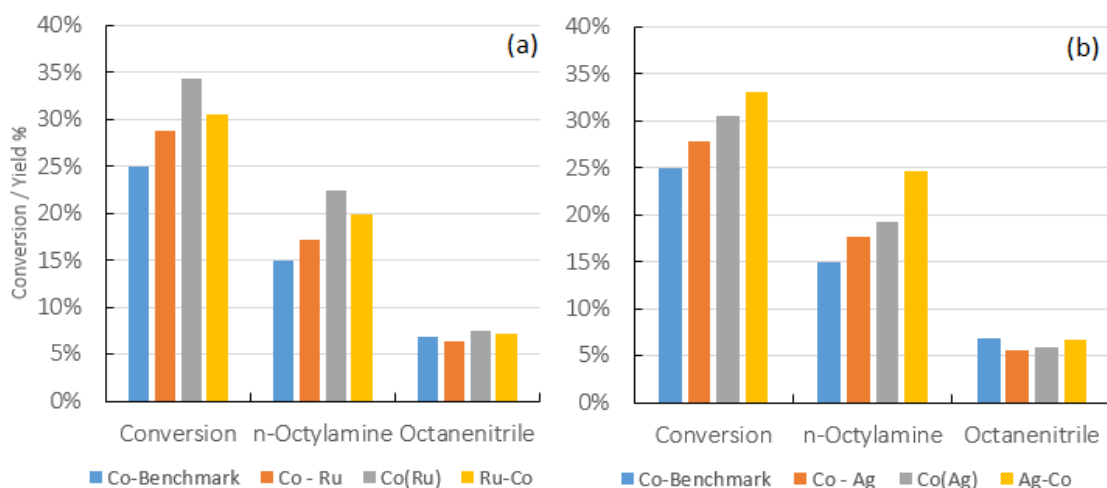


**Figure 3-3** Conversion and yields in the amination of *n*-octanol with NH<sub>3</sub> over 5%Co/γ-Al<sub>2</sub>O<sub>3</sub> doped with 1.5% Ru (a) or Ag (b) with different impregnation protocols. Reaction conditions: 180 °C; P=1 bar; NH<sub>3</sub> : H<sub>2</sub> : N<sub>2</sub> : ROH (mol%) = 9 : 2.5 : 0.9 : 1; WHSV<sub>ROH</sub> = 2.9 h<sup>-1</sup>. Carbon balance 95%-98%.

### 3.3.2 Cobalt Reducibility

The effect of the impregnation sequence on the Co reducibility was studied by H<sub>2</sub>-TPR from room temperature up to 900 °C under a 5%v/v H<sub>2</sub>-Ar flow (40 mL(STP).min<sup>-1</sup>). Table 3-3 lists the main bands observed in the reduction profiles. The H<sub>2</sub>-TPR profile of 5%Co/γ-Al<sub>2</sub>O<sub>3</sub> (Figure 3-4) comprises two differentiated bands. The first and sharper band (α), centered at ~300 °C, is generally attributed to the reduction of Co<sub>3</sub>O<sub>4</sub> to CoO, while the second band (β) in the temperature range 350-700 °C represents the subsequent conversion of CoO into metallic Co<sup>0</sup> [5,18,19]. This band is broad, covering the reduction of different CoO species. Larger Co particles with low metal-support interaction (β<sub>1</sub>) are expected to reduce at lower temperatures (~450 °C), whereas smaller Co nanoparticles (β<sub>2</sub>) with stronger interaction with alumina reduce at temperatures above ~550 °C. The observed 3:1 stoichiometry for the H<sub>2</sub> consumption is in agreement with the ratio of surface areas between both bands. The H<sub>2</sub> consumption at temperatures higher than 750-800 °C is attributed to the reduction of spinel CoAl<sub>2</sub>O<sub>4</sub> [20,21], which is generated by the diffusion of Co ions into the Al<sub>2</sub>O<sub>3</sub> lattice during calcination.

**Table 3-3** Main bands observed in the H<sub>2</sub>-TPR profiles of 5%Co/ $\gamma$ -Al<sub>2</sub>O<sub>3</sub> catalysts promoted by Ag and Co (1.5% a/a) as a function of the impregnation protocol

Catalyst	Band	Co <sub>3</sub> O <sub>4</sub> → CoO <sup>(a)</sup>		CoO → Co <sup>0</sup> <sup>(a)</sup>		Reduction Temperature <sup>(b)</sup>	CoAl <sub>2</sub> O <sub>4</sub> <sup>(b)</sup>	Ratio $\beta / \alpha$
		( $\alpha$ )	( $\beta_1$ )	( $\beta_2$ )				
5% Co/ $\gamma$ -Al <sub>2</sub> O <sub>3</sub> -Benchmark	Position	297°C	451°C	592°C	< 500°C	> 750°C	3.2	
	H <sub>2</sub> uptake (mmol·g <sup>-1</sup> )	0.22	0.55	0.18	0.52	0.02		
5% Co-0.13% Ru/ $\gamma$ -Al <sub>2</sub> O <sub>3</sub>	Position	189°C	347°C	-	< 500°C	> 750°C	2.7	
	H <sub>2</sub> uptake (mmol·g <sup>-1</sup> )	0.29	0.78	-	1.04	0.02		
0.13% Ru-5% Co/ $\gamma$ -Al <sub>2</sub> O <sub>3</sub>	Position	221°C	403°C	-	< 500°C	> 750°C	2.9	
	H <sub>2</sub> uptake (mmol·g <sup>-1</sup> )	0.24	0.71	-	0.92	0.03		
5% Co(0.13% Ru)/ $\gamma$ -Al <sub>2</sub> O <sub>3</sub>	Position	145°C	311°C	-	< 500°C	> 750°C	3.0	
	H <sub>2</sub> uptake (mmol·g <sup>-1</sup> )	0.26	0.78	-	1.02	0.03		
5% Co-0.14% Ag/ $\gamma$ -Al <sub>2</sub> O <sub>3</sub>	Position	289°C	457°C	605°C	< 500°C	> 750°C	3.1	
	H <sub>2</sub> uptake (mmol·g <sup>-1</sup> )	0.21	0.48	0.15	0.56	0.02		
0.14% Ag-5% Co/ $\gamma$ -Al <sub>2</sub> O <sub>3</sub>	Position	257°C	368°C	541°C	< 500°C	> 750°C	4.0 <sup>(c)</sup>	
	H <sub>2</sub> uptake (mmol·g <sup>-1</sup> )	0.20	0.72	0.08	0.96	0.03		
5% Co(0.14% Ag)/ $\gamma$ -Al <sub>2</sub> O <sub>3</sub>	Position	264°C	352°C	550°C	< 500°C	> 750°C	5.3 <sup>(c)</sup>	
	H <sub>2</sub> uptake (mmol·g <sup>-1</sup> )	0.14	0.64	0.11	0.80	0.04		

(a) H<sub>2</sub> consumption calculated after curve deconvolution using Gaussian distributions. (b) H<sub>2</sub> consumption calculated by integrating the H<sub>2</sub>-TPR profiles using trapezoidal numerical integration. (c) Highly overlapping bands, difficult to deconvolute

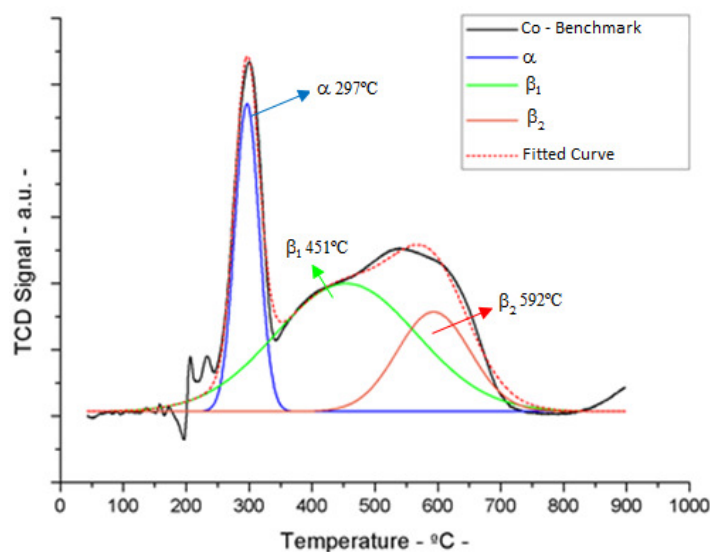


**Figure 3-4** H<sub>2</sub>-TPR band deconvolution for 5%Co/γ-Al<sub>2</sub>O<sub>3</sub>.

Figure 3-5-(a) plots the reduction profiles for the Ru-promoted 5%Co/γ-Al<sub>2</sub>O<sub>3</sub> catalysts. Regardless of the impregnation sequence, both bands shift towards lower temperature upon Ru introduction. In particular, the second band attributed to the reduction of CoO into Co<sup>0</sup> becomes significantly sharper after impregnation. A new band appears at lower temperature [79 °C for Co(Ru) and 135 °C for Co-Ru and Ru-Co sequentially impregnated catalysts], which is most likely ascribed to the reduction of RuO<sub>2</sub>. The remarkable shift towards lower temperature for the coimpregnated Co(Ru) catalyst might indicate the existence of Ru species in different combination with Co. The impregnation sequence influences to an important extent the Co reducibility. The coimpregnated Co(Ru) catalyst exhibits the largest effect, shifting the α and β bands by 152 °C and 249 °C, respectively. Both bands are very sharp, suggesting a homogeneity of Co particles with low metal-support interaction. The Co-Ru catalyst shows a temperature shift for each band by 108 °C and 213 °C, respectively. Both bands are broader than those observed for the other Ru-promoted catalysts. This observation might be explained on the basis of a higher heterogeneity of Co species for the latter catalyst, showing most likely varying interactions between Co and Ru. Finally, the Ru-Co sample displays a moderate temperature shift for both bands (76 °C and 157 °C, respectively). The same effect on the impregnation sequence was observed by Kogelbauer *et al.* [22]. Coimpregnated Co(Ru) exhibited well resolved and sharp bands, while a broader α band was observed for the Ru-Co and Co-Ru catalysts. Likewise, Cook *et al.* [12] measured a higher reducibility for coimpregnated Co(Ru) catalyst. Finally, a similar ratio of  $3 \pm 0.3$  between the surface areas of both bands is observed, supporting the assumption of two sequential reduction steps.

The reduction profiles were modified in a much different way in the presence of Ag [Figure 3-5-(b)]. The  $\alpha$  band attributed to the transformation of  $\text{Co}_3\text{O}_4$  into  $\text{CoO}$  shifts slightly by 8-40 °C towards lower temperatures. In case of the  $\beta$  band corresponding to the reduction of  $\text{CoO}$  into metallic  $\text{Co}^0$ , shows marked differences depending on the impregnation protocol considered. The  $\beta$  band in Co-Ag exhibits a small prominence by  $\sim 457$  °C, which is probably related to large  $\text{CoO}$  nanoparticles ( $\beta_1$ ) in closer contact with Ag clusters. A shoulder at  $\sim 605$  °C ( $\beta_2$ ) reveals the existence of  $\text{CoO}$  particles in strong interaction with the alumina support. These species are less prominent in the Co(Ag) and Ag-Co catalysts, showing weaker shoulders at  $\sim 550$  °C. These observations suggest the ability of Ag for decreasing the metal-support interaction when Ag is either impregnated before or concomitantly with Co. The band related to easily reducible  $\text{CoO}$  species shifts to 352 °C and 368 °C for the Co(Ag) and Ag-Co catalysts, respectively. The latter catalyst shows a more prominent  $\beta_1$  feature, achieving a higher Co reducibility. Similar  $\text{H}_2$ -TPR profiles were previously reported in the literature for Ag-promoted  $\text{Co}/\text{Al}_2\text{O}_3$  at low Ag loading ( $\sim 0.06$ - $0.55$  wt%. vs 0.14 wt.% in our case), showing a displacement of the  $\beta$  band by 100-200 °C [4,23]. Jacobs *et al.* [23] reported a displacement for both reduction bands for Ag loadings  $>0.8$  wt%. The ratio between the surface areas of both bands is 4.0 and 5.3 for Ag-Co and Co(Ag), respectively, instead of the expected value of 3.0. This observation might be related to the difficulty in deconvoluting the overlapping bands.

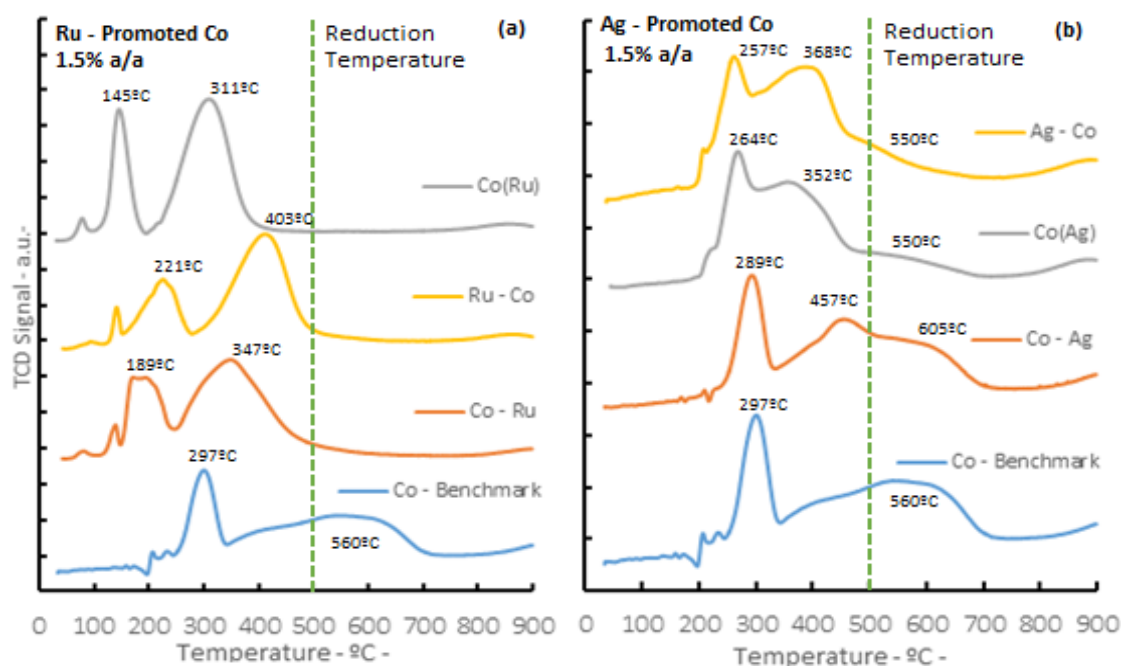


**Figure 3-5**  $\text{H}_2$ -TPR profiles for 1.5% a/a (a) Ru- and (b) Ag-promoted  $\text{Co}/\gamma\text{-Al}_2\text{O}_3$  catalysts synthesized by different impregnation protocols (coimpregnation and sequential impregnation). The dotted lines indicate the reduction temperature before the catalytic tests (500 °C).

The extent of reduction (EOR), calculated from the H<sub>2</sub> consumption below 500 °C for the different catalysts, was plotted against the OA yield [Figure 3-6-(a)]. As a rule, a higher OA yield is observed at higher EOR. However, the different catalysts show a different behavior. Ag-Co displays the highest OA yield at a slightly lower EOR than in the case of Co(Ru) or Co-Ru. This observation might be attributed to a difference in either the metal dispersion for the different catalysts, or to electronic effects induced by the dopant. Interestingly, Co-Ru displays the lowest OA production, even if this catalyst shows almost complete reduction at 500 °C. As can be observed in Figure 3-6-(b), the intrinsic activity cannot be maintained for these catalyst and the TOF decreases monotonically while increasing the EOR. This behavior might be ascribed to the existence of differentiated catalytic sites or Co<sup>0</sup> species with different intrinsic activities on the catalyst surface.

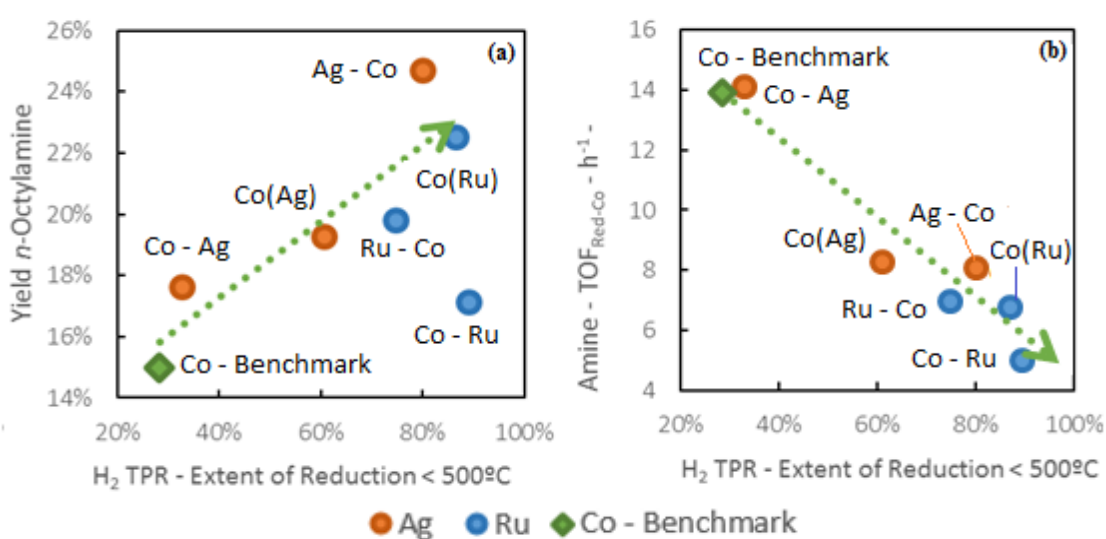


**Figure 3-6** (a) OA yield and (b) turnover frequency based on moles of OA formed per hour and per mole of reduced Co vs EOR (calculated from H<sub>2</sub> TPR <500°C). Reaction conditions: 180 °C; P=1 bar; NH<sub>3</sub> : H<sub>2</sub> : N<sub>2</sub> : ROH (mol%) = 9 : 2.5 : 0.9 : 1; WHSV<sub>ROH</sub> = 2.9 h<sup>-1</sup>. Carbon balance 95%-98%.

### 3.4 Optimization of the Dopant Loading

The effect of the Ru and Ag loading on the catalytic properties was further studied for the coimpregnated Co(Ru) and sequentially impregnated Ag-Co catalysts, which previously led to the best OA yields. The catalysts listed in Table 3-4 were synthesized according to the protocol previously described in Chapter 2 (Table 3-2).

#### 3.4.1 Catalytic activity

The catalytic performance was evaluated under the operating conditions RC-2, previously described in Table 2-5. Compared to RC-1 the reaction conditions were adjusted to obtain a higher *n*-octanol conversion and OA yield while minimizing ON formation. Below 50% conversion, the main reaction products were OA and ON (<5% yield, limited by equilibrium). DOA formation was kept <2.5% for all the promoted samples.

**Table 3-4** List of catalysts synthesized to study the influence of the promoter loading on Co(Ru) and Ag-Co (1.5% a/a)

Catalyst	Promoter	Atomic Ratio	Impregnation
5%Co/ $\gamma$ -Al <sub>2</sub> O <sub>3</sub> -Benchmark	-	-	-
12%Co/ $\gamma$ -Al <sub>2</sub> O <sub>3</sub>	-	-	-
<hr/>			
5%Co(0.003%Ru)/ $\gamma$ -Al <sub>2</sub> O <sub>3</sub>	Ru	0.03%	Coimpregnation
5%Co(0.01%Ru)/ $\gamma$ -Al <sub>2</sub> O <sub>3</sub>		0.1%	
5%Co(0.03%Ru)/ $\gamma$ -Al <sub>2</sub> O <sub>3</sub>		0.3%	
5%Co(0.06%Ru)/ $\gamma$ -Al <sub>2</sub> O <sub>3</sub>		0.75%	
5%Co(0.13%Ru)/ $\gamma$ -Al <sub>2</sub> O <sub>3</sub>		1.5%	
5%Co(0.26%Ru)/ $\gamma$ -Al <sub>2</sub> O <sub>3</sub>		3.0%	
<hr/>			
0.07%Ag-5%Co/ $\gamma$ -Al <sub>2</sub> O <sub>3</sub>	Ag	0.75%	Sequential 1 <sup>st</sup> Ag, 2 <sup>nd</sup> Co
0.14%Ag-5%Co/ $\gamma$ -Al <sub>2</sub> O <sub>3</sub>		1.5%	
0.28%Ag-5%Co/ $\gamma$ -Al <sub>2</sub> O <sub>3</sub>		3%	
0.46%Ag-5%Co/ $\gamma$ -Al <sub>2</sub> O <sub>3</sub>		5%	

The effect of the Ru loading in Co(Ru) catalysts was studied in the range 0.003-0.26 wt%, corresponding to 0.03-3% a/a (Figure 3-7-(a)). The activity of the promoted catalysts increases with the Ru loading from 0.003 wt.% to 0.03 wt.%, where an optimum performance is attained. Interestingly, the catalytic activity is unaffected by further increasing the Ru loading to 0.06 wt.%, while it becomes negatively affected at higher loadings. The optimal formulation, namely 5%Co(0.03%Ru)/ $\gamma$ -Al<sub>2</sub>O<sub>3</sub>, affords a 40% OA yield, which is comparable to that obtained over 12%Co/ $\gamma$ -Al<sub>2</sub>O<sub>3</sub> (41%), but containing 2.4 times less Co by weight.

The effect of the Ag loading on the different Ag-Co catalysts was studied in the range 0.07-0.46 wt.% corresponding to 0.75-5%a/a. All the catalysts displayed an increase of the activity compared to the benchmark catalyst. Indeed, the optimal catalytic performance was achieved at 0.28 wt.%, affording an OA yield of 42%, which is comparable to the value achieved over 12%Co/ $\gamma$ -Al<sub>2</sub>O<sub>3</sub> (41%). A further increase of the Ag loading to 5%a/a dropped the catalytic activity, the OA yield showing a value of 31%.

The results for the best performing catalysts are summarized in Table 3-5. The reported turnover frequencies (TOF) were calculated by dividing the reacted moles of *n*-octanol per hour by the amount of surface Co<sup>0</sup>. The EOR and dispersion were respectively obtained from the H<sub>2</sub> consumption during TPR at a temperature lower than 500 °C. The parent Co catalysts exhibited the highest intrinsic activity with a TOF of 191 h<sup>-1</sup>. A decrease in the TOF was observed for Ag-Co and Co(Ru) with values of 112 h<sup>-1</sup> and 70 h<sup>-1</sup> respectively. The increase of the Co<sup>0</sup> surface on the promoted catalysts does not correlate with an increase in conversion. This discrepancy could be related to a heterogeneity of Co<sup>0</sup> sites with different intrinsic activity.

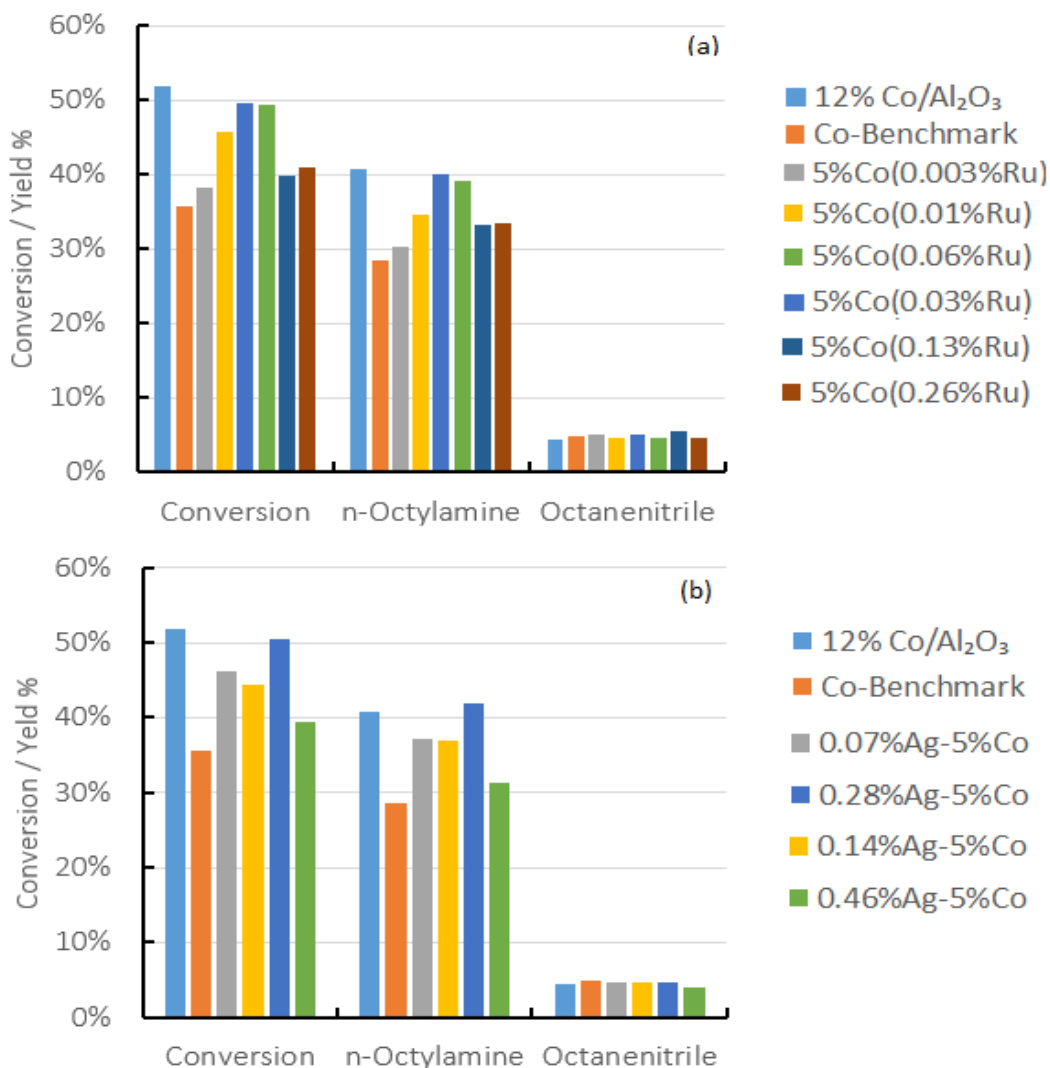


**Figure 3-7** Conversion and yields in the amination of *n*-octanol with NH<sub>3</sub> over Co(Ru) (a) and Ag-Co (b) catalysts with different promoter loadings. Reaction conditions: 180 °C; P=1 bar; NH<sub>3</sub> : H<sub>2</sub> : N<sub>2</sub> : ROH (mol%) = 9 : 3.4 : 0:1; WHSV<sub>ROH</sub> = 1.9 h<sup>-1</sup>. Carbon balance 96%-99%.

**Table 3-5** Reaction results for the best performing catalysts in operating conditions RC-2.

Catalyst	Conv.	OA yield	ON yield	DOA yield	TOF (h <sup>-1</sup> ) <sup>(a)</sup>
5%Co/γ-Al <sub>2</sub> O <sub>3</sub> -Benchmark	36%	28.5%	4.9%	1.1%	191
5%Co(0.03%Ru)/γ-Al <sub>2</sub> O <sub>3</sub>	50%	40.0%	5.0%	2.4%	70
0.28%Ag-5%Co/γ-Al <sub>2</sub> O <sub>3</sub>	51%	42.0%	4.8%	3.0%	112

(a) – TOF calculated for *n*-octanol conversion, taking into account XRD dispersion and H<sub>2</sub>-EOR extent of reduction (Table 3-8)

**Table 3-6** Reducibility of 5% Co(X% Ru)/ $\gamma$ -Al<sub>2</sub>O<sub>3</sub> catalysts with varying Ru loadings

Catalyst	Band	Co <sub>3</sub> O <sub>4</sub> → CoO <sup>(a)</sup>		CoO → Co <sup>0</sup> <sup>(a)</sup>		Reduction Temperature <sup>(b)</sup>	CoAl <sub>2</sub> O <sub>4</sub> <sup>(b)</sup>	Ratio $\beta / \alpha$
		( $\alpha$ )	( $\beta_1$ )	( $\beta_2$ )	( $\beta_2$ )			
5% Co/ $\gamma$ -Al <sub>2</sub> O <sub>3</sub> -Benchmark	Position	297°C		451°C	592°C	< 500°C	> 750°C	3.2
	H <sub>2</sub> uptake (mmol·g <sup>-1</sup> )	0.22		0.55	0.18	0.52	0.02	
5% Co(0.003% Ru)/ $\gamma$ -Al <sub>2</sub> O <sub>3</sub>	Position	274°C		446°	569°C	< 500°C	> 750°C	2.8
	H <sub>2</sub> uptake (mmol·g <sup>-1</sup> )	0.22		0.52	0.09	0.72	0.02	
5% Co(0.01% Ru)/ $\gamma$ -Al <sub>2</sub> O <sub>3</sub>	Position	222°C	255°C	436°C	-	< 500°C	> 750°C	2.7
	H <sub>2</sub> uptake (mmol·g <sup>-1</sup> )	0.11	0.15	0.67	-	0.86	0.01	
5% Co(0.03% Ru)/ $\gamma$ -Al <sub>2</sub> O <sub>3</sub>	Position	176°C	207°C	394°C	-	< 500°C	> 750°C	2.8
	H <sub>2</sub> uptake (mmol·g <sup>-1</sup> )	0.07	0.21	0.78	-	1.01	0.03	
5% Co(0.07% Ru)/ $\gamma$ -Al <sub>2</sub> O <sub>3</sub>	Position	160°C		337°C	-	< 500°C	> 750°C	2.8
	H <sub>2</sub> uptake (mmol·g <sup>-1</sup> )	0.27		0.75	-	1.01	0.03	
5% Co(0.13% Ru)/ $\gamma$ -Al <sub>2</sub> O <sub>3</sub>	Position	145°C		311°C	-	< 500°C	> 750°C	3.0
	H <sub>2</sub> uptake (mmol·g <sup>-1</sup> )	0.26		0.78	-	1.02	0.03	
5% Co(0.26% Ru)/ $\gamma$ -Al <sub>2</sub> O <sub>3</sub>	Position	143°C		271°C	-	< 500°C	> 750°C	2.8
	H <sub>2</sub> uptake (mmol·g <sup>-1</sup> )	0.26		0.73	-	0.98	0.02	

(a) H<sub>2</sub> consumption calculated after curve deconvolution using Gaussian distributions. (b) H<sub>2</sub> consumption calculated by integrating the H<sub>2</sub>-TPR profiles using trapezoidal numerical integration

**Table 3-7** Reducibility of X% Ag -5% Co/ $\gamma$ -Al<sub>2</sub>O<sub>3</sub> catalysts with varying Ag loadings

Catalyst	Band	Co <sub>3</sub> O <sub>4</sub> → CoO <sup>(a)</sup>		CoO → Co <sup>0</sup> <sup>(a)</sup>		Reduction Temperature <sup>(b)</sup>	CoAl <sub>2</sub> O <sub>4</sub> <sup>(b)</sup>	Ratio $\beta / \alpha$
		( $\alpha$ )	( $\beta_1$ )	( $\beta_2$ )				
5% Co/ $\gamma$ -Al <sub>2</sub> O <sub>3</sub> -Benchmark	Position	297°C	451°C	592°C	< 500°C	> 750°C	3.2	
	H <sub>2</sub> uptake (mmol·g <sup>-1</sup> )	0.22	0.55	0.18	0.52	0.02		
0.07% Ag-5% Co/ $\gamma$ -Al <sub>2</sub> O <sub>3</sub>	Position	260°C	375°C	564°C	< 500°C	> 750°C	5.1 <sup>(c)</sup>	
	H <sub>2</sub> uptake (mmol·g <sup>-1</sup> )	0.15	0.71	0.06	0.90	0.03		
0.14% Ag-5% Co/ $\gamma$ -Al <sub>2</sub> O <sub>3</sub>	Position	257°C	368°C	541°C	< 500°C	> 750°C	4.0 <sup>(c)</sup>	
	H <sub>2</sub> uptake (mmol·g <sup>-1</sup> )	0.20	0.72	0.08	0.96	0.03		
0.28% Ag-5% Co/ $\gamma$ -Al <sub>2</sub> O <sub>3</sub>	Position	263°C	350°C	550°C	< 500°C	> 750°C	7.2 <sup>(c)</sup>	
	H <sub>2</sub> uptake (mmol·g <sup>-1</sup> )	0.12	0.82	0.06	0.99	0.02		
0.56% Ag-5% Co/ $\gamma$ -Al <sub>2</sub> O <sub>3</sub>	Position	248°C	341°C	530°C	< 500°C	> 750°C	6.2 <sup>(c)</sup>	
	H <sub>2</sub> uptake (mmol·g <sup>-1</sup> )	0.13	0.77	0.05	0.96	0.02		

(a) H<sub>2</sub> consumption calculated after curve deconvolution using Gaussian distributions. (b) H<sub>2</sub> consumption calculated by integrating the H<sub>2</sub>-TPR profiles using trapezoidal numerical integration. (c) Highly overlapping bands, difficult to deconvolute

**Table 3-8** Summary of the properties for the optimized catalytic formulations

Catalyst	Co <sup>(a)</sup> wt%	NM <sup>(a)</sup> wt%	S <sub>BET</sub> (m <sup>2</sup> ·g <sup>-1</sup> )	Pore Vol. (cm <sup>3</sup> ·g <sup>-1</sup> ) <sup>(b)</sup>	Avg. Pore Size (nm) <sup>(b)</sup>	% H <sub>2</sub> EOR <sup>(c)</sup>	% O <sub>2</sub> EOR <sup>(d)</sup>	Co <sup>0</sup> Avg. size (nm) <sup>(e)</sup>	Dispersion %
$\gamma$ -Al <sub>2</sub> O <sub>3</sub>	-	-	150	0.49	12.8	-	-	-	-
5%Co/ $\gamma$ -Al <sub>2</sub> O <sub>3</sub>	4.9%	-	136	0.45	12.7	28 %	18 %	8.2	11.7%
5%Co(0.03%Ru)/ $\gamma$ -Al <sub>2</sub> O <sub>3</sub>	4.9%	0.02%	137	0.45	12.7	86 %	64 %	6.6	14.5%
0.28%Ag-5%Co/ $\gamma$ -Al <sub>2</sub> O <sub>3</sub>	5.0%	0.25%	134	0.45	12.7	83 %	31 %	10.1	9.5%

(a) Determined by ICP. (b) Measured from N<sub>2</sub> adsorption at 77 K using the BJH method. (c) Calculated from the H<sub>2</sub>-TPR profile below 500°C. (d) Calculated from the O<sub>2</sub>-TPO profile (reduction at 500°C, 1h). (e) Calculated from the XRD reflection at  $2\theta = 36.9^\circ$  using Scherrer equation. Contraction 0.75 Co<sub>3</sub>O<sub>4</sub>→Co<sup>0</sup> (e) D%=96/d(nm) [24,25]

The H<sub>2</sub> consumption in the H<sub>2</sub>-TPR profiles until 500 °C was used as a descriptor of the EOR of Co. The reduction degree increases linearly with the Ru loading in the range 0.003-0.03 wt.% [Figure 3-8-(a)], achieving a H<sub>2</sub> consumption equivalent to 90% of the total Co reduction. A further increase of the Ru loading does not enhance the Co reducibility. Interestingly, the catalytic performance of Co(Ru) catalysts [Figure 3-7-(a)] increases with the catalyst reducibility. However, at a Ru loading higher than 0.03 wt.%, the activity declines. Since Ru is generally related to an increase of the Co dispersion [11, 20, 21], the observed decrease of the catalytic activity appears to be most likely attributed to a poisoning effect of Ru on Co. Similarly, an enhanced reducibility was observed upon introduction of 0.07 wt.%Ag [Figure 3-8-(b)], increasing from 28% for the calcined benchmark Co catalysts up to 73%. A further increase of the Ag loading to either 0.14 wt.% or 0.28 wt.% increased the EOR to 80-83%. No further enhancement was observed at higher Ag loading, i.e. 0.46 wt.%.

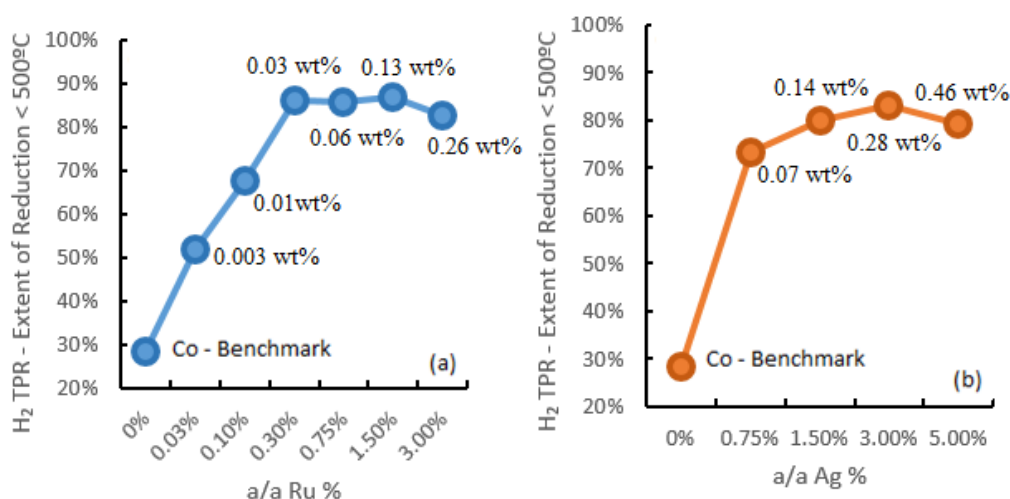


**Figure 3-8** H<sub>2</sub> consumption in the H<sub>2</sub>-TPR profiles up to 500 °C for (a) Co(Ru) and (b) Ag-Co catalysts with various promoter loadings.

The EOR was also measured by pulse O<sub>2</sub>-TPO for the best performing catalysts using the protocol described in section 2.3.6. In these tests, the catalysts were reduced following the same thermal treatment as that used before reaction. The EOR was calculated from the O<sub>2</sub> consumption, assuming total oxidation to Co<sub>3</sub>O<sub>4</sub>. The results, listed in Table 3-8, show a remarkably lower Co reducibility for the different catalysts than the values measured from the H<sub>2</sub> consumption in the H<sub>2</sub>-TPR profiles. The differences cannot be explained on the basis of a difference in the reduction protocols, since the samples were reduced for longer time prior to O<sub>2</sub>-TPO, thus expecting, if ever possible, a higher EOR for the latter experiments. The disparity in the results might be ascribed to an incomplete oxidation of Co in the O<sub>2</sub>-TPO tests. Khodakov *et al.* [27] stated that under inert atmospheres and temperatures above 350 °C, supported CoO could be more stable than Co<sub>3</sub>O<sub>4</sub>. Therefore, O<sub>2</sub> titration under inert atmosphere (Ar) could result in the oxidation of Co to CoO or to a mixture of CoO and Co<sub>3</sub>O<sub>4</sub>, thus explaining the underestimation of the EOR calculated from O<sub>2</sub>-TPO [28, 29].

### 3.4.2 X-Ray Diffraction

The crystal structure of the best performing catalysts was studied by X-ray diffraction (XRD). The XRD patterns of the calcined catalysts (Figure 3-9) confirm the presence of  $\text{Co}_3\text{O}_4$  and  $\gamma\text{-Al}_2\text{O}_3$  phases. Ru and Ag were not detected on the promoted samples. The intensity of the reflections depends both on the metal loading and on the size of the Co nanoparticles. The average crystallite size was calculated using Scherrer equation using the reflection centered at  $2\theta = 36.9^\circ$  corresponding to the (311) crystal plane of  $\text{Co}_3\text{O}_4$ . A decrease in the intensity of the (311) reflection for Co(Ru) is evidenced, indicating a smaller average particle size of Co for this latter sample. This observation is consistent earlier results reported in the literature [21,22,26]. For instance, Park *et al.* [26] observed a decrease in the Co particle size from 21.9 nm to 14.7 nm for a catalyst containing 5 wt.%Co and 0.1 wt%Ru supported over  $\gamma\text{-Al}_2\text{O}_3$ . Opposing this observation, a sharper reflection centered at  $2\theta = 36.9^\circ$  is visible for the Ag-promoted catalyst, indicating the presence of larger Co nanoparticles upon Ag promotion. The results are summarized in Table 3-8.

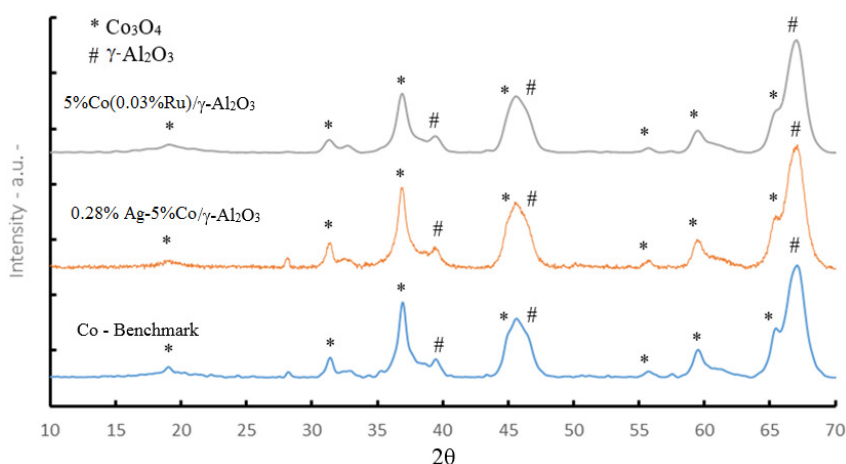
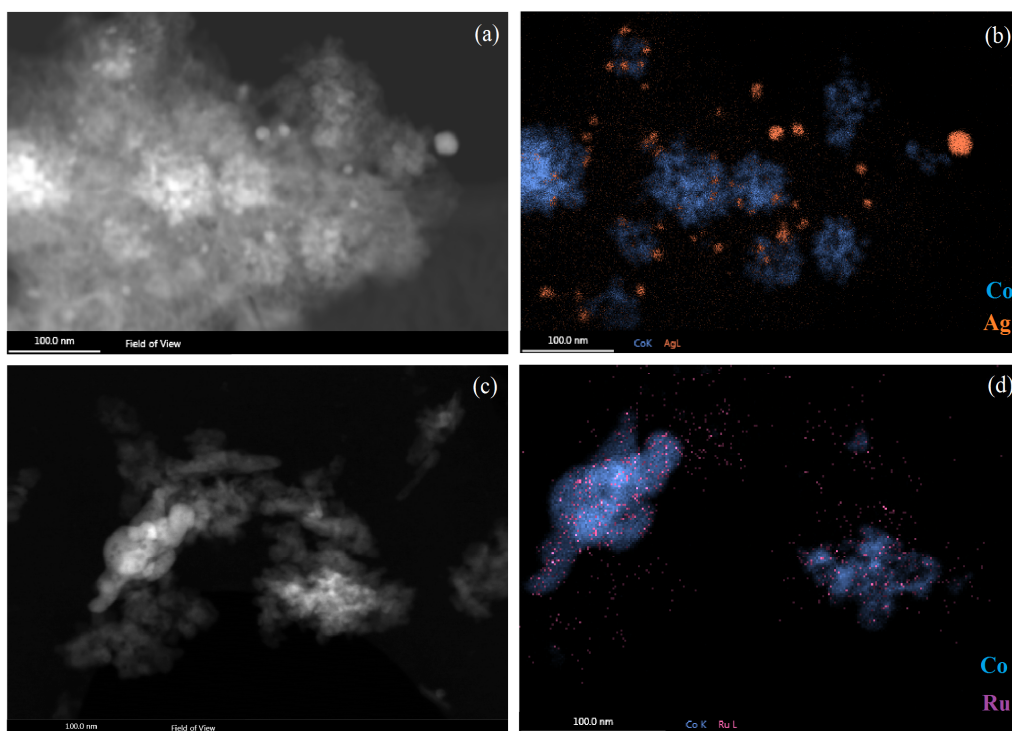


Figure 3-9 XRD patterns for the parent Co and the best performing Ru- and Ag-promoted catalysts.

### 3.4.3 STEM/EDS-SDD

STEM/EDS-SDD imaging was carried out to assess the morphology and elemental distribution of metallic species on the optimized catalysts. In Figure 3-10-(b) one can observe a catalyst consisting of ~50 nm agglomerates of Co nanoparticles (size <10 nm) decorated with Ag nanoparticles. The Ag nanoparticles appear to be selectively located around the Co agglomerates, which could diminish the Co- $\text{Al}_2\text{O}_3$  interaction and thus facilitate Co reduction. In the case of Co(Ru) [Figure 3-10-(d)] Ru seems to be homogeneously distributed within the Co particles, suggesting the formation of an alloy.



**Figure 3-10** STEM-HAADF images and elemental mapping of (a,b) Ag-Co and (c,d) Co(Ru) optimized formulations. All the images are scaled to 100 nm.

### 3.5 Effect of the H<sub>2</sub> pressure at variable NH<sub>3</sub>-to-alcohol ratios

The H<sub>2</sub> pressure has been reported to promote the catalytic activity in the amination of aliphatic alcohols operating *via* the borrowing hydrogen mechanism [30–33]. Since the rate-limiting step is generally accepted to be the alcohol dehydrogenation [32–35], H<sub>2</sub> is often regarded as a driver for maintaining the active metal sites in reduced state. The main body of published data attributes a role of H<sub>2</sub> on hindering the transformation of metal catalysts (either at the bulk or surface level) into their corresponding nitrides in the presence of NH<sub>3</sub> [28–30, 34, 35]. More recently, an alternative mechanism was proposed by Murzin *et al.* [33] correlating the activity enhancement to a partial surface regeneration of the metal centers from coke deposition in the presence of H<sub>2</sub> by the formation of light hydrocarbons. A similar type of effect was reported in the dehydrogenation of alcohols and alkanes [38, 39]. Since noble metals are known to easily activate H<sub>2</sub>, the noble metal promoted catalysts could show different responses to increasing H<sub>2</sub> pressure during amination. Keeping this hypothesis in mind, the effect of H<sub>2</sub> was studied for *n*-octanol amination at variable NH<sub>3</sub> partial pressures for Co(Ru) and Ag-Co catalysts.

Figure 3-11 plots the effect of the H<sub>2</sub> partial pressure on the performance of the benchmark Co, Co(Ru) and Ag-Co catalysts at different NH<sub>3</sub> partial pressures. At constant NH<sub>3</sub> partial pressure, the *n*-octanol conversion increases linearly with the H<sub>2</sub> pressure for all the catalysts. Benchmark Co and Co(Ru) show a similar response to a change in the H<sub>2</sub> pressure, the latter being more active and selective to OA. In contrast, Ag-Co exhibits a

flatter response, being the most active catalyst at low H<sub>2</sub> pressures. At higher H<sub>2</sub> pressures, the benchmark Co and Co(Ru) display a comparatively higher activity. The H<sub>2</sub> pressure at which Ag-Co becomes the less active catalyst shifts to higher pressures at higher NH<sub>3</sub> partial pressure. Overall, even if the NH<sub>3</sub> partial pressure impacts only slightly the catalytic activity, it affects to a higher extent the OA selectivity, especially at low NH<sub>3</sub> pressures (Figure 3-12). Likewise, an increase of the H<sub>2</sub> partial pressure promotes the formation of DOA. Among the three catalysts surveyed, Ag-Co exhibits a superior OA selectivity, affording the highest OA yields even at low *n*-octanol conversion.

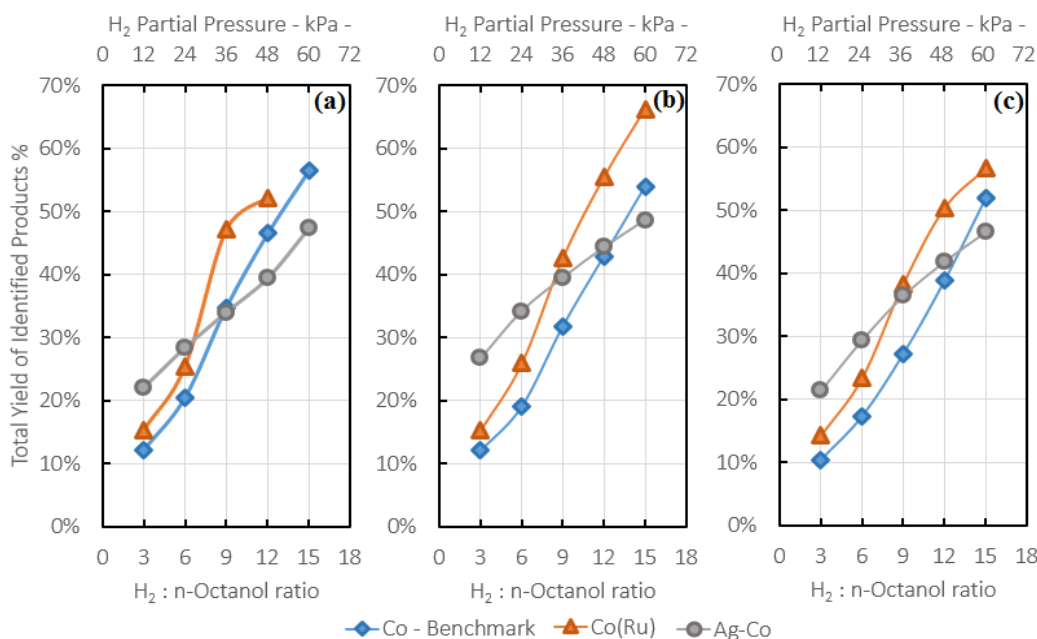


**Figure 3-11** Effect of the NH<sub>3</sub> and H<sub>2</sub> partial pressures on the catalytic activity of Co, Co(Ru) and Ag-Co catalysts. Reaction conditions: 180 °C; NH<sub>3</sub> equiv. = (a) 3; (b) 6; (c) 9; H<sub>2</sub> equiv. = 3-5; N<sub>2</sub> used to keep the total gas flow rate constant at 68 cm<sup>3</sup>(STP).min<sup>-1</sup>; WHSV<sub>ROH</sub> = 6.6 h<sup>-1</sup>; P=1 bar. Carbon balance 94-99%.

### 3.6 Optimization of Process Conditions

The effect of the total pressure, the NH<sub>3</sub> excess and the temperature were studied for the Ag-Co catalyst (0.28%Ag-5%Co/ $\gamma$ -Al<sub>2</sub>O<sub>3</sub>) to optimize the OA yield.

#### (i) Effect of the total pressure

The effect of the total pressure on the amination of *n*-octanol with NH<sub>3</sub> was surveyed in the range 1-15 bar. Figure 3-13 plots the results obtained. An increase of the total pressure from 1 to 5 bar enhances the *n*-octanol conversion from 66% to 75%. However, a further increase from 5 to 15 bar exerts a negative effect on the *n*-octanol conversion, achieving a value of 58% at 15 bar. This decreasing trend might be explained on the basis of a transition from a pure gas-phase reaction to a gas-liquid heterogeneously-catalyzed reaction at 15 bar. Similarly, an increase of the total pressure was found to promote DOA and TOA formation, dropping the OA selectivity from 75% at atmospheric pressure to 29% at 15 bar.

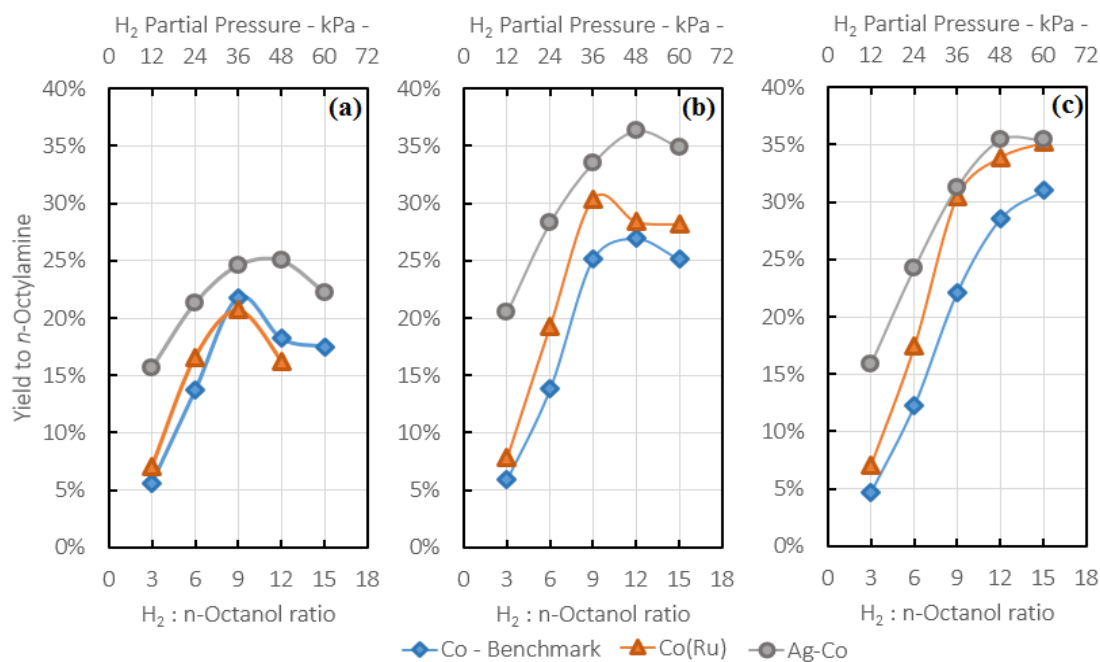


**Figure 3-12** Effect of the  $\text{NH}_3$  and  $\text{H}_2$  partial pressures on the selectivity of Co, Co(Ru) and Ag-Co catalysts. Reaction conditions:  $180\text{ }^\circ\text{C}$ ;  $P=1\text{ bar}$ ;  $\text{NH}_3$  equiv. = (a) 3; (b) 6; (c) 9;  $\text{H}_2$  equiv. = 3-15;  $\text{N}_2$  used to keep the total gas flow rate constant at  $68\text{ cm}^3(\text{STP})\cdot\text{min}^{-1}$ ;  $\text{WHSV}_{\text{ROH}} = 6.6\text{ h}^{-1}$ . Carbon balance 94-99%.

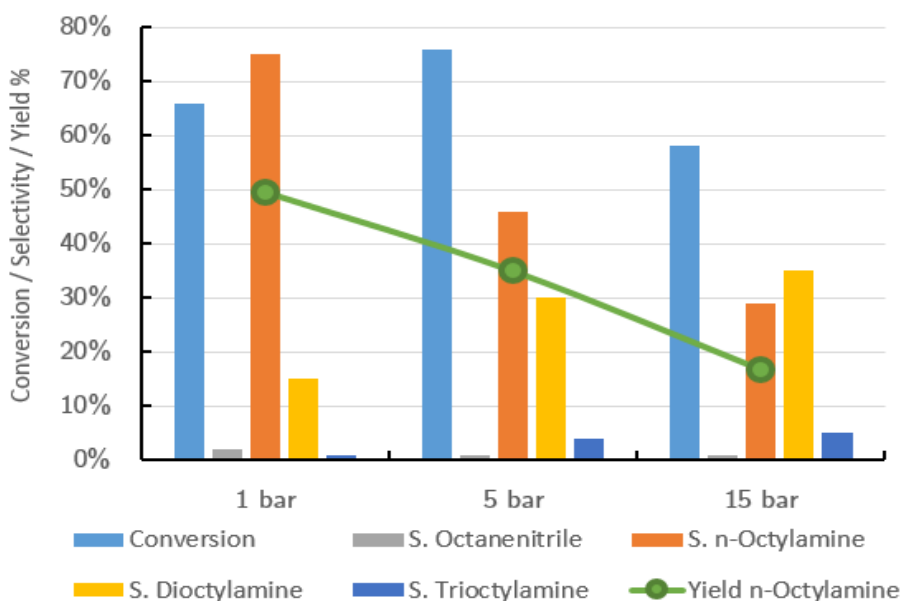


**Figure 3-13** Effect of the total pressure on the amination of *n*-octanol with  $\text{NH}_3$  over Ag-Co (0.28%Ag-5%Co/ $\gamma$ - $\text{Al}_2\text{O}_3$ ). The histograms represent the conversion and selectivities, whereas the symbol -o- represents the OA yield. Reaction conditions:  $180\text{ }^\circ\text{C}$ ;  $P=1\text{-}15\text{ bar}$ ;  $\text{NH}_3 : \text{H}_2 : \text{ROH}$  (mol%) = 9 : 6 : 1;  $\text{N}_2$  balance;  $\text{WHSV}_{\text{ROH}} = 2.1\text{ h}^{-1}$ .

(ii) Effect of the  $\text{NH}_3$  excess

The effect of the  $\text{NH}_3$  excess on the amination of *n*-octanol with  $\text{NH}_3$  was surveyed in the range 3-21 equiv. relative to *n*-octanol. As can be deduced from Figure 3-14, an increase of the  $\text{NH}_3$  excess from 3 to 15 equiv. enhances drastically the OA selectivity from

48% to 79%. A further increase to 21 equiv. enhances only slightly the OA selectivity up to 81%. The catalytic activity is slightly penalized at higher NH<sub>3</sub> partial pressures, evolving from 70% to 53% in the studied range. The stability of the catalyst was tested over 6 h on stream (Figure 3-15) using 9 equiv. of NH<sub>3</sub>, showing no appreciable loss of catalytic activity.

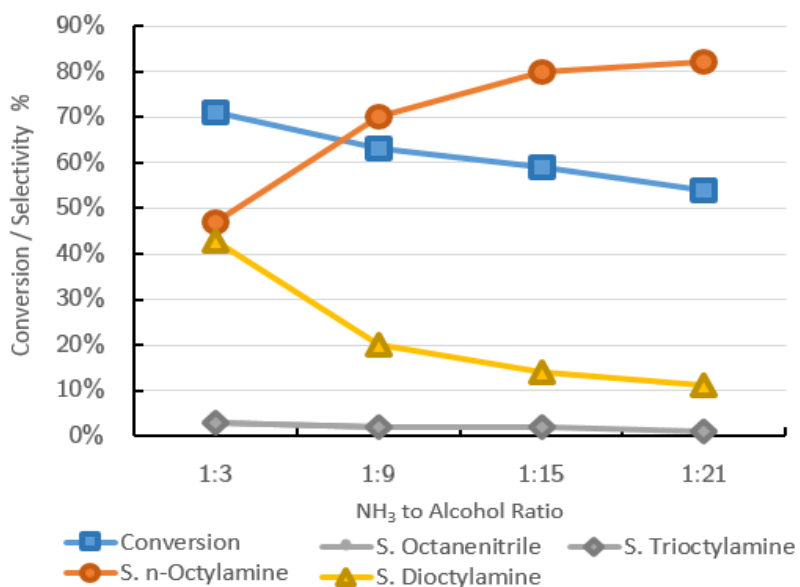


**Figure 3-14** Effect of the NH<sub>3</sub> excess on the amination of *n*-octanol with NH<sub>3</sub> over Ag-Co (0.28%Ag-5%Co/ $\gamma$ -Al<sub>2</sub>O<sub>3</sub>). Reaction conditions: 180 °C; P=1 bar; NH<sub>3</sub> : H<sub>2</sub> : ROH (mol%) = 3-21 : 6 : 1; N<sub>2</sub> balance; WHSV<sub>ROH</sub> = 2.1 h<sup>-1</sup>.

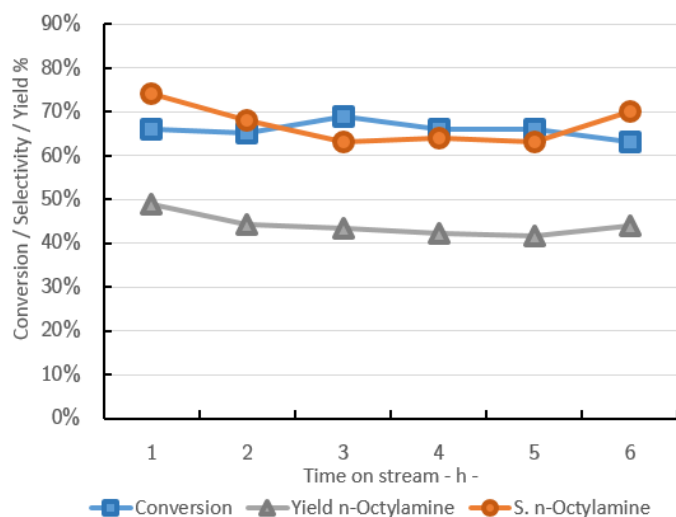


**Figure 3-15** Catalytic stability of Ag-Co (0.28%Ag-5%Co/ $\gamma$ -Al<sub>2</sub>O<sub>3</sub>) vs. time on stream. Reaction conditions: 180 °C; P=1 bar; NH<sub>3</sub> : H<sub>2</sub> : ROH (mol%) = 9 : 6 : 1; N<sub>2</sub> balance; WHSV<sub>ROH</sub> = 2.1 h<sup>-1</sup>.

### (iii) Effect of temperature

The effect of the temperature on the properties of the Ag-Co catalyst for *n*-octanol amination with NH<sub>3</sub> was surveyed in the range 160-220 °C using a ROH : H<sub>2</sub> : NH<sub>3</sub> molar ratio of 1 : 6 : 21 and balance N<sub>2</sub>. Figure 3-16 plots the results obtained. The *n*-octanol conversion increases from 40% at 160 °C to reach almost full conversion at 220 °C. Interestingly, the OA selectivity is also enhanced with the temperature, attaining 87% at 200 °C. In the meantime, the OA yield reaches a value as high as 78%. ON formation is thermodynamically favored at higher temperatures ( $\Delta H_{\text{Rx}}=+123$  kJ/mol).

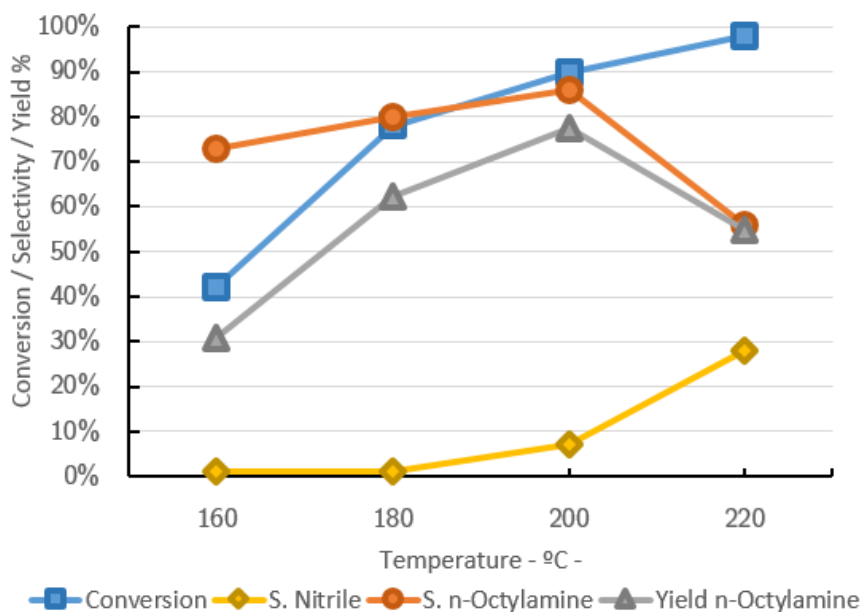


**Figure 3-16** Effect of temperature on the amination of *n*-octanol with NH<sub>3</sub> over Ag-Co (0.28%Ag-5%Co/ $\gamma$ -Al<sub>2</sub>O<sub>3</sub>). Reaction conditions: 160-220 °C; P=1 bar; NH<sub>3</sub> : H<sub>2</sub> : ROH (mol%) = 21 : 6 : 1; N<sub>2</sub> balance; WHSV<sub>ROH</sub> = 1.0 h<sup>-1</sup>.

### 3.6.1 Conclusions

In this chapter, we have presented the sequential optimization of cobalt-based catalysts promoted by noble metals for conducting the amination reaction of *n*-octanol with NH<sub>3</sub>. In a first step, we studied the effect of the promoter nature (Pt, Pd, Ag, Ru and Au) on the performance of a model 5%Co/ $\gamma$ -Al<sub>2</sub>O<sub>3</sub> catalyst. Pt and Pd were found to greatly improve the catalytic activity, but exerted at the same time a negative impact on the OA selectivity. This effect might be related to the promotion of competitive amine-amine or amine-nitrile condensation reactions, leading to the formation of the secondary amine. On the contrary, Ag and Ru enhanced the catalytic activity while keeping the selectivity of the parent catalyst towards the primary amine.

In a second step, the effect of the impregnation sequence was surveyed for the Ag- and Ru-promoted catalysts. In the case of Ag, the sequentially impregnated Ag-Co sample was found to be the most performing. A positive correlation was found between the Co

reducibility and the catalytic activity. In particular, a remarkable increase of the  $\beta_1$  band in the H<sub>2</sub>-TPR profile was observed, which can be ascribed to the reduction CoO nanoparticles with low metal-support interaction. Regarding the Ru promoted samples, the most performing catalyst was Co(Ru) prepared by coimpregnation. Likewise, the results could be related to an enhanced extent of reduction (EOR). A shift in the reduction band ascribed to Ru towards lower temperatures seems to indicate the existence of Ru in different environments for sequentially impregnated samples. Interestingly, the Co-Ru catalyst (Ru impregnated after Co), despite showing an excellent Co reducibility, displayed a comparatively lower catalytic activity.

In a third step, the promoter loading was optimized for the Ag-Co and Co(Ru) catalysts. In the former case, the catalytic activity was found to increase with the Ag loading in the range 0.07-0.28 wt.%, where an optimum was found. Co(Ru) was more efficient in promoting the Co reducibility per noble metal atom basis than Ag-Co. The catalytic activity could be correlated with the EOR, increasing for a Ru loading in the range 0.003-0.03 wt.%, where an optimal loading was found. A further increase of the Ru loading did not improve the EOR at 500 °C and exerted a negative impact on the catalytic activity, suggesting a poisoning effect of excess Ru. Further analysis of the optimized samples revealed differences in the distribution of Ru and Ag noble metals with respect to Co. On the one hand, Ag was found to be in the form of nanoparticles surrounding Co agglomerates. This could limit the metal-support interactions and boost the Co reducibility in line with the prominent  $\beta_1$  bands observed in the H<sub>2</sub>-TPR profiles. On the other hand, Ru was found to be homogeneously distributed within the Co particles, supporting the formation of a Co-Ru alloy. Noteworthy, the optimized catalysts displayed an activity that is comparable to that observed for a 12%Co/ $\gamma$ -Al<sub>2</sub>O<sub>3</sub> catalyst containing 2.4 times more Co.

In a fourth step, the effect of the NH<sub>3</sub> and H<sub>2</sub> partial pressures was studied for the Ag-Co and Co(Ru) catalysts, evidencing dissimilar behaviors upon Ag and Ru doping. Ag-Co showed the most interesting results, displaying the highest activity at low H<sub>2</sub> pressure and showing a higher OA selectivity. Interestingly, a negative effect of the H<sub>2</sub> pressure on the OA selectivity was observed for the different catalysts, being especially noticeable for the benchmark Co and Co(Ru). In addition to an enhanced EOR, the superior selectivity of Ag-Co suggests a co-catalytic role of Ag on the performance of 0.28%Ag-5%Co/ $\gamma$ -Al<sub>2</sub>O<sub>3</sub>.

Finally, the influence of the reaction parameters was studied for Ag-Co. The total pressure exerted a negative impact on the OA selectivity, especially beyond 5 bar, favoring the formation of DOA and TOA. A large NH<sub>3</sub> excess and a temperature of 200 °C were found as optimal, selectively transforming 78% of the alcohol into OA. This result presents various advantages in comparison with the existing scientific literature, exploiting an inexpensive heterogeneous catalyst [40–48], using mild conditions [49] and not involving the use of organic solvents [50].

### 3.7 References

- [1] G. Sewell, C. O'Connor, E. van Steen, Reductive amination of ethanol with silica-supported cobalt and nickel catalysts, *Appl. Catal. Gen.* 125 (1995) 99–112. doi:10.1016/0926-860X(95)00010-0.
- [2] G.S. Sewell, E. van Steen, C.T. O'Connor, Use of TPR/TPO for characterization of supported cobalt catalysts, *Catal. Lett.* 37 (1996) 255–260.
- [3] G.S. Sewell, C.T. O'Connor, E. van Steen, Effect of Activation Procedure and Support on the Reductive Amination of Ethanol Using Supported Cobalt Catalysts, *J. Catal.* 167 (1997) 513–521. doi:10.1006/jcat.1997.1596.
- [4] T. Jermwongratanachai, G. Jacobs, W. Ma, W.D. Shafer, M.K. Gnanamani, P. Gao, B. Kitiyanan, B.H. Davis, J.L.S. Klettinger, C.H. Yen, D.C. Cronauer, A.J. Kropf, C.L. Marshall, Fischer–Tropsch synthesis: Comparisons between Pt and Ag promoted Co/Al<sub>2</sub>O<sub>3</sub> catalysts for reducibility, local atomic structure, catalytic activity, and oxidation–reduction (OR) cycles, *Appl. Catal. Gen.* 464–465 (2013) 165–180. doi:10.1016/j.apcata.2013.05.040.
- [5] G. Jacobs, T.K. Das, Y. Zhang, J. Li, G. Racoillet, B.H. Davis, Fischer–Tropsch synthesis: support, loading, and promoter effects on the reducibility of cobalt catalysts, *Appl. Catal. Gen.* 233 (2002) 263–281.
- [6] D. Nabaho, J.W. (Hans) Niemantsverdriet, M. Claeys, E. van Steen, Hydrogen spillover in the Fischer–Tropsch synthesis: An analysis of platinum as a promoter for cobalt–alumina catalysts, *Catal. Today.* 261 (2016) 17–27. doi:10.1016/j.cattod.2015.08.050.
- [7] G. Jacobs, W. Ma, B. Davis, Influence of Reduction Promoters on Stability of Cobalt/g-Alumina Fischer-Tropsch Synthesis Catalysts, *Catalysts.* 4 (2014) 49–76. doi:10.3390/catal4010049.
- [8] A. Tavasoli, M. Irani, R.M.M. Abbaslou, M. Trépanier, A.K. Dalai, Morphology and deactivation behaviour of Co - Ru/  $\gamma$ -Al<sub>2</sub>O<sub>3</sub> Fischer - Tropsch synthesis catalyst, *Can. J. Chem. Eng.* 86 (2008) 1070 - 1080. doi:10.1002/cjce.20105.
- [9] D. Xu, W. Li, H. Duan, Q. Ge, H. Xu, Reaction performance and characterization of Co/Al<sub>2</sub>O<sub>3</sub> Fischer–Tropsch catalysts promoted with Pt, Pd and Ru, *Catal. Lett.* 102 (2005) 229–235. doi:10.1007/s10562-005-5861-7.
- [10] K.M. Cook, S. Poudyal, J.T. Miller, C.H. Bartholomew, W.C. Hecker, Reducibility of alumina-supported cobalt Fischer–Tropsch catalysts: Effects of noble metal type, distribution, retention, chemical state, bonding, and influence on cobalt crystallite size, *Appl. Catal. Gen.* 449 (2012) 69–80. doi:10.1016/j.apcata.2012.09.032.
- [11] M.J. Parnian, A. Taheri Najafabadi, Y. Mortazavi, A.A. Khodadadi, I. Nazzari, Ru promoted cobalt catalyst on  $\gamma$ -Al<sub>2</sub>O<sub>3</sub>: Influence of different catalyst preparation method and Ru loadings on Fischer - Tropsch reaction and kinetics, *Appl. Surf. Sci.* 313 (2014) 183 - 195. doi:10.1016/j.apsusc.2014.05.183.
- [12] K.M. Cook, H.D. Perez, C.H. Bartholomew, W.C. Hecker, Effect of promoter deposition order on platinum-, ruthenium-, or rhenium-promoted cobalt Fischer–Tropsch catalysts, *Appl. Catal. Gen.* 482 (2014) 275–286. doi:10.1016/j.apcata.2014.05.013.
- [13] G.A. Vedage, K.S. Hayes, M. Leeaphon, J.N. Armor, Multi-metallic actalysts for amination of alcohols to form alkylamines, Google Patents, 1999. <https://www.google.com/patents/US5932769> (accessed December 17, 2015).
- [14] J.D. Wulff-Doering, J.-P.D. Melder, G.D. Schulz, G.D. Voit, F. Gutschoven, W.D. Harder, Amination Catalyst for Alkylene Oxide, Alcohol, Aldehyde and Ketone and Its Production, JPH10174875 (A), 1998. [http://worldwide.espacenet.com/publicationDetails/biblio?FT=D&date=19980630&DB=EPODOC&locale=en\\_EP&CC=JP&NR=H10174875A&KC=A&ND=4](http://worldwide.espacenet.com/publicationDetails/biblio?FT=D&date=19980630&DB=EPODOC&locale=en_EP&CC=JP&NR=H10174875A&KC=A&ND=4) (accessed December 22, 2015).
- [15] J.D. Wulff-Doering, J.-P.D. Melder, G.D. Schulz, G.D. Voit, F. Gutschoven, W.D. Harder, Amination Catalyst for Alkylene Oxide, Alcohol, Aldehyde and Ketone, JPH10174874 (A), 1998..[http://worldwide.espacenet.com/publicationDetails/biblio?FT=D&date=19980630&DB=EPODOC&locale=en\\_EP&CC=JP&NR=H10174874A&KC=A&ND=4](http://worldwide.espacenet.com/publicationDetails/biblio?FT=D&date=19980630&DB=EPODOC&locale=en_EP&CC=JP&NR=H10174874A&KC=A&ND=4) (accessed December 23, 2015).

- [16] A.M. Hilmen, D. Schanke, A. Holmen, TPR study of the mechanism of rhenium promotion of alumina-supported cobalt Fischer-Tropsch catalysts, *Catal. Lett.* 38 (1996) 143–147. doi:10.1007/BF00806560.
- [17] S. Gomez, J.A. Peters, J.C. van der Waal, P.J. van den Brink, T. Maschmeyer, The rationalization of catalyst behaviour in the reductive amination of benzaldehyde with ammonia using a simple computer model, *Appl. Catal. Gen.* 261 (2004) 119–125. doi:10.1016/j.apcata.2003.10.037.
- [18] R. Bechara, D. Balloy, J.-Y. Dauphin, J. Grimblot, Influence of the Characteristics of  $\gamma$ -Aluminas on the Dispersion and the Reducibility of Supported Cobalt Catalysts, *Chem. Mater.* 11 (1999) 1703 – 1711. doi:10.1021/cm981015n.
- [19] G. Jacobs, Y. Ji, B.H. Davis, D. Cronauer, A.J. Kropf, C.L. Marshall, Fischer–Tropsch synthesis: Temperature programmed EXAFS/XANES investigation of the influence of support type, cobalt loading, and noble metal promoter addition to the reduction behavior of cobalt oxide particles, *Appl. Catal. Gen.* 333 (2007) 177–191. doi:10.1016/j.apcata.2007.07.027.
- [20] B. Jongsomjit, J. Panpranot, J.G. Goodwin, Co-Support Compound Formation in Alumina-Supported Cobalt Catalysts, *J. Catal.* 204 (2001) 98–109. doi:10.1006/jcat.2001.3387.
- [21] A. Taheri Najafabadi, A.A. Khodadadi, M.J. Parnian, Y. Mortazavi, Atomic layer deposited Co-/Al<sub>2</sub>O<sub>3</sub> catalyst with enhanced cobalt dispersion and Fischer-Tropsch synthesis activity and selectivity, *Appl. Catal. Gen.* 511 (2016) 31 – 46. doi:10.1016/j.apcata.2015.11.027.
- [22] A. Kogelbauer, J.G. Goodwin Jr, R. Oukaci, Ruthenium Promotion of Co/Al<sub>2</sub>O<sub>3</sub>Fischer–Tropsch Catalysts, *J. Catal.* 160 (1996) 125–133.
- [23] G. Jacobs, M.C. Ribeiro, W. Ma, Y. Ji, S. Khalid, P.T.A. Sumodjo, B.H. Davis, Group 11 (Cu, Ag, Au) promotion of 15%Co/Al<sub>2</sub>O<sub>3</sub> Fischer–Tropsch synthesis catalysts, *Appl. Catal. Gen.* 361 (2009) 137–151. doi:10.1016/j.apcata.2009.04.007.
- [24] R.D. Jones, C.H. Bartholomew, Improved flow technique for measurement of hydrogen chemisorption on metal catalysts, *Appl. Catal.* 39 (1988) 77–88. doi:10.1016/S0166-9834(00)80940-9.
- [25] A. Martínez, C. López, F. Márquez, I. Díaz, Fischer–Tropsch synthesis of hydrocarbons over mesoporous Co/SBA-15 catalysts: the influence of metal loading, cobalt precursor, and promoters, *J. Catal.* 220 (2003) 486–499. doi:10.1016/S0021-9517(03)00289-6.
- [26] J.-Y. Park, Y.-J. Lee, P.R. Karandikar, K.-W. Jun, J.W. Bae, K.-S. Ha, Ru promoted cobalt catalyst on -Al<sub>2</sub>O<sub>3</sub> support: Influence of pre-synthesized nanoparticles on Fischer-Tropsch reaction, *J. Mol. Catal. Chem.* 344 (2011) 153–160. doi:10.1016/j.molcata.2011.05.022.
- [27] A.Y. Khodakov, J. Lynch, D. Bazin, B. Rebours, N. Zanier, B. Moisson, P. Chaumette, Reducibility of Cobalt Species in Silica-Supported Fischer–Tropsch Catalysts, *J. Catal.* 168 (1997) 16–25. doi:10.1006/jcat.1997.1573.
- [28] A.Y. Khodakov, A. Griboval-Constant, R. Bechara, V.L. Zholobenko, Pore Size Effects in Fischer Tropsch Synthesis over Cobalt-Supported Mesoporous Silicas, *J. Catal.* 206 (2002) 230–241. doi:10.1006/jcat.2001.3496.
- [29] S. Storsater, B. Totdal, J. Walmsley, B. Tanem, A. Holmen, Characterization of alumina-, silica-, and titania-supported cobalt Fischer–Tropsch catalysts, *J. Catal.* 236 (2005) 139–152. doi:10.1016/j.jcat.2005.09.021.
- [30] J.H. Cho, J.-H. Park, T.-S. Chang, J.-E. Kim, C.-H. Shin, Reductive Amination of 2-Propanol to Monoisopropylamine Over Ni/ $\gamma$ -Al<sub>2</sub>O<sub>3</sub> Catalysts, *Catal. Lett.* 143 (2013) 1319 – 1327. doi:10.1007/s10562-013-1086-3.
- [31] J.H. Cho, J.H. Park, T.-S. Chang, G. Seo, C.-H. Shin, Reductive amination of 2-propanol to monoisopropylamine over Co/ $\gamma$ -Al<sub>2</sub>O<sub>3</sub> catalysts, *Appl. Catal. Gen.* 417 – 418 (2012) 313 – 319. doi:10.1016/j.apcata.2012.01.011.
- [32] A. Baiker, W. Caprez, W.L. Holstein, Catalytic amination of aliphatic alcohols in the gas and liquid phases: kinetics and reaction pathway, *Ind. Eng. Chem. Prod. Res. Dev.* 22 (1983) 217–225. doi:10.1021/i300010a010.
- [33] D. Ruiz, A. Aho, T. Saloranta, K. Eränen, J. Wärnå, R. Leino, D.Y. Murzin, Direct amination of dodecanol with NH<sub>3</sub> over heterogeneous catalysts. Catalyst screening and kinetic modelling, *Chem. Eng. J.* 307 (2017) 739–749. doi:10.1016/j.cej.2016.08.083.

- [34] A. Baiker, J. Kijenski, Catalytic Synthesis of Higher Aliphatic Amines from the Corresponding Alcohols, *Catal. Rev.* 27 (1985) 653–697. doi:10.1080/01614948508064235.
- [35] G.A. Kliger, L.F. Lazutina, R.A. Fridman, Y. Kryukov, A.N. Bashkirov, Y.S. Snagovskii, R. Smirnova, Several aspects of kinetics and mechanism of amination of octanol on a molten iron catalyst, *Kinet. Catal.* 16 (1975) 567–570.
- [36] A. Baiker, D. Monti, Interaction of Ammonia with Metallic Copper, Nickel and Cobalt Catalysts Studied by Temperature Programmed Desorption, *Berichte Bunsenges. Für Phys. Chem.* 87 (1983) 602–605. doi:10.1002/bbpc.19830870714.
- [37] A. Baiker, M. Maciejewski, Formation and thermal stability of copper and nickel nitrides, *J. Chem. Soc. Faraday Trans. 1 Phys. Chem. Condens. Phases.* 80 (1984) 2331–2341. doi:10.1039/F19848002331.
- [38] J.N. Keuler, L. Lorenzen, S. Miachon, The dehydrogenation of 2-butanol over copper-based catalysts: optimising catalyst composition and determining kinetic parameters, *Appl. Catal. Gen.* 218 (2001) 171–180. doi:10.1016/S0926-860X(01)00639-1.
- [39] M. Sheintuch, R.M. Dessau, Observations, modeling and optimization of yield, selectivity and activity during dehydrogenation of isobutane and propane in a Pd membrane reactor, *Chem. Eng. Sci.* 51 (1996) 535–547.
- [40] V.R. Jumde, L. Gonsalvi, A. Guerriero, M. Peruzzini, M. Taddei, A Ruthenium-Based Catalytic System for a Mild Borrowing-Hydrogen Process, *Eur. J. Org. Chem.* 2015 (2015) 1829–1833. doi:10.1002/ejoc.201403636.
- [41] X. Cui, Y. Deng, F. Shi, Reductive N-Alkylation of Nitro Compounds to N-Alkyl and N,N-Dialkyl Amines with Glycerol as the Hydrogen Source, *ACS Catal.* 3 (2013) 808–811. doi:10.1021/cs400049b.
- [42] K.O. Marichev, J.M. Takacs, Ruthenium-Catalyzed Amination of Secondary Alcohols Using Borrowing Hydrogen Methodology, *ACS Catal.* 6 (2016) 2205–2210. doi:10.1021/acscatal.6b00175.
- [43] M.H.S.A. Hamid, C.L. Allen, G.W. Lamb, A.C. Maxwell, H.C. Maytum, A.J.A. Watson, J.M.J. Williams, Ruthenium-catalyzed N-alkylation of amines and sulfonamides using borrowing hydrogen methodology, *J. Am. Chem. Soc.* 131 (2009) 1766–1774. doi:10.1021/ja807323a.
- [44] A.B. Enyong, B. Moasser, Ruthenium-catalyzed N-alkylation of amines with alcohols under mild conditions using the borrowing hydrogen methodology, *J. Org. Chem.* 79 (2014) 7553–7563. doi:10.1021/jo501273t.
- [45] K.-I. Fujita, T. Fujii, R. Yamaguchi, CpIr complex-catalyzed N-heterocyclization of primary amines with diols: a new catalytic system for environmentally benign synthesis of cyclic amines, *Org. Lett.* 6 (2004) 3525–3528. doi:10.1021/ol048619j.
- [46] K. Yuan, F. Jiang, Z. Sahli, M. Achard, T. Roisnel, C. Bruneau, Iridium-catalyzed oxidant-free dehydrogenative C-H bond functionalization: selective preparation of N-arylpiperidines through tandem hydrogen transfers, *Angew. Chem. Int. Ed Engl.* 51 (2012) 8876–8880. doi:10.1002/anie.201204582.
- [47] S. Ruch, T. Irrgang, R. Kempe, New iridium catalysts for the selective alkylation of amines by alcohols under mild conditions and for the synthesis of quinolines by acceptor-less dehydrogenative condensation, *Chem. Weinh. Bergstr. Ger.* 20 (2014) 13279–13285. doi:10.1002/chem.201402952.
- [48] A. Wetzel, S. Wöckel, M. Schelwies, M.K. Brinks, F. Rominger, P. Hofmann, M. Limbach, Selective alkylation of amines with alcohols by Cp\*-iridium(III) half-sandwich complexes, *Org. Lett.* 15 (2013) 266–269. doi:10.1021/ol303075h.
- [49] Y. Kagan, A. Bashkirov, G. Kliger, C. Chzhaodi, N. Mak, The reaction of octyl alcohols with ammonia under a pressure of hydrogen over a fused iron catalyst, *Pet. Chem. USSR.* 1 (1962) 300–310. doi:10.1016/0031-6458(62)90038-2.
- [50] K. Shimizu, K. Kon, W. Onodera, H. Yamazaki, J.N. Kondo, Heterogeneous Ni Catalyst for Direct Synthesis of Primary Amines from Alcohols and Ammonia, *ACS Catal.* 3 (2013) 112–117. doi:10.1021/cs3007473.

---

## **Chapter 4**

### **Kinetic modeling of *n*-octanol amination**

---



## 4.1 Background

As already pointed in Chapter 1, comprehensive studies focusing on the kinetic modeling of direct alcohol amination reactions are scarce [1–7]. Despite being a critical variable, the effect of exogenous H<sub>2</sub> has been generally omitted from kinetic studies, being only integrated in a recent model developed by Ruiz *et al.* [7] encompassing the direct amination of *n*-dodecanol with NH<sub>3</sub>.

Along this chapter, the reader will find a complete kinetic study of the direct amination of *n*-octanol with NH<sub>3</sub> for the Ag-Co/Al<sub>2</sub>O<sub>3</sub> catalyst presented in Chapter 3 (see Table 3-8, 4<sup>th</sup> entry for the characterization details), since this catalyst presented the most attractive performance. First, the results of a full factorial design of experiments will be analyzed to devise relevant kinetic trends and assess the main interactions between the operation variables. In a second step, these trends will be used to build kinetic models based on a set of adjustable parameters relying on a series of simplifying hypotheses. The candidate models will be further compared and discriminated in terms of goodness of fit against experimental data, physical consistency of the fitted parameters, robustness, and consistency with the initial hypotheses. As a result of this analysis, the surviving models will be listed and discussed in detail at the end of the chapter and a cartography will be presented showing the operation window affording the maximum yield and activity to the primary amine (*n*-octylamine or OA).

## 4.2 Reaction Network

The direct amination of *n*-octanol with NH<sub>3</sub> comprises a complex network of sequential and parallel reactions as shown in Figure 4-1. First, the alcohol is dehydrogenated, forming octanal and H<sub>2</sub> at rate  $r_1$ . This step is generally considered as rate limiting, controlling the overall reaction rate [1–7]. In a second step, the carbonyl compound reacts with either NH<sub>3</sub> or the as-generated amines, yielding reactive intermediates being characterized by rates  $r_2$ ,  $r_5$  and  $r_8$ . Finally, the primary and secondary intermediates are hydrogenated to generate the corresponding amines according to the reaction rates  $r_4$  and  $r_6$ , respectively. The primary imine (i.e. octylimine or OI) can also undergo dehydrogenation, favoring the formation of octanenitrile (ON) according to rate  $r_3$ . This step is equilibrated and can be limited either by decreasing the reaction temperature, or by increasing the total or the H<sub>2</sub> partial pressure. The amine distribution is determined by the relative rates of the parallel condensation ( $r_2$ ,  $r_5$ ,  $r_8$ ) and disproportionation reactions ( $r_7$ ). Regarding the former reactions, only rates  $r_2$  and  $r_5$  will be hereinafter considered, since the tertiary amine is only generated in trace amounts (i.e.  $r_8$  can be omitted) and  $r_7$  has been previously found to be negligible.

## 4.3 Experimental trends

Prior to the formulation and development of kinetic models, it is worth analyzing the experimental trends observed for the catalytic activity and selectivity over Ag-Co/ Al<sub>2</sub>O<sub>3</sub> as a function of the partial pressure of the reactants (*n*-octanol, NH<sub>3</sub>), the partial pressure of H<sub>2</sub> and the temperature, as well as of the interactions between the operation variables in

the experimental range considered in this study. Figure 4-2 summarizes the main trends observed. The main factors impacting the catalytic activity were found to be the temperature and the H<sub>2</sub> partial pressure. The effect of temperature is straightforward, since higher temperatures will lead to an increase of the frequency of molecular collisions overcoming the activation energy barriers. However, the effect of H<sub>2</sub> is rather unexpected if we assume that the first and rate-controlling step is the dehydrogenation reaction of *n*-octanol characterized by rate  $r_1$ . Both variables seem to present a slight interaction, leading the system to be more sensitive to the H<sub>2</sub> pressure at higher temperature. The *n*-octanol and NH<sub>3</sub> partial pressures exert an almost flat response on the activity, pointing out an almost *zero* reaction order for both partial pressures under the tested conditions. These trends are in line with the observations earlier reported in the literature for the direct amination of aliphatic alcohols with NH<sub>3</sub> [1–7].

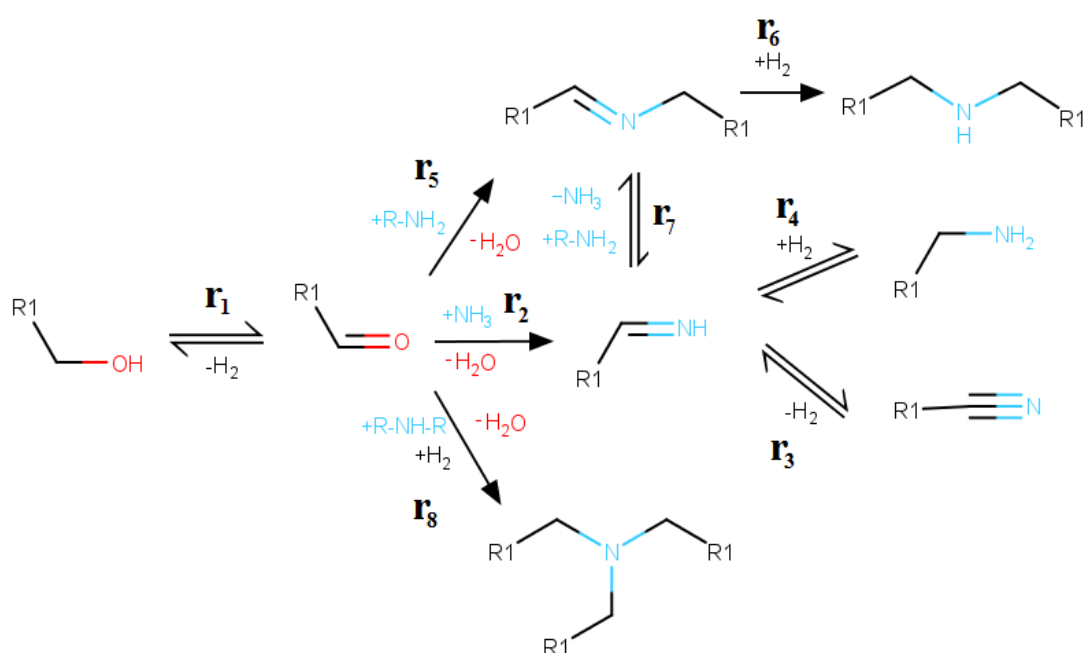


**Figure 4-1** Reaction network for the direct amination of *n*-octanol with NH<sub>3</sub>.

The effect of the reaction variables on the selectivity for consecutive reactions needs to be assessed as a function of the conversion. The OA selectivity, which is defined as the quotient between the OA yield and the total amine yield, was plotted against the *n*-octanol conversion (Figure 4-3). In this analysis, the experimental points were differentiated by the value of one operation variable at a time. The most sensitive variables (H<sub>2</sub> and NH<sub>3</sub> partial pressures) were deliberately set constant at the least selective conditions to survey the effect of the other variables at higher resolution.

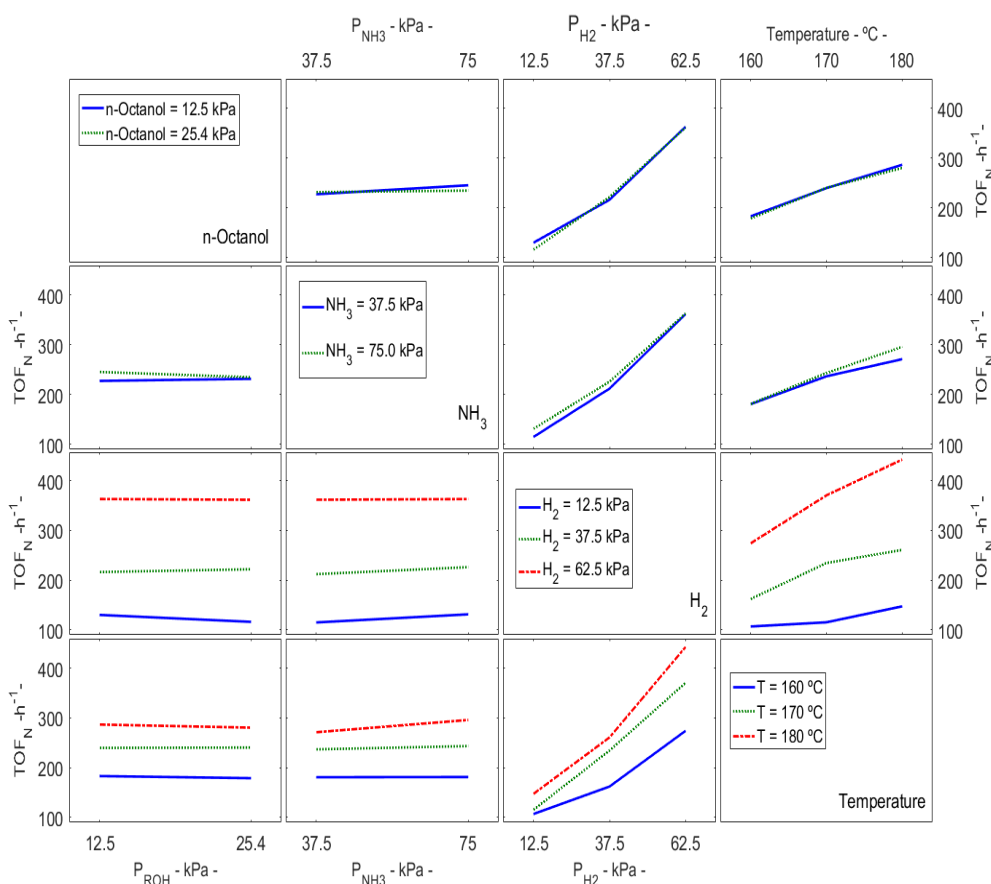


**Figure 4-2** Interaction plot showing the influence of the different operation variables on the catalytic activity over Ag-Co/Al<sub>2</sub>O<sub>3</sub> for *n*-octanol amination with NH<sub>3</sub>. The TOF<sub>N</sub> is defined as the molar flow of N-products divided by the moles of surface Co<sup>0</sup>.

Figure 4-3-(a) plots the effect of the NH<sub>3</sub> partial pressure at a constant H<sub>2</sub> pressure of 62.5 kPa and at a *n*-octanol pressure in the range of 12.5-25.4 kPa. As expected from the reaction network (Figure 4-1), the NH<sub>3</sub> partial pressure enhances the OA selectivity. This result is not surprising, since a higher NH<sub>3</sub> partial pressure is expected to promote rate  $r_2$  at the expense of rate  $r_5$ , favoring the formation of OA over DOA. Interestingly, an increase of the H<sub>2</sub> partial pressure at a constant NH<sub>3</sub> pressure of 37.5 kPa and at a *n*-octanol pressure in the range of 12.5-25.4 kPa exerts a dramatic effect on the amine selectivity (Figure 4-3-(b)), boosting DOA formation. This effect is in line with the catalytic results presented in section 3.5. More subtle effects are however observed when varying the *n*-octanol partial pressure and temperature while keeping constant the H<sub>2</sub> and NH<sub>3</sub> partial pressures at values of 62.5 kPa and 37.5 kPa, respectively: an increase of the *n*-octanol pressure promotes the OA selectivity (Figure 4-3-(c)). This result is counter-intuitive, since the NH<sub>3</sub>-to-alcohol ratio decreases at higher *n*-octanol concentration. Finally, the OA selectivity is also promoted by the temperature in the range 160-180 °C (Figure 4-3-(d)), which is consistent with the results presented in section 3.6. At first sight, this observation can be attributed to a thermodynamic effect, since DOA formation from the reaction of *n*-octanol with OA is more exothermic (-46 kJ/mol vs. -13 kJ/mol), thus shifting the chemical equilibrium

towards the least substituted amine at higher temperatures. Nonetheless, it is difficult to discern kinetic from equilibrium effects at low conversions.

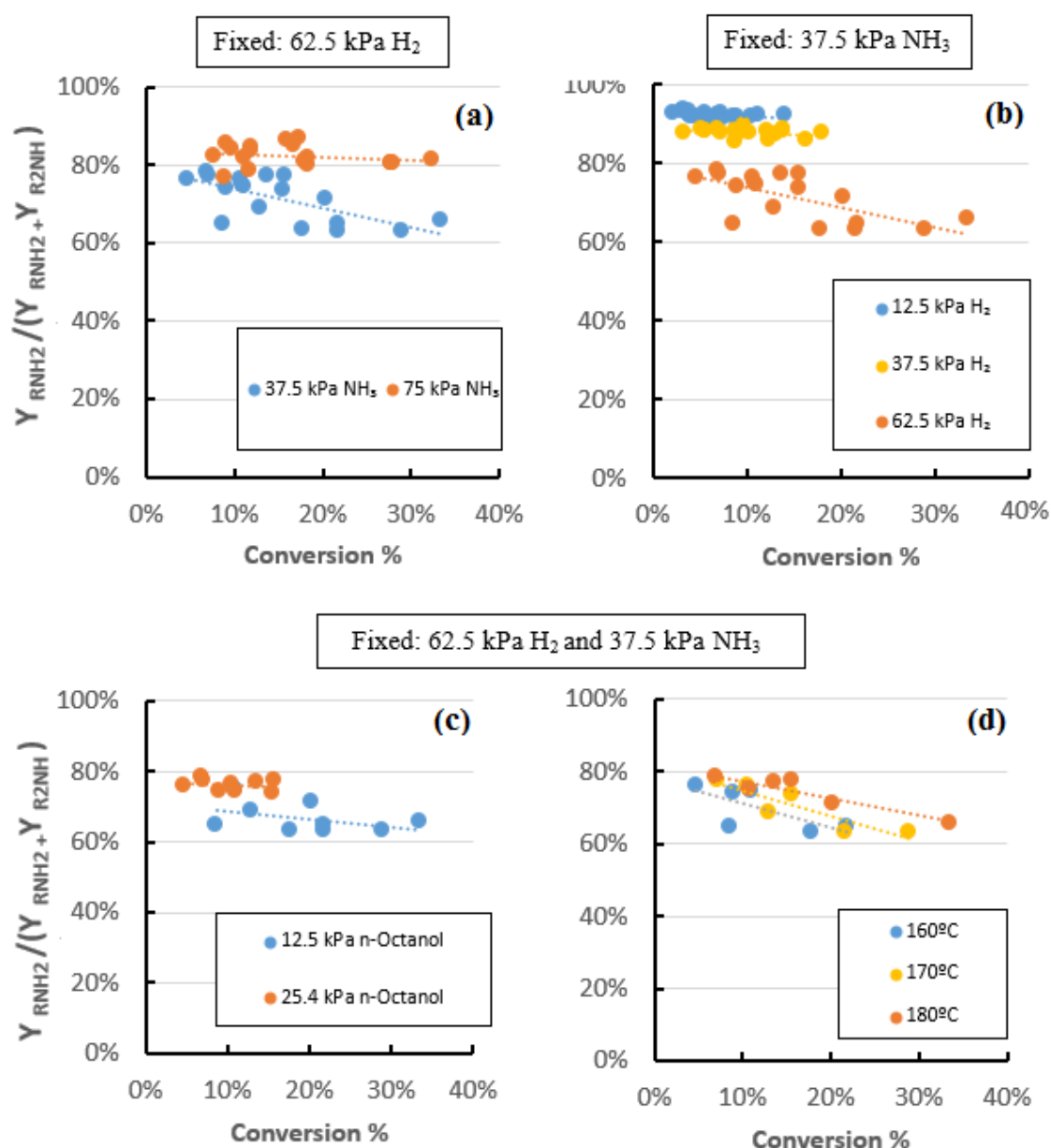


**Figure 4-3** Influence of: (a) NH<sub>3</sub> pressure, (b) H<sub>2</sub> pressure, (c) *n*-octanol pressure, and (d) temperature on the OA selectivity over Ag-Co/Al<sub>2</sub>O<sub>3</sub>. Reaction conditions: p<sub>ROH</sub>: 12.5-25.4 kPa; p<sub>H2</sub>: 12.5-62.5 kPa; p<sub>NH3</sub>: 37.5-75 kPa; Temperature: 160-180 °C. Total pressure: 200 kPa The dotted lines are a guide to the eye.

## 4.4 Development of kinetic models

### 4.4.1 Rationalization of the experimental trends

The experimental trends presented above can be used as a basis for building kinetic models for rationalizing the catalytic performance of Ag-Co/Al<sub>2</sub>O<sub>3</sub>. Among the different variables considered, the effect of the H<sub>2</sub> pressure on both the activity and selectivity for

*n*-octanol amination with NH<sub>3</sub> deserves special consideration, since this variable impacts to an important extent the catalytic performance.

On the guidance of the reaction network depicted in Figure 4-1, we can foresee *a priori* two explanations accounting for the role of H<sub>2</sub> on the catalytic activity for the Ag-Co/Al<sub>2</sub>O<sub>3</sub> catalyst: (i) enhancement of the rates  $r_4$  and  $r_6$  provided that the hydrogenation steps leading to amine formation are rate limiting, and (ii) increase of the number of available Co<sup>0</sup> catalytic sites for reaction. The first assumption can be rapidly dismissed, since reductive amination reactions starting from carbonyl compounds are known to occur fast [7], these being typically conducted at milder temperatures than those starting from the corresponding alcohols [8,9]. In this regard, considering alcohol dehydrogenation as the rate-determining step, the role of H<sub>2</sub> is more likely attributed to the second assumption encompassing a recovery of the catalytic surface from some deactivating agent. As already discussed in section 1.3, such an effect was first studied by Baiker *et al.* [10] for a Cu catalyst. It was proposed that H<sub>2</sub> could recover the active metallic phase of the catalysts being poisoned by NH<sub>3</sub> due to nitridation. Further work extended this conclusion to Ni and Co catalysts [11–14]. These studies describe a fast and reversible effect of H<sub>2</sub> on the catalytic activity as previously shown in Figure 1-12. Unfortunately, none of these studies transposed the effect of H<sub>2</sub> into kinetic models for amination. More recently, a mechanism involving a reversible catalytic deactivation of Ru catalysts triggered by coke deposition was proposed by Ruiz *et al.* [7] for the direct amination reaction of *n*-dodecanol with NH<sub>3</sub>, in line with previous findings by the same group on the amination of myrtenol [6].

Turning now our attention into the selectivity for the Ag-Co/Al<sub>2</sub>O<sub>3</sub> catalyst, three possible roles of the H<sub>2</sub> pressure can be in principle anticipated affecting the selectivity to amines (Figure 4-1): (i) promotion of the secondary imine hydrogenation rate ( $r_6$ ), favoring the genesis of the secondary amine; (ii) increase of the imine-amine coupling rate ( $r_7$ ) towards the secondary imine over the primary imine hydrogenation rate ( $r_4$ ), and (iii) promotion of rate  $r_5$  over  $r_2$ . On the guidance of the experimental results, the first mechanism can be omitted, since the secondary imine yield is enhanced by the H<sub>2</sub> pressure (Figure 4-4), pointing out a promotional effect of reactions leading to the secondary amine. The second mechanism is also unlikely, since higher H<sub>2</sub> pressures should in principle favor the primary imine hydrogenation rate  $r_4$  over  $r_7$ , increasing the selectivity towards the primary amine. In this regard, the third option, namely the promotion of rate  $r_5$  over  $r_2$ , seems to provide the most plausible explanation. Taking into account a potential role of H<sub>2</sub> on liberating Co<sup>0</sup> sites for the reaction, it appears reasonable to imagine that rate  $r_5$  might be more sensitive to the number of free Co<sup>0</sup> sites than rate  $r_2$ . This effect could be explained by a non-competitive adsorption mechanism, often considered for reactions involving bulky and small molecules [7,15]. In the adsorption of large molecules, steric hindrance or multiple-site adsorption might hinder further adsorption of large molecules before the surface is fully covered. On the contrary, lighter molecules can still be adsorbed on the remaining isolated vacant sites. In such a situation, differentiated sites would be available for non-competing adsorbents.

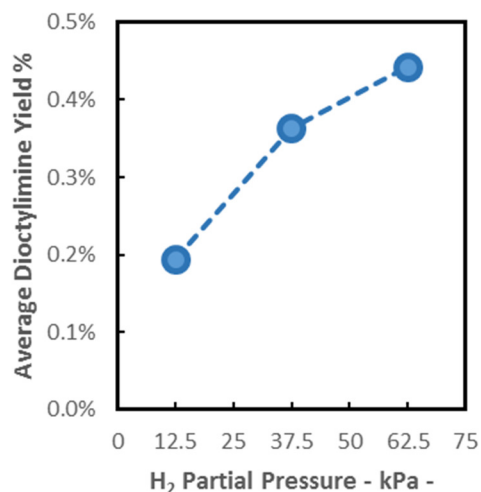


**Figure 4-4** Effect of the H<sub>2</sub> partial pressure on the average DOI yield (R=N-R) for the amination reaction of *n*-octanol with NH<sub>3</sub> over Ag-Co/Al<sub>2</sub>O<sub>3</sub>. Reaction conditions: p<sub>ROH</sub>: 12.5-25.4 kPa; p<sub>H<sub>2</sub></sub>: 12.5-62.5 kPa; p<sub>NH<sub>3</sub></sub>: 37.5-75 kPa; Temperature: 160-180 °C. Total pressure: 200 kPa The dotted lines are a guide to the eye.

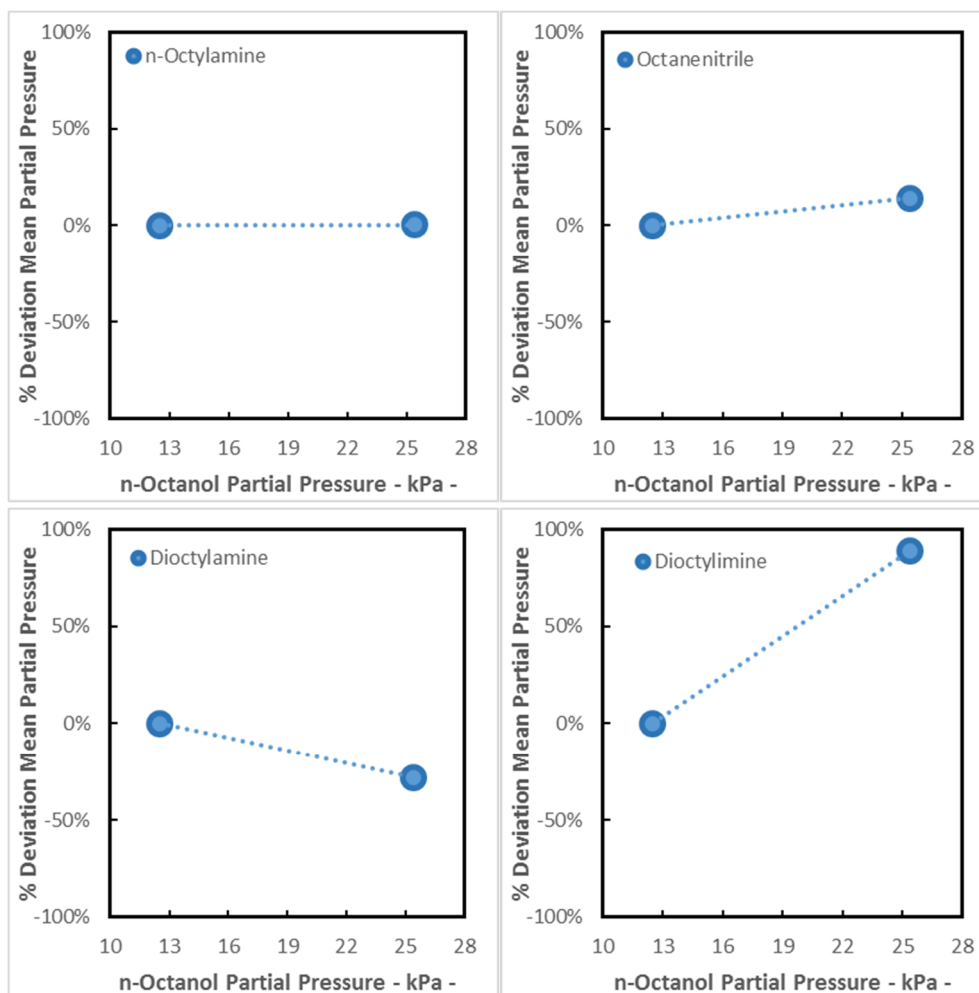
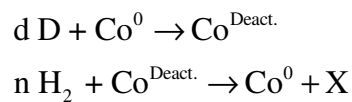


**Figure 4-5** Effect of the *n*-octanol partial pressure on the average OA, ON, DOA and DOI formation for the amination reaction of *n*-octanol with NH<sub>3</sub> over Ag-Co/Al<sub>2</sub>O<sub>3</sub>. Reaction conditions: p<sub>ROH</sub>: 12.5-25.4 kPa; p<sub>H<sub>2</sub></sub>: 12.5-62.5 kPa; p<sub>NH<sub>3</sub></sub>: 37.5-75 kPa; Temperature: 160-180 °C. Total pressure: 200 kPa The dotted lines are a guide to the eye.

In light of the comments above, the otherwise counterintuitive observation that higher OA selectivities are obtained at higher *n*-octanol partial pressures might be explained by either a direct or indirect role of such an adsorbed molecule on the reversible deactivation mechanism. As can be deduced from Figure 4-5, only ON and DOI formation appears to be promoted by the *n*-octanol partial pressure. According to the reaction network (Figure 4-1), the octanal and OI partial pressures are likely to follow the same trend as DOA. Considering that the effect of the H<sub>2</sub> pressure on catalytic activity was previously reported for secondary alcohols [13,14], where no nitrile is generated, the most likely candidates to be considered in the deactivation mechanism are *n*-octanol, octanal and the primary and secondary imine intermediates (i.e. OI and DOI).

On the guidance of the analysis above, the effect of the H<sub>2</sub> partial pressure will be ascribed hereinafter to a catalytic deactivation-regeneration mechanism, as described in Reaction 4-1, where *D* is the deactivating agent and *d* and *n* refer to the stoichiometric coefficients.



**Reaction 4-1**

#### 4.4.2 Hypotheses and approximations

As a rule, the catalytic transformation of chemicals on heterogeneous catalysts can be described as a result of 7 consecutive steps [16]: (1) mass-transfer of the reactants from the bulk phase to the catalyst surface, (2) intraparticle mass-transfer of the reactants, (3) adsorption of the reactants on the catalytic sites, (4) surface reaction, (5) desorption of the products from the catalytic sites, (6) intraparticle mass-transfer of the products, and (7) mass-transfer of the products from the catalyst surface to the bulk phase. To develop kinetic models, a series of assumptions and approximations needs to be considered allowing the description of the complexity of a system with simpler mathematical expressions. In line with the experimental trends described in section 4.3, the following general and particular assumptions were taken into account:

(i) **General assumptions**

1. **Plug flow model:** We assume that the reactor hydrodynamics can be described by an ideal plug-flow model in the absence of heat and mass transfer limitations, as pointed out in section 2.5.1. In this model, the mass balance of a component in an elemental volume can be described by Eq. 4-1 using the reactant flowrate at the reactor inlet as boundary condition:

$$\frac{dF_i}{dM_c} = v_i r_i \quad \text{with } M_c = 0 \rightarrow F_i = F_{i,0}$$

**Eq. 4-1**

2. **Quasi-equilibrium approximation (QEA):** We assume that the concentration of surface species encompassing fast adsorption or generation can be described by an adsorption or chemical equilibrium expression. This affords an easy way for relating

the surface coverage of the different species to the corresponding partial pressure in the gas phase. This approximation was applied here to all adsorption processes and to the second step of reversible hydrogenation/dehydrogenation reactions (entries 10 and 13, Table 4-1). The adsorption equilibria were described using Langmuir-type isotherms (Eq. 4-2) [17] based on monolayer adsorption on an ideal homogeneous surface and with constant adsorption enthalpy

$$\theta_i = \frac{K_i p_i}{1 + \sum K_x p_x} \quad \Bigg| \quad \text{Eq. 4-2}$$

3. Quasi-steady state approximation: We assume that the surface coverage of intermediate species that are rapidly consumed can be estimated by considering equal rates of formation and consumption. This approximation has been hereinafter used for calculating the surface coverage of the intermediate primary imine and the extent of surface deactivation (entries 9, 12 and 20, 21 of Table 4-1, respectively).

(ii) Particular assumptions

1. Reversible / irreversible surface reactions: We assume that the primary imine surface hydrogenation reaction is fully reversible, whereas the forward reaction is dominant for the other surface reactions.
2. Reversible deactivation: We assume a deactivation mechanism for the catalyst, where a reactant, an intermediate or a reaction product partially inhibits the catalytic activity *via* coke formation. The H<sub>2</sub> partial pressure is expected to regenerate the catalyst surface, increasing the number of active sites for reaction. This process can be regarded as fast if we assume instantaneous change of the extent of deactivation the concentration of either the coke source or the H<sub>2</sub> partial pressure. In line with the kinetic trends drawn in section 4.4.1, the possible coke sources are: *n*-octanol, octanal, OA and DOI.
3. Non-competitive adsorption between bulky and small molecules: We assume the presence of two different catalytic sites (Y and Z) with independent site balances for small (Y) and bulky (Z) adsorbed species.
4. We assume that the deactivation mechanism only affects the catalytic sites for larger molecules (Z) in line with the observed trends relating the OA selectivity with the H<sub>2</sub> partial pressure.

**Table 4-1** List of elementary steps for *n*-octanol amination with NH<sub>3</sub> (QEA: quasi-equilibrium approximation; QSSA: quasi-steady state approximation)

#	Elementary steps <sup>1</sup>	Approximation	Rate
1	$\text{R-OH}_{(g)} + \text{Z} \longrightarrow \text{R-OH}^{\text{Z}}$	QEA	
2	$\text{R-OH}^{\text{Z}} + \text{Y} \longrightarrow \text{R-OH-I}^{\text{Z}} + \text{H}^{\text{Y}}$	-	r <sub>1</sub>
3	$\text{R-OH-I}^{\text{Z}} + \text{Y} \longrightarrow \text{R=O}^{\text{Z}} + \text{H}^{\text{Y}}$	QSSA	
4	$\text{H}_{2(g)} + 2\text{Y} \rightleftharpoons 2\text{H}^{\text{Y}}$	QEA	
5	$\text{R=O}_{(g)} + \text{Z} \rightleftharpoons \text{R=O}^{\text{Z}}$	QEA	
6	$\text{NH}_{3(g)} + \text{Y} \rightleftharpoons \text{NH}_3^{\text{Y}}$	QEA	
7	$\text{R=O}^{\text{Z}} + \text{NH}_3^{\text{Y}} \longrightarrow \text{R=NH}^{\text{Z}} + \text{H}_2\text{O}^{\text{Y}}$	-	r <sub>2</sub>
8	$\text{H}_2\text{O}_{(g)} + \text{Y} \rightleftharpoons \text{H}_2\text{O}^{\text{Y}}$	QEA	
9	$\text{R=NH}^{\text{Z}} + \text{Y} \rightleftharpoons \text{R-CN-I}^{\text{Z}} + \text{H}^{\text{Y}}$	-	r <sub>3</sub>
10	$\text{R-CN-I}^{\text{Z}} + \text{Y} \rightleftharpoons \text{R-CN}^{\text{Z}} + \text{H}^{\text{Y}}$	QEA	
11	$\text{R=NH}^{\text{Z}} + \text{H}^{\text{Y}} \rightleftharpoons \text{R-NH}_2\text{-I}^{\text{Z}} + \text{Y}$	-	r <sub>4</sub>
12	$\text{R-NH}_2\text{-I}^{\text{Z}} + \text{H}^{\text{Y}} \rightleftharpoons \text{R-NH}_2^{\text{Z}} + \text{Y}$	QEA	
13	$\text{R-NH}_{2(g)} + \text{Z} \rightleftharpoons \text{R-NH}_2^{\text{Z}}$	QEA	
14	$\text{R-CN} + \text{Z} \rightleftharpoons \text{R-CN}^{\text{Z}}$	QEA	
15	$\text{R=O}^{\text{Z}} + \text{R-NH}_2^{\text{Z}} \longrightarrow \text{R=N-R}^{\text{Z}} + \text{H}_2\text{O}^{\text{Y}}$	-	r <sub>5</sub>
16	$\text{R=N-R}_{(g)} + \text{Z} \rightleftharpoons \text{R=N-R}^{\text{Z}}$	QEA	
17	$\text{R=N-R}^{\text{Z}} + \text{H}^{\text{Y}} \longrightarrow \text{R}_2\text{-NH-I}^{\text{Z}} + \text{Y}$	-	r <sub>6</sub>
18	$\text{R}_2\text{-NH-I}^{\text{Z}} + \text{H}^{\text{Y}} \longrightarrow \text{R}_2\text{-NH}^{\text{Z}} + \text{Y}$	QSSA	
19	$\text{R}_2\text{-NH}_{(g)} + \text{Z} \rightleftharpoons \text{R}_2\text{-NH}^{\text{Z}}$	QEA	
20	$\text{d D}^{\text{Z}} \longrightarrow \text{Z}^{\text{Deact}}$	QSSA	r <sub>D</sub>
21	$\text{Z}^{\text{Deact.}} + n \text{H}^{\text{Y}} \rightarrow \text{Z} + n \text{Y} + \text{X}$	QSSA	r <sub>R</sub>

<sup>1</sup> The labels Y and Z refer to active sites

#### 4.4.3 Formulation of kinetic expressions

A series of kinetic expressions was developed using the set of chemical transformations listed in Table 4-1. In Table 4-2, each chemical transformation is related to the rate of an elementary step in Table 4-1. The surface coverage of the different species,  $\theta_j^{\text{Z}}$  or  $\theta_j^{\text{Y}}$ , was computed using Langmuir-type expressions accounting for adsorption equilibrium (Eq. 4-3) with the exception of  $\theta_{\text{R=NH}}^{\text{Z}}$ ,  $\theta_{\text{D}}^{\text{Z}}$ ,  $\theta_{\text{RCN-I}}^{\text{Z}}$  and  $\theta_{\text{RNH}_2\text{-I}}^{\text{Z}}$  corresponding to the surface coverage of the OI, coke, ON and OA intermediates, respectively, all

considered here as non-desorbable species. Table 4-3 compiles the expressions obtained for the rate of the different surface reactions.

$$\theta_i^x = K_i p_i \theta_v^x \quad \text{Eq. 4-3}$$

Incorporating Eq. 4.3 for the adsorption equilibria into Eqs. 4.4-4.11, the expressions listed in Table 4.4 are obtained for reactions r<sub>1</sub>-r<sub>6</sub>.

**Table 4-2** List of surface reactions leading to the main reaction products and deactivation-regeneration mechanism

RDS # (Table 4-1)	Chemical Transformation	Reaction #
2	$R-OH^Z + 2Y \xrightarrow{r_1} R=O^Z + 2H^Y$	Reaction 4-2
7	$R=O^Z + NH_3^Y \xrightarrow{r_2} R=NH^Z + H_2O^Y$	Reaction 4-3
9	$R=NH^Z + 2Y \xrightleftharpoons[r_{-3}]{r_{+3}} R-CN^Z + 2H^Y$	Reaction 4-4
11	$R-NH^Z + 2H^Y \xrightleftharpoons[r_{-4}]{r_{+4}} R-NH_2^Z + 2Y$	Reaction 4-5
15	$R=O^Z + R-NH_2^Z \xrightarrow{r_5} R=N-R^Z + H_2O^Y$	Reaction 4-6
17	$R=N-R^Z + 2H^Y \xrightarrow{r_6} R_2-NH^Z + 2Y$	Reaction 4-7
20	$d D^Z \xrightarrow{r_D} Z^{Deact.}$	Reaction 4-8
21	$Z^{Deact.} + n H^Y \xrightarrow{r_R} Z + n Y + X$	Reaction 4-9

**Table 4-3** Reaction rates for the elementary steps in Table 4-1

$r_1 = k_1 \theta_{R-OH}^Z \theta_V^Y$	Eq. 4-4
$r_2 = k_2 \theta_{R=O}^Z \theta_{NH_3}^Y$	Eq. 4-5
$r_3 = k_{+3} \theta_{R=NH}^Z \theta_V^Y - k_{-3} \theta_{R-CN-I}^Z \theta_H^Y$	Eq. 4-6
$r_4 = k_{+4} \theta_{R=NH}^Z \theta_H^Y - k_{-4} \theta_{R-NH_2-I}^Y \theta_V^Y$	Eq. 4-7
$r_5 = k_5 \theta_{R=O}^Z \theta_{R-NH_2}^Z$	Eq. 4-8
$r_6 = k_6 \theta_{R=N-R}^Z \theta_H^Y$	Eq. 4-9
$r_D = k_D (\theta_x^Z)^d$	Eq. 4-10
$r_R = k_R (\theta_H^Y)^n \theta_D^Z$	Eq. 4-11

**Table 4-4** Expressions for the different reaction rates leading to chemical transformations

$r_1 = k'_1 p_{R-OH} \theta_V^Y \theta_V^Z$	<b>Eq. 4-12</b>
$r_2 = k'_2 p_{R=O} p_{NH_3} \theta_V^Y \theta_V^Z$	<b>Eq. 4-13</b>
$r_3 = \left( k'_{+3} A_{R=NH} - k'_{-3} p_{R-CN} p_{H_2} \right) \theta_V^Y \theta_V^Z$	<b>Eq. 4-14</b>
$r_4 = \left( k'_{+4} A_{R=NH} p_{H_2}^{1/2} - k'_{-4} p_{R-NH_2} p_{H_2}^{-1/2} \right) \theta_V^Y \theta_V^Z$	<b>Eq. 4-15</b>
$r_5 = k'_5 p_{R=O} p_{R-NH_2} \left( \theta_V^Z \right)^2$	<b>Eq. 4-16</b>
$r_6 = k'_6 p_{R=N-R} p_{H_2}^{1/2} \theta_V^Z \theta_V^Y$	<b>Eq. 4-17</b>

The OI and coke surface coverages (i.e.  $\theta_{R=NH}^Z$  and  $\theta_D^Z$ ) were computed by applying the quasi-steady state approximation, thus obtaining the expressions:

$$\begin{aligned} \text{QSSA: } r_2 &= r_3 + r_4 \\ \theta_{R=NH}^Z &= \frac{k_2 \theta_{R=O}^Z \theta_{NH_3}^Y + k_{-3} \theta_{R-CN-I}^Z \theta_H^Y + k_{-4} \theta_{R-NH_2-I}^Y \theta_V^Y}{k_{+3} \theta_V^Y + k_{+4} \theta_H^Y} \end{aligned} \quad \text{Eq. 4-18}$$

$$\begin{aligned} \text{QSSA: } r_R &= r_D \\ \theta_D^Z &= \frac{k_D \left( \theta_X^Z \right)^d}{k_R \left( \theta_H^Y \right)^n} \end{aligned} \quad \text{Eq. 4-19}$$

where D = R-OH, R=O, R=NH, R<sub>2</sub>=N

In contrast, the surface coverage of ON and OA surface intermediates  $\theta_{R-CN-I}^Z$  and  $\theta_{R-NH_2-I}^Z$  were computed by applying the quasi-equilibrium approximation, thus obtaining the following expressions:

$$\begin{aligned} \text{QEA: \#13 in Table 4.1} \\ \theta_{R-CN-I}^Z &= \frac{p_{R-CN} p_{H_2}^{1/2}}{K_{R-CN-I}} \end{aligned} \quad \text{Eq. 4-20}$$

$$\begin{aligned} \text{QEA: \#10 in Table 4.1} \\ \theta_{R-NH_2-I}^Z &= K_{R-NH_2-I}^{-1} p_{R-NH_2} p_{H_2}^{-1/2} \end{aligned} \quad \text{Eq. 4-21}$$

Introducing Eq. 4-20 and Eq. 4-21 into Eq. 4-18 and rearranging, the following expression can be obtained, where  $k_i'$  is defined as a global constant collecting the corresponding kinetic and equilibrium constants:

$$\theta_{R=NH}^Z = \frac{k'_2 p_{R=O} p_{NH_3} + k'_{-3} p_{RCN} p_{H_2} + k'_{-4} p_{R-NH_2} p_{H_2}^{-1/2}}{k'_{+3} + k'_{+4} p_{H_2}^{1/2}} \theta_V^Z = A_{R=NH} \theta_V^Z \quad \text{Eq. 4-22}$$

The fraction of Z and Y vacant sites (i.e.  $\theta_j^Z$  and  $\theta_j^Y$ ) was calculated from the corresponding Z and Y site balances using Eq. 4-23, where only the reactant, intermediate imine and deactivated coverages were considered. The expression for the Y site balance, corresponding to smaller molecules, is presented in Eq. 4-24. In the case of Z sites, two different expressions were developed as a function of the stoichiometry of the deactivation reaction ( $d=1$  or  $2$ ), resulting in Eq. 4-25 and Eq. 4-26, where  $K_D'$  is a global constant that collects the deactivation constant and the respective adsorption constants. In the case of Eq. 4-26, a quadratic equation was obtained with only one positive solution.

$$\theta_V^x = 1 - \sum \theta_i^x \quad (x = Z \text{ or } Y) \quad \text{Eq. 4-23}$$

**i) Y sites**

$$1 = \theta_V^Y + \theta_{NH_3}^Y + \theta_H^Y$$

$$\theta_V^Y = \frac{1}{1 + K_{NH_3} p_{NH_3} + \sqrt{K_{H_2} p_{H_2}}} \quad \text{Eq. 4-24}$$

**ii) Z sites**

Stoichiometry  $d = 1$

$$1 = \theta_V^Z + \theta_{R-OH}^Z + \theta_{R=NH}^Z + \theta_D^Z$$

$$\theta_V^Z = \frac{1}{1 + K_{R-OH} p_{R-OH} + A_{R=NH} + K_D' p_D (p_{H_2}^{1/2} \theta_V^Y)^{-n}} \quad \text{Eq. 4-25}$$

with  $D = R-OH, R=O, R=NH, R_2=N$

Stoichiometry  $d = 2$

$$1 = \theta_V^Z + \theta_{R-OH}^Z + \theta_{R=NH}^Z + \theta_D^Z$$

$$1 = \theta_V^Z + K_{R-OH} p_{R-OH} \theta_V^Z + A_{R=NH} \theta_V^Z + K_D' p_D^2 (p_{H_2}^{1/2} \theta_V^Y)^{-n} (\theta_V^Z)^2 \quad \text{Eq. 4-26}$$

with  $D = R-OH, R=O, R=NH, R_2=N$

The kinetic expressions for  $r_1$  to  $r_6$  in Table 4-4 were included in the material balances, as expressed in Table 4-5. The deactivation reaction was only included in the site balance, since the fraction of mass loss *via* this route was considered negligible.

**Table 4-5** Expressions for the differential material balances

$\frac{dF_{R-OH}}{dW} = -r_1$	<b>Eq. 4-27</b>
$\frac{dF_{R=O}}{dW} = r_1 - r_2 - r_5$	<b>Eq. 4-28</b>
$\frac{dF_{R-NH_2}}{dW} = r_4 - r_5$	<b>Eq. 4-29</b>
$\frac{dF_{R-CN}}{dW} = r_3$	<b>Eq. 4-30</b>
$\frac{dF_{R_2=N}}{dW} = r_5 - r_6$	<b>Eq. 4-31</b>
$\frac{dF_{R_2-NH}}{dW} = r_6$	<b>Eq. 4-32</b>
$\frac{dF_{NH_3}}{dW} = -r_2$	<b>Eq. 4-33</b>
$\frac{dF_{H_2}}{dW} = r_1 + r_3 - r_4 - r_6$	<b>Eq. 4-34</b>

Finally, the temperature dependency of the apparent rate and equilibrium constants was expressed by Eq. 4-35 and Eq. 4-36, respectively.

$$k'_i(T) = k'_i(T_M) \exp \left[ -\frac{E_{a,app i}}{R} \left( \frac{1}{T} - \frac{1}{T_M} \right) \right] \quad \text{Eq. 4-35}$$

$$K'_i(T) = K'_i(T_M) \exp \left[ -\frac{\Delta H_i}{R} \left( \frac{1}{T} - \frac{1}{T_M} \right) \right] \quad \text{Eq. 4-36}$$

## 4.5 Kinetic Fitting

### 4.5.1 Discrimination of the different deactivation mechanisms

In light of the experimental trends drawn in section 4.3 and the theoretical corpus of section 4.4, several molecules were selected as plausible candidates for controlling the deactivation process over Ag-Co/Al<sub>2</sub>O<sub>3</sub>. Initially, 8 models (I-VIII) were fitted to the experimental results, comprising the following permutations:

- (i) Source of coke: *n*-octanol, octanal, OA and DOA
- (ii) Deactivation stoichiometry: *d* = 1 and *d* = 2

The initial models were constructed as presented in section 4.4.2, encompassing the fitting of 25 variables. The thermodynamic consistency of the fitted variables was initially

imposed by forcing positive values of both the kinetic and equilibrium constants, as well as negative adsorption enthalpies. The parameters were adjusted by minimizing sum of squares difference ( $SS_E$ ) between the computed and experimental pressures of *n*-octanol, OA, ON and DOA, which were scaled around their mean value (Eq. 4-37). Complementarily, the goodness of fit was also judged in terms of the coefficient of determination, which was computed according to Eq. 4-38.

$$SS_E = \sum_{x=1} \sum_{i=1} \left[ (p_{x,j} - \widehat{p}_{x,j})^2 \right] w_{x,i} \quad \text{Eq. 4-37}$$

$$R^2 = 1 - \frac{(p_{x,j} - \widehat{p}_{x,j})^2}{(p_{x,j} - \bar{p}_{x,j})^2} \quad \text{Eq. 4-38}$$

The results of the fittings to the different models are summarized in Table 4-6. Overall, the best fittings were achieved for models M.V and M.VI relying on a deactivation mechanism triggered by the primary imine (OI), and model M.VII considering the secondary imine (DOI) as coke source. The least representative models were those based on *n*-octanol and octanal driven deactivation. Regarding the stoichiometry, without exception, the models considering  $d=2$  led to higher  $SS_E$  when compared to models considering  $d=1$ . The analysis of residuals (Figure 4-6) confirmed the superiority of model M.V, showing the lowest  $SS_E$ . Models M.VI and M.VII exhibited a pronounced negative correlation for OA, while model M.V exhibited an almost random pattern. Overall, all the models exhibited deviations at higher yields and conversions, most likely due to a lack of experimental data at higher product concentrations. A correction of model M.V to circumvent these deviations will be proposed in the forthcoming chapter.

**Table 4-6** Summary of fitting results for discrimination among different deactivation mechanisms

Model #	Coke Source	d	SS <sub>E</sub>	R <sup>2</sup>		Highest Correlation Factor
				p <sub><i>n</i>-octanol</sub>	p <sub>products</sub>	
M.I	R-OH	d = 1	40.5	99.1%	95.7%	$k'_3 - k'_4 = 99.9\%$
M.II	R-OH	d = 2	188.3	98.5%	84.5%	$E_{a,app2} - E_{a,app5} = 99.9\%$
M.III	R=O	d = 1	45.8	99.1%	94.7%	$k'_3 - k'_4 = 99.9\%$
M.IV	R=O	d = 2	133.1	98.6%	91.2%	$k'_3 - k'_4 = 99.9\%$
M.V	R=NH	d = 1	29.7	99.0%	96.8%	$E_{a,app1} - H_{ROH} = 99.1\%$
M.VI	R=NH	d = 2	33.2	98.3%	95.9%	$k'_3 - H_{ROH} = 99.9\%$
M.VII	R <sub>2</sub> =N	d = 1	34.5	99.0%	94.8%	$k'_3 - k'_4 = 99.9\%$
M.VIII	R <sub>2</sub> =N	d = 2	45.7	98.9%	93.6%	$k'_3 - k'_4 = 99.9\%$

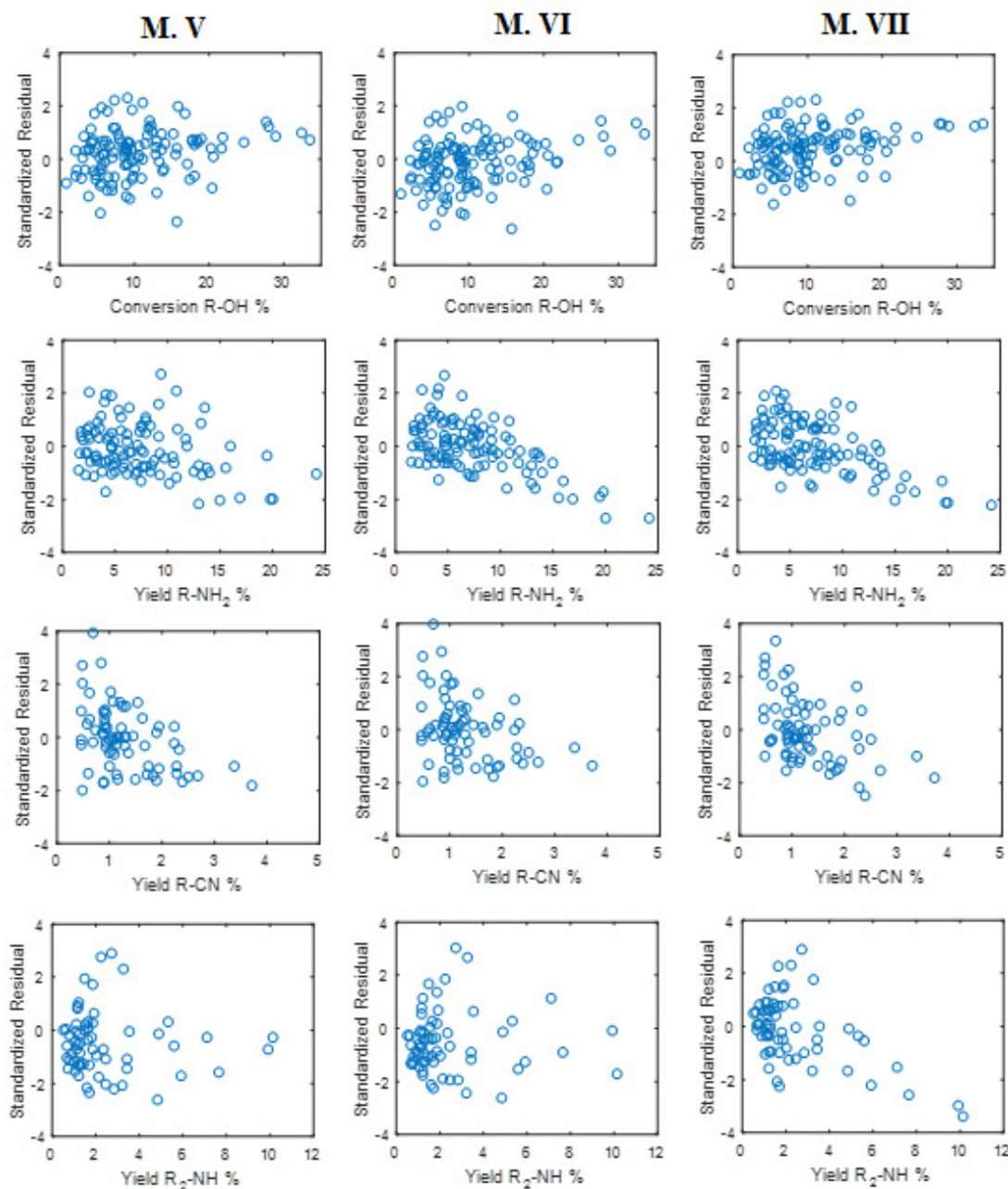


**Figure 4-6** Standardized residual analysis for the kinetic models M.V, M.VI and M.VII.

The fitted parameters for model M.V are listed in Table 4-7. The kinetic constants affecting the *n*-octanol conversion, as well as the adsorption constants, could be safely estimated with moderate standard errors. In contrast, the parameters defining the product distribution showed correlation. This issue can be circumvented either by a mathematical transformation of model M.V, or by removing parameters with low sensitivity, as described in the next section.

**Table 4-7** Fitted parameters for model M.V

Parameter	Unit	Mean value	% RSE (95% C.I.) <sup>a</sup>	> 95% Correlation
$k'_1$	mmol h <sup>-1</sup> bar <sup>-1</sup> mg <sub>cat</sub> <sup>-1</sup>	4.97	0.01%	-
$k'_2$	mmol h <sup>-1</sup> bar <sup>-2</sup> mg <sub>cat</sub> <sup>-1</sup>	292.37	89.4%	$k'_5$
$k'_{+3}$	mmol h <sup>-1</sup> mg <sub>cat</sub> <sup>-1</sup>	1.90	122.3%	$k'_{+4}$
$k'_{-3}$	mmol h <sup>-1</sup> bar <sup>-1</sup> mg <sub>cat</sub> <sup>-1</sup>	287.06	35.0%	-
$k'_{+4}$	mmol h <sup>-1</sup> bar <sup>-0.5</sup> mg <sub>cat</sub> <sup>-1</sup>	13.22	115.4%	K <sub>D</sub> , $k'_{+3}$
$k'_{-4}$	mmol h <sup>-1</sup> bar <sup>-0.5</sup> mg <sub>cat</sub> <sup>-1</sup>	17.20	45.2%	-
$k'_5$	mmol h <sup>-1</sup> bar <sup>-2</sup> mg <sub>cat</sub> <sup>-1</sup>	2.71E+04	100.4%	$k'_2$
$k'_6$	mmol h <sup>-1</sup> bar <sup>-1.5</sup> mg <sub>cat</sub> <sup>-1</sup>	1.55E+04	195.5%	-
E <sub>a,app 1</sub>	kJ mol <sup>-1</sup>	27.75	4.4%	-
E <sub>a,app 2</sub>	kJ mol <sup>-1</sup>	36.26	128.7%	-
E <sub>a,app +3</sub>	kJ mol <sup>-1</sup>	116.81	49.1%	-
E <sub>a,app -3</sub>	kJ mol <sup>-1</sup>	-32.03	137.8%	-
E <sub>a,app +4</sub>	kJ mol <sup>-1</sup>	49.34	102.5%	-
E <sub>a,app -4</sub>	kJ mol <sup>-1</sup>	-106.12	55.3%	-
E <sub>a,app 5</sub>	kJ mol <sup>-1</sup>	-41.11	126.3%	-
E <sub>a,app 6</sub>	kJ mol <sup>-1</sup>	550.25	95.5%	-
K <sub>R-OH</sub>	bar <sup>-1</sup>	5.04E-04	192.1%	-
H <sub>R-OH</sub>	kJ mol <sup>-1</sup>	-101.50	8.8%	-
K <sub>NH<sub>3</sub></sub>	bar <sup>-1</sup>	2.48E-04	198.0%	-
H <sub>NH<sub>3</sub></sub>	kJ mol <sup>-1</sup>	-99.90	9.6%	-
K <sub>H<sub>2</sub></sub>	bar <sup>-1</sup>	0.71	6.7%	-
H <sub>H<sub>2</sub></sub>	kJ mol <sup>-1</sup>	-30.01	9.9%	-
K <sub>D</sub>	bar <sup>b/2</sup>	62.96	116.0%	$k'_{+4}$
H <sub>D</sub>	kJ mol <sup>-1</sup>	60.94	82.5%	-
N	-	1.84	18.3%	-

<sup>a</sup> C.I. = Confidence Interval

## 4.5.2 Kinetic Model Optimization

As pointed out in the previous section, model M.V showed the best fitting to the experimental data. Nonetheless, some of the obtained parameters, presented in Table 4-7, were found to be non-significant from a statistical viewpoint. As an attempt to improve the statistical quality of the fittings, we decided to simplify the kinetic expressions included in model M.V. using the following set of approximations:

- (i) *N*-octanol adsorption is negligible ( $K_{ROH} p_{ROH} \ll 1$ )
- (ii)  $NH_3$  adsorption is negligible ( $K_{NH3} p_{NH3} \ll 1$ )
- (iii) The deactivation stoichiometry factor was set to the closest integer:  $n=2$

Moreover, model M.V predicts non-negligible octanal concentrations at the reactor outlet, whereas this molecule was not experimentally detected. In the same line, only small amounts of DOI were formed (<1% yield). Keeping these ideas in mind, two additional simplifications were introduced to the model:

- (iv) Quasi-steady state approximation for octanal ( $r_1 = r_2 + r_5$ ) if we consider its concentration negligible in the global mass balance.
- (v) Quasi-steady state approximation for DOI ( $r_5 = r_6$ ) if we consider its concentration negligible in the global mass balance.

By introducing the aforementioned 5 approximations into model M.V, new expressions for the coverages and reaction rates  $r_1$ - $r_6$  could be derived, which are compiled in Annex IV. The kinetic parameters for the model were reduced from an initial number of 25 to 18 after simplification, and were again optimized. To increase the chance of finding global minima, different fittings were run using different starting points. Overall, the simplified model converged into two different solutions, resulting in models M.V\_A and M.V\_B, for which the fitted parameters are compiled in Table 4-8 and Table 4-9, respectively. Both models show excellent standard errors for the fitted parameters. The highest determination errors are related to the backward reaction rates (i.e.  $r_3$  and  $r_4$ ) and the secondary amine formation rate ( $r_5$ ). This could be explained by the use of experimental data covering only low *n*-octanol conversions. Moreover, none of the fitted parameters exhibited correlation factors above 95%. On the contrary, most of the parameters in model M.V\_A presented non-negligible variance inflation factors (VIF >10), implying the existence of multi-collinearity (see Eq- 2-15 in Chapter 2 for further information). This fact indicates that a change in one of the parameters during the fitting can be compensated by the simultaneous change of multiple parameters, helping to explain the existence of variable convergent solutions based on different combinations of values for the parameters. VIF values were comparatively lower for model M.V\_B with only two pairs of parameters with VIF >10 (i.e.  $k'_{-5}$  and  $E_{a,app 5}$ ;  $k'_{-4}$ , and  $E_{a,app -4}$ ).

The statistics of the fittings for models M.V\_A and M.V\_B are compared in Table 4-10. Overall, model M.V\_B provided a better fitting with the smallest  $SS_E$ . As can be observed in the corresponding parity plots (Figure 4-7 and Figure 4-8), model M.V\_B was

able to improve the prediction of DOI formation, while the other variables were similarly predicted by both models. As in section 4.5.1, the ill-poisoned prediction of DOA formation at high conversions can be ascribed to the relatively low number of experiments in our matrix leading to high DOA partial pressures. Keeping this idea in mind, models M.V\_A and M.V\_B were further refined and tested to improve the predictive level at higher conversions. Figure 4-9 compares the reaction profile predicted by both models up to 70% conversion. Overall, both models showed an excellent agreement with the experimental data for OA and ON formation. In contrast, DOA formation was more accurately predicted by model M.V\_B, while model M.V\_A presented severe deviations at conversions >50%. In light of the smaller SS<sub>E</sub>, lack of correlation between the fitted parameters and superior prediction level at higher conversions, model M.V\_B was selected hereinafter as the best performing model.

**Table 4-8** Fitted parameters for model M.V\_A

Parameter	Unit	Value	% RSE (95% C.I.) <sup>a</sup>	VIF <sup>b</sup>
$k_1'$	(mmol h <sup>-1</sup> bar <sup>-1</sup> mg <sub>cat</sub> <sup>-1</sup> )	5.53	1%	14
$k_2'$	(mmol h <sup>-1</sup> bar <sup>-2</sup> mg <sub>cat</sub> <sup>-1</sup> )	278.95	1%	22
$k_{+3}'$	(mmol h <sup>-1</sup> mg <sub>cat</sub> <sup>-1</sup> )	1.97	1%	15
$k_{-3}'$	(mmol h <sup>-1</sup> bar <sup>-1</sup> mg <sub>cat</sub> <sup>-1</sup> )	380.03	25%	4
$k_{+4}'$	(mmol h <sup>-1</sup> bar <sup>-0.5</sup> mg <sub>cat</sub> <sup>-1</sup> )	12.51	1%	16
$k_{-4}'$	(mmol h <sup>-1</sup> bar <sup>-0.5</sup> mg <sub>cat</sub> <sup>-1</sup> )	18.85	29%	12
$k_5'$	(mmol h <sup>-1</sup> bar <sup>-2</sup> mg <sub>cat</sub> <sup>-1</sup> )	2.77E+04	20%	14
E <sub>a,app 1</sub>	kJ mol <sup>-1</sup>	26.10	1%	23
E <sub>a,app 2</sub>	kJ mol <sup>-1</sup>	36.01	2%	81
E <sub>a,app +3</sub>	kJ mol <sup>-1</sup>	116.09	1%	48
E <sub>a,app -3</sub>	kJ mol <sup>-1</sup>	-24.22	>100%	4
E <sub>a,app +4</sub>	kJ mol <sup>-1</sup>	48.74	1%	17
E <sub>a,app -4</sub>	kJ mol <sup>-1</sup>	-62.36	81%	9
E <sub>a,app 5</sub>	kJ mol <sup>-1</sup>	-8.98	>100%	10
K <sub>H<sub>2</sub></sub>	bar <sup>-1</sup>	0.78	1%	8
H <sub>H<sub>2</sub></sub>	kJ mol <sup>-1</sup>	-62.86	1%	25
K <sub>D</sub>	bar	49.87	1%	16
H <sub>D</sub>	kJ mol <sup>-1</sup>	62.37	1%	40

<sup>a</sup> C.I. = Confidence Interval; <sup>b</sup> VIF = Variance Inflation Factor

**Table 4-9** Fitted parameters for model M.V\_B

Parameter	Unit	Value	% RSE (95% C.I.) <sup>a</sup>	VIF <sup>b</sup>
$k'_1$	(mmol h <sup>-1</sup> bar <sup>-1</sup> mg <sub>cat</sub> <sup>-1</sup> )	119.55	<1%	4
$k'_2$	(mmol h <sup>-1</sup> bar <sup>-2</sup> mg <sub>cat</sub> <sup>-1</sup> )	12.42	<1%	3
$k'_{+3}$	(mmol h <sup>-1</sup> mg <sub>cat</sub> <sup>-1</sup> )	15.07	<1%	3
$k'_{-3}$	(mmol h <sup>-1</sup> bar <sup>-1</sup> mg <sub>cat</sub> <sup>-1</sup> )	8757.47	24%	4
$k'_{+4}$	(mmol h <sup>-1</sup> bar <sup>-0.5</sup> mg <sub>cat</sub> <sup>-1</sup> )	97.91	<1%	3
$k'_{-4}$	(mmol h <sup>-1</sup> bar <sup>-0.5</sup> mg <sub>cat</sub> <sup>-1</sup> )	498.39	24%	14
$k'_5$	(mmol h <sup>-1</sup> bar <sup>-2</sup> mg <sub>cat</sub> <sup>-1</sup> )	2.74E+04	18%	15
E <sub>a,app 1</sub>	kJ mol <sup>-1</sup>	116.16	<1%	2
E <sub>a,app 2</sub>	kJ mol <sup>-1</sup>	-469.65	<1%	4
E <sub>a,app +3</sub>	kJ mol <sup>-1</sup>	127.12	<1%	3
E <sub>a,app -3</sub>	kJ mol <sup>-1</sup>	36.49	>100%	5
E <sub>a,app +4</sub>	kJ mol <sup>-1</sup>	85.44	<1%	4
E <sub>a,app -4</sub>	kJ mol <sup>-1</sup>	52.74	97%	13
E <sub>a,app 5</sub>	kJ mol <sup>-1</sup>	-446.07	8%	14
K <sub>H<sub>2</sub></sub>	bar <sup>-1</sup>	0.69	<1%	2
H <sub>H<sub>2</sub></sub>	kJ mol <sup>-1</sup>	-25.46	<1%	4
K <sub>D</sub>	bar	398.76	<1%	3
H <sub>D</sub>	kJ mol <sup>-1</sup>	56.06	<1%	3

<sup>a</sup> C.I. = Confidence Interval; <sup>b</sup> VIF = Variance Inflation Factor

**Table 4-10** Summary of statistics of fitting for discriminating models M.V, M.V\_A and M.V\_B

Model #	Coke Source	d	SSE	R <sup>2</sup> p <sub>n-octanol</sub>	R <sup>2</sup> p <sub>products</sub>	Highest Correlation Factor
M.V	R=NH	d = 1	29.7	99.0 %	96.8 %	E <sub>a,app1</sub> - H <sub>ROH</sub> = -99.1%
M.V_A	R=NH	d = 1	30.9	99.1 %	96.3 %	k'_{-4} - k'_5 = 93.7%
M.V_B	R=NH	d = 1	25.9	99.2%	96.8 %	k'_{-4} - k'_5 = 94.4%

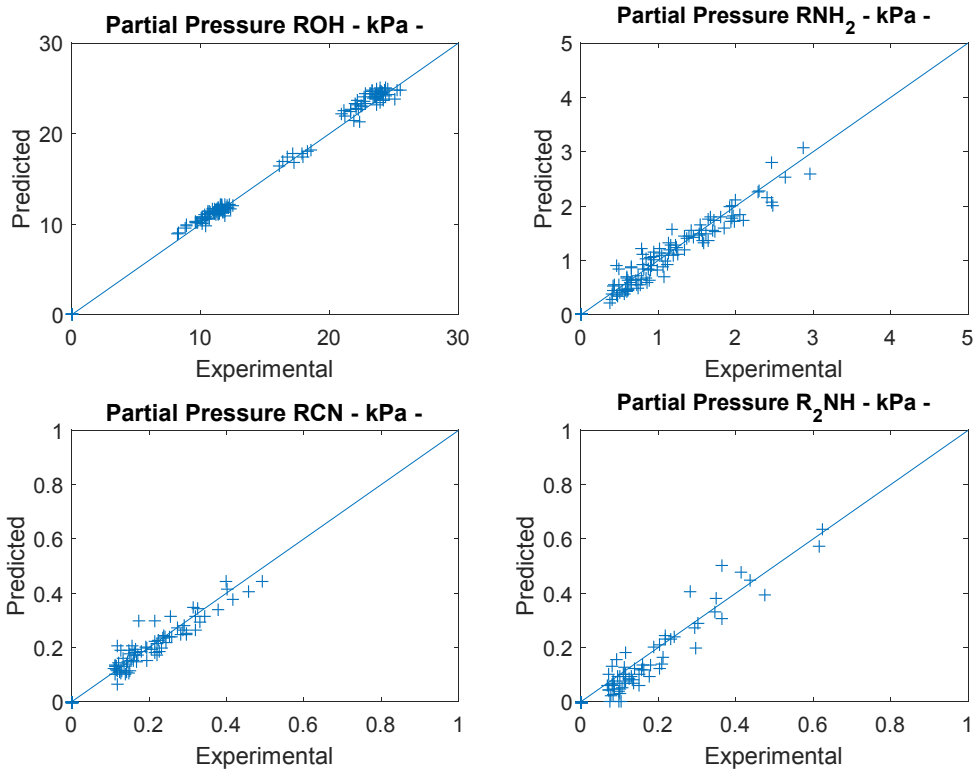


**Figure 4-7** Experimental vs. predicted partial pressures for *n*-octanol, OA, ON and DOA for model M.V\_A.

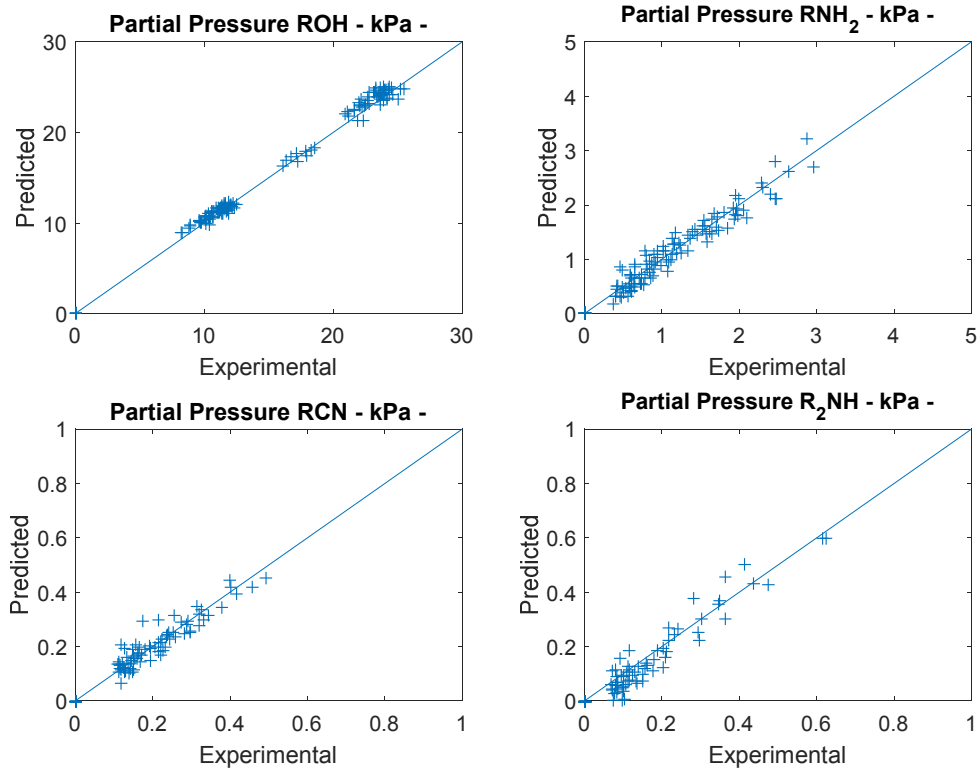


**Figure 4-8** Experimental vs. predicted partial pressures for *n*-octanol, OA, ON and DOA for model M.V\_B.

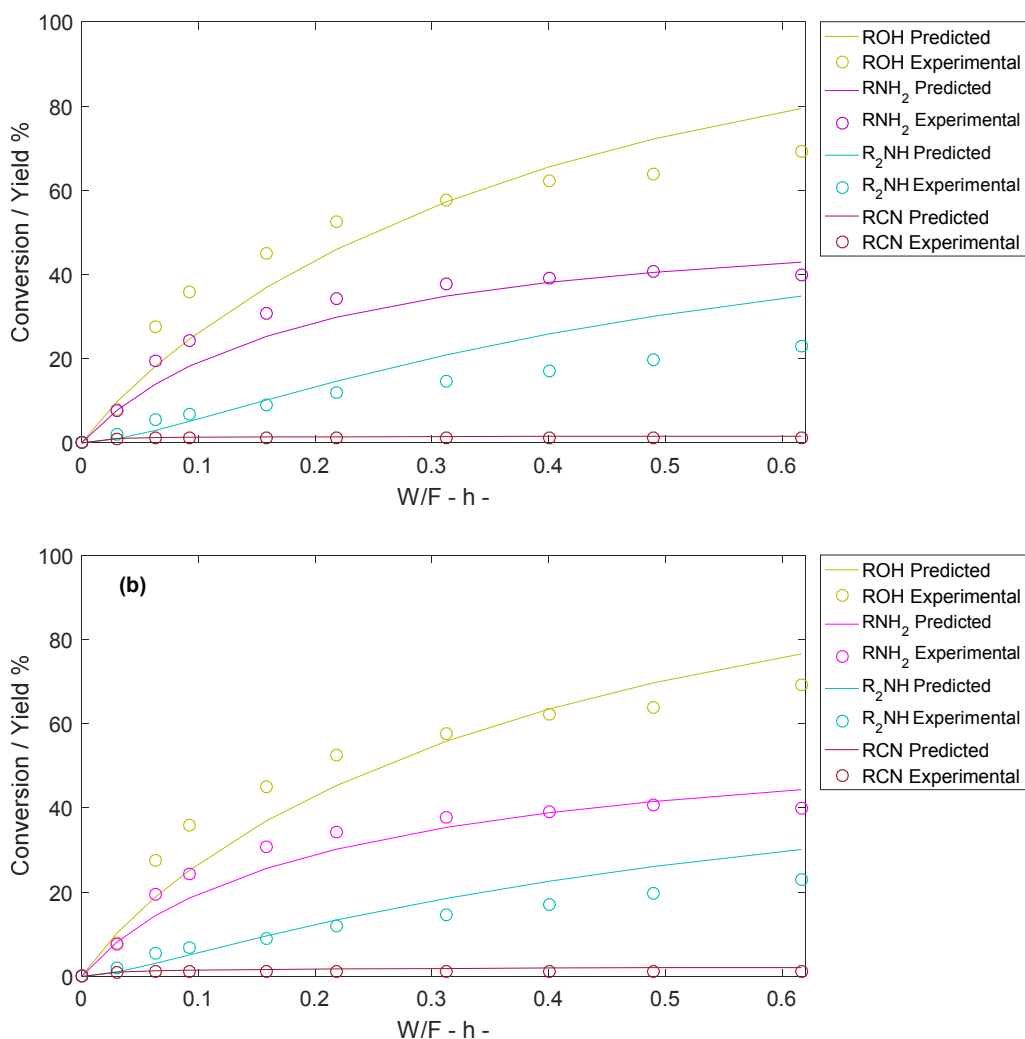


**Figure 4-9** Experimental vs. predicted product distribution profiles at high conversions for models (a) M.V\_A and (b) M.V\_B. Reaction conditions: *n*-octanol feed: 0.4 mL·h<sup>-1</sup>; T = 180 °C, P = 200 kPa, [NH<sub>3</sub>:H<sub>2</sub>:N<sub>2</sub>:ROH] = [3 : 3 : 4.5 : 1]).

### 4.5.3 Validation of experimental trends for model M.V\_B

As pointed out above, model M.V\_B was able to describe successfully the whole body of experimental data for *n*-octanol amination over Ag-Co/Al<sub>2</sub>O<sub>3</sub> at low and high conversions. Figure 4-10 compares the experimental and predicted trends. Overall, the experimental trends are in agreement with those predicted by model M.V\_B:

- (i) Reaction order close to zero for NH<sub>3</sub> and *n*-octanol;
- (ii) Positive reaction order for H<sub>2</sub>;
- (iii) Enhanced sensitivity to H<sub>2</sub> pressure at higher temperature.

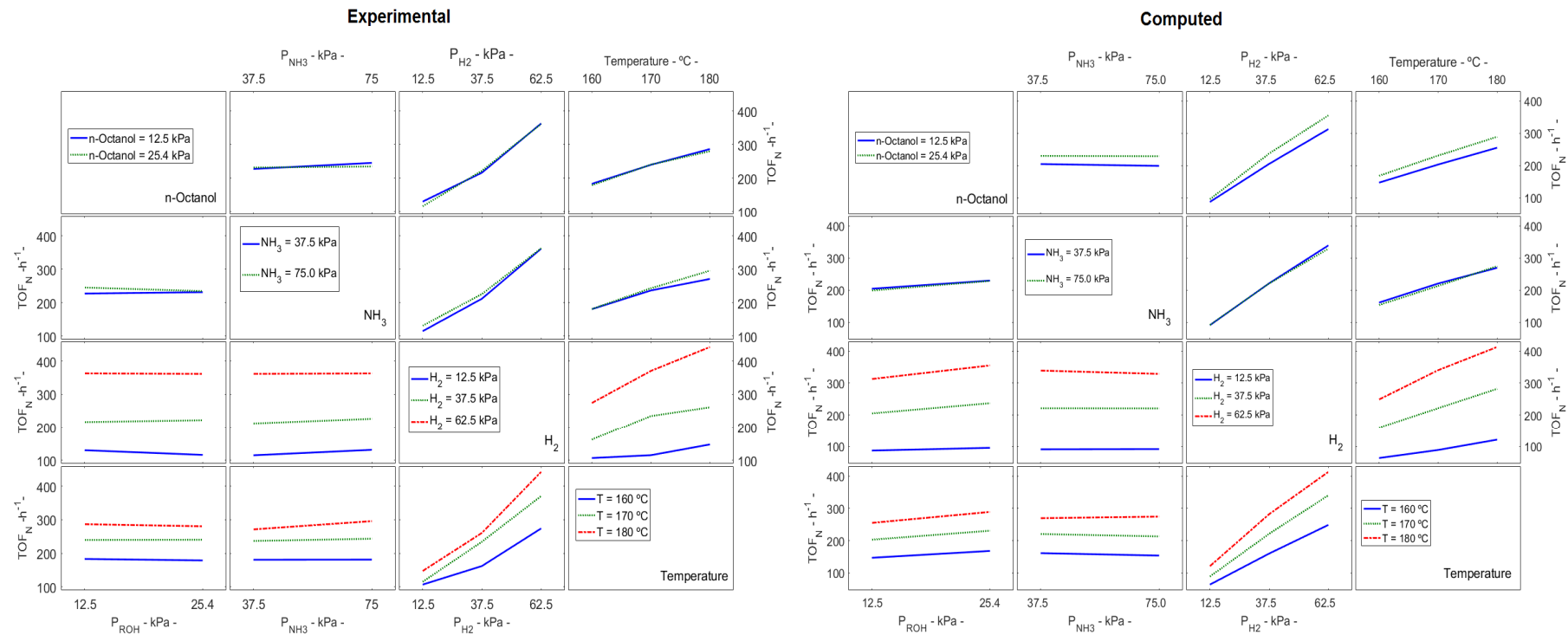


**Figure 4-10** Experimental vs. predicted interaction plots by model M.V\_B showing the influence of the operation variables on the catalytic activity for *n*-octanol amination with NH<sub>3</sub> over Ag-Co/Al<sub>2</sub>O<sub>3</sub>. The TOF<sub>N</sub> is defined as the molar flow of identified products divided by the moles surface Co<sup>0</sup>. Reaction conditions: *n*-octanol pressure: 12.5-25.4 kPa; H<sub>2</sub> pressure: 12.5-62.5 kPa; NH<sub>3</sub> pressure: 37.5-75 kPa; Total pressure: 200 kPa Temperature: 160-180 °C.

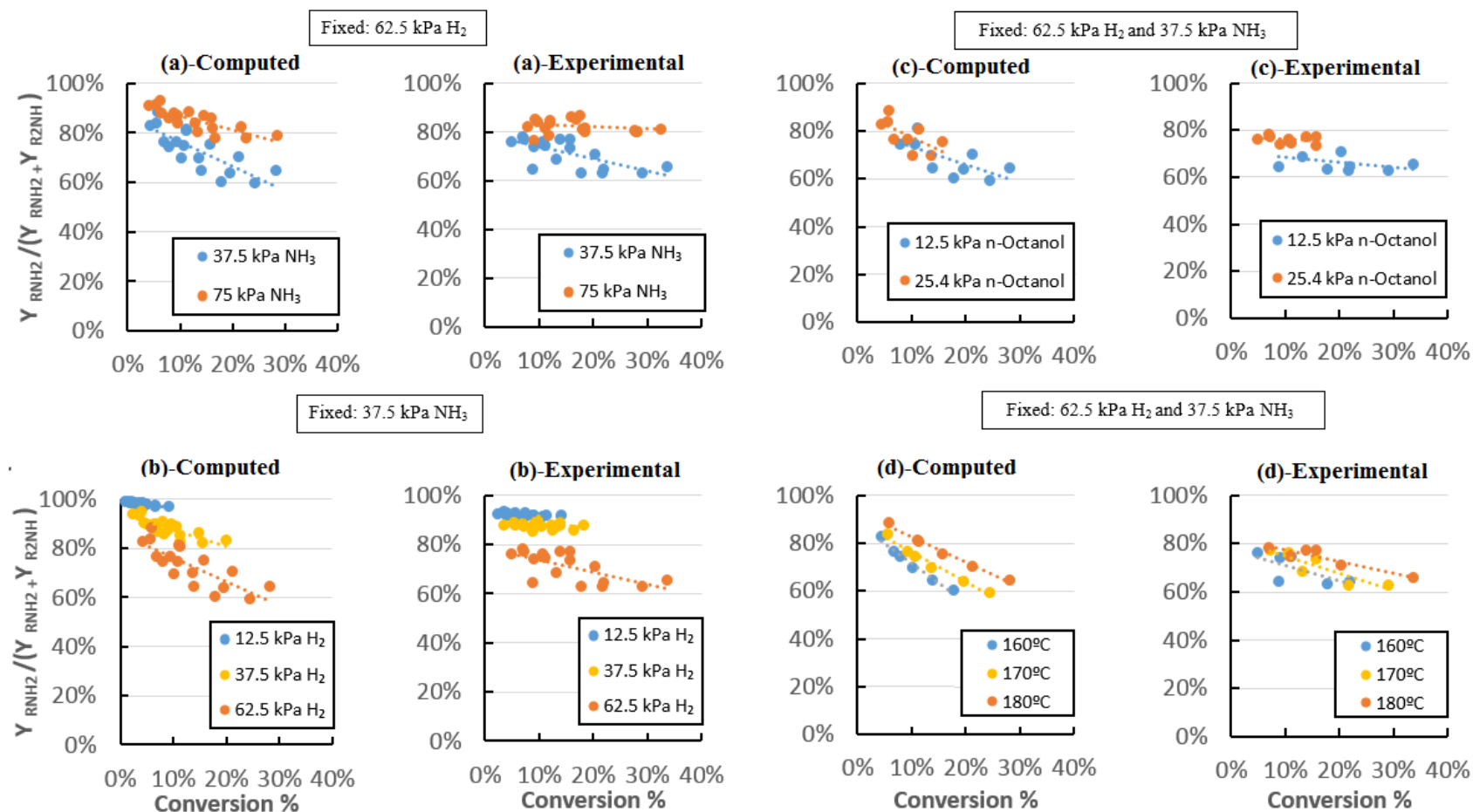


**Figure 4-11** Experimental vs. predicted trends by model M.V\_B for OA selectivity in the amination reaction of *n*-octanol with NH<sub>3</sub> over Ag-Co/Al<sub>2</sub>O<sub>3</sub> as a function of: (a) NH<sub>3</sub> partial pressure (b) H<sub>2</sub> partial pressure, (c) *n*-octanol partial pressure, and (d) temperature. Reaction conditions: *n*-octanol pressure: 12.5-25.4 kPa; H<sub>2</sub> pressure: 12.5-62.5 kPa; NH<sub>3</sub> pressure: 37.5-75 kPa; Temperature: 160-180 °C. Total pressure: 200 kPa The dotted curves are a guide to the eye.

Despite the good prediction level of model M.V\_B, some deviations from the experimental trends can be observed. For instance, a slightly positive order for the *n*-octanol pressure is noticeable, especially at high H<sub>2</sub> pressure. This could be attributed to the fact that coke formation is not considered in the computed mass balance. Indeed, a higher carbon loss is experimentally observed when increasing the *n*-octanol pressure, evolving from 0.7% to 2.7% on average relative to total *n*-octanol in the feed. This deviation induces the model to overestimate the rate of product formation as a compensation for the non-accounted carbon loss. Overall, these deviations are small and do not exert an important influence under the tested conditions. More interestingly, a deviation is observed regarding the response to the H<sub>2</sub> pressure. While the experimental trends show a non-linear response in a broad range of *n*-octanol and NH<sub>3</sub> partial pressures, the predicted trend is almost linear and deviates especially on the central point. This could be well accounted by different effects, such as by a non-langmuirian adsorption pattern for H<sub>2</sub>, or by a dual-site deactivation mechanism.

Figure 4-11 compares the experimental and predicted trends by model M.V\_B affecting the OA selectivity. Noteworthy, the main experimental trends listed below are accurately reproduced by the model:

- (i) Selectivity increase at higher NH<sub>3</sub> pressure;
- (ii) Selectivity loss at higher H<sub>2</sub> pressure;
- (iii) Slight selectivity increase at higher *n*-octanol pressure;
- (iv) Slight selectivity increase at higher temperature;

However, as a rule, the predicted selectivity at very low conversions (<10%) is higher than the experimental values. This observation might be attributed to an ill definition of the reaction rates leading to the secondary amine formation, as already pointed out in section 4.5.2. This deviation vanishes at higher conversions, where the kinetic predictions are of greater interest for industrial production.

Overall, the experimental and predicted trends by model M.V\_B show very good agreement. Despite some deviations, the model offers a good compromise between the accuracy of the prediction and its complexity. The introduction of additional parameters could lead to an over-fitting of the experimental data and to a loss of physical significance of the fitted parameters under the body of the assumptions made.

#### 4.5.4 Mapping of Process Conditions

In view of the high prediction ability of Model M.V\_B, this model was further used to compute the product distribution by interpolation within the fitted experimental plane. This exercise can help the engineer to identify the optimal conditions for the production of the targeted amines (in our case primary amines).

As an illustrative example, the results of the product distribution at a constant contact time (W/F) of 0.5 h are presented in Figure 4-12. The effect of the H<sub>2</sub> and NH<sub>3</sub> partial pressures were screened over the experimental plane. For the sake of visual clarity, the

effect of the temperature was computed in different plots. The predicted trends for the *n*-octanol conversion are in agreement with those presented in Figure 4-11. The parallel vertical lines indicate that the H<sub>2</sub> partial pressure is the variable exerting the most relevant effect. Interestingly, the lines become steeper at the highest H<sub>2</sub> pressures, pointing out a slightly negative effect of the NH<sub>3</sub> partial pressure over this range. As expected, the *n*-octanol conversion increases with the temperature. The maximum conversion (80%) is achieved at the maximum temperature (180 °C) and H<sub>2</sub> pressure (62.5 kPa).

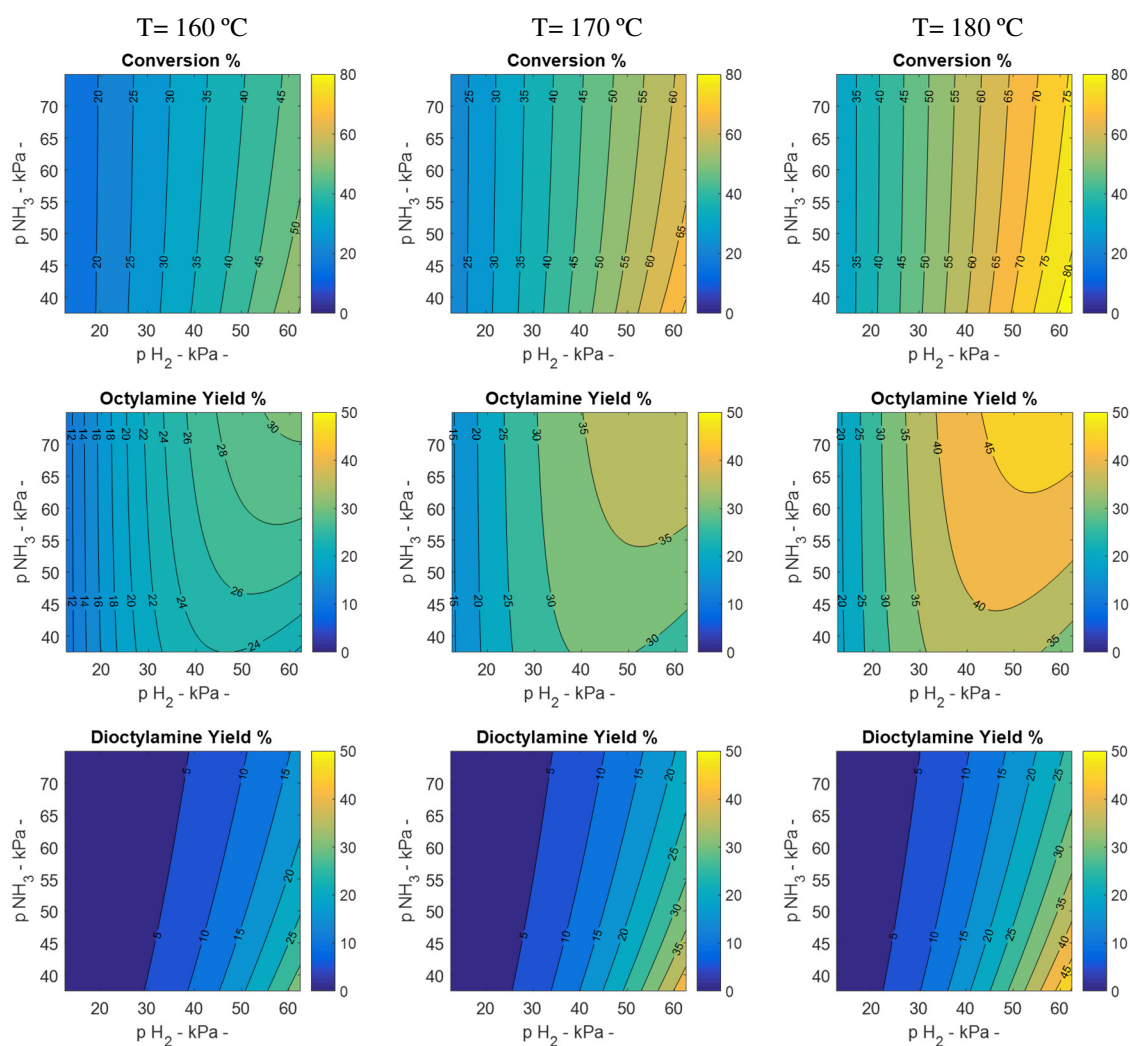


**Figure 4-12** Contour plots showing the estimated conversions and product yields for model M.V\_B over the fitted experimental plane. Conditions: P=200 kPa, W/F = 0.5 h<sup>-1</sup>, p<sub>ROH</sub> = 12.5 kPa).

Interesting patterns can be underlined regarding the primary amine (OA) formation. At low H<sub>2</sub> partial pressures, encompassing low conversions, the OA yield appears to be virtually independent of the NH<sub>3</sub> pressure. In contrast, at higher H<sub>2</sub> pressures, an optimal operation zone for the OA yield is observed. As a matter of fact, the H<sub>2</sub> pressure exerts a net positive effect on the OA selectivity from 12 to 40 kPa, while a further increase exerts a negative effect. This negative effect can be somehow compensated by the NH<sub>3</sub> pressure, reaching a maximum value of 45% at 180 °C for a H<sub>2</sub> and NH<sub>3</sub> pressure of ~55 kPa and ~70 kPa, respectively. DOA is favored at lower NH<sub>3</sub> pressures, being mainly dictated by

the H<sub>2</sub> pressure and the *n*-octanol conversion. The iso-yield lines tend to get closer and steeper at higher H<sub>2</sub> pressures and conversions, which is mainly due to the competition between the NH<sub>3</sub> and the OA pressure. A maximum DOA yield of 45% can be achieved at 180 °C at minimum NH<sub>3</sub> (37.5 kPa) and maximum H<sub>2</sub> (62.5 kPa) pressures. The position of the maximum indicates that a higher yield could be *a priori* obtained under conditions out of the experimental plane covered in this work.

## 4.6 Conclusions

In this chapter, we have presented the development and fitting of a kinetic model describing the direct amination of *n*-octanol with NH<sub>3</sub> over a 0.28%Ag-5%Co/ $\gamma$ -Al<sub>2</sub>O<sub>3</sub> catalyst. In a first step, a set of experimental data was gathered, covering *n*-octanol pressures between 12.5-25.4 kPa, NH<sub>3</sub> pressures between 37.5-75 kPa and H<sub>2</sub> pressures in the range 12.5-62.5 kPa. The temperature was varied between 160 °C and 180 °C. Finally, the total pressure was set to 200 kPa. The analysis of the experimental trends observed in the range of conditions considered in this study leads to the following conclusions:

- The *n*-octanol partial pressure exerts no relevant effect on the catalytic activity, but promotes slightly the OA selectivity;
- The NH<sub>3</sub> partial pressure exerts no relevant effect on the *n*-octanol conversion, but promotes the OA selectivity;
- The H<sub>2</sub> partial pressure impacts to an important extent the catalytic performance, enhancing the *n*-octanol conversion and decreasing the OA selectivity;
- The temperature enhances the catalytic activity and favors slightly the OA selectivity.

In light of the observed experimental trends, a set of kinetic models was build aiming at predicting the behavior of the Ag-Co/Al<sub>2</sub>O<sub>3</sub> catalyst for amination with special focus on rationalizing the role of the H<sub>2</sub> pressure on the catalytic properties. While direct alcohol amination is expected to obey to a H<sub>2</sub> borrowing mechanism, which *a priori* does not require exogenous H<sub>2</sub>, the H<sub>2</sub> pressure was surprisingly found to be the most impacting variable on the catalytic performance. A series of models were built based on a deactivation-regeneration mechanism, where H<sub>2</sub> would recover the catalytic surface from coke deposition. The non-competitive adsorption between OA and NH<sub>3</sub> was proposed as the underlying mechanism explaining the selectivity loss at higher H<sub>2</sub> partial pressures: while the bulkier OA rapidly reaches saturation at conditions favoring high coke coverage, NH<sub>3</sub> could still be adsorbed on isolated vacant sites. As a result, higher H<sub>2</sub> pressures would decrease the coke coverage and facilitate OA adsorption, promoting in turn the formation of DOA. Finally, the fact that higher OA selectivities were obtained at higher *n*-octanol partial pressures suggests a relation between this molecule and the catalyst deactivation process.

All this considered, a set of kinetic models were fitted to the whole body of experimental data comprising different deactivation mechanisms and stoichiometries. The best fitting model considers the primary imine (OI) as the coke source, affording an

excellent fitting to the experimental data. In a further step, the as-obtained model was simplified, decreasing the confidence interval of the fitted parameters while maintaining the original goodness of fit. Two converging solutions were obtained for the simplified model and discriminated based on their prediction accuracy for a set of high conversion data, originally excluded from the fitting.

To sum up, a kinetic model was rationally developed accounting for gas-phase *n*-octanol amination with NH<sub>3</sub> over Ag-Co/Al<sub>2</sub>O<sub>3</sub>, which was able to successfully reproduce the experimental trends for the *n*-octanol conversion and OA and DOA selectivities in a broad range of conditions. A plausible deactivation mechanism was proposed, explaining the *a priori* non-intuitive effect of the H<sub>2</sub> partial pressure on the catalytic activity and selectivity. The present model might be extrapolated to other amination reactions and industrially applied for the optimization of process conditions.

## 4.7 Nomenclature

$r$	Reaction rate ( $\text{mmol} \cdot \text{g-cat}^{-1} \cdot \text{h}^{-1}$ )
$\theta$	surface coverage
$\widehat{p}_{x,j}$	Computed partial pressure (kPa)
$p_{x,j}$	Experimental partial pressure (kPa)
$\bar{p}_{x,j}$	Mean partial pressure (kPa)
$D$	Deactivating agent
$d$	Deactivation stoichiometry
DOA	= Dioctylamine
DOI	= Dioctylimine
$E_{a,app}$	= Apparent activation energy
$H$	= Enthalpy of reaction/adsorption
$K'_I$	= Apparent equilibrium constant
$K'_1$	= Apparent kinetic constant
$K_i$	= Equilibrium constant
$k_i$	= Kinetic constant
$n$	= Regeneration stoichiometry
OA	= <i>n</i> -octylamine
ON	= Octanenitrile
R=NH	= Octylimine
R=O	= Octanal
$R^2$	= Coefficient of determination
$R_2=N$	= Di- <i>n</i> -octylimine
$R_2-NH$	= Di- <i>n</i> -octylamine
R-CN	= Octanenitrile
R-CN-I	= Nitrile formation intermediate
R-NH <sub>2</sub>	= <i>N</i> -octylamine
R-NH <sub>2</sub> -I	= Amine formation intermediate
R-OH	= <i>N</i> -octanol
$SS_E$	= Sum of squared errors
TOA	= Trioctylamine
$TOF_N$	= Turnover Frequency of Nitrogen containing Products ( $\text{h}^{-1}$ )
VIF	= Variance Inflation Factor
$W$	= Weight of catalyst (mg)
$W/F$	= Contact time ( $\text{g catalyst} \cdot \text{g } n\text{-octanol}^{-1} \cdot \text{h}$ )
$w_{x,i}$	= Weight matrix scaling fitting values around its mean
$Y$	= Site for small molecules
$Y_i$	= Yield component <i>i</i> (%)
$Z$	= Site for bulky molecules

## 4.8 References

- [1] G.A. Kliger, L.F. Lazutina, R.A. Fridman, Y. Kryukov, A.N. Bashkirov, Y.S. Snagovskii, R. Smirnova, Several Aspects of Kinetics and Mechanism of Amination of Octanol on a Molten Iron Catalyst, *Kinet. Catal.* 16 (1975) 567–570.
- [2] A. Baiker, J. Kijenski, Catalytic Synthesis of Higher Aliphatic Amines from the Corresponding Alcohols, *Catal. Rev.* 27 (1985) 653–697. doi:10.1080/01614948508064235.
- [3] A. Baiker, W. Caprez, W.L. Holstein, Catalytic amination of aliphatic alcohols in the gas and liquid phases: kinetics and reaction pathway, *Ind. Eng. Chem. Prod. Res. Dev.* 22 (1983) 217–225. doi:10.1021/i300010a010.
- [4] V. A. Bassili, A. Baiker, Catalytic amination of 1-methoxypropan-2-ol over silica supported nickel : Modeling of reaction kinetics, *Appl. Catal.* 70 (1991) 325–338. doi:10.1016/S0166-9834(00)84174-3.
- [5] N. Zotova, F.J. Roberts, G.H. Kelsall, A.S. Jessiman, K. Hellgardt, K.K. (Mimi) Hii, Catalysis in flow: Au-catalysed alkylation of amines by alcohols, *Green Chem.* 14 (2012) 226–232. doi:10.1039/C1GC16118K.
- [6] Y.S. Demidova, I.L. Simakova, M. Estrada, S. Beloshapkin, E.V. Suslov, D.V. Korchagina, K.P. Volcho, N.F. Salakhutdinov, A.V. Simakov, D.Y. Murzin, One-pot myrtenol amination over Au nanoparticles supported on different metal oxides, *Appl. Catal. Gen.* 464–465 (2013) 348–356. doi:10.1016/j.apcata.2013.06.013.
- [7] D. Ruiz, A. Aho, T. Saloranta, K. Eränen, J. Wärnå, R. Leino, D.Y. Murzin, Direct amination of dodecanol with NH<sub>3</sub> over heterogeneous catalysts. Catalyst screening and kinetic modeling, *Chem. Eng. J.* 307 (2017) 739–749. doi:10.1016/j.cej.2016.08.083.
- [8] P. Roose, M.G. Turcotte, Amines, Lower Aliphatic, in: *Kirk-othmer Encycl. Chem. Technol.*, John Wiley & Sons, Inc., 2000. doi:10.1002/0471238961.1215230520211803.a01.pub3.
- [9] G. Ertl, ed., *Handbook of heterogeneous catalysis: 8 volumes, 2., completely rev. and enl. ed.*, WILEY-VCH, Weinheim, 2008.
- [10] A. Baiker, Catalytic amination of aliphatic alcohols. Role of hydrogen as inhibitor for catalyst deactivation, *Ind. Eng. Chem. Prod. Res. Dev.* 20 (1981) 615–618. doi:10.1021/i300004a006.
- [11] A. Baiker, M. Maciejewski, Formation and thermal stability of copper and nickel nitrides, *J. Chem. Soc. Faraday Trans. 1 Phys. Chem. Condens. Phases.* 80 (1984) 2331–2341. doi:10.1039/F19848002331.
- [12] A. Baiker, D. Monti, Interaction of Ammonia with Metallic Copper, Nickel and Cobalt Catalysts Studied by Temperature Programmed Desorption, *Berichte Bunsenges. Für Phys. Chem.* 87 (1983) 602–605. doi:10.1002/bbpc.19830870714.
- [13] J.H. Cho, J.-H. Park, T.-S. Chang, J.-E. Kim, C.-H. Shin, Reductive Amination of 2-Propanol to Monoisopropylamine Over Ni/  $\gamma$ -Al<sub>2</sub>O<sub>3</sub> Catalysts, *Catal. Lett.* 143 (2013) 1319 - 1327. doi:10.1007/s10562-013-1086-3.
- [14] J.H. Cho, J.H. Park, T.-S. Chang, G. Seo, C.-H. Shin, Reductive amination of 2-propanol to monoisopropylamine over Co/  $\gamma$ -Al<sub>2</sub>O<sub>3</sub> catalysts, *Appl. Catal. Gen.* 417 - 418 (2012) 313 - 319. doi:10.1016/j.apcata.2012.01.011.
- [15] G.B. Rogers, M.M. Lih, O.A. Hougen, Catalytic hydrogenation of propylene and isobutylene over platinum. Effect of noncompetitive adsorption, *AIChE J.* 12 (1966) 369–377. doi:10.1002/aic.690120230.
- [16] R. Dittmeyer, G. Emig, Simultaneous Heat and Mass Transfer and Chemical Reaction, in: G. Ertl, H. Knözinger, F. Schüth, J. Weitkamp (Eds.), *Handb. Heterog. Catal.*, Wiley-VCH Verlag GmbH & Co. KGaA, Weinheim, Germany, 2008. doi:10.1002/9783527610044.hetcat0094.
- [17] I. Langmuir, The adsorption of gases on plane surfaces of glass, mica and platinum., *J. Am. Chem. Soc.* 40 (1918) 1361–1403.



---

## **Chapter 5**

### **General conclusions and perspectives**

---



## 5.1 General Conclusions

As presented over the introductory chapter, synthetic amines are extensively used in the chemical industry as platform molecules for the production of agrochemicals, surfactants, polymers, water treatment chemicals, pharmaceuticals, solvents and dyes. Despite the maturity of amine manufacturing technologies, there are still several unsolved challenges, especially related to the production of primary amines. The current industrial processes often lack selectivity, involve hazardous reagents, generate salts as residues or consume H<sub>2</sub> stoichiometrically. In the meantime, biomass upgrading is expected to supply a large portfolio of alcohols in the near future, potentially becoming interesting platform molecules for the synthesis of amines *via* the so-called *borrowing hydrogen* mechanism. The growing interest on this pathway has been manifest over the last decade, as evidenced by the steady increase in the number of patents and scientific literature related to the matter. As of today, the best performing formulations rely on expensive homogeneous catalysts based on organometallic Ru or Ir complexes and ligands, difficult to be recovered and reused. These shortcomings limit their scale-up viability, focusing the industrial interest in the development of efficient heterogeneous formulations. In this context, this work centered its efforts in the development of selective novel heterogeneous catalysts for the direct amination of alcohols. Furthermore, aiming at better understanding the effect of the different reaction parameters, a thorough kinetic study was carried out.

To meet the aforementioned objectives, the work comprised in this thesis was divided in two sections:

(i) Sequential design and optimization of metal supported catalysts:

The interest of Co/ $\gamma$ -Al<sub>2</sub>O<sub>3</sub> as a selective catalyst for the synthesis of *n*-octylamine was evidenced from a preliminary high-throughput screening of a library of catalysts covering the use of different active phase and support combinations. The parent catalyst was improved *via* noble metal doping, following a sequential optimization strategy. First, the effect of the nature of the dopant was studied obtaining the best results for Ru and Ag doped catalysts. In a second and third steps, the impregnation sequence and the noble metal content were optimized, leading to the best following formulations: 5%Co(0.03%Ru)/ $\gamma$ -Al<sub>2</sub>O<sub>3</sub> (obtained by coimpregnation) and 0.28%Ag-5%Co/ $\gamma$ -Al<sub>2</sub>O<sub>3</sub> (obtained by sequential impregnation). Both dopants enhanced the reducibility of the parent catalyst, but presented noticeable differences in their catalytic behavior:

- (a) Ru was found to be in solid solution within the Co crystallites and presented higher efficiency in boosting the Co reducibility in a *per* atom basis relative to Ag. The parent and promoted catalysts responded similarly to changes in H<sub>2</sub> and NH<sub>3</sub> pressures. These results suggested a role of Ru limited to the enhancement of the Co reduction.
- (b) Ag was present as isolated nanoparticles, selectively dispersed around the corners of Co agglomerates. The promoted catalyst showed an enhanced selectivity towards the *n*-octylamine over the range of studied conditions, suggesting a co-catalytic effect of Ag.

Finally, the influence of the reaction parameters was briefly studied for Ag-Co/Al<sub>2</sub>O<sub>3</sub>, achieving a 78% OA yield at the optimal conditions. This result, in parallel with the use of an inexpensive heterogeneous catalyst, the use of mild conditions and the absence of need of organic solvents represents a significant step forward in comparison to the existing open literature.

(ii) Kinetic study of *n*-octanol amination over a Ag-Co/ $\gamma$ -Al<sub>2</sub>O<sub>3</sub> catalyst

The second body of this thesis was focused on the development of a kinetic model, serving a double objective. Firstly, the coverage of a broad range of experimental conditions is of great industrial interest for the purpose of process optimization. Secondly, the kinetic models claimed in the open literature typically exclude the effect of exogenous H<sub>2</sub> pressure, which we found, in contrast, to be the most sensitive parameter.

With this in mind, a kinetic study was designed, comprising a full factorial DoE that covered 126 experimental conditions. The analysis of the experimental kinetic regularities allowed the development of various kinetic models in agreement with different proposed mechanisms. The kinetic models were checked for thermodynamic consistency, discriminated following statistical criteria and simplified in a final step. As a result of this work, a kinetic model was obtained, successfully predicting the product distribution over a wide range of experimental conditions. A deactivation-regeneration mechanism was proposed, rationalizing the role of H<sub>2</sub> on the activity and selectivity of the reaction. This last contribution complements the existing open literature and opens a discussion for further studies on the matter. The proposed kinetic model could easily be extrapolated to other amination reactions and different catalysts, considered that the same mechanism applies. Moreover, the kinetic model could be exploited industrially for the purpose of process optimization, implementing economic and technical constraints.

## 5.2 Perspectives

Based on the obtained results along this thesis, some perspectives can be proposed for future research on the subject:

(i) Fundamental studies on the role of Ag and Co in the bimetallic Ag-Co optimized formulation:

It would be interesting to better understand the role of Ag and Co during the catalytic cycle. For instance, the use of *in operando* infrared spectroscopy could be envisaged in order to identify and quantify the surface species at different reaction conditions. The comparison of the data between the parent Co and the Ag promoted samples could provide valuable information relative to the nature of the promoting effect.

(ii) DFT modelling of Ag-Co catalysts and extrapolation to new formulations:

The information obtained from *in operando* spectroscopy techniques could potentially be used for the refinement of DFT models. This could allow the prediction of novel promising formulations and provide a better picture of the reaction mechanism.

(iii) SSITKA studies

The analysis of transient state kinetics would provide valuable information for the improvement of the kinetic models. The use of labeled isotopic experiments would help to understand the mechanism behind the hydrogen transfer process and provide valuable information regarding the effect of exogenous H<sub>2</sub> pressure.

(iv) Industrial process optimization

Provided the economic and technical constraints the proposed kinetic model could be used to optimize the process conditions for the industrial production of n-octylamine. The kinetic expressions could be adapted to conditions out of the studied experimental space and/or to other amination reactions after optimization using the corresponding experimental data.



---

## **Annexes**

---



## **Annex I. Summary of the screening of mono-metallic catalysts**

### **I.1. Introduction**

Along this annex, the results of the screening of an existing library of catalysts for the amination reaction of *n*-octanol with NH<sub>3</sub> will be presented. The library consisted of metal-supported formulations based on Ni, Co, Pd, Pt, Au and Cu supported over different metal oxides such as Al<sub>2</sub>O<sub>3</sub>, TiO<sub>2</sub>, CeO<sub>2</sub>, Fe<sub>2</sub>O<sub>3</sub> and SiO<sub>2</sub>. First, a high-throughput (HT) screening of catalysts was carried out to assess the most active formulations as an attempt to discern the relative role of the metal and the support on the catalytic properties, as well as metal-support synergistic effects. Subsequently, the selectivity of the most promising catalysts towards the synthesis of the target product, i.e. *n*-octylamine (OA), was explored under optimized conditions.

### **I.2. Materials and Methods**

All the chemical reagents used in this section are listed in section 2.1. All the catalysts were prepared by incipient wetness impregnation. The bulk metal content was measured by ICP.

An initial HT screening was conducted in the Flowrence unit (Avantium, Netherlands) available at the REALCAT platform (UCCS, Lille). The details on the equipment used can be found in section 2.4.3, while the experimental conditions S-A used are compiled in Table A-2. The second screening at optimized conditions was conducted in a MPRS-3TC reactor (Yashentech, China) available at E2P2L (Solvay, Shanghai). Further details on the equipment are presented in section 2.4.1, while the experimental conditions S-B used are compiled in Table A-2.

### **I.3. Results**

#### **I.3.1. Primary High-Throughput screening of monometallic supported catalysts**

A library of 26 metal-supported catalysts was screened under the reaction conditions S-A (Table A-2). The reference and composition of the catalysts can be found in Table A-1, whereas the *n*-octanol conversions and OA yields are listed in Table A-3 to Table A-6. It is important to note that the operational conditions were not optimized at this point and low carbon balances were generally obtained. Similarly, the use of NH<sub>3</sub> in stoichiometric amounts limited the OA selectivity. Accordingly, the activity of the catalysts was assessed in terms of yield to amine products, as shown in Table A-6.

##### **(i) Effect of the support**

The influence of the support on the catalytic activity varied among the different supported metals. Among the different catalysts, Ni and Co supported over Al<sub>2</sub>O<sub>3</sub> exhibited the highest yield to amines, while Pd and Pt exhibited the best results when supported over TiO<sub>2</sub> (Table A-6). The different metals supported over Fe<sub>2</sub>O<sub>3</sub> displayed low activities. Regarding the carbon balance (Table A-4), a negative effect of CeO<sub>2</sub> was observed. The online GC-FID analysis of gas effluents showed an increased formation of volatile products

for the latter catalysts (see Figure A-1). A further offline GC-MS analysis of the products pointed out the formation of dehydration and hydrogenolysis products (see Figure A-2), suggesting a promoting effect of CeO<sub>2</sub> for these reactions.

(ii) Effect of the metal nature

A difference in terms of activity was evident among the different metal-supported catalysts. Irrespective of the support, Cu and Au catalysts showed very low activity. On the contrary, Ni catalysts afforded amine yields >10% except for the Fe<sub>2</sub>O<sub>3</sub>-supported catalyst, whereas Pd and Pt afforded the highest amine yields (30% and 33%, respectively) when supported over TiO<sub>2</sub>. These results suggest a synergistic effect between TiO<sub>2</sub> and noble metals. Finally, Co-supported catalysts displayed a moderate activity, showing the best result when supported over Al<sub>2</sub>O<sub>3</sub>. No clear trend could be devised between the metal and the carbon balance.

**Table A-1** List of metal-supported catalysts and references used in the HT screening

Metal	Support	Reference	ICP wt%
Co	CeO <sub>2</sub>	SHAC - 28	16.6 %
Co	TiO <sub>2</sub>	SHAC - 40	14.3 %
Co	Fe <sub>2</sub> O <sub>3</sub>	SHAC - 48	9.7%
Co	Al <sub>2</sub> O <sub>3</sub>	SHAC - 27	14.7 %
Co	SiO <sub>2</sub>	SHAC - 39	13.1 %
Co - CD <sup>(b)</sup>	CeO <sub>2</sub>	SHAC - 30	14.9 %
Co - CD <sup>(b)</sup>	Al <sub>2</sub> O <sub>3</sub>	SHAC - 19	15.6 %
Pd	CeO <sub>2</sub>	SHAC - 56	1.3 %
Pd	TiO <sub>2</sub>	SHAC - 54	1.5 %
Pd	Fe <sub>2</sub> O <sub>3</sub>	SHAC - 50	1.5 %
Pd	Al <sub>2</sub> O <sub>3</sub>	SHAC - 55	0.5 %
Pd	SiO <sub>2</sub>	SHAC - 53	0.9 %
Pd - M <sup>(c)</sup>	CeO <sub>2</sub>	SHAC - 4	2.4 %
Ni	CeO <sub>2</sub>	SHAC - 12	8.1 %
Ni	TiO <sub>2</sub>	SHAC - 54	9.0 %
Ni	Fe <sub>2</sub> O <sub>3</sub>	SHAC - 47	8.3 %
Ni	Al <sub>2</sub> O <sub>3</sub>	SHAC - 11	9.8% <sup>(a)</sup>
Ni	SiO <sub>2</sub>	SHAC - 9	12.6 %
Cu	CeO <sub>2</sub>	SHAC - 60	8.8 %
Cu	TiO <sub>2</sub>	SHAC - 58	11.8 %
Cu	Al <sub>2</sub> O <sub>3</sub>	SHAC - 59	9.1 %
Pt	TiO <sub>2</sub>	SHAC - 36	0.6 %
Pt	Fe <sub>2</sub> O <sub>3</sub>	SHAC - 52	0.6 %
Pt	Al <sub>2</sub> O <sub>3</sub>	SHAC - 37	0.6 %
Au	TiO <sub>2</sub>	SHAC - 44	2.0 %
Au	Fe <sub>2</sub> O <sub>3</sub>	SHAC - 51	1.9 %
Au	Al <sub>2</sub> O <sub>3</sub>	SHAC - 45	1.7 %

(a) Nominal metal loading values; (b) CD stands for cyclodextrin-assisted impregnation; (c) M stands for manual synthesis.

**Table A-2** Experimental conditions used for the catalytic screening of supported monometallic formulations

	S - A		S - B	
	Flow (STD mL/min)	Equivalents	Flow (STD mL/min)	Equivalents
NH <sub>3</sub>	3.65	1	38.3	9
H <sub>2</sub>	3.65	1	11.3	2.5
n-octanol	3.65	1	4.3	1
N <sub>2</sub>	32.85	9	3.8	0.9
He	10.0	2.7	-	-
Mass of Catalyst	100 mg		510 mg	
W/F	0.08 h		0.34 h	
Temperature	220°C		180 °C	
Pressure	1 bar		1 bar	

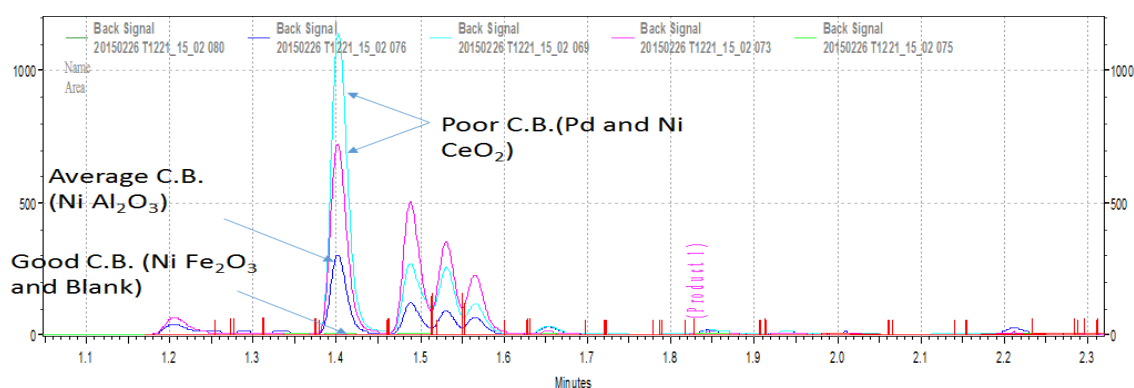


**Figure A-1** Online GC-FID results for the gas reaction products of catalysts with different carbon balances.

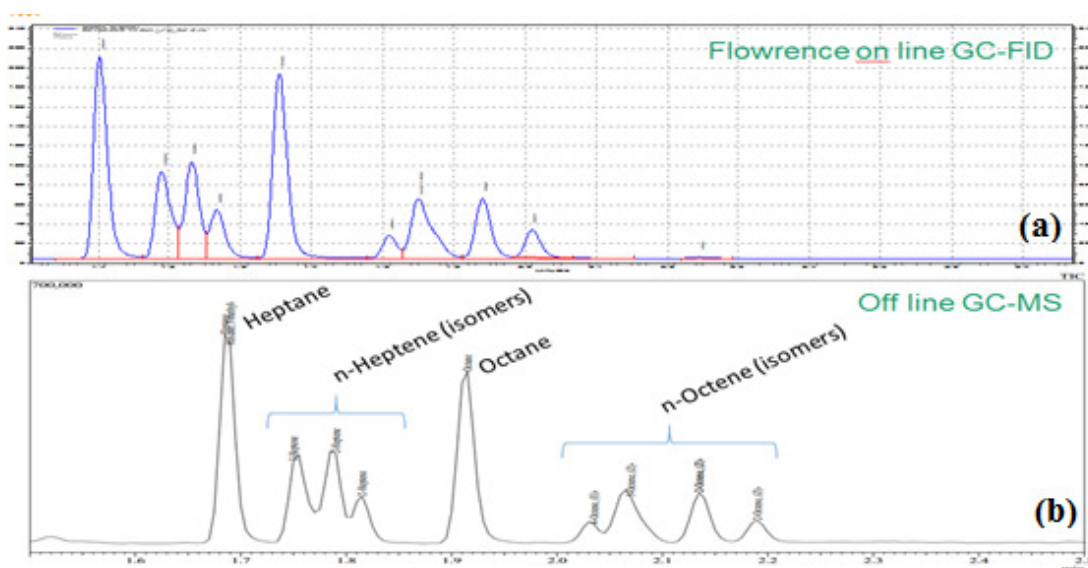


**Figure A-2** (a) Online GC-FID and (b) off line GC-MS chromatograms example for the gas reaction products of CeO<sub>2</sub> supported catalyst.

**Table A-3** *N*-octanol conversion on the screening of metal-supported catalysts

Conversion	CeO <sub>2</sub>	TiO <sub>2</sub>	Fe <sub>2</sub> O <sub>3</sub>	Al <sub>2</sub> O <sub>3</sub>	SiO <sub>2</sub>
Co	32%	36%	3%	60%	58%
Pd	54%	68%	35%	9%	1%
Ni	86%	73%	18%	98%	95%
Cu	41%	9%		7%	
Au		0%	7%	18%	
Pt		68%	8%	16%	
Pd M	69%				
Co CD	33%				

**Table A-4** Carbon balance obtained on the screening of metal-supported catalysts

C. B.	CeO <sub>2</sub>	TiO <sub>2</sub>	Fe <sub>2</sub> O <sub>3</sub>	Al <sub>2</sub> O <sub>3</sub>	SiO <sub>2</sub>
Co	71%	82%	98%	82%	65%
Pd	51%	74%	70%	97%	100%
Ni	37%	70%	85%	63%	41%
Cu	66%	93%		97%	
Au		100%	94%	84%	
Pt		69%	94%	99%	
Pd M	38%				
Co CD	71%				

**Table A-5** OA yield on the screening of metal-supported catalysts

Yield to R-NH <sub>2</sub>	CeO <sub>2</sub>	TiO <sub>2</sub>	Fe <sub>2</sub> O <sub>3</sub>	Al <sub>2</sub> O <sub>3</sub>	SiO <sub>2</sub>
Co	0%	4%	0%	8%	1%
Pd	2%	8%	1%	3%	0%
Ni	1%	6%	0%	5%	4%
Cu	0%	0%		3%	
Au		0%	0%	1%	
Pt		6%	1%	4%	
Pd M	2%				
Co CD	0%				

**Table A-6** Yield to amines on the screening of metal-supported catalyst

Yield to Amines	CeO <sub>2</sub>	TiO <sub>2</sub>	Fe <sub>2</sub> O <sub>3</sub>	Al <sub>2</sub> O <sub>3</sub>	SiO <sub>2</sub>
Co	0%	5%	0%	10%	4%
Pd	4%	33%	4%	4%	0%
Ni	13%	17%	1%	26%	12%
Cu	2%	1%		3%	
Au		0%	0%	2%	
Pt		30%	2%	6%	
Pd M	6%				
Co CD	1%				

**Table A-7** Results summary for the best performing catalysts

Metal	Loading wt %	Support	Conversion	C.B.	Y. R-NH <sub>2</sub>	Yield to Amines	Yield to RCN	R-NH <sub>2</sub> to amine ratio
Pt	0.6 %	TiO <sub>2</sub>	68 %	69 %	6 %	30 %	7 %	0.20
Pd	1.5 %	TiO <sub>2</sub>	68 %	74 %	8 %	33 %	9 %	0.24
Ni	9.8 %	Al <sub>2</sub> O <sub>3</sub>	98 %	63 %	5 %	26 %	35 %	0.19
Co	14.7 %	Al <sub>2</sub> O <sub>3</sub>	60 %	82 %	8 %	10 %	31 %	0.80
Ni	9.0 %	TiO <sub>2</sub>	73 %	70 %	6 %	17 %	26 %	0.35

The OA yield was in all cases lower than 10 % (Table A-5), obtaining the best results for Pd/TiO<sub>2</sub> and Co/Al<sub>2</sub>O<sub>3</sub> followed by Ni/TiO<sub>2</sub>, Pt/TiO<sub>2</sub> and Ni/Al<sub>2</sub>O<sub>3</sub>. This low yield is not surprising regarding the low amount of NH<sub>3</sub> fed. A net effect of the catalysts on the selectivity was difficult to assess because of the very different conversions obtained. Overall, a higher selectivity was noticeable for Co/Al<sub>2</sub>O<sub>3</sub> and Co/TiO<sub>2</sub>, for which ≈80% of the amine yield corresponded to OA, but this was only ≈20% to 35% for the Ni, Pd and Pt catalysts.

### (iii) Summary

A library of 26 catalysts comprising Co, Pd, Pt, Ni, Au and Cu supported over CeO<sub>2</sub>, TiO<sub>2</sub>, Fe<sub>2</sub>O<sub>3</sub>, Al<sub>2</sub>O<sub>3</sub> and SiO<sub>2</sub> were tested for 3 HT runs. The most promising results are shown in Table A-7. However, the results must be analyzed with care because of the differences in conversion, metal loading and as a rule low carbon balances. Despite these limitations, we can conclude that the most promising catalysts from the screened library are: **Ni/Al<sub>2</sub>O<sub>3</sub>, Pt/TiO<sub>2</sub>, Pd/TiO<sub>2</sub>, Co/Al<sub>2</sub>O<sub>3</sub> and Ni/TiO<sub>2</sub>**. It is also especially noticeable a positive effect on the OA selectivity for **Co/Al<sub>2</sub>O<sub>3</sub>**.

### **I.3.2. Secondary screening of mono-metallic supported catalysts**

In light of the results presented above, a second screening was conducted, covering combinations of the best performing metals and supports (Pd, Pt, Ni and Co supported over  $\text{Al}_2\text{O}_3$  and  $\text{TiO}_2$ ). The reaction conditions S-B (Table A-2) were used, adapted to decrease the impact of side reactions leading to low carbon balances.

As can be observed in Figure A-3, the best results in terms of OA yield were obtained for Ni and Co supported over  $\text{Al}_2\text{O}_3$ . These catalysts over-performed their counterparts supported over  $\text{TiO}_2$ , suggesting a positive effect of amphoteric  $\text{Al}_2\text{O}_3$ . Nonetheless, the Pt formulations afforded the highest activities per metal atom basis. It is important to analyze these results with care, since differences in metal dispersion and extent of reduction were not taken into account. Despite these differences, the superior selectivity of  $\text{Co}/\text{Al}_2\text{O}_3$  is evident, affording the highest OA yield (43%) with only 5% DOA yield. In contrast,  $\text{Pt}/\text{TiO}_2$  afforded the same DOA yield while generating <10% of OA. In light of these results,  $\text{Co}/\text{Al}_2\text{O}_3$  was selected in this study as the most promising formulation for the synthesis of OA.

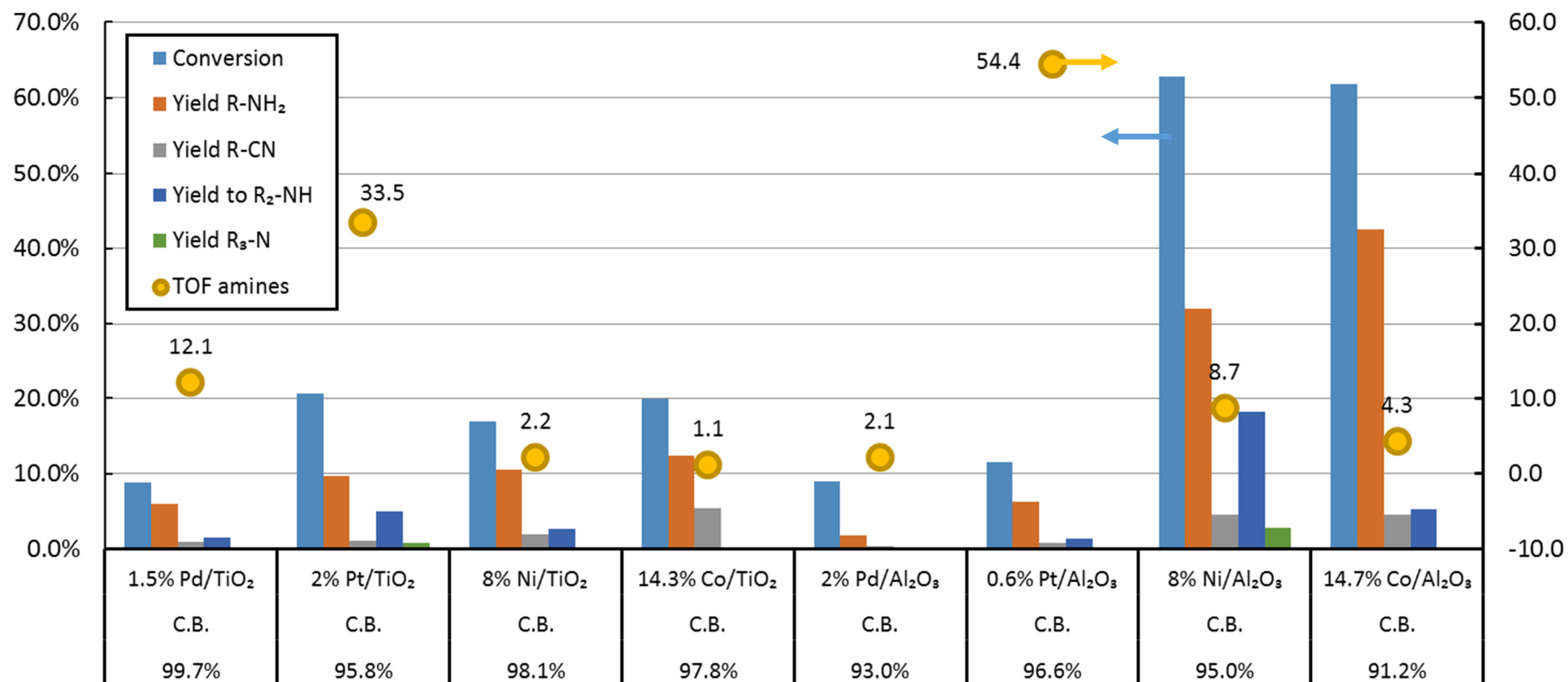


**Figure A-3** Conversion and yield results on the screening of mono-metallic supported catalyst in the amination of *n*-octanol with ammonia. Reaction conditions: *n*-octanol feed: 1.8 mL·h<sup>-1</sup>; T = 180 °C, P = 1 bar, [NH<sub>3</sub>:H<sub>2</sub>:N<sub>2</sub>:ROH] = [9 : 2.5 : 0.9 : 1]). (TOF calculated as moles of amines produced *per* total metal atom and hour)

## Annex II. Kinetic experiments and table of results

As presented in section 2.4.3, a full factorial design of experiments comprising two central points was designed to assess the influence of the different operation variables. The full list of experiments is presented in Table A-7. Each of the 14 listed conditions was tested at 3 different temperatures (160 °C, 170 °C and 180 °C) and 3 catalyst weights (10 mg, 20 mg and 30 mg), resulting in 126 experimental points. Table A-8 summarizes the experimental results obtained.

**Table A-7** List of reaction conditions tested for the kinetic modelling of *n*-octanol amination with NH<sub>3</sub> in chapter 4.

Condition reference	p <sup>0</sup> ROH (kPa)	p <sup>0</sup> NH <sub>3</sub> (kPa)	p <sup>0</sup> H <sub>2</sub> (kPa)
1	12.5	37.5	12.5
2	12.5	37.5	37.5
3	12.5	37.5	62.5
4	12.5	75.0	12.5
5	12.5	75.0	37.5
6	12.5	75.0	62.5
7	25.4	37.5	12.5
8	25.4	37.5	37.5
9	25.4	37.5	62.5
10	25.4	75.0	12.5
11	25.4	75.0	37.5
12	25.4	75.0	62.5
13	19.0	37.5	37.5
14	12.5	56.3	37.5

Table A-8 Summary of kinetic results for reactions conditions listed in Table A-7

Condition Reference	1								
Temperature - °C -	180	180	180	170	170	170	160	160	160
Catalyst weight –mg -	12.3	20.7	30.8	10.5	20	30	10.5	19.7	30.1
p R-NH <sub>2</sub> – kPa -	0.40	0.61	0.88	0.36	0.51	0.72	0.28	0.48	0.61
p R-OH – kPa -	11.66	11.06	10.60	11.52	11.49	10.93	11.86	12.10	12.10
p R-CN – kPa -	0.18	0.33	0.46	0.14	0.21	0.30	0.09	0.15	0.20
p R <sub>2</sub> -NH – kPa -	0.02	0.03	0.04	0.02	0.02	0.03	0.01	0.02	0.02
Conversion	5.9%	10.6%	14.1%	6.3%	8.7%	11.4%	4.1%	5.6%	7.4%
Yield R-NH <sub>2</sub>	3.2%	5.0%	7.1%	2.9%	4.0%	5.8%	2.3%	3.7%	4.7%
Yield R-CN	1.4%	2.7%	3.7%	1.1%	1.7%	2.4%	0.7%	1.2%	1.5%
Yield R <sub>2</sub> -NH	0.4%	0.5%	0.6%	0.3%	0.4%	0.5%	0.2%	0.3%	0.4%
Carbon Balance	99.4%	97.8%	97.7%	98.2%	97.6%	97.6%	99.2%	99.7%	99.4%
Condition Reference	2								
Temperature - °C -	180	180	180	170	170	170	160	160	160
Catalyst weight –mg -	12.3	20.7	30.8	10.5	20	30	10.5	19.7	30.1
p R-NH <sub>2</sub> – kPa -	0.65	1.13	1.68	0.60	0.94	1.34	0.42	0.81	1.13
p R-OH – kPa -	11.71	10.65	10.13	11.61	11.38	10.63	11.95	11.93	11.86
p R-CN – kPa -	0.15	0.23	0.29	0.10	0.14	0.16	0.06	0.07	0.08
p R <sub>2</sub> -NH – kPa -	0.04	0.07	0.12	0.04	0.05	0.09	0.03	0.05	0.08
Conversion	5.6%	13.9%	18.1%	5.6%	9.7%	13.9%	3.4%	7.0%	9.3%
Yield R-NH <sub>2</sub>	5.3%	9.1%	13.6%	4.9%	7.5%	10.9%	3.4%	6.3%	8.7%
Yield R-CN	1.2%	1.9%	2.3%	0.8%	1.1%	1.3%	0.5%	0.6%	0.6%
Yield R <sub>2</sub> -NH	0.7%	1.1%	1.9%	0.6%	0.9%	1.5%	0.5%	0.8%	1.2%
Carbon Balance	102.1%	98.8%	100.5%	101.0%	100.1%	100.3%	101.2%	101.1%	101.5%

Condition Reference	3								
Temperature - °C -	180	180	180	170	170	170	160	160	160
Catalyst weight –mg -	9.4	19.8	28.1	10.7	22	29.2	10.7	21.2	28.8
p R-NH <sub>2</sub> – kPa -	0.94	1.71	2.40	0.91	1.61	2.10	0.74	1.26	1.59
p R-OH – kPa -	11.42	10.40	8.21	10.60	9.70	8.81	11.52	10.16	9.62
p R-CN – kPa -	0.13	0.14	0.12	0.06	0.06	0.06	0.03	0.03	0.03
p R <sub>2</sub> -NH – kPa -	0.16	0.35	0.63	0.21	0.47	0.62	0.20	0.37	0.44
Conversion	10.9%	20.4%	33.5%	13.0%	21.7%	29.0%	8.7%	17.8%	21.8%
Yield R-NH <sub>2</sub>	7.3%	13.1%	19.4%	7.5%	13.0%	16.9%	5.9%	10.2%	12.9%
Yield R-CN	1.0%	1.1%	1.0%	0.5%	0.5%	0.5%	0.3%	0.3%	0.2%
Yield R <sub>2</sub> -NH	2.4%	5.3%	10.1%	3.4%	7.7%	9.9%	3.2%	5.9%	7.1%
Carbon Balance	100.5%	100.0%	98.0%	98.9%	100.0%	98.9%	101.0%	98.9%	98.8%
Condition Reference	4								
Temperature - °C -	180	180	180	170	170	170	160	160	160
Catalyst weight –mg -	9.4	19.8	28.1	10.7	22	29.2	10.7	21.2	28.8
p R-NH <sub>2</sub> – kPa -	0.33	0.57	0.85	0.33	0.59	0.76	0.28	0.46	0.61
p R-OH – kPa -	12.54	12.34	11.27	11.64	11.36	11.28	12.22	11.62	11.32
p R-CN – kPa -	0.14	0.29	0.42	0.11	0.21	0.28	0.08	0.13	0.17
p R <sub>2</sub> -NH – kPa -	0.03	0.05	0.10	0.03	0.07	0.10	0.03	0.05	0.08
Conversion	2.1%	5.4%	8.5%	4.5%	8.2%	8.9%	3.1%	5.9%	7.9%
Yield R-NH <sub>2</sub>	2.6%	4.4%	6.9%	2.7%	4.7%	6.2%	2.2%	3.7%	5.0%
Yield R-CN	1.1%	2.2%	3.4%	0.9%	1.7%	2.3%	0.6%	1.0%	1.4%
Yield R <sub>2</sub> -NH	0.5%	0.8%	1.7%	0.5%	1.1%	1.6%	0.4%	0.8%	1.2%
Carbon Balance	102.2%	102.2%	103.8%	99.8%	99.5%	101.4%	100.3%	99.8%	99.8%

Condition Reference	5								
Temperature - °C -	180	180	180	170	170	170	160	160	160
Catalyst weight –mg -	12.4	20.5	29.4	10	19.3	29.8	11.5	22.5	29.8
p R-NH <sub>2</sub> – kPa -	1.06	1.64	1.97	0.71	1.20	1.73	0.63	1.09	1.34
p R-OH – kPa -	10.99	10.15	9.78	11.37	11.10	10.47	12.14	11.80	11.16
p R-CN – kPa -	0.16	0.24	0.27	0.09	0.11	0.13	0.05	0.07	0.06
p R <sub>2</sub> -NH – kPa -	0.08	0.11	0.13	0.05	0.07	0.11	0.05	0.07	0.08
Conversion	12.8%	17.7%	20.3%	6.7%	10.4%	15.5%	5.3%	9.8%	9.7%
Yield R-NH <sub>2</sub>	8.4%	13.3%	16.0%	5.8%	9.6%	14.0%	4.9%	8.4%	10.9%
Yield R-CN	1.3%	1.9%	2.2%	0.7%	0.9%	1.1%	0.4%	0.5%	0.5%
Yield R <sub>2</sub> -NH	1.2%	1.7%	2.0%	0.8%	1.1%	1.8%	0.8%	1.1%	1.3%
Carbon Balance	98.6%	99.8%	100.5%	100.8%	101.6%	101.7%	101.0%	100.4%	103.1%
Condition Reference	6								
Temperature - °C -	180	180	180	170	170	170	160	160	160
Catalyst weight –mg -	12.4	20.5	29.4	10	19.3	29.8	11.5	22.5	29.8
p R-NH <sub>2</sub> – kPa -	1.57	2.47	2.96	1.12	1.71	2.46	0.90	1.38	1.85
p R-OH – kPa -	10.29	8.93	8.30	10.75	10.11	8.93	11.67	9.43	10.14
p R-CN – kPa -	0.11	0.11	0.11	0.05	0.05	0.05	0.03	0.03	0.03
p R <sub>2</sub> -NH – kPa -	0.18	0.30	0.35	0.15	0.21	0.30	0.14	0.17	0.22
Conversion	18.3%	27.7%	32.4%	11.8%	18.5%	28.0%	9.0%	27.9%	18.1%
Yield R-NH <sub>2</sub>	12.5%	20.0%	24.1%	9.2%	13.8%	19.8%	7.0%	10.5%	14.9%
Yield R-CN	0.9%	0.9%	0.9%	0.4%	0.4%	0.4%	0.3%	0.2%	0.2%
Yield R <sub>2</sub> -NH	2.8%	4.8%	5.6%	2.5%	3.4%	4.9%	2.1%	2.6%	3.5%
Carbon Balance	98.4%	98.5%	98.7%	100.6%	99.5%	97.4%	100.5%	85.6%	100.8%

Condition Reference	7								
Temperature - °C -	180	180	180	170	170	170	160	160	160
Catalyst weight –mg -	11.7	20.1	29.6	10.8	20.9	31.6	10.2	19.2	30.4
p R-NH <sub>2</sub> – kPa -	0.20	0.57	0.84	0.23	0.42	0.65	0.27	0.40	0.48
p R-OH – kPa -	25.50	23.16	23.57	24.52	23.95	23.75	24.31	24.29	23.97
p R-CN – kPa -	0.09	0.26	0.40	0.06	0.12	0.17	0.09	0.12	0.17
p R <sub>2</sub> -NH – kPa -	0.01	0.03	0.04	0.01	0.02	0.03	0.01	0.01	0.02
Conversion	3.8%	7.5%	9.1%	2.2%	3.9%	7.0%	3.3%	3.4%	4.6%
Yield R-NH <sub>2</sub>	0.8%	2.3%	3.2%	0.9%	1.7%	2.5%	1.1%	1.6%	1.9%
Yield R-CN	0.3%	1.0%	1.5%	0.3%	0.5%	0.7%	0.4%	0.5%	0.7%
Yield R <sub>2</sub> -NH	0.1%	0.2%	0.3%	0.1%	0.1%	0.2%	0.1%	0.1%	0.2%
Carbon Balance	97.4%	96.3%	96.4%	99.2%	98.6%	96.7%	98.4%	99.1%	98.4%
Condition Reference	8								
Temperature - °C -	180	180	180	170	170	170	160	160	160
Catalyst weight –mg -	9.3	19.7	27.8	9.9	19.8	29.5	9.3	19.4	33
p R-NH <sub>2</sub> – kPa -	0.35	1.40	1.88	0.59	1.24	1.94	0.43	0.85	1.20
p R-OH – kPa -	23.82	21.97	20.60	23.24	24.12	22.50	22.76	22.44	22.44
p R-CN – kPa -	0.07	0.33	0.42	0.12	0.23	0.26	0.06	0.10	0.13
p R <sub>2</sub> -NH – kPa -	0.02	0.11	0.15	0.04	0.08	0.14	0.04	0.06	0.08
Conversion	5.3%	12.3%	16.3%	7.3%	8.9%	13.3%	8.7%	10.4%	12.2%
Yield R-NH <sub>2</sub>	1.4%	5.6%	7.6%	2.4%	4.7%	7.5%	1.7%	3.4%	4.7%
Yield R-CN	0.3%	1.3%	1.7%	0.5%	0.9%	1.0%	0.2%	0.4%	0.5%
Yield R <sub>2</sub> -NH	0.2%	0.9%	1.2%	0.3%	0.6%	1.1%	0.3%	0.5%	0.6%
Carbon Balance	96.8%	96.1%	95.0%	96.2%	97.7%	97.0%	93.7%	94.2%	94.1%

Condition Reference	9								
Temperature - °C -	180	180	180	170	170	170	160	160	160
Catalyst weight –mg -	9.4	19.4	28.2	10.4	18.5	28.8	11	18.3	29.1
p R-NH <sub>2</sub> – kPa -	0.95	1.99	2.47	0.89	1.55	2.31	0.65	1.16	1.65
p R-OH – kPa -	24.17	21.59	22.30	23.35	22.46	21.18	24.36	22.69	22.28
p R-CN – kPa -	0.15	0.22	0.24	0.09	0.10	0.10	0.05	0.05	0.05
p R <sub>2</sub> -NH – kPa -	0.13	0.30	0.36	0.13	0.24	0.41	0.10	0.20	0.28
Conversion	6.9%	13.7%	15.7%	7.1%	10.7%	15.6%	4.7%	9.0%	11.1%
Yield R-NH <sub>2</sub>	3.6%	8.0%	9.3%	3.5%	6.2%	9.2%	2.5%	4.7%	6.6%
Yield R-CN	0.6%	0.9%	0.9%	0.4%	0.4%	0.4%	0.2%	0.2%	0.2%
Yield R <sub>2</sub> -NH	1.0%	2.4%	2.7%	1.0%	1.9%	3.3%	0.8%	1.6%	2.2%
Carbon Balance	98.8%	98.3%	98.3%	98.2%	98.4%	98.0%	99.2%	97.8%	98.3%
Condition Reference	10								
Temperature - °C -	180	180	180	170	170	170	160	160	160
Catalyst weight –mg -	11.7	20.1	29.6	10.8	20.9	31.6	10.2	19.2	30.4
p R-NH <sub>2</sub> – kPa -	0.30	0.73	1.07	0.30	0.54	0.79	0.37	0.56	0.65
p R-OH – kPa -	25.25	22.76	23.46	23.67	23.32	22.83	23.94	23.29	24.06
p R-CN – kPa -	0.13	0.32	0.49	0.08	0.16	0.22	0.12	0.15	0.22
p R <sub>2</sub> -NH – kPa -	0.01	0.02	0.04	0.01	0.02	0.02	0.01	0.01	0.02
Conversion	4.7%	9.0%	9.4%	5.6%	6.4%	10.6%	4.7%	7.3%	4.2%
Yield R-NH <sub>2</sub>	1.1%	2.9%	4.1%	1.2%	2.2%	3.1%	1.5%	2.2%	2.6%
Yield R-CN	0.5%	1.3%	1.9%	0.3%	0.6%	0.8%	0.5%	0.6%	0.9%
Yield R <sub>2</sub> -NH	0.1%	0.2%	0.3%	0.1%	0.1%	0.2%	0.1%	0.1%	0.2%
Carbon Balance	97.0%	95.6%	97.2%	96.1%	96.6%	93.7%	97.4%	95.8%	99.6%

<b>Condition Reference</b>	<b>11</b>								
<b>Temperature - °C -</b>	180	180	180	170	170	170	160	160	160
<b>Catalyst weight –mg -</b>	9.3	19.7	27.8	9.9	19.8	29.5	9.3	19.4	33
<b>p R-NH<sub>2</sub> – kPa -</b>	0.35	1.53	1.96	0.59	1.22	1.96	0.43	0.84	1.18
<b>p R-OH – kPa -</b>	24.58	22.76	21.62	24.00	25.05	23.62	23.92	23.61	23.89
<b>p R-CN – kPa -</b>	0.07	0.31	0.40	0.10	0.19	0.24	0.05	0.09	0.12
<b>p R<sub>2</sub>-NH – kPa -</b>	0.01	0.07	0.09	0.02	0.04	0.07	0.00	0.01	0.02
<b>Conversion</b>	2.3%	9.2%	12.2%	4.3%	5.4%	9.0%	4.1%	5.8%	6.5%
<b>Yield R-NH<sub>2</sub></b>	1.4%	6.1%	8.0%	2.4%	4.6%	7.5%	1.7%	3.3%	4.6%
<b>Yield R-CN</b>	0.3%	1.3%	1.6%	0.4%	0.7%	0.9%	0.2%	0.3%	0.5%
<b>Yield R<sub>2</sub>-NH</b>	0.1%	0.5%	0.7%	0.2%	0.3%	0.5%	0.0%	0.1%	0.2%
<b>Carbon Balance</b>	99.6%	99.1%	98.6%	98.8%	100.5%	100.5%	97.8%	98.0%	98.8%
<b>Condition Reference</b>	<b>12</b>								
<b>Temperature - °C -</b>	180	180	180	170	170	170	160	160	160
<b>Catalyst weight –mg -</b>	9.4	19.4	28.2	10.4	18.5	28.8	11	18.3	29.1
<b>p R-NH<sub>2</sub> – kPa -</b>	1.15	2.29	2.87	1.05	1.80	2.64	0.79	1.37	1.93
<b>p R-OH – kPa -</b>	23.60	21.05	21.84	22.71	22.10	20.92	23.60	22.17	22.09
<b>p R-CN – kPa -</b>	0.16	0.22	0.25	0.10	0.10	0.10	0.05	0.05	0.05
<b>p R<sub>2</sub>-NH – kPa -</b>	0.10	0.18	0.22	0.10	0.16	0.23	0.09	0.15	0.19
<b>Conversion</b>	9.1%	15.9%	17.5%	9.7%	12.0%	16.8%	7.7%	11.1%	11.9%
<b>Yield R-NH<sub>2</sub></b>	4.4%	9.1%	10.9%	4.2%	7.2%	10.5%	3.1%	5.5%	7.7%
<b>Yield R-CN</b>	0.6%	0.9%	1.0%	0.4%	0.4%	0.4%	0.2%	0.2%	0.2%
<b>Yield R<sub>2</sub>-NH</b>	0.8%	1.4%	1.6%	0.8%	1.3%	1.9%	0.7%	1.2%	1.5%
<b>Carbon Balance</b>	97.0%	96.0%	96.4%	95.9%	97.1%	96.3%	96.4%	96.0%	97.8%

Condition Reference	13								
Temperature - °C -	180	180	180	170	170	170	160	160	160
Catalyst weight –mg -	11.3	22.8	27.8	10.4	20.6	28	10.9	18.4	27.5
p R-NH <sub>2</sub> – kPa -	0.87	1.55	2.05	0.30	1.02	1.42	0.30	0.47	0.78
p R-OH – kPa -	17.12	17.22	16.05	18.28	16.72	16.37	18.59	17.82	17.90
p R-CN – kPa -	0.21	0.34	0.38	0.06	0.16	0.20	0.03	0.07	0.09
p R <sub>2</sub> -NH – kPa -	0.10	0.11	0.16	0.01	0.07	0.11	0.01	0.03	0.06
Conversion	8.6%	13.0%	17.2%	2.9%	9.5%	12.8%	0.9%	4.5%	6.4%
Yield R-NH <sub>2</sub>	4.6%	7.9%	10.6%	1.6%	5.5%	7.6%	1.6%	2.5%	4.1%
Yield R-CN	1.1%	1.7%	1.9%	0.3%	0.9%	1.0%	0.2%	0.4%	0.5%
Yield R <sub>2</sub> -NH	1.1%	1.1%	1.6%	0.1%	0.7%	1.2%	0.1%	0.3%	0.6%
Carbon Balance	98.9%	98.5%	97.8%	99.2%	98.1%	97.5%	101.0%	99.0%	99.1%
Condition Reference	14								
Temperature - °C -	180	180	180	170	170	170	160	160	160
Catalyst weight –mg -	11.3	22.8	27.8	10.4	20.6	28	10.9	18.4	27.5
p R-NH <sub>2</sub> – kPa -	0.98	1.52	1.98	0.35	1.02	1.46	0.33	0.49	0.80
p R-OH – kPa -	10.66	10.36	9.64	11.66	10.32	10.04	11.65	11.20	11.36
p R-CN – kPa -	0.23	0.30	0.32	0.07	0.14	0.15	0.04	0.07	0.08
p R <sub>2</sub> -NH – kPa -	0.08	0.08	0.12	0.01	0.05	0.09	0.01	0.03	0.06
Conversion	13.7%	20.6%	24.6%	6.1%	15.3%	18.9%	5.8%	9.0%	9.9%
Yield R-NH <sub>2</sub>	8.0%	11.7%	15.5%	2.8%	8.3%	11.8%	2.7%	4.0%	6.3%
Yield R-CN	1.8%	2.3%	2.5%	0.6%	1.2%	1.2%	0.3%	0.5%	0.7%
Yield R <sub>2</sub> -NH	1.4%	1.3%	1.8%	0.2%	0.9%	1.5%	0.1%	0.5%	0.9%
Carbon Balance	97.9%	95.1%	95.9%	97.6%	95.4%	96.0%	97.4%	96.2%	98.1%

## Annex III. Validation of the proposed hydrodynamic model

### (i) Evaluation of the axial dispersion – Mears criterion

According to Mears, axial dispersion in packed bed reactors can be neglected when the following criterion is satisfied [1]:

$$\frac{L}{d_p} > \frac{20}{Pe_a} \ln \frac{1}{1-x} \quad \text{Eq. A-1}$$

where  $L$  is the bed length ( $\sim 3$  cm in our case),  $d_p$  is the particle diameter ( $\sim 0.015$  cm in our case),  $Pe_a$  is the axial Péclet number and  $x$  is the reaction conversion.

Assuming a conservative 50% *n*-octanol conversion (the maximum conversion achieved in the kinetic tests is 34%), an axial  $Pe_a > 0.07$  should imply negligible axial dispersion. The  $Pe_a$  number represents the ratio of advective transport to diffusive transport rates and its value reflects the predominant flow regime in the reactor. The  $Pe_a$  number can be usually estimated using empirical correlations. In Figure A-4, the axial and radial  $Pe_a$  numbers are plotted against the Reynolds number ( $Re$ ) for packed-bed reactors.  $Re$  can be calculated using A-2 taking an average density and viscosity in the reactor.

$$Re = \frac{d_p u \rho_f}{\mu} = \frac{1.5 \cdot 10^{-2} * 4.4 * 1.6 \cdot 10^{-3}}{1.9 \cdot 10^{-4}} = 0.56 \quad \text{Eq. A-2}$$

where  $d_p$  is particle diameter [cm],  $u$  is the spatial velocity [cm/s],  $\rho_f$  is the fluid density [ $\text{g} \cdot \text{cm}^{-3}$ ] and  $\mu_f$  is the fluid viscosity [ $\text{g} \cdot \text{cm}^{-1} \cdot \text{s}^{-1}$ ]. The fluid viscosity was estimated using the UNIQUAC property package in Aspen Hysys software.

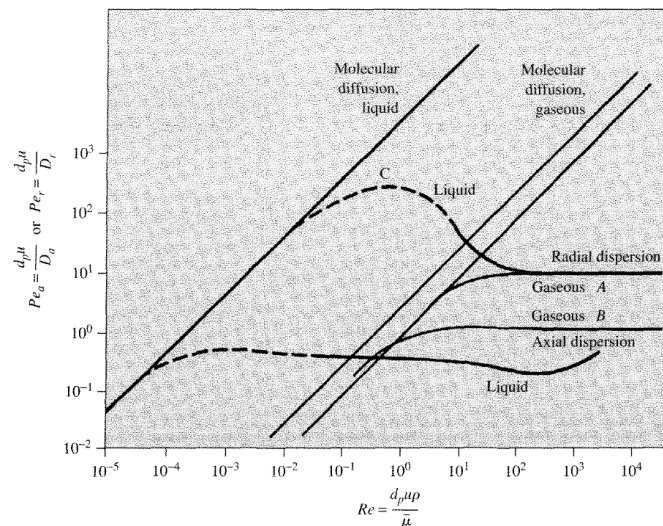


**Figure A-4** Axial and radial Péclet numbers as a function of the Reynolds number for packed-bed reactors (Adapted from ref. [2]).

According to Figure, for  $Re = 0.56$ , the axial  $Pe_a$  can be estimated in the range 0.5-1, well above the limiting value of 0.07. This result confirms the absence of axial dispersion in our reactor during the catalytic tests.

(ii) Estimation of *n*-octanol diffusivity

The gas-phase mass molecular diffusivity in a multicomponent mixture can be calculated according to the theory of diffusion in a semi-infinite column as expressed in Eq. A-3. [3]

$$D'_A = \frac{1 - y_A}{\sum \frac{Y_X}{D_{AX}}} \quad \text{Eq. A-3}$$

where  $D'_A$  is the effective diffusion coefficient of gas A,  $y_x$  is the molar fraction of the X component and  $D_{AX}$  is the binary diffusion coefficient of A in X.

The binary diffusion coefficients for mixtures of polar components at low pressure can be calculated using the adaptation of the Chapman-Enskog correlation proposed by Brokaw [4] according to Eq. A-4:

$$D_{AB} = \frac{0.001858 \cdot T^{3/2} \left( \frac{1}{M_A} + \frac{1}{M_B} \right)^{1/2}}{P \sigma_{AB}^2 \Omega_D} \quad \text{Eq. A-4}$$

where  $D_{AB}$  is the binary diffusion coefficient [ $\text{cm}^2 \cdot \text{s}^{-1}$ ],  $T$  is the temperature [K],  $M_A$  and  $M_B$  are the molecular weights of A and B [ $\text{g} \cdot \text{mol}^{-1}$ ], respectively,  $P$  is pressure [atm],  $\sigma_{AB}$  is the geometric mean of the characteristic length [ $\text{\AA}$ ], and  $\Omega_D$  is the integration of the diffusion collision value [-]. The corrected value of  $\Omega_D$  for polar mixtures can be calculated using Eq. A-5, where  $T^*$  is the characteristic temperature (Eq. A-6)

$$\Omega_D = \left( 44.54 T^{*-4.909} + 1.911 T^{*-1.575} \right)^{0.10} + 0.19 \frac{\delta_{AB}^2}{T^*} \quad \text{Eq. A-5}$$

$$T^* = \frac{kT}{\epsilon_{AB}} \quad \text{Eq. A-6}$$

where  $\epsilon_{AB}$  and  $\delta_{AB}$  are the geometric means of the Lennard-Jones energy and the polarity correction term of the pure components, which can be calculated using the correlations grouped in Eq. A-7.

$$\begin{aligned} \sigma_{AB^\circ} &= (\sigma_{A^\circ} \sigma_{B^\circ})^{1/2} & \sigma_{i^\circ} &= [1.585 V_{bi} / (1 + 1.3 \delta_i^2)]^{1/3} \\ \delta_{AB} &= (\delta_A \delta_B)^{1/2} & \delta_i &= 1.94 \times 10^3 \mu_i^2 / V_{bi} T_{bi} \\ \epsilon_{AB^\circ} &= (\epsilon_{A^\circ} \epsilon_{B^\circ})^{1/2} & \epsilon_{i^\circ} / k &= 1.18 (1 + 1.3 \delta_i^2) T_{bi} \end{aligned} \quad \text{Eq. A-7}$$

where  $T_b$  is the boiling point temperature [K],  $V_b$  is the liquid molar volume at  $T_b$  [ $\text{mL} \cdot \text{mol}^{-1}$ ] and  $\mu$  is the dipole moment [-] (Table A-9). The estimated effective diffusion coefficients for *n*-octanol, according to Eq. A-3 and Eq. A-4, are summarized in Table A-10.

**Table A-9** Parameters of the pure components to calculate  $D_{AB}$  by the Brokaw's method.

Parameter	<i>n</i> -octanol	N <sub>2</sub>	H <sub>2</sub>	NH <sub>3</sub>
T <sub>b</sub> (K) <sup>[5]</sup>	468.0	77.4	20.3	239.8
V <sub>b</sub> (mL·mol <sup>-1</sup> ) <sup>[5]</sup>	158.0	34.7	28.5	19.8
μ (-) <sup>[6]</sup>	1.76	0	0	1.47

**Table A-10** D'<sub>ROH</sub> estimated values by the Brokaw's method

T (K)	D' <sub>ROH</sub> (cm <sup>2</sup> ·s <sup>-1</sup> )
433	7.5·10 <sup>-2</sup> ± 0.007
443	7.9·10 <sup>-2</sup> ± 0.008
453	8.2·10 <sup>-2</sup> ± 0.008

**(iii) External mass transfer**

The influence of the external mass transfer on the reaction rate can be assessed using the Mears criterion as expressed by Eq. A-8 [1,7]

$$\frac{-r_{ROH(obs)}\rho_b R_p n}{k_g C_{ROH}} < 0.15 \quad \left| \quad \text{Eq. A-8} \right.$$

where  $r_{ROH(obs)}$  is the reaction rate [mmol·g-cat<sup>-1</sup>·s<sup>-1</sup>],  $\rho_b$  is the bed density [g·cm<sup>-3</sup>],  $R_p$  is the particle radius [cm],  $n$  is the reaction order,  $k_g$  is the mass transfer coefficient [cm·s<sup>-1</sup>] and  $C_{ROH}$  is the *n*-octanol concentration [mmol·cm<sup>-3</sup>].

The mass transfer coefficient at low Re number (Re=0.56) can be calculated from the Froessling correlation: [8,9]

$$k_g = \frac{D}{d_p} (2.0 + 0.6 Sc^{1/3} Re^{1/2}) \quad \left| \quad \text{Eq. A-9} \right.$$

where  $D$  is the mass diffusivity (previously estimated to be >0.068 cm<sup>2</sup>·s<sup>-1</sup> at 160 °C),  $d_p$  is the particle diameter and  $Sc$  is the Schmidt number.

The Schmidt number describes the ratio of viscous diffusion to molecular diffusion rates and can be calculated using Eq. A-10, where  $\mu_f$  is the fluid viscosity [g·cm<sup>-1</sup>·s<sup>-1</sup>] and  $\rho_f$  is the fluid density [g·cm<sup>-3</sup>]:

$$Sc = \frac{\mu}{\rho_f D} = \frac{1.9 \cdot 10^{-4}}{1.6 \cdot 10^{-3} \cdot 0.068} = 1.7 \quad \left| \quad \text{Eq. A-10} \right.$$

By substituting the  $Sc$  and  $Re$  numbers into Eq. A-9, the mass transfer coefficient can be estimated as follows:

$$k_g = \frac{0.068}{1.5 \cdot 10^{-2}} (2 + 0.6 \cdot 1.7^{1/3} \cdot 0.56^{1/2}) = 11.5 \text{ cm} \cdot \text{s}^{-1} \quad \left| \quad \text{Eq. A-11} \right.$$

By applying the calculated mass transfer coefficient to Eq. , we obtain a value of 0.017 for the Mears criterion, far below the limiting value of 0.15. Having considered a reaction rate 1.5 times higher than the highest value measured experimentally, as well as the least favorable diffusivity, we can safely conclude the absence of external mass transfer limitations under the working conditions.

$$\frac{-r_{\text{ROH}(obs)} \rho_b R_p^n}{k_g C_{\text{ROH}}} = \frac{0.2 \cdot 0.9 \cdot 7.5 \cdot 10^{-3} \cdot 1}{11.5 \cdot 6.7 \cdot 10^{-3}} = 0.017 \ll 0.15 \quad \text{Eq. A-12}$$

(iv) Internal mass transfer

The contribution of internal mass transfer to the reaction rate can be assessed using the Weisz-Prater criterion (Eq. A-13) [10,11]. Considering the bulk phase effective diffusion coefficient previously calculated to be  $0.068 \text{ cm}^2 \cdot \text{s}^{-1}$ , since Knudsen diffusion is unlikely at  $160 \text{ }^\circ\text{C}$  in  $13 \text{ nm}$  pores, the Weisz-Prater criterion gives a value of 0.09, implying no relevant resistance due internal mass transfer.

$$\frac{-r_{\text{ROH}(obs)} \rho_c R_p^2}{D_{\text{ROH}} C_{\text{ROH}}} = \frac{0.2 \cdot 3.65 \cdot (7.5 \cdot 10^{-3})^2}{0.068 \cdot 6.7 \cdot 10^{-3}} = 0.09 \ll 0.6 \quad \text{Eq. A-13}$$

## Annex IV. Development of the kinetic expressions

In this annex section we present the development of the kinetic expressions corresponding to the kinetic models M.V\_A and M.V\_B presented in section 4.5.2. The different elementary reactions and the corresponding approximations applied are listed in Table A-11.

**Table A-11** List of elementary steps for *n*-octanol amination with NH<sub>3</sub> relying on models M.V\_A and M.V\_B (QEA: quasi-equilibrium approximation; QSSA: quasi-steady state approximation)

#	Elementary steps <sup>1</sup>	Approximation	Rate
1	$\text{R-OH}_{(g)} + \text{Z} \longrightarrow \text{R-OH}^{\text{Z}}$	QEA	
2	$\text{R-OH}^{\text{Z}} + \text{Y} \longrightarrow \text{R-OH-I}^{\text{Z}} + \text{H}^{\text{Y}}$	-	r <sub>1</sub>
3	$\text{R-OH-I}^{\text{Z}} + \text{Y} \longrightarrow \text{R=O}^{\text{Z}} + \text{H}^{\text{Y}}$	QSSA	
4	$\text{H}_{2(g)} + 2\text{Y} \rightleftharpoons 2\text{H}^{\text{Y}}$	QEA	
5	$\text{R=O}_{(g)} + \text{Z} \rightleftharpoons \text{R=O}^{\text{Z}}$	QEA	
6	$\text{NH}_{3(g)} + \text{Y} \rightleftharpoons \text{NH}_3^{\text{Y}}$	QEA	
7	$\text{R=O}^{\text{Z}} + \text{NH}_3^{\text{Y}} \longrightarrow \text{R=NH}^{\text{Z}} + \text{H}_2\text{O}^{\text{Y}}$	QSSA	r <sub>2</sub>
8	$\text{H}_2\text{O}_{(g)} + \text{Y} \rightleftharpoons \text{H}_2\text{O}^{\text{Y}}$	QEA	
9	$\text{R=NH}^{\text{Z}} + \text{Y} \rightleftharpoons \text{R-CN-I}^{\text{Z}} + \text{H}^{\text{Y}}$	QSSA	r <sub>3</sub>
10	$\text{R-CN-I}^{\text{Z}} + \text{Y} \rightleftharpoons \text{R-CN}^{\text{Z}} + \text{H}^{\text{Y}}$	QEA	
11	$\text{R=NH}^{\text{Z}} + \text{H}^{\text{Y}} \rightleftharpoons \text{R-NH}_2\text{-I}^{\text{Z}} + \text{Y}$	QSSA	r <sub>4</sub>
12	$\text{R-NH}_2\text{-I}^{\text{Z}} + \text{H}^{\text{Y}} \rightleftharpoons \text{R-NH}_2^{\text{Z}} + \text{Y}$	QEA	
13	$\text{R-NH}_{2(g)} + \text{Z} \rightleftharpoons \text{R-NH}_2^{\text{Z}}$	QEA	
14	$\text{R-CN} + \text{Z} \rightleftharpoons \text{R-CN}^{\text{Z}}$	QEA	
15	$\text{R=O}^{\text{Z}} + \text{R-NH}_2^{\text{Z}} \longrightarrow \text{R=N-R}^{\text{Z}} + \text{H}_2\text{O}^{\text{Y}}$	-	r <sub>5</sub>
16	$\text{R=N-R}_{(g)} + \text{Z} \rightleftharpoons \text{R=N-R}^{\text{Z}}$	QEA	
17	$\text{R=N-R}^{\text{Z}} + \text{H}^{\text{Y}} \longrightarrow \text{R}_2\text{-NH-I}^{\text{Z}} + \text{Y}$	QSSA	
18	$\text{R}_2\text{-NH-I}^{\text{Z}} + \text{H}^{\text{Y}} \longrightarrow \text{R}_2\text{-NH}^{\text{Z}} + \text{Y}$	QSSA	
19	$\text{R}_2\text{-NH}_{(g)} + \text{Z} \rightleftharpoons \text{R}_2\text{-NH}^{\text{Z}}$	QEA	
20	$\text{d D}^{\text{Z}} \longrightarrow \text{Z}^{\text{Deact}}$	QSSA	r <sub>D</sub>
21	$\text{Z}^{\text{Deact}} + n \text{H}^{\text{Y}} \rightarrow \text{Z} + n \text{Y} + \text{X}$	QSSA	r <sub>R</sub>

<sup>1</sup> The labels Y and Z refer to active sites

(i) **Balance of surface species**

The existence of two differentiated catalytic sites is proposed, namely Y and Z. Y sites correspond to the adsorption sites for lighter molecules (NH<sub>3</sub>, H<sub>2</sub> and H<sub>2</sub>O), while bulkier molecules (C<sub>8</sub>-X) are expected to adsorb in the Z sites. The consideration of two site balances is justified by the non-competitive nature of the adsorption between lighter and bulkier molecule [12,13]. According to the fitting results for model M.V, only the following molecules were considered to compete for adsorption:

- (i) H<sub>2</sub> adsorption in Y site
- (ii) Octanal adsorption in Z site
- (iii) Octylimine (OI) adsorption in Z site
- (iv) Coke coverage - deactivated Z sites

The adsorption rates are considered fast, reaching equilibrium during the reaction. A Langmuir isotherm, as expressed in Eq. 4-3, is considered. Certain molecules are proposed to be non-desorbable, being fast consumed as they are formed on the catalyst surface. This approximation is in agreement with the experimental observation of virtually 0 kPa partial pressure for such molecules. The surface coverage is instead calculated via the quasi-steady state approximation, as expressed in Eq. A-14 to Eq- A-17..

$\theta_i^x = K_i p_i \theta_v^x$	<b>Eq. A-14</b>
QSSA: $r_1 = r_2 + r_5$ $\theta_{R=O}^Z = \frac{k_1 \theta_{R-OH}^Z \theta_v^Y}{k_2 \theta_{NH_3}^Y + k_5 \theta_{R-NH_2}^Z}$	<b>Eq. A-15</b>
QSSA: $r_2 = r_3 + r_4$ $\theta_{R=NH}^Z = \frac{k_2 \theta_{R=O}^Z \theta_{NH_3}^Y + k_{-3} \theta_{R-CN-I}^Z \theta_H^Y + k_{-4} \theta_{R-NH_2-I}^Y \theta_v^Y}{k_{+3} \theta_v^Y + k_{+4} \theta_H^Y}$	<b>Eq. A-16</b>
QSSA: $r_D = r_R$ $\theta_D^Z = \frac{k_D (\theta_{R=NH}^Z)}{k_R (\theta_H^Y)^2}$	<b>Eq. A-17</b>

The incorporation of the Langmuir isotherms and the quasi-steady state intermediates into the Y and Z site balances provides the following expressions for the balances:

(i) **Y site balance**

$1 = \theta_v^Y + \theta_H^Y$ $\theta_v^Y = \frac{1}{1 + \sqrt{K_{H_2} p_{H_2}}}$	<b>Eq. A-18</b>
---	-----------------

(ii) Z site balance

$$1 = \theta_V^Z + \theta_{R=O}^Z + \theta_{R=NH}^Z + \theta_D^Z$$

$$\theta_V^Z = 1 - (\theta_{R=O}^Z + \theta_{R=NH}^Z + \theta_D^Z)$$

Where:

$$\theta_{R=O}^Z = \frac{k_1 \theta_{R-OH}^Z \theta_V^Y}{k_2 \theta_{NH_3}^Y + k_5 \theta_{R-NH_2}^Z}$$

$$\theta_{R=NH}^Z = \frac{k_2 \theta_{R=O}^Z \theta_{NH_3}^Y + k_{-3} \theta_{R-CN-I}^Z \theta_H^Y + k_{-4} \theta_{R-NH_2-I}^Y \theta_V^Y}{k_{+3} \theta_V^Y + k_{+4} \theta_H^Y}$$

$$\theta_D^Z = \frac{k_D (\theta_{R=NH}^Z)}{k_R (\theta_H^Y)^2}$$

Eq. A-19

The expression for the Z balance becomes in this case implicit. The vacancies of Z sites need to be calculated using an iterative process at each integration step. Only one solution with physical meaning ( $0 \leq \theta_V^Z \leq 1$ ) is found.

Finally, by applying the QSSA to  $r_5=r_6$  and integrating the coverage expressions into the rate equations, the rate expressions listed in Table A-12 are obtained. The incorporation of these rate expressions into the mass balances gives the expressions listed in Table A-13.

**Table A-12** Expressions for the different reaction rates

$r_3 = k_{+3} \theta_{R=NH}^Z \theta_V^Y - k_{-3} p_{R-CN} p_{H_2} \theta_V^Z \theta_V^Y$	Eq. A-20
$r_4 = k_{+4} \theta_{R=NH}^Z p_{H_2}^{1/2} \theta_V^Y - k_{-3} p_{R-NH_2} p_{H_2}^{-1/2} \theta_V^Z \theta_V^Y$	Eq. A-21
$r_5 = r_6 = k'_5 p_{R=O} p_{R-NH_2} (\theta_V^Z)^2$	Eq. A-22

**Table A-13** Expressions for the differential material balances

$\frac{dF_{R-OH}}{dW} = - (r_3 + r_4 + r_5)$	<b>Eq. A-23</b>
$\frac{dF_{R=O}}{dW} = 0$	<b>Eq. A-24</b>
$\frac{dF_{R-NH_2}}{dW} = r_4 - r_5$	<b>Eq. A-25</b>
$\frac{dF_{R-CN}}{dW} = r_3$	<b>Eq. A-26</b>
$\frac{dF_{R_2=N}}{dW} = 0$	<b>Eq. A-27</b>
$\frac{dF_{R_2-NH}}{dW} = r_5$	<b>Eq. A-28</b>
$\frac{dF_{NH_3}}{dW} = - (r_3 + r_4)$	<b>Eq. A-29</b>
$\frac{dF_{H_2}}{dW} = + 2 r_3$	<b>Eq. A-30</b>

Finally, the temperature dependency of the apparent rate and equilibrium constants was expressed by Eq. A-31 and Eq. E-32, respectively.

$$k'_i(T) = k'_i(T_M) \exp \left[ -\frac{E_{a,app i}}{R} \left( \frac{1}{T} - \frac{1}{T_M} \right) \right] \quad \text{Eq. A-31}$$

$$K'_i(T) = K'_i(T_M) \exp \left[ -\frac{\Delta H_i}{R} \left( \frac{1}{T} - \frac{1}{T_M} \right) \right] \quad \text{Eq. A-32}$$

## Annex V. Matlab code for the kinetic optimization of model M.V\_B

Matlab® code for the kinetic optimization of model M.V\_B in section 4.5.2.

```
function MV_II
clc
close all
clear all
% Load experimental Data
data_profile=xlsread('Kinetic_data');

% Create vector of experimental conditions
Initial_conditions=data_profile(2:5,2:127);

% Create Vector of experimental partial pressures
EP_RNH2(:,1)=data_profile(15,2:127);
EP_R2NH(:,1)=data_profile(18,2:127);
EP_R2N(:,1)=data_profile(19,2:127);
EP_RCN(:,1)=data_profile(17,2:127);
EP_ROH(:,1)=data_profile(16,2:127);

%Create vector of experimental yields and conversions
EY_RNH2(:,1)=data_profile(22,2:127).*100;
EY_R2NH(:,1)=data_profile(24,2:127).*100;
EY_R2N(:,1)=data_profile(25,2:127).*100;
EY_RCN(:,1)=data_profile(23,2:127).*100;
EC_ROH(:,1)=data_profile(21,2:127).*100;

% Weights for experimental data - Eliminate experimental points out of the
% calibration sensitivity
W_RNH2(:,1)=data_profile(28,2:127);
W_R2NH(:,1)=data_profile(30,2:127);
W_RCN(:,1)=data_profile(29,2:127);
W_ROH(:,1)=data_profile(32,2:127);
W_R2N(:,1)=data_profile(31,2:127);

% Scale the experimental pressures around its central value
Pw_RNH2(:,1)=EP_RNH2./0.9948.*W_RNH2;
Pw_R2NH(:,1)=EP_R2NH./0.0912.*W_R2NH;
Pw_RCN(:,1)=EP_RCN./0.1211.*W_RCN;
Pw_ROH(:,1)=EP_ROH./15.6568.*W_ROH;
Pw_R2N(:,1)=EP_R2N./0.031.*W_R2N;

% Create vector with the experimental values for the mass of catalyst
Mc=data_profile(7,2:127); % mass of cat in mg

R=8.314*1e-3; % Ideal Gas Constant
```

```

Pt=2; % Total Pressure, bar
In=zeros(10,1); % Empty vector of Inlet conditions
Temp=[453.15 443.15 433.15]; % Vector of experimental temperatures

```

1) % Empty Vectors for optimization function

```

p_RNH2opt=zeros(126,1);
p_RCNopt=zeros(126,1);
p_R2NHopt=zeros(126,1);
p_ROHopt=zeros(126,1);
p_R2Nopt=zeros(126,1);
p_RNHopt=zeros(126,1);

```

% Experimental Values for optimization

```
Exp=[Pw_RNH2;Pw_R2NH;Pw_RCN;Pw_ROH];
```

% Initial Values for Optimization

```
BETA0=[119.55 12.42 15.07 8757.47 97.91 498.39 27378.9 116.16 -469.65 127.12 36.49 85.44 52.74 -446.07 0.69 -25.46
398.76 56.06];
```

% Optimization function

```
optionsLSQ=optimoptions('lsqcurvefit','UseParallel',true,'Display','iter','Algorithm','levenberg-marquardt');
[BETA,ResNorm,Res,ExitFlag,Output,~,J]= lsqcurvefit(@fopt,BETA0,[],Exp,[],[],optionsLSQ);
```

%----- Data Statistics-----

% Confidence Interval

```
CI = nlparci(BETA,Res,'jacobian',J);
Err=abs((CI(:,1)-BETA)./BETA)*100;
Nvar=1:length(BETA');
```

% Output Table with Variables and 95% CI

```
Table1=table(Nvar,BETA,CI,Err)
```

SSE=(Res\*Res); % Standard Error

```
MSE=(Res*Res)/(length(Exp)-length(BETA0)); % Mean Squared Error
```

```
cov=(inv(J*J))*MSE; % variance-covariance matrix
```

```
corr=cov./sqrt(diag(cov)*diag(cov)); % correlation matrix
```

```
VIF=diag(inv(corr)); % Variance Inflation Factor
```

% Standardized Residuals R-NH2

```
Res_RNH2=Res(1:126);
MSE_RNH2=(Res_RNH2*Res_RNH2)/(126-length(BETA0));
Std_RNH2=Res_RNH2./sqrt(MSE_RNH2);
Std_RNH2(Std_RNH2 == 0) = NaN;
```

% Standardized Residuals R2-NH

```
Res_R2NH=Res(127:252);
MSE_R2NH=(Res_R2NH*Res_R2NH)/(126-length(BETA0));
Std_R2NH=Res_R2NH./sqrt(MSE_R2NH);
Std_R2NH(Std_R2NH == 0) = NaN;
```

```

% Standardized Residuals R-CN
Res_RCN=Res(253:378);
MSE_RCN=(Res_RCN*Res_RCN)/(126-length(BETA0));
Std_RCN=Res_RCN./sqrt(MSE_RCN);
Std_RCN(Std_RCN == 0) = NaN;
% Standardized Residuals R-OH
Res_ROH=Res(379:504);
MSE_ROH=(Res_ROH*Res_ROH)/(126-length(BETA0));
Std_ROH=Res_ROH./sqrt(MSE_ROH);
Std_ROH(Std_ROH == 0) = NaN;

```

```

% Calculate determination coefficients R2

```

```

% R2 global;

```

```

a=[Pw_R2NH.*0.0912.*W_R2NH;Pw_RNH2.*0.9948.*W_RNH2;Pw_ROH.*15.6568.*W_ROH;Pw_RCN.*0.1211.*W_RCN];

```

```

b=[pw_R2NHopt.*0.0912.*W_R2NH;pw_RNH2opt.*0.9948.*W_RNH2;pw_ROHopt.*15.6568.*W_ROH;pw_RCNopt.*0.1211.*W_RCN];

```

```

a=a(a~=0);

```

```

b=b(b~=0);

```

```

Rg2=corrcoef([a b]).^2;

```

```

% R2 Products

```

```

a=[Pw_R2NH.*0.0912.*W_R2NH;Pw_RNH2.*0.9948.*W_RNH2;Pw_RCN.*0.1211.*W_RCN];

```

```

b=[pw_R2NHopt.*0.0912.*W_R2NH;pw_RNH2opt.*0.9948.*W_RNH2;pw_RCNopt.*0.1211.*W_RCN];

```

```

a=a(a~=0);

```

```

b=b(b~=0);

```

```

R_PROD=corrcoef([a b]).^2;

```

```

% R2 ROH

```

```

a=Pw_ROH.*15.6568.*W_ROH;

```

```

b=pw_ROHopt.*15.6568.*W_ROH;

```

```

a=a(a~=0);

```

```

b=b(b~=0);

```

```

R2_ROH=corrcoef([a b]).^2;

```

```

R2_All=[SSE R2_ROH(2) Rg2(2) R_PROD(2)];

```

```

% Output Table with R2

```

```

R2_tn={'SSE';'R^2 ROH';'R^2 Global';'R^2 Products'};

```

```

Table2=table(R2_All,'RowNames',R2_tn)

```

```

%-----Plot figures-----

```

```

%Parity Plots

```

```

figure(1)

```

```

subplot(2,2,2)

```

```

plot(Pw_RNH2.*0.9948.*W_RNH2,pw_RNH2opt.*0.9948.*W_RNH2,'+');

```

```

title('Partial Pressure RNH_2 - kPa -')

```

```

xlabel('Experimental');ylabel('Predicted')

```

```

axis([0 5 0 5])

```

```

refline(1)

```

```

subplot(2,2,3)

```

```

plot(Pw_RCN.*0.1211.*W_RCN,pw_RCNopt.*0.1211.*W_RCN,'+');

```

```

axis([0 1 0 1])
title('Partial Pressure RCN - kPa -')
xlabel('Experimental');ylabel('Predicted')
refline(1)

subplot(2,2,4)
plot(Pw_R2NH.*0.0912.*W_R2NH,pw_R2NHopt.*0.0912.*W_R2NH,'+');
axis([0 1 0 1])
title('Partial Pressure R_2NH - kPa -')
xlabel('Experimental');ylabel('Predicted')
refline(1)

subplot(2,2,1)
plot(Pw_ROH.*15.6568.*W_ROH,pw_ROHopt.*15.6568.*W_ROH,'+');
axis([0 30 0 30])
title('Partial Pressure ROH - kPa -')
xlabel('Experimental');ylabel('Predicted')
refline(1)
%Residual Plots
figure(2)

subplot(2,2,1)
plot(EC_ROH,Std_ROH,'o');
axis([0 35 -4 4])
title('ROH')
xlabel('Conversion ROH %');ylabel('Normalized Residual')

subplot(2,2,2)
plot(EY_RNH2,Std_RNH2,'o');
title('RNH_2')
xlabel('Yield RNH_2 %');ylabel('Normalized Residual')
axis([0 25 -4 4])
subplot(2,2,3)
plot(EY_RCN,Std_RCN,'o');
axis([0 5 -4 4])
title('RCN')
xlabel('Yield RCN %');ylabel('Normalized Residual')

subplot(2,2,4)
plot(EY_R2NH,Std_R2NH,'o');
axis([0 12 -4 4])
title('R_2NH')
xlabel('Yield R_2NH %');ylabel('Normalized Residual')
snapnow

save VARIABLES

% Optimization function
function fx=fopt(p,~)

```

```
% Reaction & Equilibrium constants
```

```
k1=p(1);  
k2=p(2);  
k3=p(3);  
k_3=p(4);  
k4=p(5);  
k_4=p(6);  
k5=p(7);  
Ea1=p(8);  
Ea2=p(9);  
Ea3=p(10);  
Ea_3=p(11);  
Ea4=p(12);  
Ea_4=p(13);  
Ea5=p(14);  
K_H2=p(15);  
H_H2=p(16);  
KD1=p(17);  
HD1=p(18);  
a=1;  
b=2;
```

```
%----- LOOP FOR ALL EXPERIMENTAL CONDITIONS -----
```

```
for cn=1:14
```

```
    In(1:3)=Initial_conditions(1:3,9*cn-8); %mmol/h  
    nROHi=In(1);  
    nNH3i=In(2);  
    nH2i=In(3);
```

```
    for i=3*cn-2:3*cn
```

```
        T=Temp(i-3*cn+3);  
        M(2:4)=Mc(3*i-2:3*i); %mg of catalyst
```

```
    % ODE Solver
```

```
    optionsODE=odeset('RelTol',1e-3);  
    [~,yo]=ode15s(@fun,M,In,optionsODE);
```

```
    F=sum(Initial_conditions(:,9*cn-8))+yo(2:4,10)+2.*yo(2:4,4); %mmol/h total
```

```
    % Vectors of computed partial pressures in kPa
```

```
    p_RNH2opt(3*i-2:3*i)=yo(2:4,5)/F.*200 ;  
    p_RNHopt(3*i-2:3*i)=yo(2:4,9)/F.*200 ;  
    p_RCNOpt(3*i-2:3*i)=yo(2:4,4)/F.*200 ;  
    p_R2NHopt(3*i-2:3*i)=yo(2:4,6)/F.*200 ;  
    p_R2NOpt(3*i-2:3*i)=yo(2:4,10)/F.*200 ;  
    p_ROHopt(3*i-2:3*i)=yo(2:4,1)/F.*200;
```

```
    end
```

```
end
```

```

% Weighted and Scaled Vectors of computed partial pressures
pw_RNH2opt(:,1)=p_RNH2opt./0.9948.*W_RNH2;
pw_R2NHopt(:,1)=p_R2NHopt./0.0912.*W_R2NH;
pw_RCNopt(:,1)=p_RCNopt./0.1211.*W_RCN;
pw_ROHopt(:,1)=p_ROHopt./15.6568.*W_ROH;
pw_R2Nopt(:,1)=p_R2Nopt./0.031.*W_R2N;

% Objective Function
fx=[pw_RNH2opt;pw_R2NHopt;pw_RCNopt;pw_ROHopt];

%System of differential Equations
function dydt=fun(-,y)
Tm=443.15; % Tm temperature
F=sum(Initial_conditions(:,9*cn-8))+2*y(4); % mmol/h total

%----- CONSTANTS vs Temp -----
% Equilibrium Constants
KD1t=KD1*exp(-HD1/R*(1/T-1/Tm));
KH2t=K_H2*exp(-H_H2/R*(1/T-1/Tm));

% Rate Constants
k1t=k1*exp(-Ea1/R*(1/T-1/Tm));
k2t=k2*exp(-Ea2/R*(1/T-1/Tm));
k3t=k3*exp(-Ea3/R*(1/T-1/Tm));
k_3t=k_3*exp(-Ea_3/R*(1/T-1/Tm));
k4t=k4*exp(-Ea4/R*(1/T-1/Tm));
k_4t=k_4*exp(-Ea_4/R*(1/T-1/Tm));
k5t=k5*exp(-Ea5/R*(1/T-1/Tm));

%Partial pressures in bar
P_ROH=y(1)/F*Pt;
P_NH3=y(2)/F*Pt;
P_H2=y(3)/F*Pt;
P_RCN=y(4)/F*Pt;
P_RNH2=y(5)/F*Pt;
P_R2NH=y(6)/F*Pt;
P_H2O=y(7)/F*Pt;
P_RO=y(8)/F*Pt;
P_R2N=y(10)/F*Pt;

%----- SITE BALANCES -----
% Site Balance Y site (Light Molecules)
S2=1/(1+(KH2t*P_H2)^.5);
% Site Balance Z site (Bulky Molecules)
S=fzero(@fs,[0 1]);
function f=fs(S)
f=1-k1t*P_ROH*S2*S/(k2t*P_NH3*S2+k5t*P_RNH2*S)-
(k2t*k1t*P_ROH*S2*S/(k2t*P_NH3*S2+k5t*P_RNH2*S)*P_NH3+k_3t*P_RCN*P_H2*S+k_4t*P_RNH2/P_H2^.5*S)/(k3t+k4t*P

```

```

_H2^5)-
KD1t/(P_H2^5*S2)^b*(k2t*k1t*P_ROH*S2*S/(k2t*P_NH3*S2+k5t*P_RNH2*S)*P_NH3+k_3t*P_RCN*P_H2*S+k_4t*P_RNH2/
P_H2^5*S)/(k3t+k4t*P_H2^5)-S;
    end
O_RO=k1t*P_ROH*S*S2/(k2t*P_NH3*S2+k5t*P_RNH2*S);           % aldehyde coverage
O_RNH=(k2t*O_RO*P_NH3+k_3t*P_RCN*P_H2*S+k_4t*P_RNH2/P_H2^5*S)/(k3t+k4t*P_H2^5); % Primary Imine Coverage
O_D=KD1t*O_RNH^a/(P_H2^5*S2)^b;                             % Fraction of deactivated catalyst

% Reaction rates
r3=k3t*O_RNH*S2-k_3t*P_RCN*P_H2*S2*S;           % 1ary imine to Nitrile
r4=k4t*O_RNH*P_H2^5*S2-k_4t*P_RNH2/P_H2^5*S*S2; % 1ary imine to Amine
r5=k5t*O_RO*P_RNH2*S;                             % Aldehyde to 2ary amine

%----- MASS BALANCES -----
dydt=zeros(10,1);
dydt(1)=-r3-r4-r5; %ROH
dydt(8)=0;        %R=O
dydt(9)=0;        % R=NH
dydt(10)=0;       % R2=N
dydt(2)=-r3-r4;   %NH3R
dydt(3)=+2*r3;    %H2
dydt(4)=r3;       %RCN
dydt(5)=r4-r5;    %RNH2
dydt(6)=r5;       %R2NH
dydt(7)=r3+r4+r5; %H2O

end
end
end

```

Iteration	Func-count	First-order Residual	Norm of optimality	Lambda	step
0	19	25.9386	269	0.01	
1	39	25.9371	93.9	0.1	0.480324

Local minimum possible.

lsqcurvefit stopped because the relative size of the current step is less than the default value of the step size tolerance.

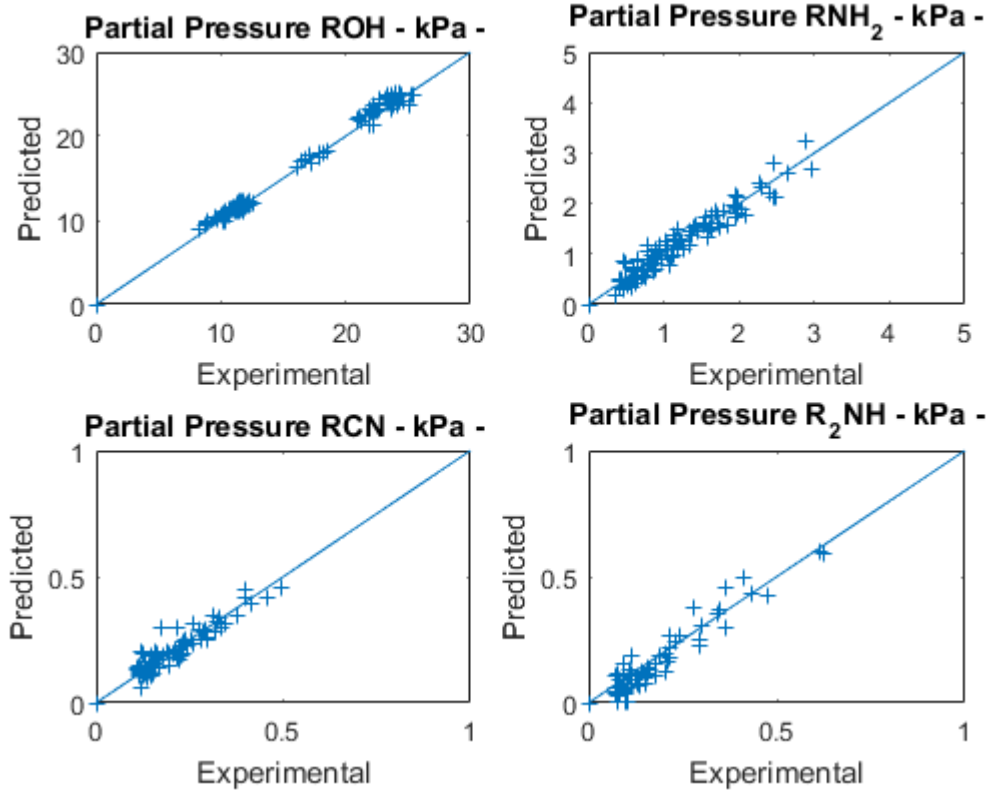
Table1 =

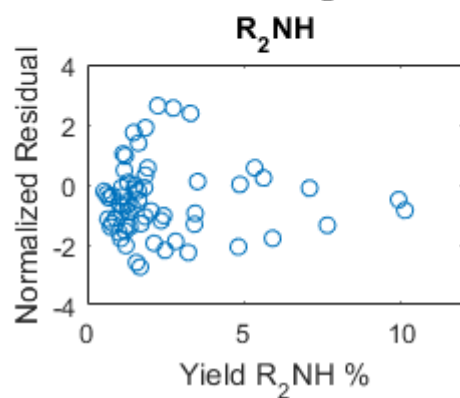
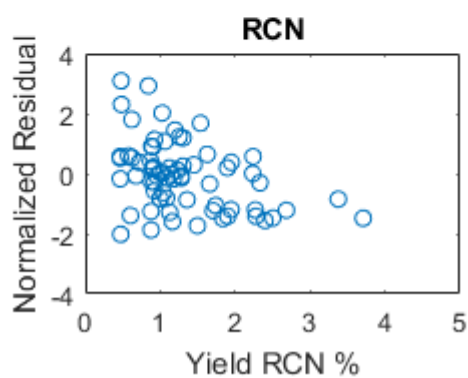
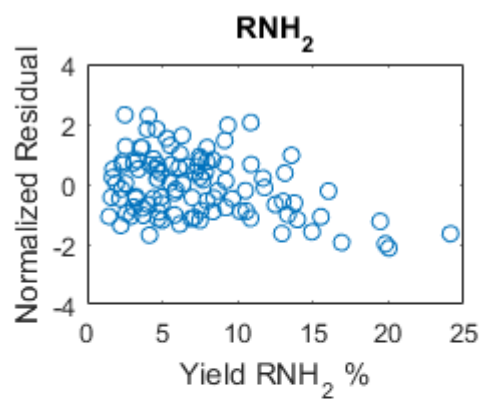
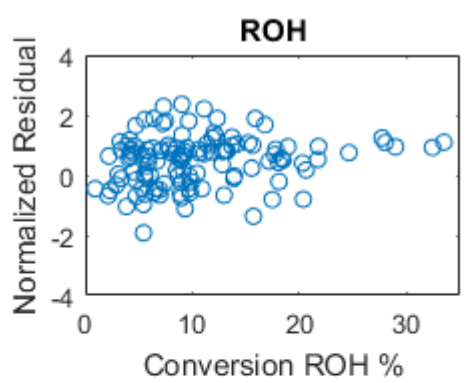
Var1	Var2	CI	Err
1	119.51	119.4	0.089161
2	12.424	12.415	0.073218
3	15.081	15.071	0.067096
4	8757.5	7736	9778.9

5	97.898	97.827	97.969	0.072097
6	498.38	437.36	559.4	12.244
7	27379	24866	29892	9.1794
8	116.12	116.03	116.22	0.080505
9	-469.81	-470.3	-469.32	0.10418
10	126.99	126.88	127.09	0.084442
11	36.438	12.856	60.019	64.717
12	85.416	85.333	85.5	0.097516
13	52.925	27.001	78.849	48.982
14	-446.34	-465.02	-427.66	4.1849
15	0.6895	0.68876	0.69025	0.10823
16	-25.465	-25.49	-25.44	0.098087
17	399.03	398.75	399.31	0.070333
18	56.049	55.984	56.114	0.11567

Table2 =

Var1	
SSE	25.937
R <sup>2</sup> ROH	0.99172
R <sup>2</sup> Global	0.9984
R <sup>2</sup> Products	0.96805





## References of the annexes

- [1] D.E. Mears, Tests for transport limitations in experimental catalytic reactors, *Ind. Eng. Chem. Process Des. Dev.* 10 (1971) 541–547.
- [2] R.H. Wilhelm, Progress towards the a priori design of chemical reactors, *Pure Appl. Chem.* 5 (1962). doi:10.1351/pac196205030403.
- [3] D.F. Fairbanks, C.R. Wilke, Diffusion coefficients in multicomponent gas mixtures, *Ind. Eng. Chem.* 42 (1950) 471–475.
- [4] R.S. Brokaw, Predicting transport properties of dilute gases, *Ind. Eng. Chem. Process Des. Dev.* 8 (1969) 240–253.
- [5] WebBook de Chimie NIST, (n.d.). <http://webbook.nist.gov/> (accessed May 16, 2017).
- [6] Chemical Rubber Company, D.R. Lide, eds., *CRC handbook of chemistry and physics: a ready-reference book of chemical and physical data*, 85. ed, CRC Press, Boca Raton, 2004.
- [7] H.F. Rase, *Fixed-Bed Reactor Design and Diagnostics: Gas-Phase Reactions*, Butterworth-Heinemann, 2013.
- [3] R.H. Perry, D.W. Green, eds., *Perry's chemical engineers' handbook*, 8th ed, McGraw-Hill, New York, 2008. p. 5-79
- [9] N. Froessling, Über die verdunstung fallender tropfen, *Gerlands Beitr. Zur Geophys.* 52 (1938) 170–215.
- [10] P.B. Weisz, C.D. Prater, Interpretation of Measurements in Experimental Catalysis, *Adv. Catal.* 6 (1954) 143–196. doi:10.1016/S0360-0564(08)60390-9.
- [11] O. Levenspiel, *Chemical reaction engineering*, 3rd ed, Wiley, New York, 1999.
- [12] D. Ruiz, A. Aho, T. Saloranta, K. Eränen, J. Wärnå, R. Leino, D.Y. Murzin, Direct amination of dodecanol with NH<sub>3</sub> over heterogeneous catalysts. Catalyst screening and kinetic modelling, *Chem. Eng. J.* 307 (2017) 739–749. doi:10.1016/j.cej.2016.08.083.
- [13] G.B. Rogers, M.M. Lih, O.A. Hougen, Catalytic hydrogenation of propylene and isobutylene over platinum. Effect of noncompetitive adsorption, *AIChE J.* 12 (1966) 369–377. doi:10.1002/aic.690120230.